PSDF

Power Systems Development Facility

Technical Progress Report
Gasification Test Run GCT 3

December 1, 2000 -
February 1, 2001

DOE Cooperative Agreement Number
DE-FC21-90MC25140

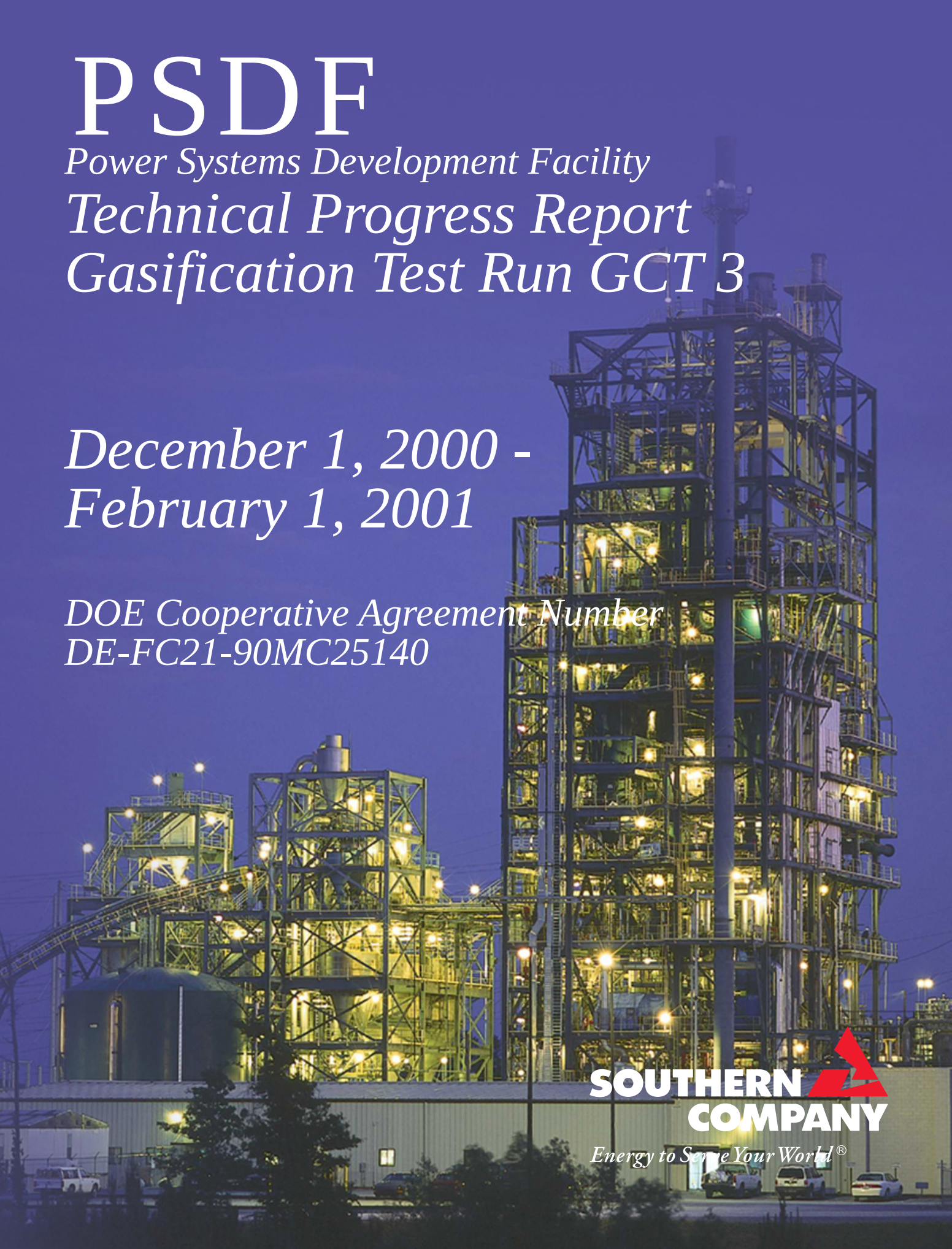

POWER SYSTEMS DEVELOPMENT FACILITY

TECHNICAL PROGRESS REPORT
GASIFICATION TEST RUN GCT3

DECEMBER 1, 2000 – FEBRUARY 1, 2001

DOE Cooperative Agreement Number
DE-FC21-90MC25140

Prepared by:
Southern Company Services, Inc.
Power Systems Development Facility
P.O. Box 1069
Wilsonville, AL 35186
Tel: 205-670-5840
Fax: 205-670-5843
http://psdf.southernco.com

May 2002

POWER SYSTEMS DEVELOPMENT FACILITY

DISCLAIMER

Available to the public from the National Technical Information Service, U.S. Department of Commerce, 5285 Port Royal Road, Springfield, VA 22161. Phone orders accepted at (703) 487-4650.

ACKNOWLEDGEMENT

The authors wish to acknowledge the contributions and support provided by various project managers: Jim Longanbach (DOE), Neville Holt (EPRI), Gene Cover (KBR), Zal Sanjana (Westinghouse), and Vann Bush (SRI). Also, the enterprising solutions to problems and the untiring endeavors of many personnel at the site during commissioning of the transport reactor train in gasification mode of operation are greatly appreciated. The project was sponsored by the U.S. Department of Energy National Energy Technology Laboratory under contract DE-FC21-90MC25140.

CONTENTS

Section Page

This Page Intentionally Left Blank

Listing of Tables

Listing of Figures

1.0 EXECUTIVE SUMMARY

1.1 SUMMARY

This report discusses test campaign GCT3 of the Halliburton KBR transport reactor train with a Siemens Westinghouse Power Corporation (Siemens Westinghouse) particle filter system at the Power Systems Development Facility (PSDF) located in Wilsonville, Alabama. The transport reactor is an advanced circulating fluidized-bed reactor designed to operate as either a combustor or a gasifier using one of two possible particulate control devices (PCDs). The transport reactor was operated as a pressurized gasifier during GCT3.

GCT3 was planned as a 250-hour test run to commission the loop seal and continue the characterization of the limits of operational parameter variations using a blend of several Powder River Basin coals and Bucyrus limestone from Ohio. The primary test objectives were:

- *Loop Seal Commissioning* – Evaluate the operational stability of the loop seal with sand and limestone as a bed material at different solids circulation rates and establish a maximum solids circulation rate through the loop seal with the inert bed.

- *Loop Seal Operations* – Evaluate the loop seal operational stability during coal feed operations and establish maximum solids circulation rate.

Secondary objectives included the continuation of reactor characterization, including:

- *Operational Stability* – Characterize the reactor loop and PCD operations with short-term tests by varying coal feed, air/coal ratio, riser velocity, solids circulation rate, system pressure, and air distribution.

- *Reactor Operations* – Study the devolatilization and tar cracking effects from transient conditions during transition from start-up burner to coal. Evaluate the effect of process operations on heat release, heat transfer, and accelerated fuel particle heat-up rates. Study the effect of changes in reactor conditions on transient temperature profiles, pressure balance, and product gas composition.

- *Effects of Reactor Conditions on Syngas Composition* – Evaluate the effect of air distribution, steam/coal ratio, solids circulation rate, and reactor temperature on CO/CO_2 ratio, H_2/converted carbon ratio, gasification rates, carbon conversion, and cold and hot gas efficiencies.

Test run GCT3 was started on December 1, 2000, with the startup of the thermal oxidizer fan, and was completed on February 1, 2001. This test was conducted in two parts; the loop seal was commissioned during the first part of this test run from December 1 through 15, which consisted of hot inert solids circulation testing. These initial tests provided preliminary data necessary to understand different parameters associated with the operation

and performance of the loop seal. The loop seal was tested with coal feed during the second part of the test run and additional data was gathered to analyze reactor operations and to identify necessary modifications to improve equipment and process performance. In the second part of GCT3, the gasification portion of the test, from January 20 to February 1, 2001, the mixing zone and riser temperatures were varied between 1,675 and 1,825°F at pressures ranging from 200 to 240 psig. There were 306 hours of solid circulation and 184 hours of coal feed attained in GCT3.

1.2 PSDF ACCOMPLISHMENTS

The PSDF has achieved over 4,985 hours of operation on coal feed and about 6,470 hours of solids circulation in combustion mode, and 979 hours of solid circulation and 634 hours of coal feed in gasification mode. The major accomplishments during GCT1, GCT2, and GCT3 are summarized below. (For combustion-related accomplishments, see the technical progress report for the TC05 test campaign.)

1.2.1 Transport Reactor Train

The major accomplishments and observations in GCT1, GCT2, and GCT3 included the following:

Commercial

- With subbituminous coal, more than 95-percent carbon conversion and 100 Btu/scf syngas heating value can be attained. The syngas characteristics were sufficient to support existing pressurized syngas burners without further dilution by nitrogen or saturation by water vapor. Moisture content in the syngas is sufficient for NO_X control. The contacted turbine vendor is uncertain of the role that ammonia in syngas will play in NO_X formation/reduction in CT.

- Transport reactor generated syngas can be combusted without propane enrichment. The thermal oxidizer (atmospheric syngas burner) operated well using syngas with different heating values and was run for short periods of time without propane addition while maintaining an exit temperature near 2,000°F.

Process

- In GCT1, the reactor was operated using two bituminous coals and a Powder River Basin (PRB) coal with different sorbents. Gasifier operations were stable, but carbon conversions were low due to disengager and cyclone inefficiencies.

- During GCT2, the longest continuous run of 184 hours in gasification mode of operation was achieved with PRB coal. Reactor operations were smooth without any incident of oxygen breakthrough, temperature excursions, deposits, clinkers, or any other operational problem. The reactor loop was run consistently at about 50 percent of the design circulation rate, and the carbon content of circulating solids was sufficient to maintain a reactor temperature of 1,800°F at the coal-feed rates tested. For the most part, the cyclone dipleg operated well with high solids flow due to the inefficiency of disengager. However, there were brief cyclone dipleg upsets.

- In GCT3, stable gasification reactor operation was achieved at a range of coal-feed rates, solids circulation rates, and reactor pressures ranging as high as 240 psig on PRB coal. The loop seal performed well, needing little attention, and promoted

much higher solids circulation rates and higher coal-feed rates that resulted in lower relative solids loading to the PCD and higher char retention in the reactor. Tar generation was also lower and could be completely eliminated by varying reactor operating parameters. It was also demonstrated that coal feed can safely be restarted after more than 30 minutes of down time without lighting the reactor start-up burner.

- The new loop seal located below the primary cyclone performed well, preventing reverse flow and increasing the cyclone efficiency. Also, the filter vessel loading was much lower at comparable coal-feed rates in GCT3 than during previous test runs. The changes made to the disengager and cyclone dipleg, as well as the addition of the new loop seal, contributed greatly to the lower loading values.

- In GCT3 the reactor experienced much higher circulation rates than in previous runs. The level in the disengager standpipe reached its highest levels ever, attaining heights beyond expectations without difficulties.

- The GCT3 test run registered the highest coal-feed rates ever fed to the transport reactor. The carbon conversion was much higher than in any of the previous test runs. The high coal-feed rate also caused the syngas produced to have the highest heating value of any syngas produced in the transport reactor to date.

- The transition from the start-up burner to coal feed can be made smoothly without any incidents of oxygen breakthrough. The reactor is heated up from ambient temperature to 1,200°F in about 14 hours, then using cokebreeze the reactor temperature can be increased to the desired operating temperature in less than 2 hours.

- Since the high carbon conversion in the transport gasifier significantly reduced the amount of remaining char, the sulfator did not receive enough char to maintain a high temperature. Thus, the sulfator required additional heating from its start-up burner and fuel oil injection system.

- Limestone calcination of 90 percent was achieved in the transport gasifier. The CO_2 partial pressures ranged from 20 to 23 psia.

- The overall mass balance was excellent with only ± 2 percent error.

- With PRB, the corrected fuel gas heating values ranged from 100 to 120 Btu/scf, depending on the test conditions. In the test range, the solids circulation rates, gas and solids residence times, and reactor temperatures do not show much effect on the fuel gas heating values. The observed increase in raw syngas heating value at higher coal-feed rates is mainly due to the reduced effect of added nitrogen (dilution and relatively less energy consumption for heatup).

- For PRB coal, the corrected cold gas efficiency (syngas latent heat to coal latent heat) remained between 60 and 70 percent based on gas analyses. The corrected hot gas efficiency (syngas latent + sensible heat to coal latent heat) was between 80 and 90 percent and the remaining coal latent heat was mainly present in the ash/char stream from the process.

- The H_2S concentration in the syngas was equilibrium constrained and varied from 100 to 200 ppm. On a larger unit the H_2S concentration will be less, due to lower partial pressures of H_2O and CO_2 in the syngas.

Equipment

- The PCD operates extremely well at the conditions tested in GCT3, with a low and stable DP when little or no tar is present in the gas. The fines removal system also performed well.

- After initial problems with the coal-feed line plugging with coal fines, the coal feed system operated flawlessly in GCT2. High coal-feed rates (up to 110 percent of design) were achieved with room to increase rates further (to 120 percent of design). However, the GCT3 test run was unusually characterized by numerous problems associated with the coal feed system. During operations, it was thought that the problems were related to the increased amount of fines in the ground coal. However, near the end of the run it was determined that a filter bag from the coal feed system filter vessel had fallen into the surge bin and partially blocked the path to the coal feed lock hopper. Eventually, the bag, with its respective cage, fell into the lock hopper, prevented the valves from operating, and caused the feed system to shut down. Due to these problems additional interlocks were identified to prevent oxygen breakthrough to the PCD from occurring in the event of coal feeder disruption.

- The primary gas cooler operated well, with no signs of plugging. There were no signs of tar deposits based on low pressure drop across the gas cooler and high heat-transfer rates.

- With logic changes made to the reactor, the char/ash removal system (FD0510) operated well without any line plugging during gasification.

- Modifications to the gas analysis system continued to improve its operation. The tar removal probe proved effective, allowing longer operation of the analyzers without plugging the tar removal probe.

- Standpipe gas and solids samples were collected for the first time during GCT3.

- The sulfator fuel oil injection system performed well. However, due to high carbon-feed rates at minimum motor speed, insufficient air flow to allow complete

combustion remains a problem. During GCT3, superheated steam from the sulfator was used as feed for reactor steam for the first time.

- The steam and condensate system also worked well, requiring little attention. There were no sulfator-related trips due to low steam flow.

- With additional improvements, the flare pilot sensors functioned satisfactorily, and the flow sensing of both the propane and syngas flow to the flare was reliable.

- The economizer was effective in moderating the baghouse temperature. The high exhaust temperatures seen previously were the result of the combination of higher-than-design coal-feed rates to the transport gasifier along with higher-than-design flue gas-flow rates from the sulfator, and lower-than-design cooling dilution air availability.

1.2.2 PCD

The major highlights for the PCD during GCT3 are summarized below.

1. PCD successfully operated for about 184 on-coal hours during the GCT3 test run with low outlet loading and no filter failures.

2. Testing continued on iron aluminide filters specifically designed for gasification environments. Iron aluminide filters were tested during the combustion test runs and GCT1A and performed well. Visual inspection of these filters after shutdown showed that they were intact. The char cake was thin and relatively uniform after the clean shutdown.

3. Testing continued on monolithic silicon carbide filters from Pall and Schumacher which performed well and without any mechanical failures. The visual inspection showed that the filters were intact and that the char cake was thin and uniform after the clean shutdown.

4. New filter holders developed by PSDF personnel performed well; the outlet loading never exceeded 1 ppmw throughout the run.

5. SRI successfully measured inlet and outlet particulate loading and char samples from the inlet sampling as well as char cake were analyzed and tested.

6. The ash removal system (FD0502/FD0520) worked well in GCT3; due to the lower inlet particulate loading to the PCD, solid accumulation in the cone of the PCD was not a problem. However, ceramic candle pieces plugged the discharge line of the dense-phase vessel at the end of the run. (These pieces were from the broken filter in the sand circulation run.)

7. The post-run PCD inspection showed that the shroud and liner sections were relatively clean. The plenums and tubesheet were also clean compared to previous gasification runs.

8. The 10 new Siemens Westinghouse fail-safes that were tested in GCT2 were installed for the GCT3 gasification run. After exposure in GCT3, two fail-safes were flow tested and weighed. The fail-safes will be continuously tested in the following runs and their performance will be further evaluated.

9. After the modification to the transport reactor there were dramatic changes in the particle characteristics in GCT3. Compared to the GCT2 run, the particles that carried over to the PCD during GCT3 were smaller in mean size and had a larger specific surface area. Despite these changes, control over the PCD pressure drop was maintained.

1.3 FUTURE PLANS

A 250-hour characterization test run (GCT4) with the transport reactor train operating in gasification mode is planned for March 2001. During GCT4, the direct sulfur recovery process (DSRP) operated by Research Triangle Institute (RTI) will be commissioned. A 1,000-hour test campaign (TC06) is planned to start in July 2001. After completing TC06 the modifications necessary to operate the transport reactor as an oxygen-blown gasifier will be completed.

The next test (TC07) will be in air blown mode during the first quarter of 2002 to characterize the modifications made following TC06. Then, there is a 250-hour oxygen-blown characterization test (TC08) scheduled to begin in the second quarter of 2002.

2.0 INTRODUCTION

This report provides an account of the GCT3 test campaign with the Halliburton KBR transport reactor and the Siemens Westinghouse Power Corporation (Siemens Westinghouse) filter vessel at the Power Systems Development Facility (PSDF) located in Wilsonville, Alabama, 40 miles southeast of Birmingham. The PSDF is sponsored by the U. S. Department of Energy (DOE) and is an engineering-scale demonstration of two advanced coal-fired power systems. In addition to DOE, Southern Company Services, Inc., (SCS), Electric Power Research Institute (EPRI), and Peabody Holding Company are cofunders. Other cofunding participants supplying services or equipment currently include Halliburton KBR and Siemens Westinghouse. SCS is responsible for constructing, commissioning, and operating the PSDF.

2.1 THE POWER SYSTEMS DEVELOPMENT FACILITY

SCS entered into an agreement with DOE/National Energy Technology Laboratory (NETL) for the design, construction, and operation of a hot-gas, clean-up test facility for pressurized gasification and combustion. The purpose of the PSDF is to provide a flexible test facility that can be used to develop advanced power system components, evaluate advanced turbine system configurations, and assess the integration and control issues of these advanced power systems. The facility was designed as a resource for rigorous, long-term testing and performance assessment of hot-stream, clean-up devices and other components in an integrated environment.

The PSDF will consist of five modules for systems and component testing. These modules include:

- An advanced pressurized, fluidized-bed combustion (APFBC) module.
- A transport reactor module.
- A hot-gas, clean-up module.
- A compressor/turbine module.
- A fuel cell module.

The APFBC module consists of FW technology for second-generation PFBC. This module relies on the partial conversion of the coal to fuel gas in a carbonizer, with the remaining char converted in a PFBC. Both the fuel gas and PFBC exhaust gas streams are filtered to remove particulates, then combined to fire a combustion turbine. The advanced gasifier module includes KBR transport reactor technology for pressurized combustion and gasification to provide either an oxidizing or reducing gas for parametric testing of hot particulate control devices. The filter systems that will be tested at PSDF include particulate control devices (PCDs) supplied by Siemens Westinghouse.

2.2 TRANSPORT REACTOR SYSTEM DESCRIPTION

The transport reactor is an advanced circulating fluidized-bed reactor operating as either a combustor or as a gasifier, using one of two possible hot-gas, clean-up filter technologies (particulate control devices, or PCDs) at a component size readily scaleable to commercial systems. The transport reactor train operating in gasification mode is shown schematically in Figure 2.2-1. A taglist of all major equipment in the process train and associated balance-of-plant is provided in Tables 2.2-1 and -2.

The transport reactor consists of a mixing zone, a riser, a disengager, a cyclone, a standpipe, a loop seal, a solids cooler, and two J-legs. The fuel, sorbent, and air are mixed together in the mixing zone, along with the solids from the standpipe and solids cooler J-legs. The mixing zone, located below the riser, has a slightly larger diameter compared to the top part of the riser. Provision is made to inject air at several different points along the riser to control the formation of NO_X during combustion mode of operation. The gas and solids move up the riser together, make two turns and enter the disengager. The disengager removes larger particles by gravity separation. The gas and remaining solids then move to the cyclone, which removes most of the particles not collected by the disengager. The gas then exits the transport reactor and goes to the primary gas cooler and the PCD for final particulate clean-up. The solids collected by the disengager and cyclone are recycled back to the reactor mixing zone through the standpipe and a J-leg. In the combustion mode of operation, the solids cooler controls the reactor temperature by generating steam and provides solids surge volume. A part of the solids stream from the standpipe flows through the solids cooler. The solids from the solids cooler then return to the bottom of the reactor mixing zone through another J-leg. The solids cooler is not used in gasification. The nominal transport reactor operating temperatures are 1,800 and 1,600°F for gasification and combustion modes, respectively. The reactor system is designed to have a maximum operation pressure of 294 psig, with a thermal capacity of about 21 million Btu/hr for combustion mode and 41 million Btu/hr for gasification mode.

For start-up purposes, a burner (BR0201) is provided at the reactor mixing zone. Liquefied propane gas (LPG) is used as start-up fuel. The fuel and sorbent are separately fed into the transport reactor through lock hoppers. Coal is ground to a nominal average particle diameter of 250 and 350 μm when the transport reactor is operated in gasification mode and combustion mode, respectively. Sorbent is ground to a nominal average particle diameter of 20 μm. Limestone or dolomitic sorbents are fed into the reactor for sulfur capture, thus eliminating the need for downstream facilities to reduce plant sulfur emissions. The gas leaves the transport reactor cyclone and goes to the primary gas cooler which cools the gas prior to entering the Siemens Westinghouse PCD barrier filter. The PCD uses ceramic or metal elements to filter out dust from the reactor. The filters remove almost all the dust from the gas stream to prevent erosion of a downstream gas turbine in a commercial plant. The operating temperature of the PCD is controlled both by the reactor temperature and by an upstream gas cooler. For test purposes, the gas from the transport reactor can flow through the gas cooler from zero to 100 percent. The PCD gas temperature can range from 700 to 1,600°F. The filter elements are back-pulsed by high-pressure nitrogen or air in a desired time interval or at a given maximum pressure difference across the elements. There is a secondary gas cooler after the filter vessel to cool the gas before discharging to the stack or thermal oxidizer (atmospheric syngas combustor). In a

commercial process, the gas from the PCD would be sent to a combustion gas turbine. The flue gas or fuel gas is sampled for on-line analysis after traveling through the secondary gas cooler.

After exiting the secondary gas cooler, the gas is then let down to about 2 psig through a pressure control valve. In gasification, the fuel gas is then sent to a thermal oxidizer to burn the gas and oxidize all reduced sulfur compounds (H_2S, COS, CS_2) and reduced nitrogen compounds (NH3, HCN). The thermal oxidizer uses propane as a supplemental fuel. In combustion, the thermal oxidizer can be bypassed and fired on propane to make startup steam. The gas from the thermal oxidizer goes to the baghouse and then to the stack.

The transport reactor produces both fine solids collected by the PCD and coarse solids extracted from the transport reactor standpipe. The two solids streams are cooled using screw coolers, reduced in pressure in lock hoppers, and then combined. The combustion solids (ash) are suitable for commercial use or landfill as produced. In gasification, any fuel sulfur captured by sorbent should be present as calcium sulfide (CaS). The gasification solids (char) are processed in the sulfator to oxidize the CaS to calcium sulfate ($CaSO_4$) and burn any residual carbon. The waste solids are then suitable for commercial use or disposal. Neither the sulfator nor the thermal oxidizer would be part of a commercial process. In a commercial process, the gasification solids could be burned to recover the solids heat value.

Table 2.2-1

Major Equipment in the Transport Reactor Train

TAG NAME	DESCRIPTION
BR0201	Reactor Start-up Burner
BR0401	Thermal Oxidizer
BR0602	Sulfator Start-up/PCD Preheat Burner
CO0201	Main Air Compressor
CO0401	Recycle Gas Booster Compressor
CO0601	Sulfator Air Compressor
CY0201	Primary Cyclone in the Reactor Loop
CY0207	Disengager in the Reactor Loop
CY0601	Sulfator Cyclone
DR0402	Steam Drum
DY0201	Feeder System Air Dryer
FD0206	Spent Solids Screw Cooler
FD0210	Coal Feeder System
FD0220	Sorbent Feeder System
FD0502	Fines Screw Cooler
FD0510	Spent Solids Transporter System
FD0520	Fines Transporter System
FD0530	Spent Solids Feeder System
FD0602	Sulfator Solids Screw Cooler
FD0610	Sulfator Sorbent Feeder System
FL0301	PCD — Siemens Westinghouse
FL0302	PCD — Combustion Power
FL0401	Compressor Intake Filter
HX0202	Primary Gas Cooler
HX0203	Combustor Heat Exchanger
HX0204	Transport Air Cooler
HX0402	Secondary Gas Cooler
HX0405	Compressor Feed Cooler
HX0601	Sulfator Heat Recovery Exchanger
ME0540	Heat Transfer Fluid System
RX0201	Transport Reactor
SI0602	Spent Solids Silo
SU0601	Sulfator

Table 2.2-2 (Page 1 of 3)

Major Equipment in the Balance-of-Plant

TAG NAME	DESCRIPTION
BO2920	Auxiliary Boiler
BO2921	Auxiliary Boiler – Superheater
CL2100	Cooling Tower
CO2201A-D	Service Air Compressor A-D
CO2202	Air-Cooled Service Air Compressor
CO2203	High-Pressure Air Compressor
CO2601A-C	Reciprocating N_2 Compressor A-C
CR0104	Coal and Sorbent Crusher
CV0100	Crushed Feed Conveyor
CV0101	Crushed Material Conveyor
DP2301	Baghouse Bypass Damper
DP2303	Inlet Damper on Dilution Air Blower
DP2304	Outlet Damper on Dilution Air Blower
DY2201A-D	Service Air Dryer A-D
DY2202	Air-Cooled Service Air Compressor Air Dryer
DY2203	High-Pressure Air Compressor Air Dryer
FD0104	MWK Coal Transport System
FD0111	MWK Coal Mill Feeder
FD0113	Sorbent Mill Feeder
FD0140	Coke Breeze and Bed Material Transport System
FD0154	MWK Limestone Transport System
FD0810	Ash Unloading System
FD0820	Baghouse Ash Transport System
FL0700	Baghouse
FN0700	Dilution Air Blower
HO0100	Reclaim Hopper
HO0105	Crushed Material Surge Hopper
HO0252	Coal Surge Hopper
HO0253	Sorbent Surge Hopper
HT2101	MWK Equipment Cooling Water Head Tank
HT2103	SCS Equipment Cooling Water Head Tank
HT0399	60-Ton Bridge Crane
HX2002	MWK Steam Condenser
HX2003	MWK Feed Water Heater

Table 2.2-2 (Page 2 of 3)

Major Equipment in the Balance-of-Plant

TAG NAME	DESCRIPTION
HX2004	MWK Subcooler
HX2103A	SCS Cooling Water Heat Exchanger
HX2103C	MWK Cooling Water Heat Exchanger
LF0300	Propane Vaporizer
MC3001-3017	MCCs for Various Equipment
ME0700	MWK Stack
ME0701	Flare
ME0814	Dry Ash Unloader for MWK Train
ML0111	Coal Mill for MWK Train
ML0113	Sorbent Mill for Both Trains
PG2600	Nitrogen Plant
PU2000A-B	MWK Feed Water Pump A-B
PU2100A-B	Raw Water Pump A-B
PU2101A-B	Service Water Pump A-B
PU2102A-B	Cooling Tower Make-Up Pump A-B
PU2103A-D	Circulating Water Pump A-D
PU2107	SCS Cooling Water Make-Up Pump
PU2109A-B	SCS Cooling Water Pump A-B
PU2111A-B	MWK Cooling Water Pump A-B
PU2300	Propane Pump
PU2301	Diesel Rolling Stock Pump
PU2302	Diesel Generator Transfer Pump
PU2303	Diesel Tank Sump Pump
PU2400	Fire Protection Jockey Pump
PU2401	Diesel Fire Water Pump #1
PU2402	Diesel Fire Water Pump #2
PU2504A-B	Waste Water Sump Pump A-B
PU2507	Coal and Limestone Storage Sump Pump
PU2700A-B	Demineralizer Forwarding Pump A-B

Table 2.2-2 (Page 3 of 3)

Major Equipment in the Balance-of-Plant

TAG NAME	DESCRIPTION
PU2920A-B	Auxiliary Boiler Feed Water Pump A-B
SB3001	125-V DC Station Battery
SB3002	UPS
SC0700	Baghouse Screw Conveyor
SG3000-3005	4,160-V, 480-V Switchgear Buses
SI0101	MWK Crushed Coal Storage Silo
SI0103	Crushed Sorbent Storage Silo
SI0111	MWK Pulverized Coal Storage Silo
SI0113	MWK Limestone Silo
SI0114	FW Limestone Silo
SI0810	Ash Silo
ST2601	N_2 Storage Tube Bank
TK2000	MWK Condensate Storage Tank
TK2001	FW Condensate Tank
TK2100	Raw Water Storage Tank
TK2300A-D	Propane Storage Tank A-D
TK2301	Diesel Storage Tank
TK2401	Fire Water Tank
XF3000A	230/4.16-kV Main Power Transformer
XF3001B-5B	4,160/480-V SS Transformer No. 1-5
XF3001G	480/120-V Miscellaneous Transformer
XF3010G	120/208 Distribution Transformer
XF3012G	UPS Isolation Transformer
VS2203	High-Pressure Air Receiver

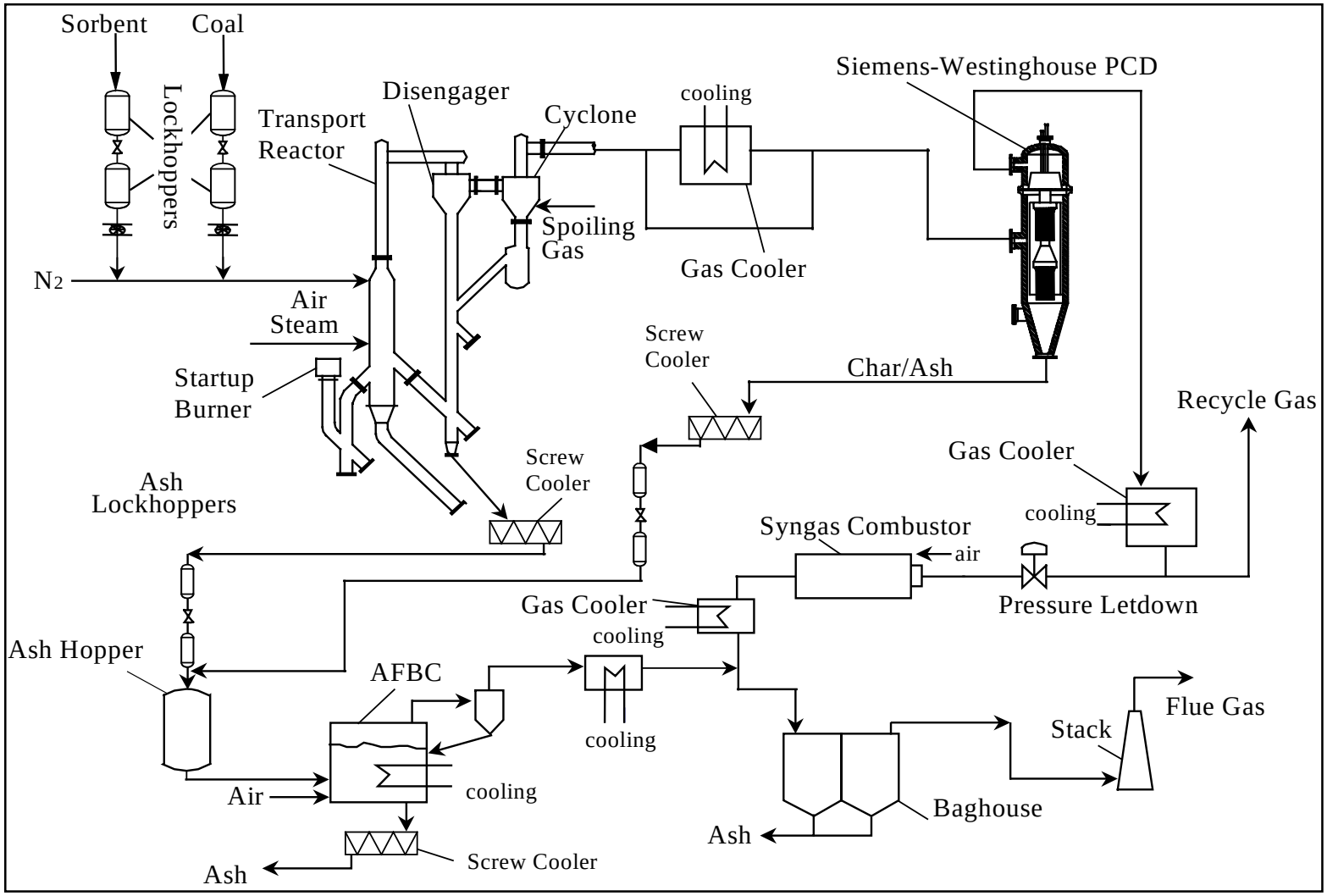

Figure 2.2-1 Flow Diagram of the Transport Reactor Train

2.3 SIEMENS WESTINGHOUSE PARTICULATE CONTROL DEVICE

Different PCDs will be evaluated on the transport reactor train. The first PCD that was commissioned in 1996, and has been used in all of the testing to date, was the filter system designed by Siemens Westinghouse. In this system, the dirty gas enters the PCD below the tubesheet, flows through the filter elements, and the ash collects on the outside of the filter. The clean gas passes from the plenum/filter element assembly through the plenum pipe to the outlet pipe. As the ash collects on the outside surface of the filter elements, the pressure drop across the filter system gradually increases. The filter cake is periodically dislodged by injecting a high-pressure gas pulse to the clean side of the filter elements. The cake then falls to the discharge hopper.

Until the first gasification run in late 1999, the transport reactor had been operated only in the combustion mode. Initially, high-pressure air was used as the pulse gas for the PCD, however, the pulse gas was changed to nitrogen early in 1997. The pulse gas was routed individually to the two-plenum/filter element assemblies via injection tubes mounted on the top head of the PCD vessel. The pulse duration was typically 0.1 to 0.5 seconds.

A sketch of the Siemens Westinghouse PCD is shown in Figure 2.3-1.

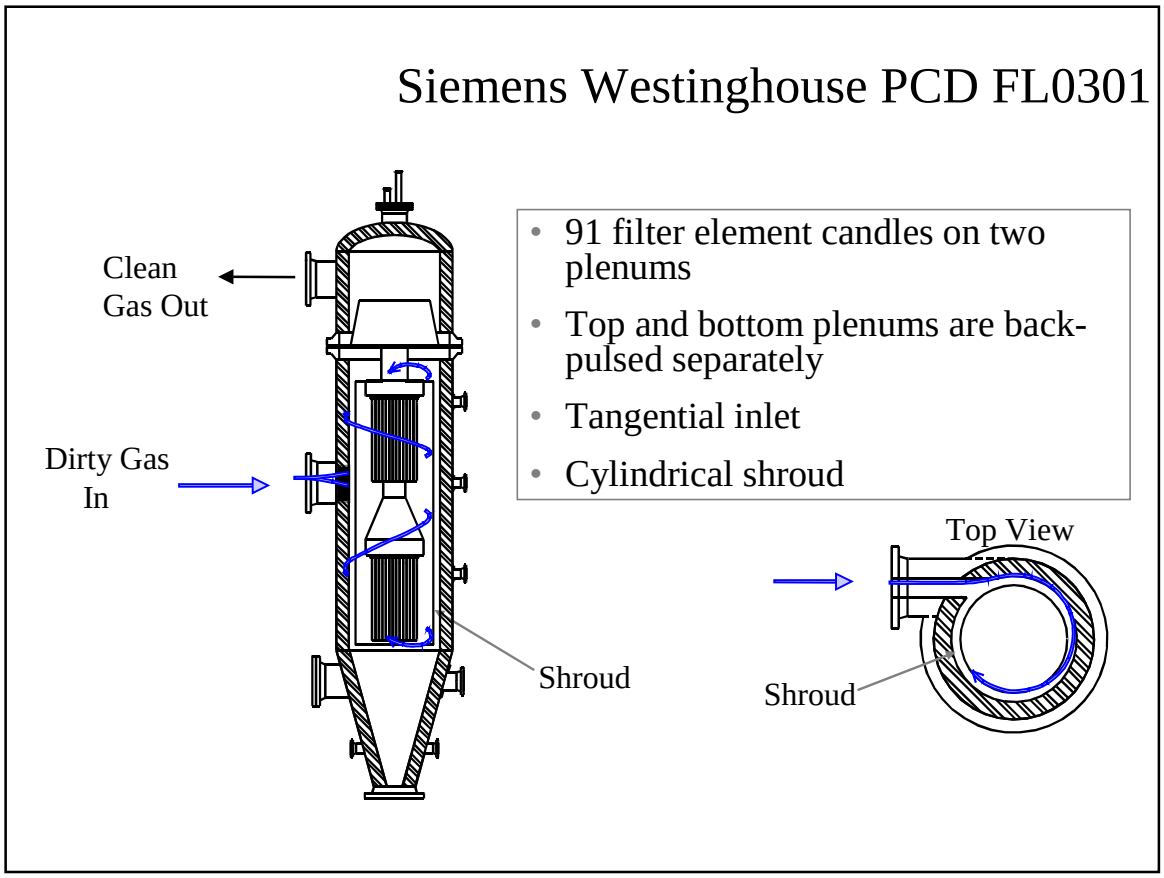

Figure 2.3-1 Siemens Westinghouse PCD

2.4 OPERATION STATUS

Commissioning activities began in September 1995 and proceeded in parallel with construction activities. Design and construction of the transport reactor and associated equipment was completed in early summer of 1996. All separate components and subsystems were fully operational by midsummer and commissioning work was focused on integration issues for the entire transport reactor train. The first coal fire in combustion mode of operation was achieved on August 18, 1996. A series of characterization tests was initiated to develop an understanding of reactor system operations. Test runs CCT1, CCT2, and CCT3 were completed by December 1996. Solids carryover from the reactor to the PCD was found to be excessive during these test runs. A number of startup and design problems associated with various equipment were successfully addressed.

During 1997 three additional sets of characterization test runs, CCT4, CCT5, and CCT6, and one major test campaign, TC01, were undertaken. TC01 focused on exposing the PCD filter elements to process gas for 1,000 hours at temperatures from 1,350 to 1,400°F and achieving stable reactor operations. An Alabama bituminous coal from the Calumet mine in the Mary Lee seam and Plum Run dolomite were used in these test runs.

Two test campaigns (TC02 and TC03) were successfully completed during 1998. TC02 was planned for reactor parametric testing to better quantify the effect of different variables on reactor and filter element operation. Test run TC02 was started on April 5, 1998, and completed on May 11, 1998. Based on TC02 observations, TC03 was planned for additional reactor parametric testing to better quantify the effect of different variables on reactor and PCD operation and to evaluate operation with an Eastern Kentucky bituminous coal and a Gregg Mine limestone from Florida. The third major test campaign, TC03, was performed from May 31, 1998, to August 10, 1998. Stable operations were demonstrated using the Eastern Kentucky coal and Plum Run dolomite, Bucyrus limestone, and Longview limestone during TC03. There were, however, circulation problems using the Eastern Kentucky coal and Florida Gregg Mine limestone because of deposits resulting from excessive fines (segregated) in the Eastern Kentucky feed. One additional test run, TC04, was started on October 14, 1999, but was prematurely ended due to a temperature excursion in the PCD during the initial heatup of the transport reactor system.

The final combustion test campaign (TC05) was started on January 10, 1999, in combustion mode of operation and was completed May 2, 1999. During TC05, steady state operations with a variety of fuel and sorbent feed materials was demonstrated (including petroleum coke with two different sorbents) and reactor parametric testing with different feed combinations was performed. Overall, TC05 was a successful test run with 10 different feed combinations tested.

Conversion of the transport reactor train to gasification mode of operations was performed from May to September 1999. The first gasification test run, GCT1, was planned as a 250-hour test run to commission the transport reactor train in gasification mode of operation and to characterize the limits of operational parameter variations. GCT1 was started on September 9, 1999, with the first part completed on September 15, 1999 (GCT1A). The

second part of GCT1 was started on December 7, 1999, and completed on December 15, 1999 (GCT1B through D). This test run provided the data necessary for preliminary analysis of reactor operations and for identification of necessary modifications to improve equipment and process performance. Five different feed combinations of coal and sorbent were tested to gain a better understanding of the reactor solids collection system efficiency.

GCT2, planned as a 250-hour characterization test run, was started on April 10, 2000, and completed on April 27, 2000. Additional data was taken to analyze the effect of different operating conditions on reactor performance and operability. A blend of several Powder River Basin (PRB) coals was used with Longview limestone from Alabama. In the outage following GCT2, the transport reactor underwent a major modification to improve the operation and performance of the reactor solids collection system. The most fundamental change was the addition of the loop seal underneath the primary cyclone.

GCT3 was planned as a 250-hour characterization with the primary objective to commission the loop seal. A hot-solids circulation test was started on December 1, 2000, and completed December 15, 2000. After a 1-month outage to address maintenance issues with the main air compressor, GCT3 was continued. The second part of GCT3 (the actual gasification portion) was started on January 20, 2001, and completed on February 1, 2001. During this test portion a blend of several PRB coals was used with Bucyrus limestone from Ohio. The loop seal performed well, needing little attention and promoting much higher solids-circulation rates, higher coal-feed rates that resulted in lower relative solids loading to the PCD, and higher char retention in the reactor. Figure 2.4-1 shows a summary of operating test hours achieved with the transport reactor at the PSDF.

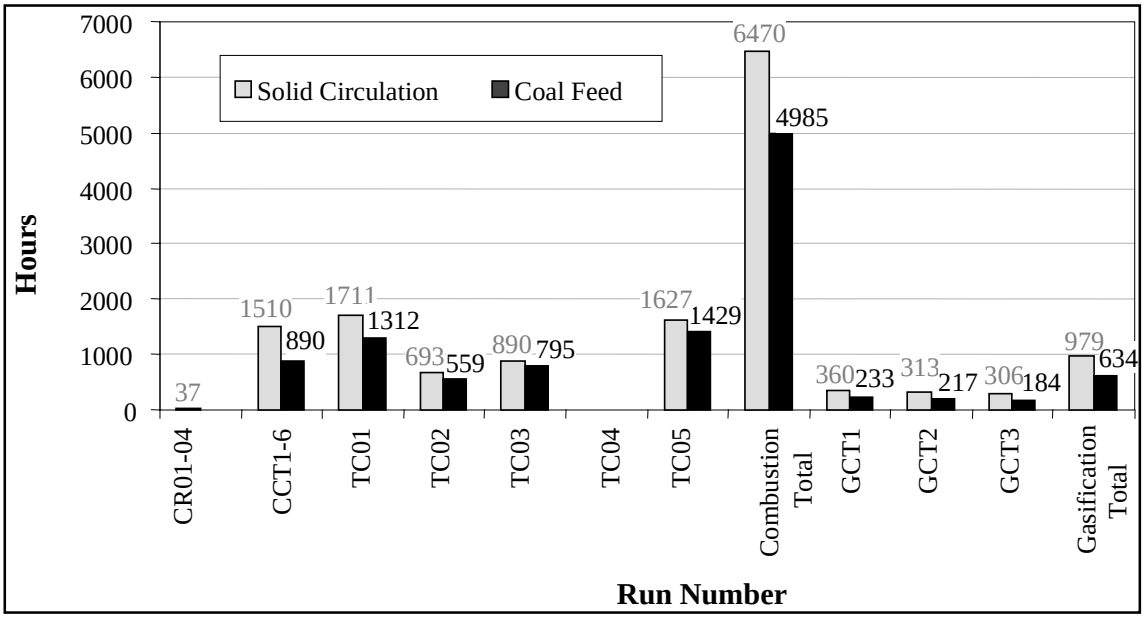

Figure 2.4-1 Operating Hours Summary for the Transport Reactor Train

3.0 PARTICLE FILTER SYSTEM

3.1 GCT3 RUN OVERVIEW

The GCT3 gasification run was the third gasification run for the Halliburton KBR transport reactor. GCT3 was divided into two components: 1) the sand circulation run and 2) the gasification run. The sand circulation run portion of GCT3 began on December 1, 2000, with sand addition occurring from December 13 to December 15, 2000. Major modifications were made to the transport reactor between the GCT2 and GCT3 gasification runs. The purpose of the sand circulation run was to cure new refractory lined pipes added as a result of these modifications. One ceramic filter failed during the sand circulation and ended the run. As a result, the failed filter as well as seven other nearby filters were replaced before the startup of the gasification run.

The second component of GCT3 was the gasification run, from January 20 to February 1, 2001. The particulate control device (PCD) performed well during the GCT3 gasification run. This was mainly due to lessons learned during the first two gasification runs. The following actions were taken prior to the GCT3 run: 1) all filter elements were installed with the new filter holder designed by PSDF personnel, 2) a new fail-safe gasket developed by Siemens Westinghouse was installed, 3) all instrument wires were directed through a nozzle on the vessel wall rather than through the plenum, and 4) all new iron aluminide and monolithic silicon carbide filters were installed. With these changes the PCD outlet loading did not exceed 1 ppmw. Major achievements were:

1. PCD successfully operated for about 184 on-coal hours during the GCT3 test run. This is based on low outlet loading and no filter failures.

2. Continued testing iron aluminide filters specifically designed for gasification environments. Iron aluminide filters were tested during the combustion test runs as well as GCT1A and performed well. Visual inspection of these filters after shutdown showed that they were intact. The char cake was thin and relatively uniform after the clean shutdown.

3. Continued testing monolithic silicon carbide filters from Pall and Schumacher, which performed well without any mechanical failures. The visual inspection showed that the filters were intact. The char cake was thin and uniform after the clean shutdown.

4. The new filter holders developed by PSDF personnel performed well. The outlet loading never exceeded 1 ppmw throughout the run.

5. SRI successfully measured inlet and outlet particulate loading during the run. Char samples from the inlet sampling and char cake were analyzed and tested.

6. The ash removal system (FD0502/FD0520) worked very well in GCT3. Due to the lower inlet particulate loading to the PCD, solid accumulation in the cone of the PCD

was not a problem. However, ceramic candle pieces plugged the discharge line of the dense-phase vessel, becoming one reason for ending the run.

7. The post-run PCD inspection showed that the shroud and liner sections were relatively clean. The plenums and tubesheet were also clean when compared to previous gasification runs.

8. The 10 new Siemens Westinghouse fail-safes that were tested in GCT2 were installed for the GCT3 gasification run. After exposure in GCT3, two fail-safes were flow tested and weighed. The fail-safes will be continuously tested in the following runs and their performance will be further evaluated.

The GCT3 test run was the first gasification test run in which the PCD operated with the new loop seal modification in the transport reactor. The purpose of the modification was to increase the carbon conversion in the reactor. It was predicted that the reactor modification would decrease particle size to the PCD and increase the pressure drop across the PCD. As predicted, the pressure drop in the PCD was higher during the GCT3 gasification run than in the GCT2 gasification run. However, the reason for the higher pressure drop was not limited to the reduced particle size. During the GCT3 test run the coal feeder tripped many times, exacerbating the higher pressure drop across the PCD. During these coal feeder trips the temperature dropped below 1,600°F. Below this temperature the reactor was producing tars. It was suspected that tar condensation in the PCD made the dustcake sticky. As a result, the baseline pressure drop increased.

After the GCT3 test run, the PCD plenum was pulled out of the PCD vessel for inspection. During inspection, char bridging on the bottom plenum was noticed. It was suspected that tar condensation was a factor in causing the char bridging. To achieve stable operation in the PCD, the coal feeder trips must be eliminated or minimized.

The temperature in the PCD was lower during GCT3 than in GCT2. The temperature in the PCD ranged from 600 to 950°F. During the steady-state periods in GCT3 the temperature in the PCD was below 800°F. However, there was one major thermal transient in the PCD. The thermal transient was the result of a coal feeder trip, which allowed oxygen breakthrough to the PCD. During the thermal transient the filter temperatures increased approximately 300°F in one minute. Fortunately, there were no filter failures in this event.

3.2 GCT3 RUN REPORT

3.2.1 Introduction

The GCT3 run was divided into two components: 1) the sand circulation run and 2) the gasification run. The purpose of the sand circulation run was to cure the new refractory lined additions to the transport reactor. The sand circulation run was December 1 through December 15, 2000. On December 15, Southern Research Institute (SRI) collected an outlet sample from the PCD. The outlet loading measured was approximately 17 ppmw. At around 17:00, ceramic candle pieces were found in the fine solids removal system. It was determined at this point to end the run. The filter vessel was disassembled and inspected. The inspection revealed that a Schumacher TF20 filter had failed. No reason has been reported for this filter failure and no process upsets have been linked to this filter failure. The failed filter element, as well as seven nearby filters, were replaced during the outage between the sand circulation and gasification runs.

The GCT3 gasification run started on January 20. From a PCD standpoint the GCT3 gasification run was considered a successful run. This statement is based on the fact that the PCD did not experience any filter failures with coal feeding and the outlet loading from the PCD was below 1 ppmw. However, the PCD did experience several significant challenges throughout the GCT3 gasification run, including high pressure drop across the filter vessel, a major thermal transient event, ash removal system plugging, and char bridging in the filter vessel.

The low outlet loading was attributed to lessons learned during the earlier gasification runs. During GCT1A through GCT1B, C, and D gasification runs, high outlet loading was attributed to several factors including char penetration through filters, leakage around the sealing gaskets, and leakage through instrumentation fittings. Before the GCT2 gasification run the following changes or modifications were made to the PCD:

- Removed filters that did not perform well in previous gasification runs or needed further evaluation, therefore leaving only monolithic SiC filters.
- A modified filter holder designed by PSDF personnel was used to support and seal the filters to the tubesheet.
- All instrumentation fittings were routed from the dirty side of the PCD directly to the atmosphere through a nitrogen-purged flange on the pressure vessel rather than from the dirty side of the tubesheet to the clean side.

The outlet loading during the GCT2 gasification run was less than 1 ppmw. Therefore, all these changes were implemented for the GCT3 gasification run. Also, prior to the GCT3 gasification test run iron aluminide filters were installed. Figure 3.2-1 shows the filter layout for the GCT3 test run.

As expected, the pressure drop across the PCD was higher during GCT3 than GCT2. The higher pressure drop was attributed to two reasons: 1) a transport reactor modification and 2) coal feeder reliability problems. Between the GCT2 gasification run and the GCT3 gasification run the transport reactor underwent a major modification. This modification increased the carbon conversion in the reactor, thereby increasing the performance of the gasifier. As a result, the particle characteristics were altered, which increased the drag of the particles carried over to the PCD (See Section 3.4). Another reason suspected to have contributed to the high pressure drop was low reliability of the coal feeder. During the GCT3 gasification run the coal feeder tripped on many occasions. This resulted in the reactor temperature dropping into a temperature regime in which tar was produced. If this tar condensed in the PCD the result would be a sticky filter cake, which would increase the baseline pressure drop. Despite the higher pressure drop in the PCD vessel the filters and the filter sealing arrangement did not leak.

In the GCT3 gasification run the PCD experienced a thermal transient event during one of the coal feeder trips. At this time fuel was not being injected into the reactor and the air compressor was not shut off promptly, allowing an oxygen breakthrough to the PCD. Char cake on the filters and syngas in the PCD combusted causing a temperature increase of approximately 300°F in 1 minute.

The fine ash removal system tripped at the end of the run due to ceramic filter pieces plugging the outlet pipe of the dense-phase transport vessel. Originally, it was believed that one of the monolithic SiC filters had failed, however, during inspection it was discovered that none of the filters had failed. Therefore, it was suspected that pieces from a past filter failure had worked their way through the fine ash removal system. Throughout the entire run the fine ash removal system performed well. Other than minor seal leaks, the screw cooler operated without any problems. Also, the lock vessel system operated without any mechanical failures. Operationally, the lock vessel system required significant attention because a reliable level probe has not been found. Therefore, a timer was necessary to control the lock vessel cycle. The lock vessel cycle timer was adjusted often to keep solids from backing up into the PCD cone.

Finally, during the inspection of the PCD, char bridging between the filter elements was discovered. It was suspected that the char bridging was a result of the filter support brackets and possibly tar condensation in the filter vessel. Prior to the GCT3 gasification run all the 1.5-meter iron aluminide filters were supported on the mid-level weld joint (See Figure 3.2-1). These brackets were thought to have provided an origination point for the char bridging. Also, tar condensation in the PCD was suspected to cause the char cake to become sticky, forming an adherent coating which may have aided in char bridging.

3.2.2 Test Objectives

The primary test objectives for the GCT3 run included:

- Continue testing new filter holder design. Based on the performance of the new filter holder design during GCT2, it was decided to continue testing the new design.

- Evaluate PCD performance after the transport reactor modification. During the outage between GCT2 and GCT3 the transport reactor underwent a major modification.

- Test Pall iron aluminide filter performance. The iron aluminide filters were specifically designed for reducing environments. Therefore, 57 of these filters were installed.

- Evaluate Siemens Westinghouse fail-safe. Ten prototype fail-safes designed by Siemens Westinghouse were installed in the PCD. Each prototype fail-safe contains metal fibers. These fail-safes will be evaluated by taking weight and flow measurements following each run.

3.2.3 Run Summary

The GCT3 gasification run began with the PCD warm-up sequence on January 20, 2001. The purpose of this sequence was to warm up the PCD to 200°F and hold for 1 hour. In order to heat up the PCD, cold nitrogen was passed through the primary heat exchanger where the nitrogen was heated to approximately 270°F. At this time, the back-pulse system was started. The back-pulse timer and pressure were set at 30 minutes and 285 psig, respectively. The system pressure was increased to 90 from 40 psig at 14:40 and the back-pulse pressure was increased to 330 from 285 psig. Once the PCD temperature approached a plateau, the process was lined up for the start-up burner. At 17:00 the main air compressor was started. Shortly after, the start-up burner was lit. During the next 11 hours the PCD temperature was increased to about 500°F.

Table 3.2-1 provides a brief description of the major events during the GCT3 gasification run that can be used in conjunction with Figures 3.2-2 through -7. Also, Table 3.2-2 outlines the major run statistics for the GCT3 gasification run.

A loss-of-propane flow at 06:05 on January 21, 2001, caused the start-up burner to trip. As a result, the PCD temperature began to decrease. Over the next 5 hours the start-up burner was started and tripped. The start-up burner was successfully started at around 13:45 and, as a result, the PCD temperature, pressure drop, and face velocity began to increase.

The system pressure was increased on three different occasions on January 22, 2001. The first increase was at 00:00 when the system pressure was increased to 90 psig. The second increase was at 07:30 when the system pressure was increased to 95 psig. Finally, the system pressure was increased to 110 psig. In preparation for coal feed, the back-pulse pressure and timer were changed to 500 psig and 5 minutes, respectively. At 15:45 the coal feeder was started, but was immediately shut down due to a plug in the coal feed to the reactor mixing zone. At this time the back-pulse pressure and timer were changed to 350 psig and 30 minutes, respectively. Once the exit line was unplugged and the reactor was heated up, the coal feeder was started (at 21:50). At this time the back-pulse pressure and timer were changed to 500 psig and 5 minutes. After the coal feed was started the PCD temperature, pressure drop, and face velocity began to increase. At 22:08 the system pressure was increased to 180 psig to help lower the pressure drop in the PCD.

On January 23, 2001, at 01:00 the spent solids conveying system (FD0530) was experiencing trouble conveying solids to the sulfator. To prevent solids from building up in the spent solids conveying system, the coal-feed rate was decreased. An attempt was made to force the FD0530 system to convey solids to the sulfator while the process was online. Eventually, it was determined that the solids were plugged in the cone of the FD0530 vessel. At 08:40 the coal feeder was shut down. Also, the fine ash removal (FD0502/FD0520) system was shut down. This allowed maintenance personnel to remove the spool piece from between the spent solids surge bin and lock vessel to unplug the system. At 19:50 the start-up burner was lit to maintain the reactor temperature at around 1,000°F, and subsequently the PCD temperature began to increase.

On January 24, 2001, at 04:00 the system pressure was decreased to 65 psig to help stabilize the reactor burner flame intensity and the back-pulse pressure was decreased to 310 psig. By 05:26 the reactor burner flame had stabilized; therefore, the reactor pressure was increased to 80 psig. At this time the back-pulse pressure was increased to 320 psig. At 10:15 the system and back-pulse pressure were increased to 90 and 330 psig, respectively. At 09:00 a leak on the nondrive end of the screw cooler (FD0502) was detected. The packing follower bolts were tightened and the leak was stopped. By 15:25 the spent solids system was back online. At this time the fine ash removal system was started up to remove all the solids that were carried over to the PCD. At 18:20 the coal feeder was started. At this time the pressure drop, face velocity, and temperature increased in the PCD. Over the next 5 hours the system pressure was increased incrementally to help decrease the pressure drop across the PCD. The system pressure range over this time span was from 90 to 210 psig. Shortly after the coal feeder was started the start-up burner was tripped. At 21:00 the back-pulse pressure was increased to 570 psig and at 22:00 to 580 psig. At 23:00 the coal feeder tripped. During this time the main air compressor unloaded and the PCD temperatures began to drop. The coal feeder and main air compressor were immediately started back up.

On January 25, 2001, at 00:23 the main air compressor and the coal feeder tripped. As a result the PCD temperatures began to decrease. By 00:53 the main air compressor was started and by 01:15 the coal feeder was started. The system pressure was increased to 210 psig on January 25, 2001, at 04:30. At 11:15 the coal feeder was shut down because coal was not being transferred from the surge bin to the lock vessel. To make sure oxygen did not break through to the PCD, the main air compressor was shut down. During this time the system pressure was decreased to 170 psig. At 11:45 the main air compressor and the coal feeder were restarted. At 15:20 the system pressure was increased to 220 psig to help decrease the pressure drop in the PCD.

On January 26, 2001, at 02:11 the system pressure was increased to 235 psig. At 03:30 the coal feeder tripped due to solids packing in the lock vessel. Once the solids began to flow out of the lock vessel into the feeder vessel the coal feeder was restarted. After the coal feeder was started, the pressure drop, face velocity, and temperature began to increase in the PCD. At 05:20 the process and back-pulse pressures were increased to 225 and 620 psig, respectively. At 23:08 the coal feeder speed was reduced because coal was not transferring from the surge bin to the lock vessel. This action was taken to maintain a coal inventory in the coal feeder vessel; during this time the air flow rate was decreased.

On January 27, 2001, at 00:10 the solids flow between the surge bin and the lock vessel was regained and the coal feeder speed was increased. At 21:08 the coal feeder lock vessel became packed with solids. In order to maintain the coal inventory in the feeder vessel the coal-feed rate was reduced. Also, the airflow rate was decreased. By 21:30 the coal feeder lock vessel was unpacked and the coal feeder speed was increased.

On January 28, 2001, at 08:30 the coal feeder tripped. Once again, the main air compressor was tripped to prevent oxygen breakthrough to the PCD. By 08:45 the coal feeder and main air compressor were back online. At 09:30 the coal feeder tripped, but was restarted by 10:00. It was suspected that the coal size was too fine, thereby exacerbating the packing problems in the lock vessels. Therefore, it was decided to increase the coal grind size from the mills.

On January 29, 2001, at 01:50 the coal feeder tripped. Again, coal was not dropping into the lock vessel from the surge bin. During this time oxygen broke through to the PCD and caused a temperature increase on the filters of approximately 300°F in 1 minute. At 06:30 the coal feeder was experiencing trouble transferring coal from the surge bin to the lock vessel; therefore, the coal-feed rate was reduced. At 12:50 a gasket leak was detected on the discharge line of the fine ash removal system, which was then stopped in order to replace the gasket. The gasket was replaced and the system was restarted by 17:40. The system and back-pulse pressures were decreased to 200 and 610 psig, respectively, at 19:09. At 20:07 the coal feeder tripped but was restarted by 20:20. At 21:30 the system pressure was decreased to 200 psig.

On January 30, 2001, at 00:30 the coal feeder continued to experience problems. The dispense vessel level probe was not showing covered at appropriate times. This indicated that solids were not falling out of the lock vessel into the dispense vessel. The coal-feed rate was decreased, and to prevent a thermal event in the PCD the airflow rate was reduced. At 01:30 the back-pulse pressure was decreased to 590 psig. At 02:30 the system and back-pulse pressures were increased to 220 and 610 psig, respectively. At 03:30 the system and back-pulse pressures were increased to 225 and 620 psig, respectively. At 13:18 the back-pulse timer was changed to 10 from 5 minutes; at 18:18 the back-pulse timer was changed to 15 from 10 minutes; and at 19:51 the back-pulse timer was changed to 20 from 15 minutes. At 20:46 the coal feeder experienced problems with the transfer of solids to the dispense vessel.

On January 31, 2001, at 01:10 the coal feeder experienced trouble transferring coal to the dispense vessel from the lock vessel. At 08:15 the FD0210 baghouse was leaking dust to the atmospheric vent on the ninth floor. At 22:48 the coal feeder tripped when operations attempted to fluff the lock vessel. The coal feeder was placed back online at 23:54.

On February 1, 2001, at 00:52 the coal feeder tripped. By 00:56 the coal feeder was back online. At 01:00 the top spheri-valve on the lock vessel failed to close causing the coal feeder to trip. One of the baghouse filters fell into the surge bin and blocked the valves from closing, so maintenance personnel were called in to fix the valve. At 02:45 the start-up burner was lit. At 03:00 the fine ash removal system tripped. The outlet line of the discharge vessel was plugged with ceramic candle pieces found in the discharge vessel exit line. It was believed that one of the filters had failed. Therefore, based on the problems with the coal feeder and the fine ash removal system, the decision was made to stop the run.

3.2.4 GCT3 Data Analysis

One of the objectives stated in Section 3.2.2 is to evaluate the PCD performance after modifications were made to the transport reactor between GCT2 and GCT3. During the outage, the transport reactor recycle loop was modified to improve carbon retention, and a larger motor was installed on the coal feeder to increase the coal-feed rate. The net effect of these changes on PCD performance was difficult to predict in advance because there could be simultaneous changes in particle mass loading, particle size, dust cake drag, and other particle properties. This section describes how the modifications affected PCD pressure drop. In Section 3.6, the pressure drop effects are related to the changes in particle properties and are reported there in more detail.

3.2.4.1 Gas Flow Analysis

In comparing PCD performance between two test programs, it is important to ensure that changes in face velocity, temperature, and pressure do not bias comparisons of pressure drops. The face velocities during GCT2 and GCT3 are shown in Figures 3.2-8 and -9. The horizontal arrows on the graphs mark the periods of stable operation that were used for analysis. Comparison of the face velocities recorded during the marked time periods shows that GCT2 and GCT3 were conducted over a similar range of face velocities. Despite the similarity of the face velocities, Figures 3.2-10 and -11 show that the gas mass-flow rate through the PCD was higher in GCT3 than during GCT2. The higher mass-flow rate would be related to the increased coal-feed rate during GCT3. Since the GCT2 and GCT3 tests were run over a similar range of face velocities, the difference in mass-flow rates must have been compensated for by differences in gas temperature and pressure. As shown in Figures 3.2-12 and -13, the PCD gas temperature during GCT2 varied between 850 and 950°F, while the PCD gas temperature during GCT3 remained below 800°F for most of the run. During much of GCT3 the PCD pressure was about 230 psig, while gas pressure varied from 200 to 230 psig in GCT2 (see Figures 3.2-14 and -15). Because of the combined effects of the temperature and pressure differences, there was little difference between the GCT2 and GCT3 face velocities, even though there was a significant difference in gas mass-flow rates.

3.2.4.2 PCD Pressure Drop Analysis

To prevent the changes in gas flow, temperature, and pressure from affecting the analysis of PCD performance, the pressure drop data from both tests were normalized to a temperature of 850°F and a filter face velocity of 3.5 ft/min. Figure 3.2-16 shows the normalized peak and baseline pressure drops recorded during GCT2. During the stable operating period marked on Figure 3.2-16 the baseline pressure drop varied from 60 to 75 inWC. The peak pressure drop during the same time period varied from 75 to 180 inWC.

The normalized peak and baseline pressure drops during GCT3 are shown in Figure 3.2-17. During the stable operating period marked on this figure the baseline pressure drop varied from 60 to 140 inWC and the peak pressure drop ranged between 140 and 350 inWC. When Figures 3.2-16 and -17 are compared, it is apparent that there were major pressure drop differences between the two runs. The rest of this section will address some of the major differences between GCT2 and GCT3.

Tables 3.2-3 and -4 show the inlet particulate loadings to the PCD during the two runs. On average, the loading to the PCD was lower during GCT3 than during GCT2, even though the coal-feed rate to the reactor was 20 percent higher in GCT3 than in GCT2. Figures 3.2-18 and -19 show the coal-feed rate for periods of steady-state operation during each run. The highest coal-feed rate during GCT2 was approximately 4,300 lb/hr, while during GCT3 it was about 1,000 lb/hr higher. Despite the higher coal-feed rates during GCT3, the solids return loop, disengager and cyclone dip leg seal modifications reduced the loading to the PCD.

Even though the inlet loading to the PCD was lower, the peak pressure drop during GCT3 was much higher than the peak pressure drop during GCT2. During both runs, the back-pulse time interval was changed on several different occasions (see Figures 3.2-20 and -21). To account for the effect of the increased back-pulse time interval, the normalized transient pressure drop rise was divided by the back-pulse time interval and plotted for both runs, as shown in Figures 3.2-22 and -23, as the rate of pressure drop rise. When comparing these figures it is apparent that the rate of pressure drop rise was substantially higher during GCT3 than during GCT2. Again, this result was contrary to what would be expected from the differences in mass loadings alone, but it was not surprising given the other potential changes in particle size, drag, and other particle properties.

From the differences in the rate of pressure drop rise discussed above, it can be concluded that the drag of the char particles must have increased between the two runs. Based on the drag measurements reported in Section 3.6, the transient dustcake drags for GCT2 and GCT3 were 53 and 129 inWC/(ft/min)/(lb/ft^2), respectively. This difference in normalized drag is sufficient to account for the increased transient pressure drop observed during GCT3, as explained in more detail in .

Like the transient pressure drop, the baseline pressure drop after cleaning was also significantly higher during GCT3, consistent with the drag values measured for the transient dust. Following the completion of the run, the PCD was disassembled and the residual dustcake examined. Unfortunately, because of repeated back-pulsing after shutdown, very little of the residual dustcake remained, and the areal loading was not believed to be representative of normal operation. This uncertainty in areal loading made it difficult to evaluate the drag of the residual dustcake, as discussed in Section 3.6.

As mentioned in Section 3.2, there were many process upsets during GCT3 as a result of coal feeder problems. These coal feeder problems periodically caused the reactor temperature to drop to a level where tars could no longer be cracked. The tars that were released from the reactor during these episodes could be deposited on char particles, thereby making them sticky. The tars could also be deposited within the PCD dustcake and, therefore, contribute to the formation of bridged deposits within the PCD (see Section 3.3). Alteration of the residual dustcake by tar deposition and formation of bridged deposits can lead to increased baseline pressure drop. The effect of tar deposition on dustcake drag and the potential effect of bridged deposits on filter face velocity are discussed in more detail in Section 3.6.

3.2.4.3 Summary of PCD Operation

To summarize, the changes to the transport reactor recycle loop produced fundamental changes in the char particles sent to the PCD. These changes resulted in an increased peak and baseline pressure drop during GCT3. The increased pressure drop in the PCD was attributed to the increased drag of the solid particles and possibly tar condensation in the PCD during coal feeder upsets, which may have contributed to bridging.

Table 3.2-1
(Page 1 of 2)

GCT3 Major Events for January 20, 2001, Through February 2, 2001
(See Figures 3.3-2 through -7)

Event	Description	Date at Time
A	System Pressure Increased to 40 psig	01/20/01 at 00:50
B	PCD Warm-up Sequence Started	01/20/01 at 06:45
C	System Pressure Increased to 90 psig	01/20/01 at 14:40
D	Main Air Compressor Started	01/20/01 at 17:00
E	Start-up Burner Lit	01/20/01 at 18:30
F	System Pressure Decreased to 70 psig	01/20/01 at 22:00
G	Start-up Burner Tripped	01/21/01 at 06:05
H	Start-up Burner Lit	01/21/01 at 08:30
I	Start-up Burner Tripped	01/21/01 at 10:00
J	Start-up Burner Lit	01/21/01 at 13:45
K	System Pressure Increased to 90 psig	01/22/01 at 00:00
L	System Pressure Increased to 95 psig	01/22/01 at 07:30
M	System Pressure Increased to 110 psig	01/22/01 at 14:50
N	Coal Feeder Started	01/22/01 at 15:45
O	Coal Feeder Started	01/22/01 at 21:50
P	System Pressure Increased to 180 psig	01/22/01 at 22:08
Q	Coal-Feed Rate Decreased	01/23/01 at 01:00
R	System Pressure Decreased to 90 psig	01/23/01 at 07:50
S	Start-up Burner Lit	01/23/01 at 19:50
T	System Pressure Decreased to 75 psig	01/23/01 at 21:00
U	Back-Pulse Timer Changed to 15 Minutes	01/23/01 at 23:00
V	System Pressure Decreased to 65 psig	01/24/01 at 04:00
W	System Pressure Increased to 80 psig	01/24/01 at 06:05
X	System Pressure Increased to 90 psig	01/24/01 at 10:15
Y	Coal Feeder Started	01/24/01 at 18:20
Z	Back-Pulse Pressure Increased to 570 psig	01/24/01 at 21:00

Table 3.2-1
(Page 2 of 2)

AA	Back-Pulse Pressure Increased to 580 psig	01/24/01 at 22:00
BB	Coal Feeder Tripped	01/24/01 at 22:50
CC	Coal Feeder Started	01/24/01 at 23:00
DD	Main Air Compressor Tripped	01/25/01 at 00:23
EE	Coal Feeder Stopped	01/25/01 at 11:15
FF	Main Air Compressor Started	01/25/01 at 11:45
GG	System Pressure Increased to 220 psig	01/25/01 at 15:20
HH	System Pressure Increased to 235 psig	01/26/01 at 02:11
II	Coal Feeder Tripped	01/26/01 at 03:30
JJ	Coal Feeder Started	01/26/01 at 04:30
KK	System Pressure Increased to 225 psig	01/26/01 at 05:20
LL	Reduced Coal Feeder Speed	01/26/01 at 23:08
MM	Increased Coal Feeder Speed	01/27/01at 00:10
NN	Coal Feeder Tripped	01/28/01 at 08:30
OO	Coal Feeder Tripped	01/28/01 at 09:30
PP	System Pressure Decreased to 200 psig	01/29/01 at 19:09
QQ	Back-Pulse Pressure Decreased to 590 psig	01/30/01 at 01:30
RR	System Pressure Increased to 220 psig	01/30/01 at 02:30
SS	Back-Pulse Pressure Increased to 620 psig	01/30/01 at 03:30
TT	Coal Feeder Tripped	02/01/01 at 01:30
UU	Run Ended	02/01/01 at 06:00

Table 3.2-2

GCT3 Run Statistics
January 20 Through February 1, 2000

Start Time:	01/20/00 00:50
End Time:	02/01/00 06:00
Coal Type:	Powder River Basin
Hours on Coal:	Approximately 184 hr
Sorbent Type:	Ohio Limestone
Number of Filter Elements:	90
Filter Element Layout No.:	18 (Figure 3.2-1)
Filtration Area:	261.3 ft^2 (24.3 m^2)
Pulse Valve Open Time:	0.2 sec
Pulse Time Trigger:	5 to 30 min
Pulse Pressure:	350 to 620 psig
Pulse DP Trigger:	250 inH_20

Table 3.2-3

GCT2 PCD Inlet Loading

Date	Time	Inlet Loading (ppmw)	Gas Flow (lb/hr)	Solids Loading (lb/hr)
4/17/00	10:00	34,000	24,981	849
4/19/00	10:00	31,100	21,607	672
4/20/00	13:35	31,000	22,653	702
4/21/00	08:21	28,300	21,628	612
4/22/00	10:10	25,700	18,264	469
4/24/00	12:35	29,600	21,506	637
4/25/00	10:07	30,900	21,204	655

Table 3.2-4

GCT3 PCD Inlet Loading

Date	Time	Inlet Loading (ppmw)	Gas Flow (lb/hr)	Solids Loading (lb/hr)
1/25/01	10:45	11,000	23,620	260
1/26/01	09:30	25,900	26,779	694
1/27/01	08:25	20,700	24,972	517
1/29/01	10:30	19,300	23,371	451
1/30/01	09:35	28,700	25,241	724
1/31/01	09:27	15,500	25,355	393

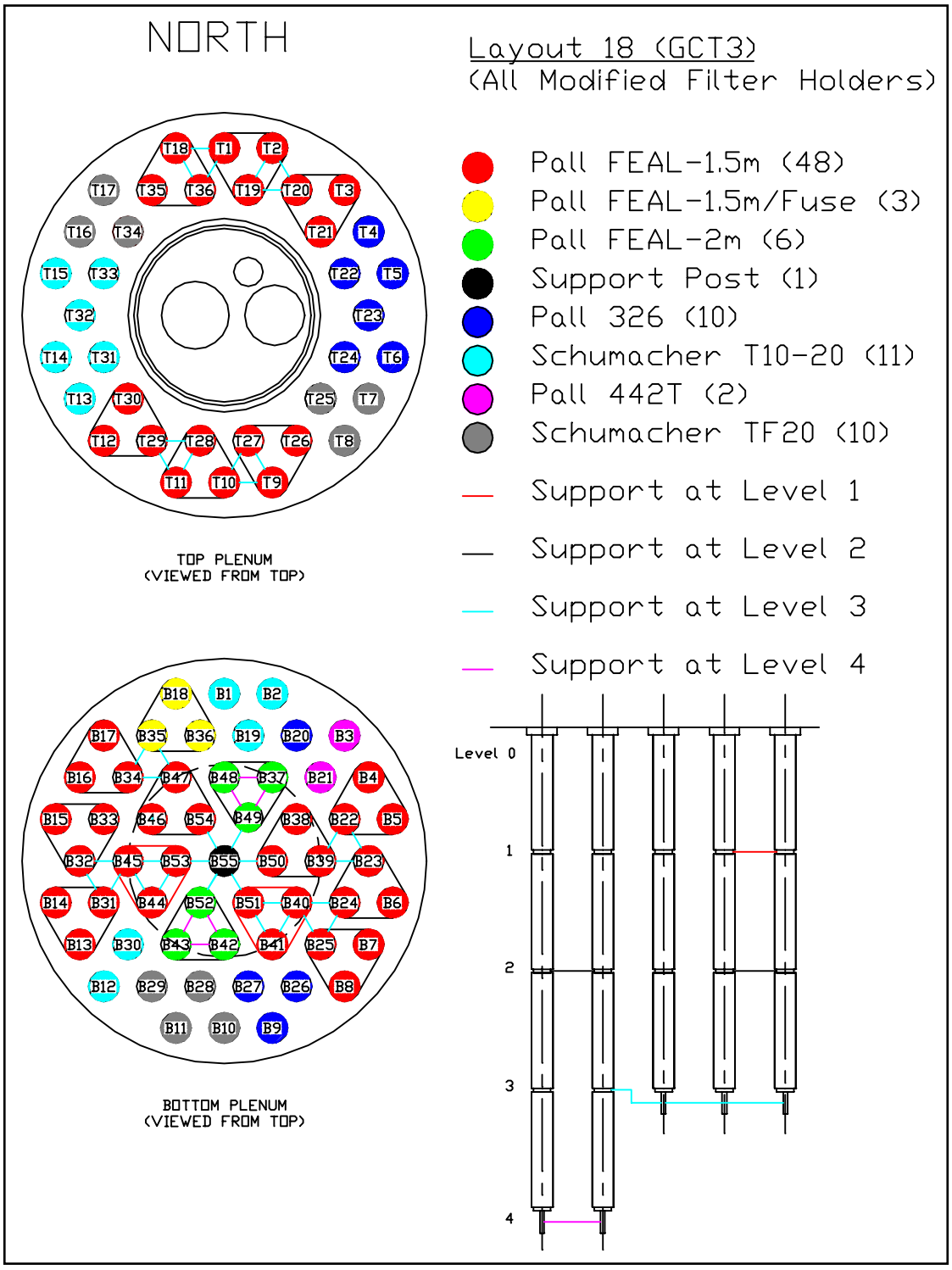

Figure 3.2-1 Filter Layout for GCT3

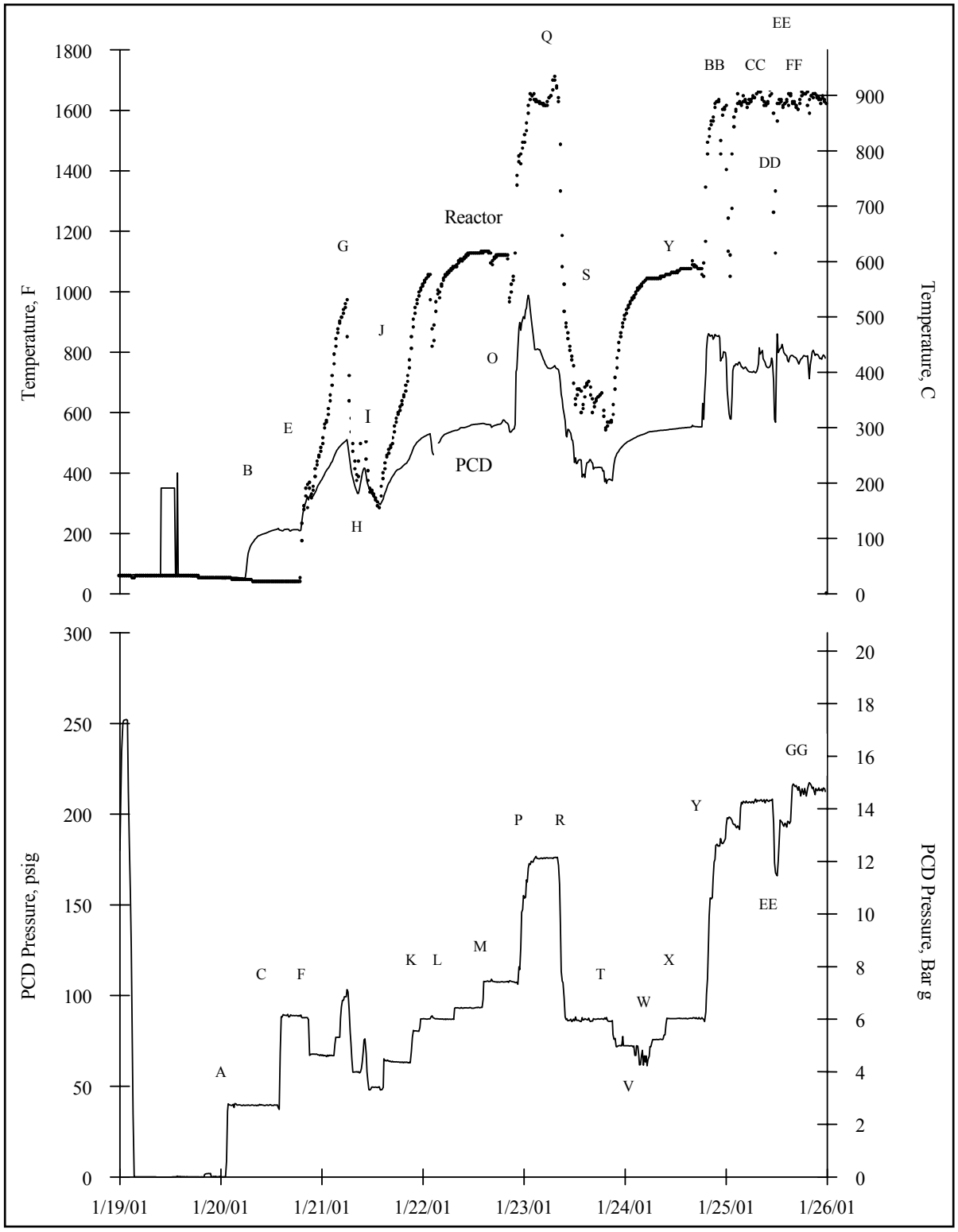

Figure 3.2-2 GCT3 Temperature and Pressure for January 19 Through 26

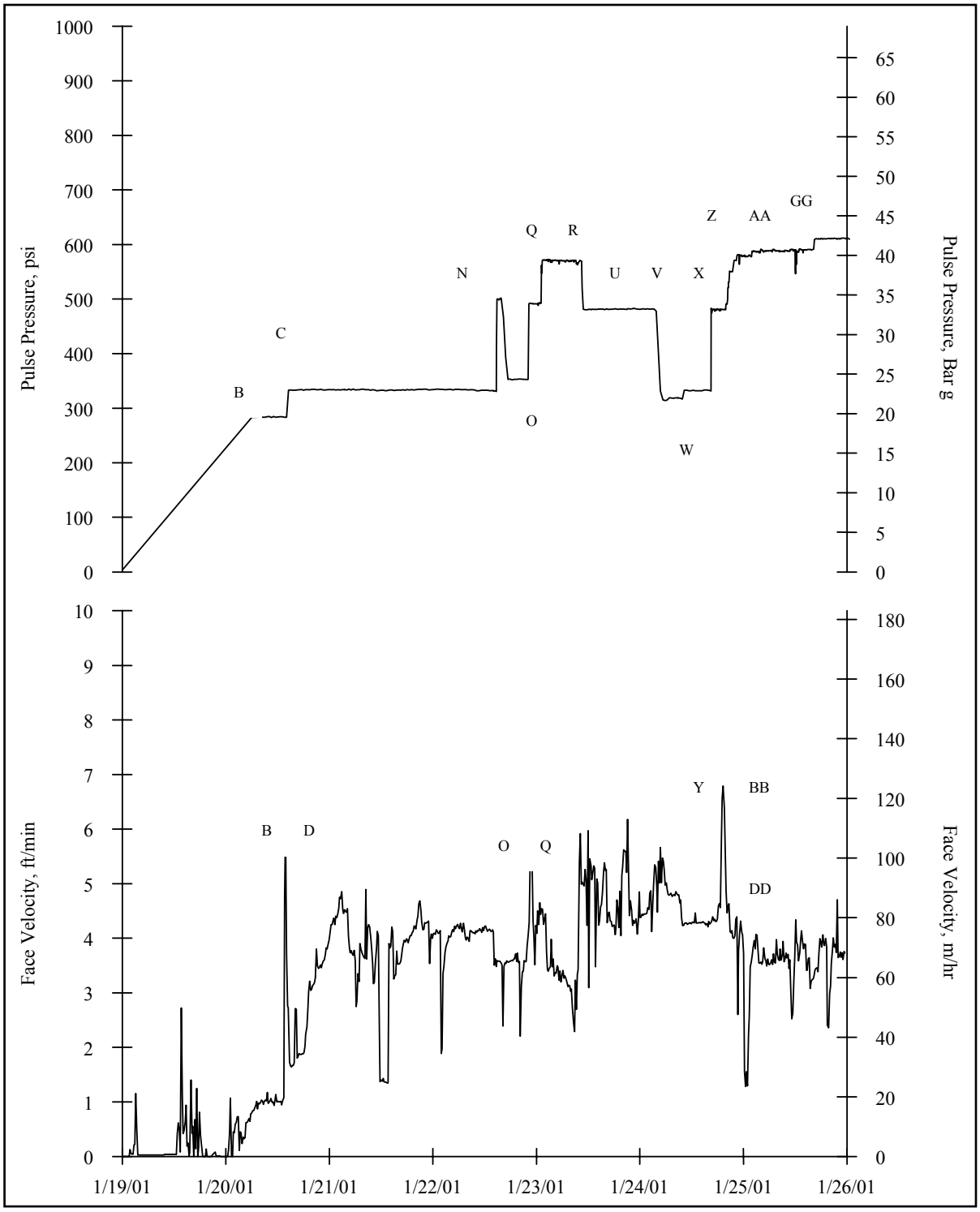

Figure 3.2-3 GCT3 Back-Pulse Pressure and Face Velocity for January 19 Through 26

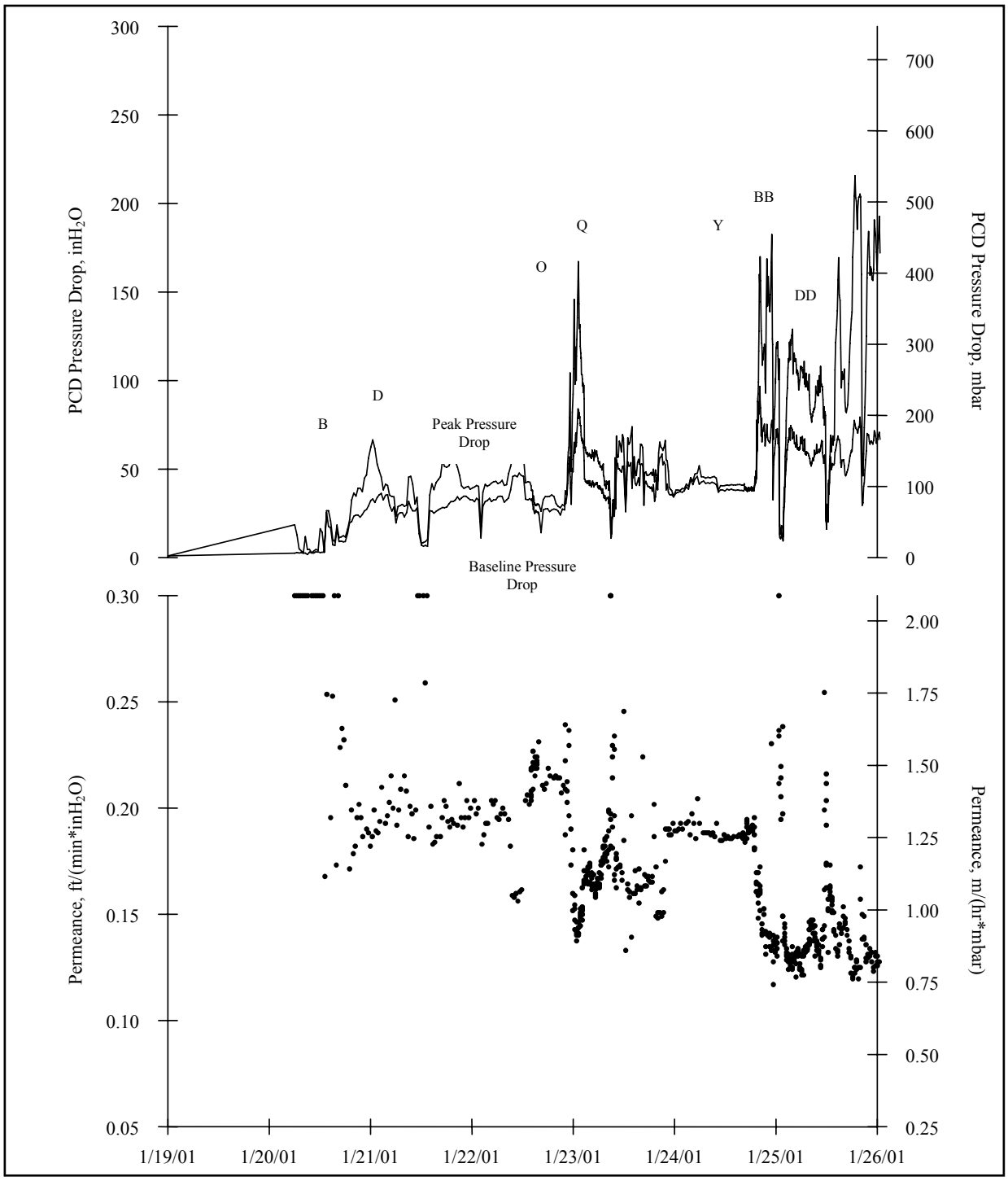

Figure 3.2-4 GCT3 Pressure Drop and Permeance for January 19 Through 26

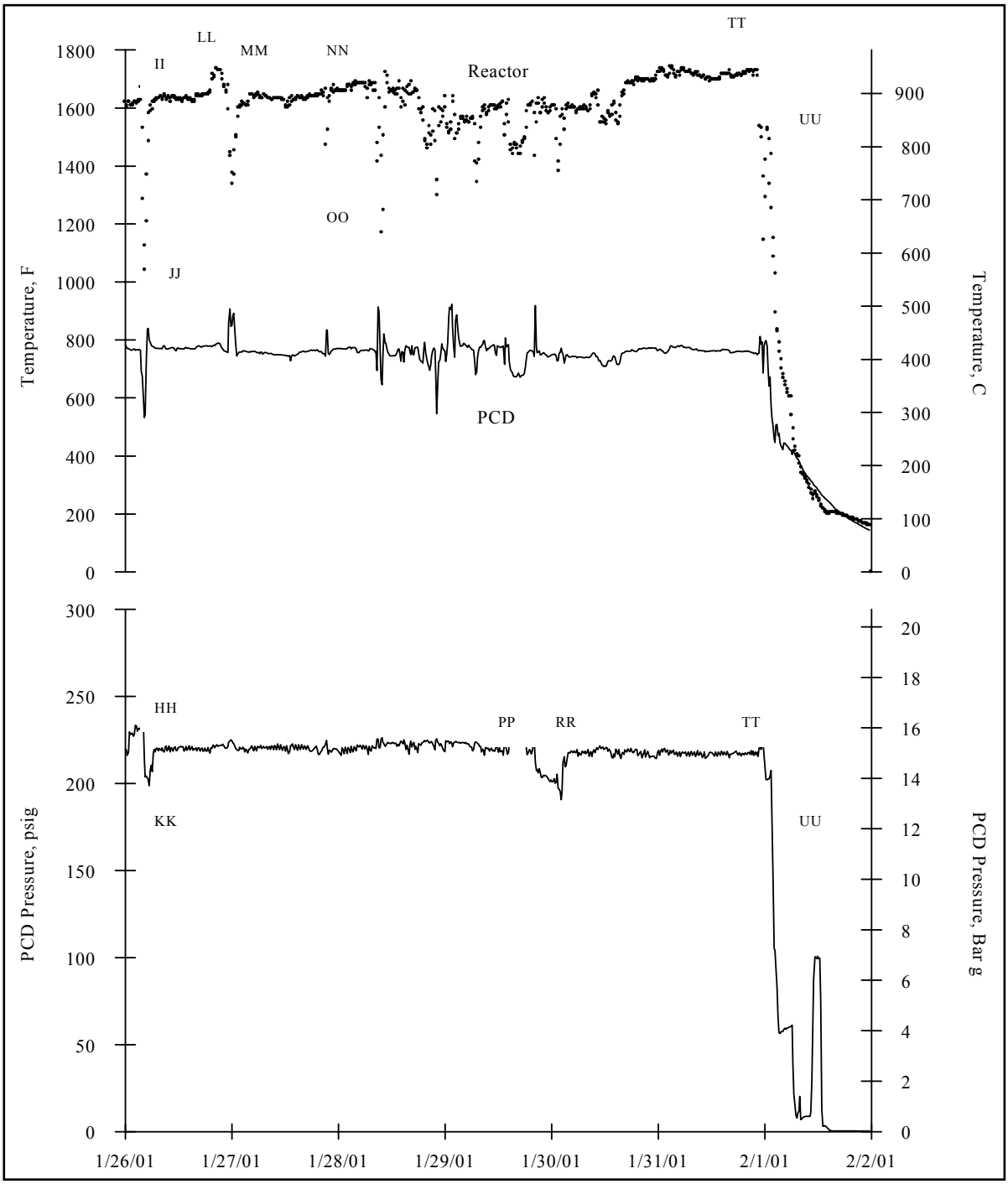

Figure 3.2-5 GCT3 Temperature and Pressure for January 26 Through February 2

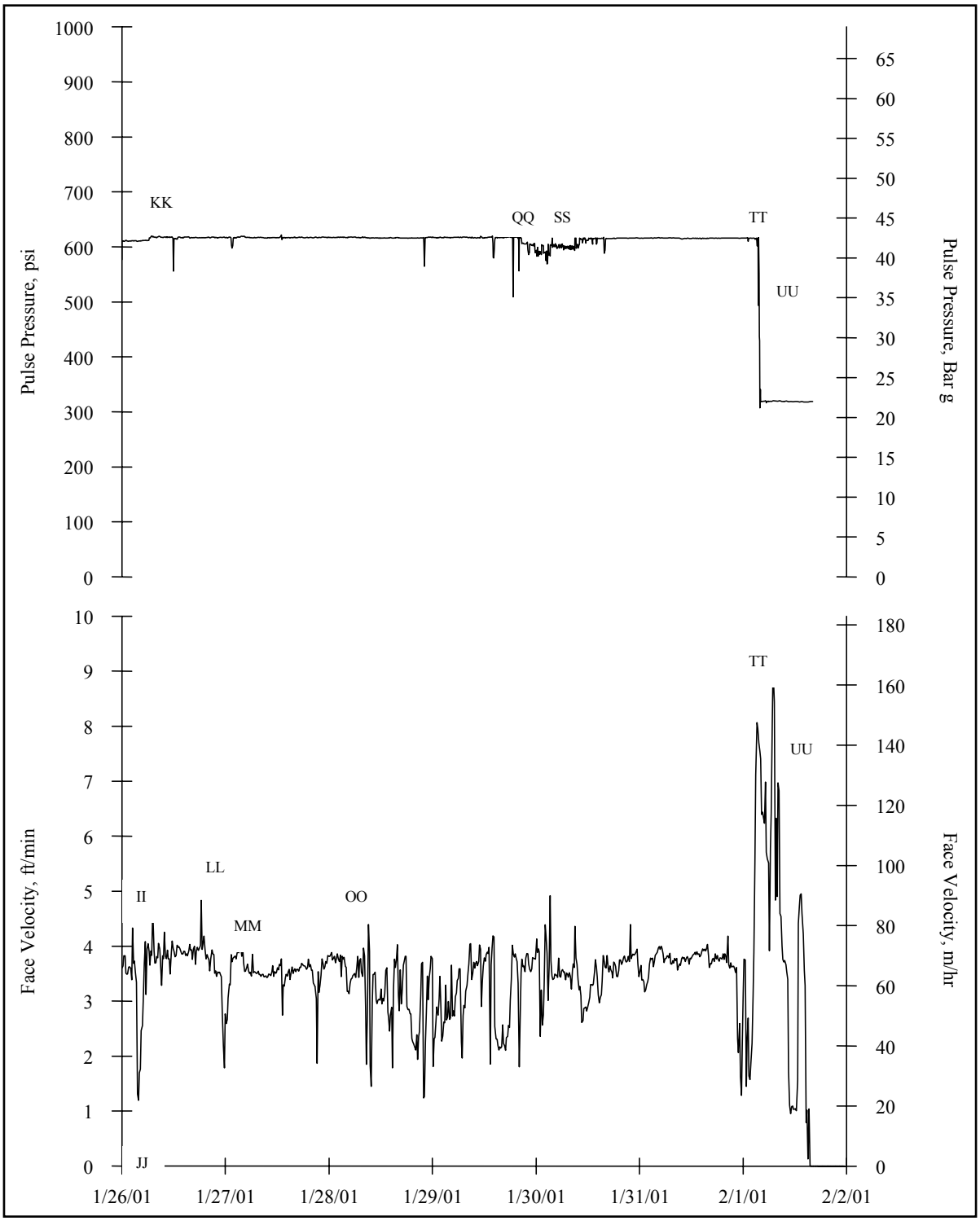

Figure 3.2-6 GCT3 Back-Pulse Pressure and Face Velocity for January 26 Through February 2

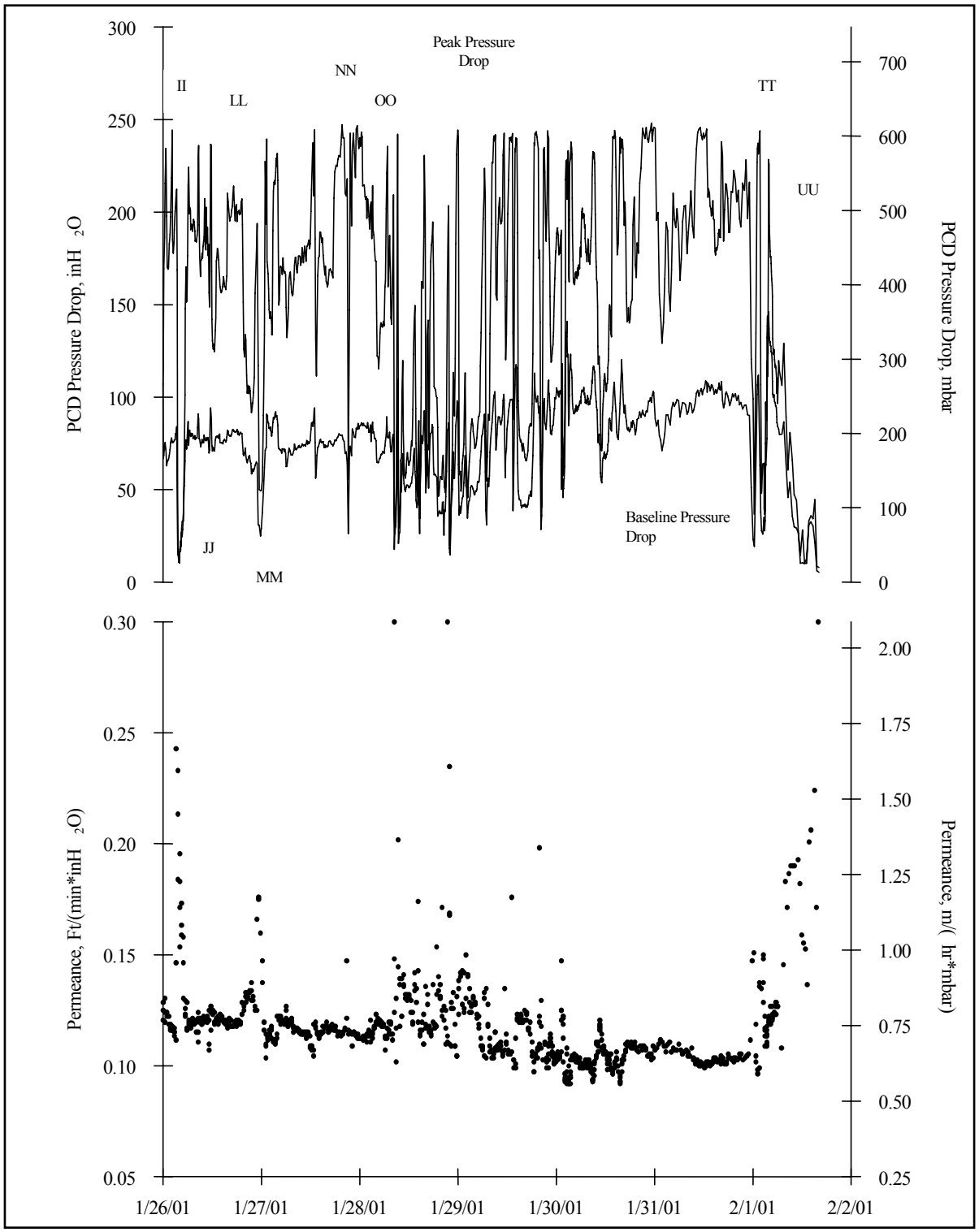

Figure 3.2-7 GCT3 Pressure Drop and Permeance for January 26 Through February 2

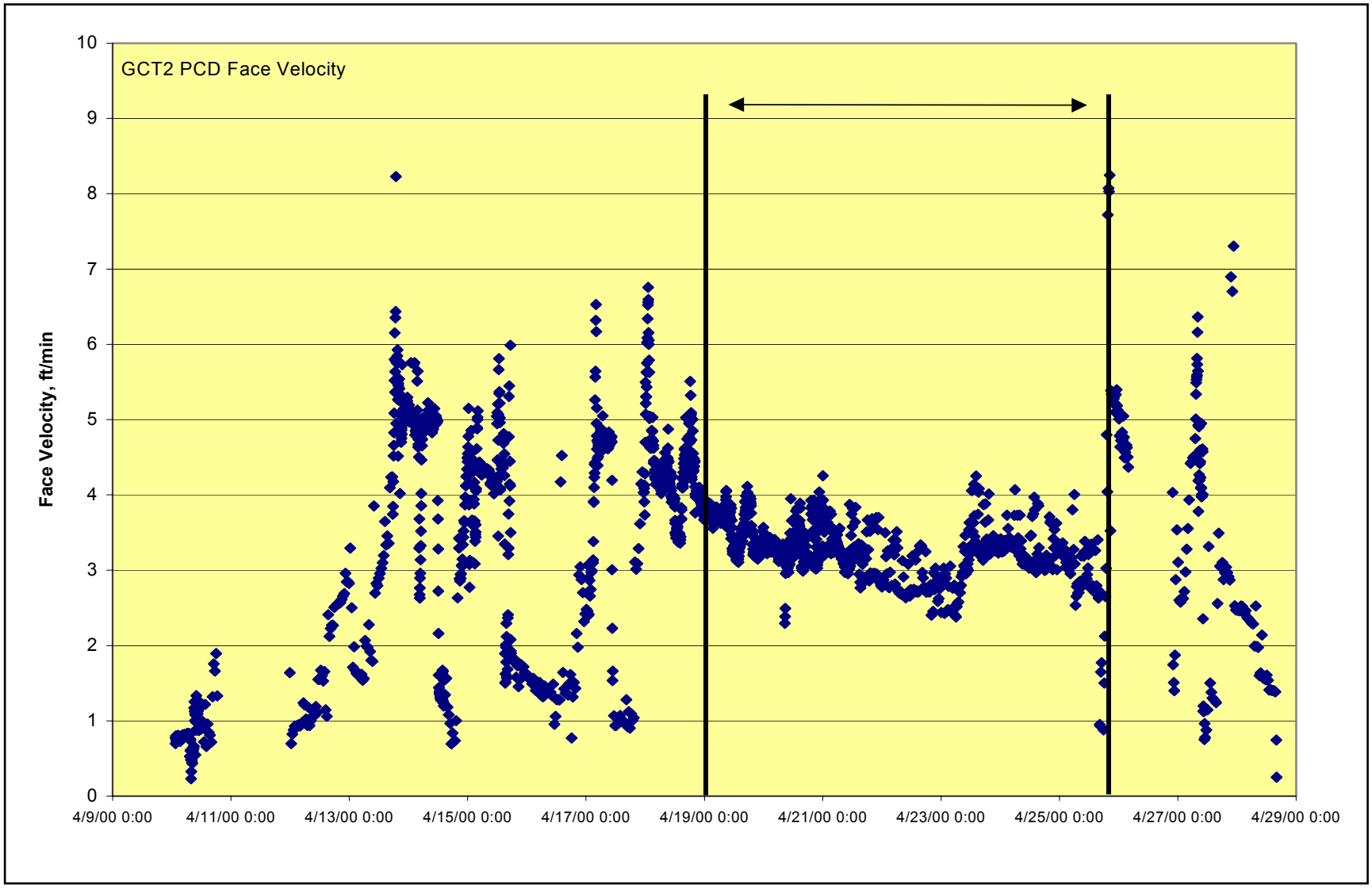

Figure 3.2-8 GCT2 PCD Face Velocity

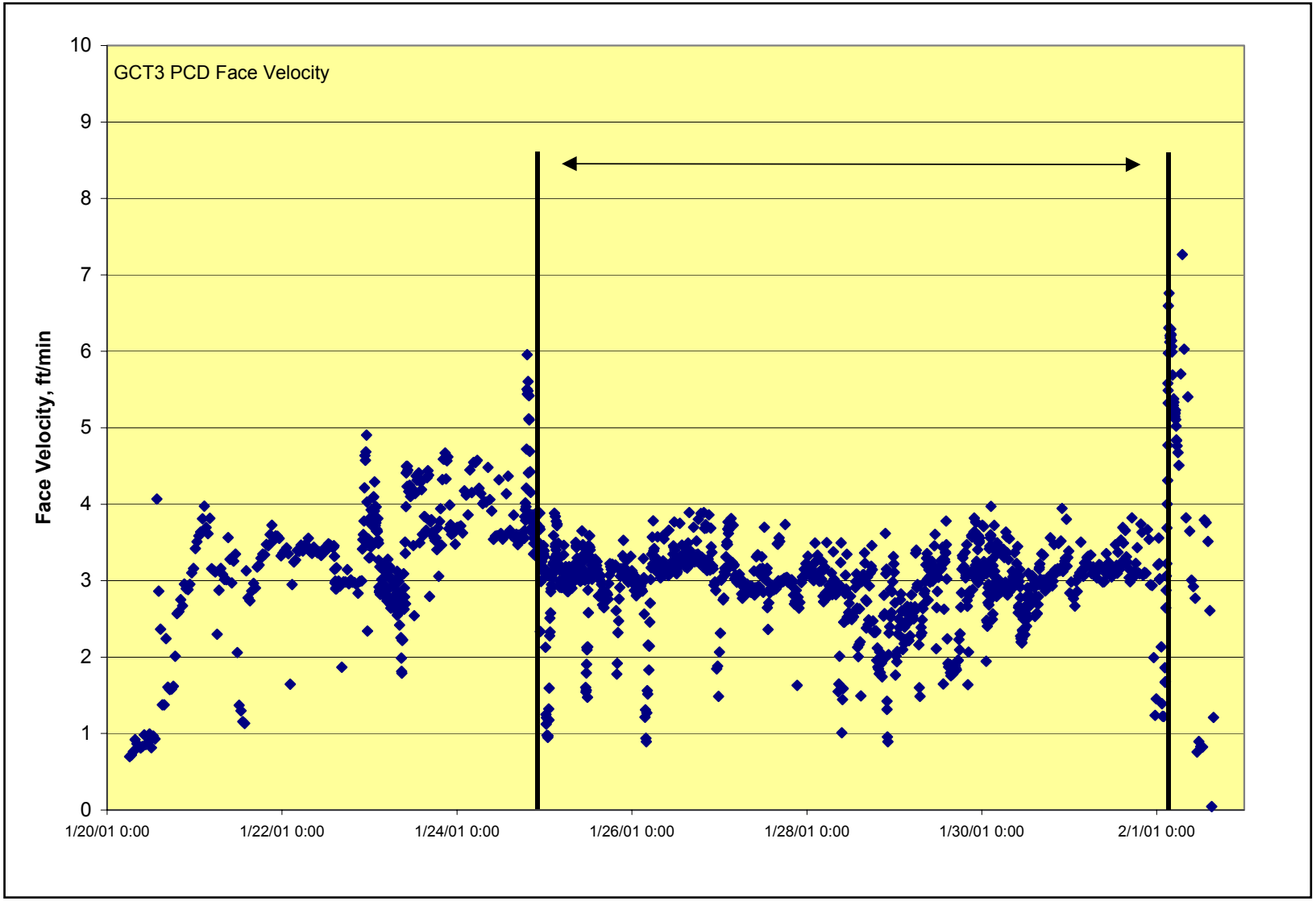

Figure 3.2-9 GCT3 PCD Face Velocity

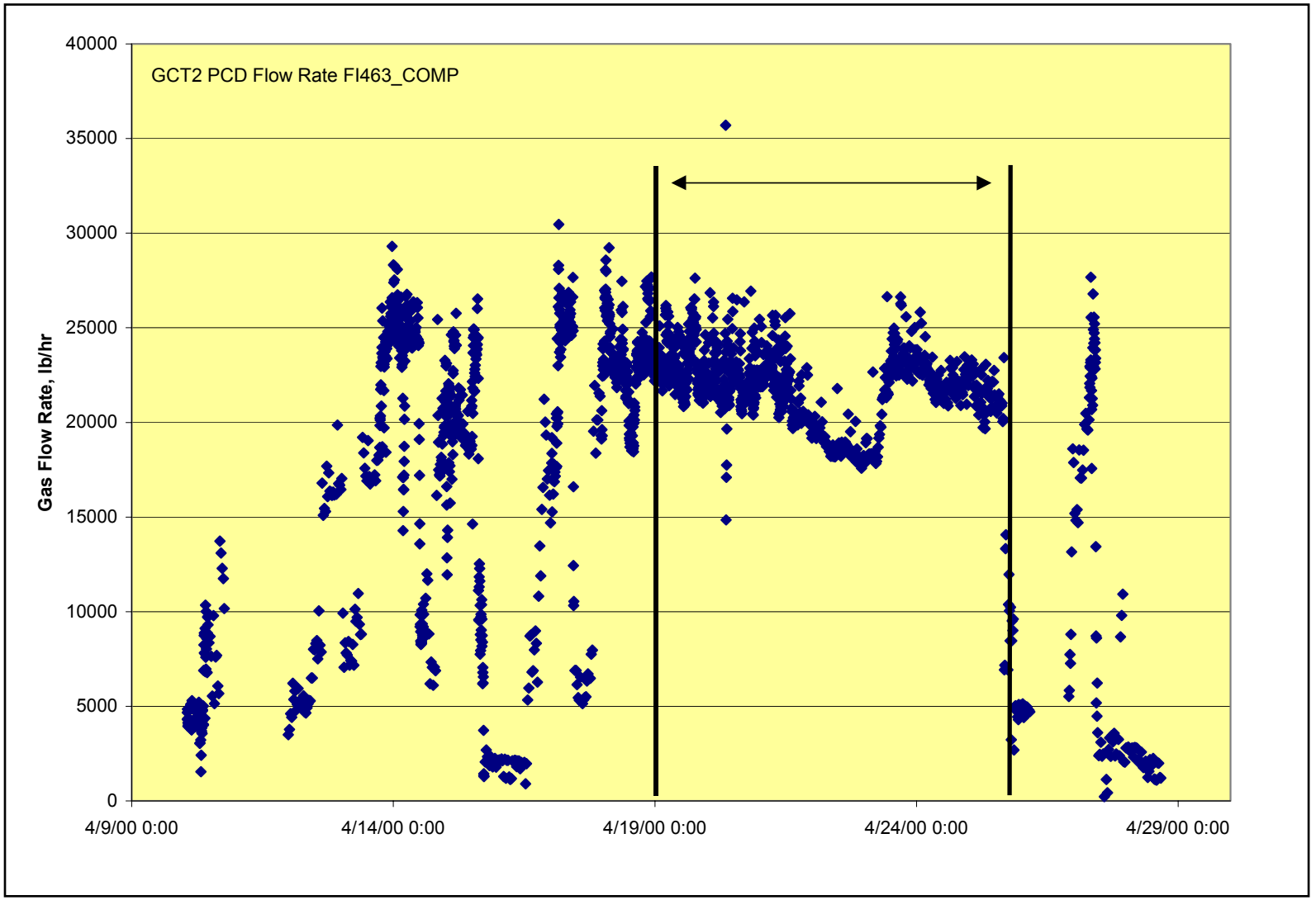

Figure 3.2-10 GCT2 PCD Gas Flow Rate

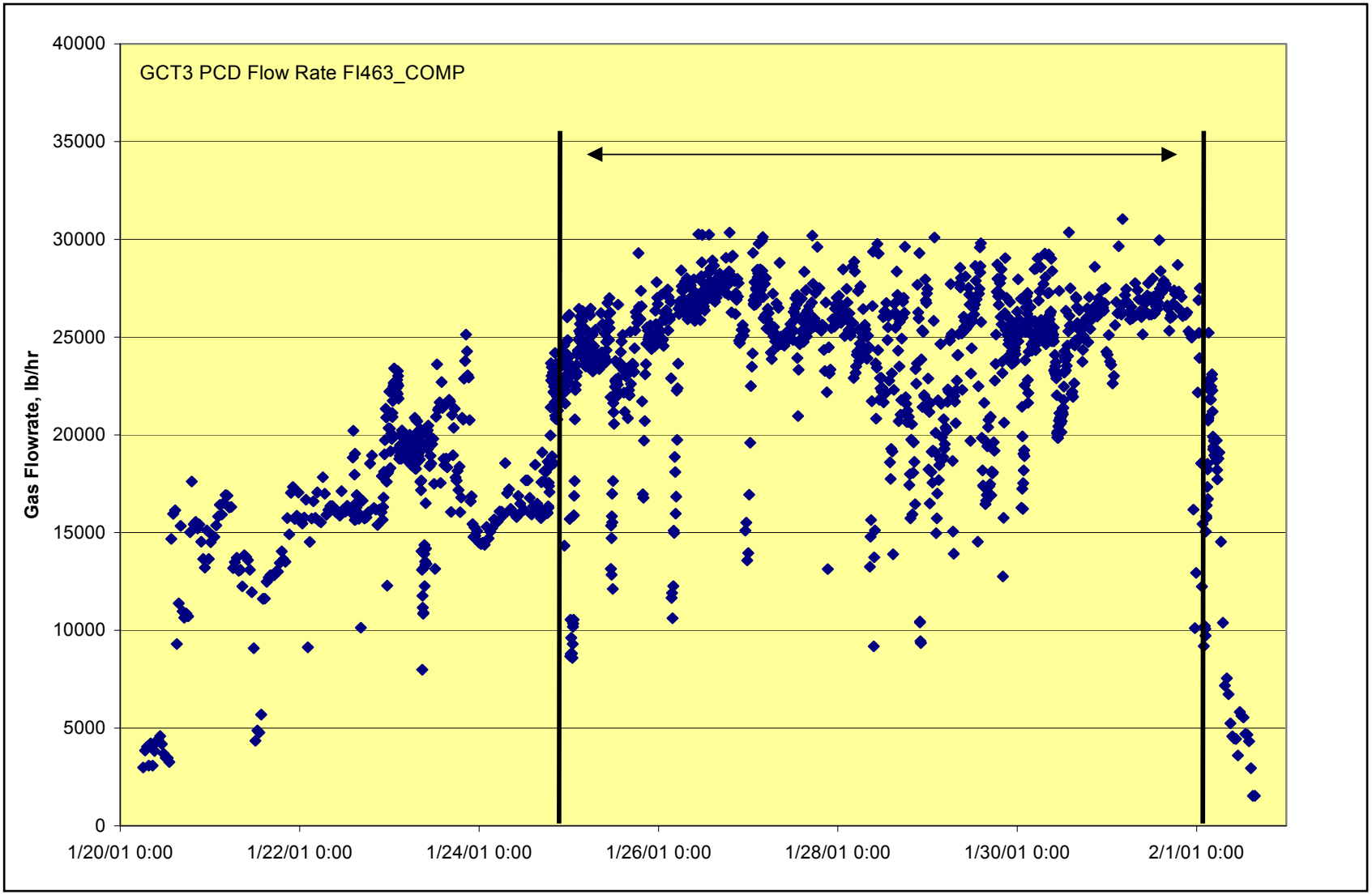

Figure 3.2-11 GCT3 PCD Gas Flow Rate

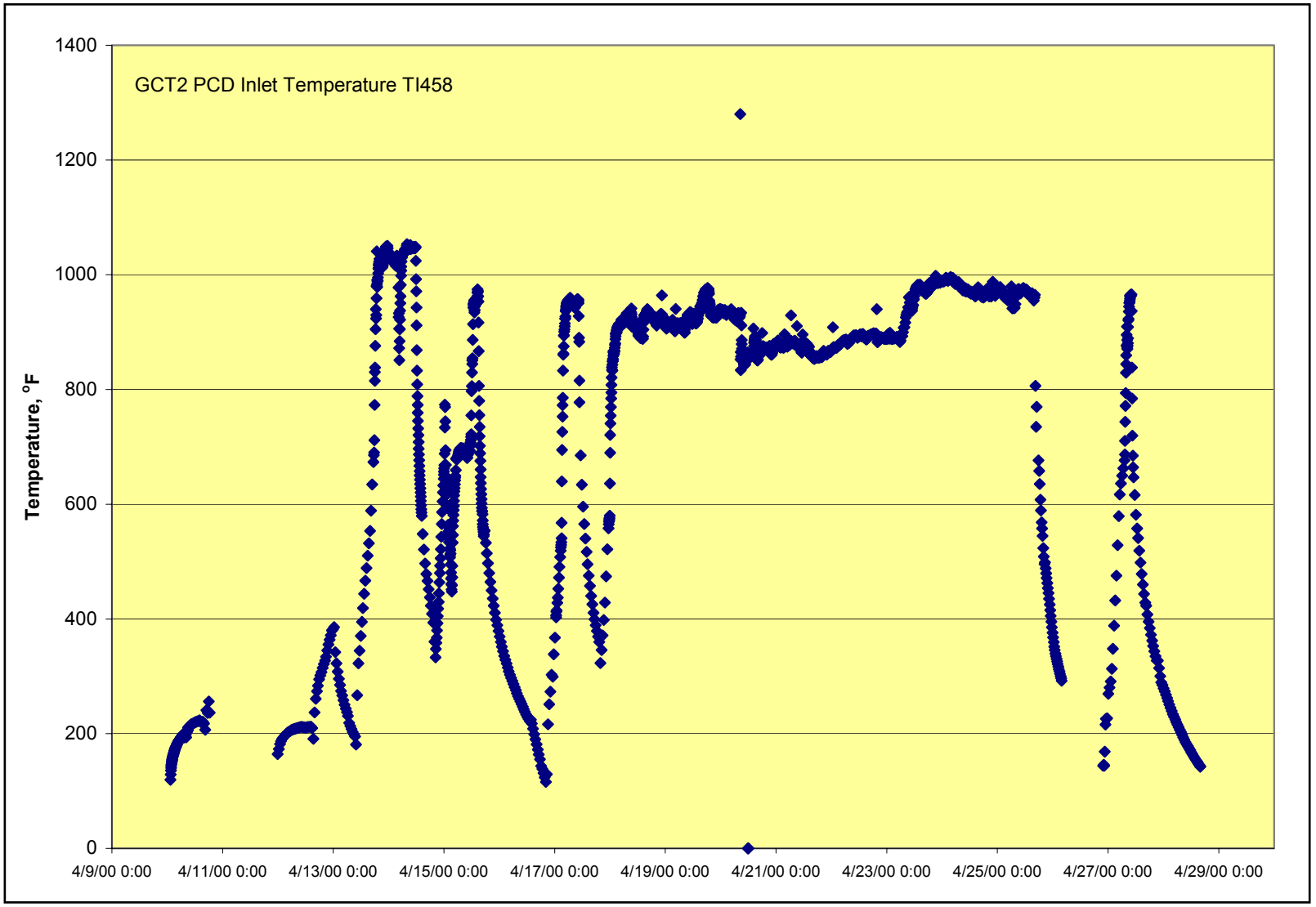

Figure 3.2-12 GCT2 PCD Inlet Temperature

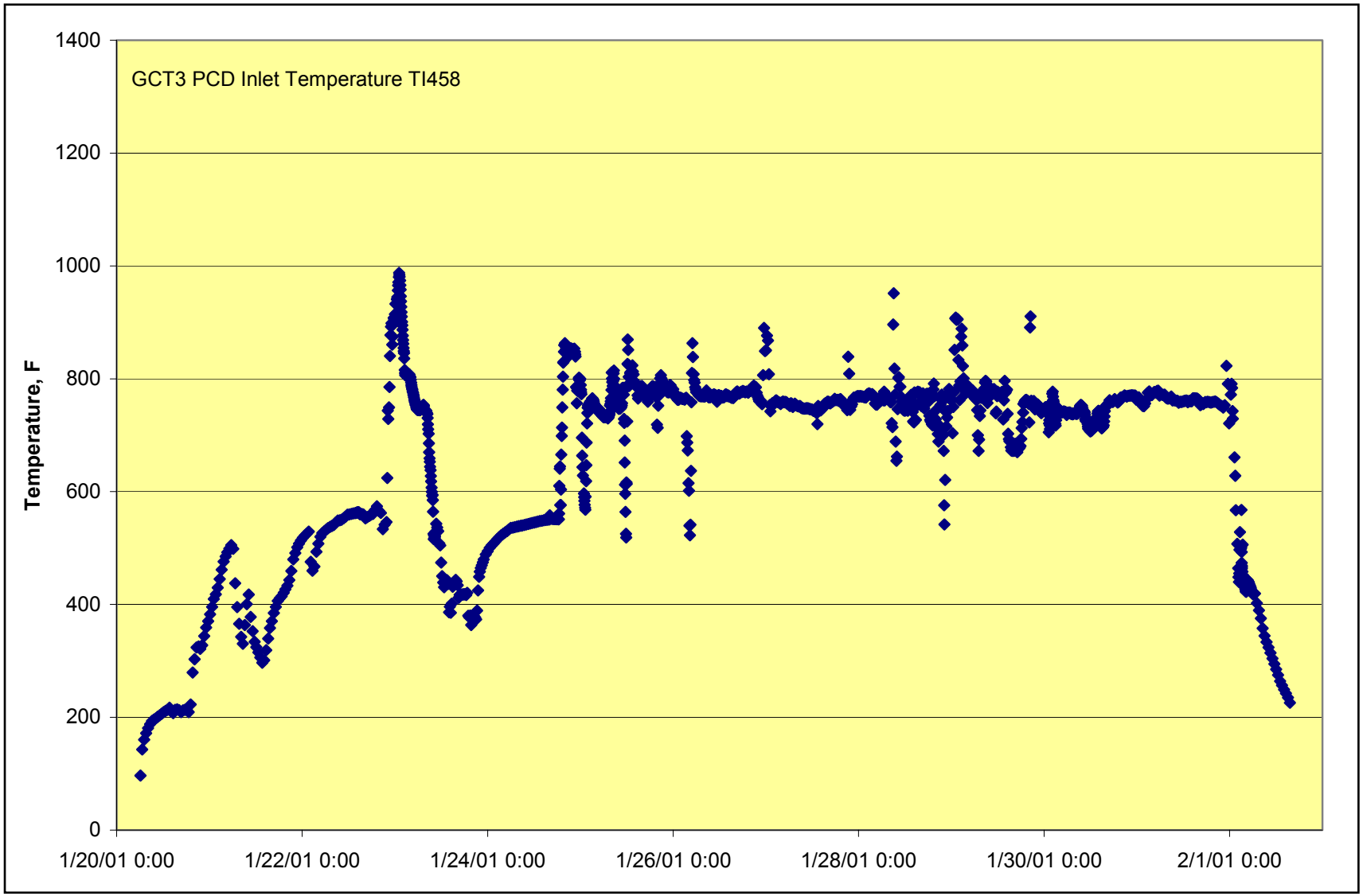

Figure 3.2-13 GCT3 PCD Inlet Temperature

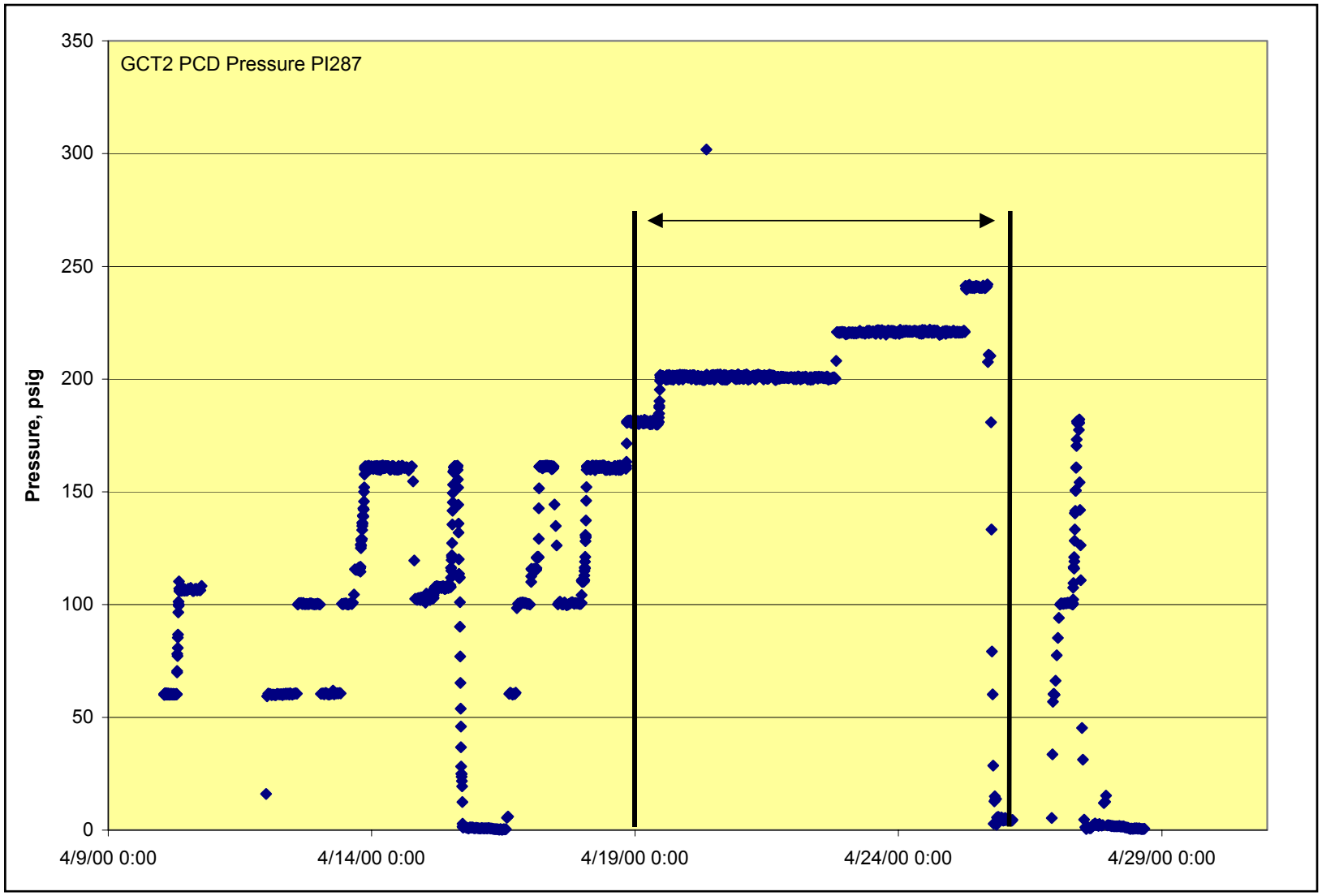

Figure 3.2-14 GCT2 PCD Pressure

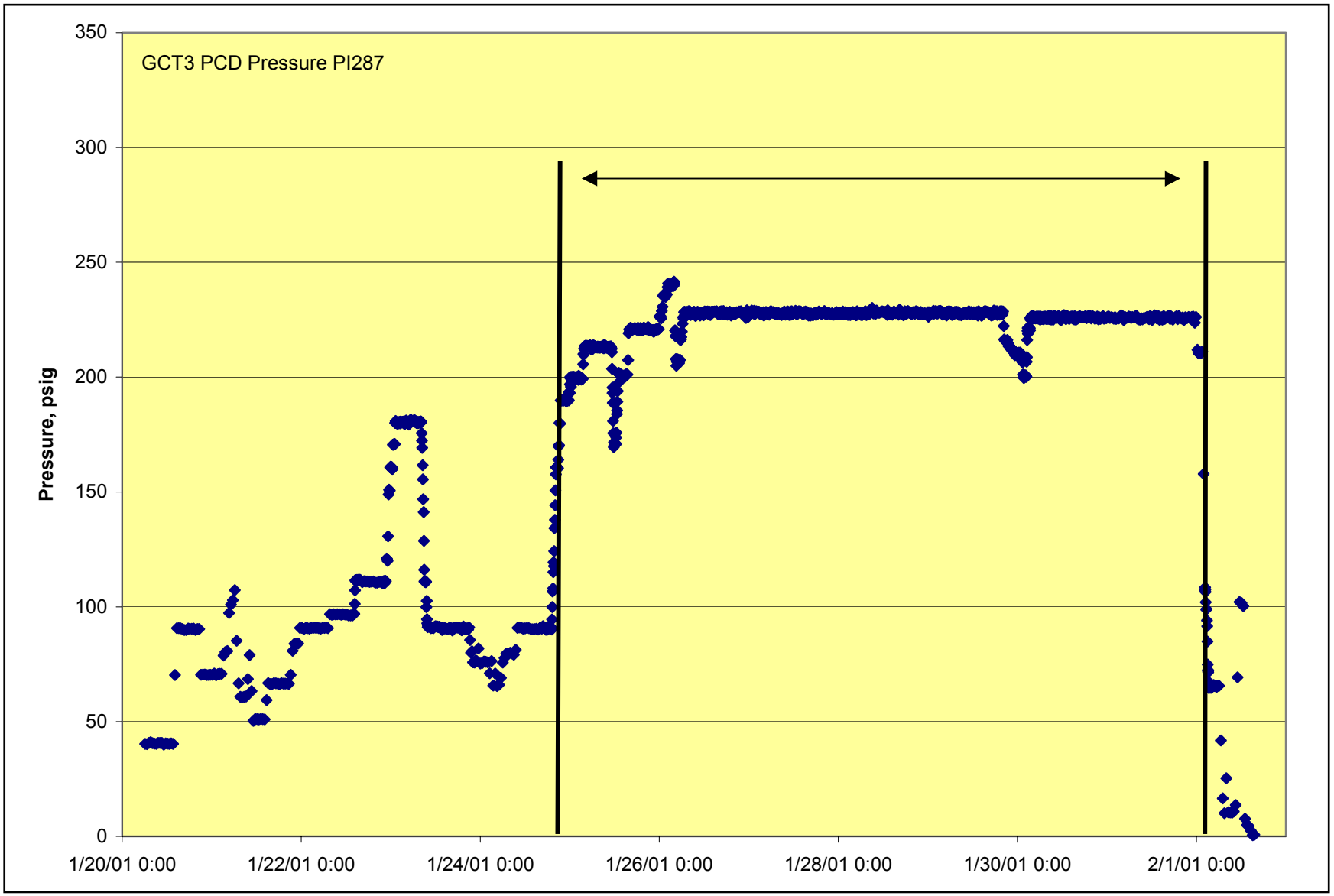

Figure 3.2-15 GCT3 PCD Pressure

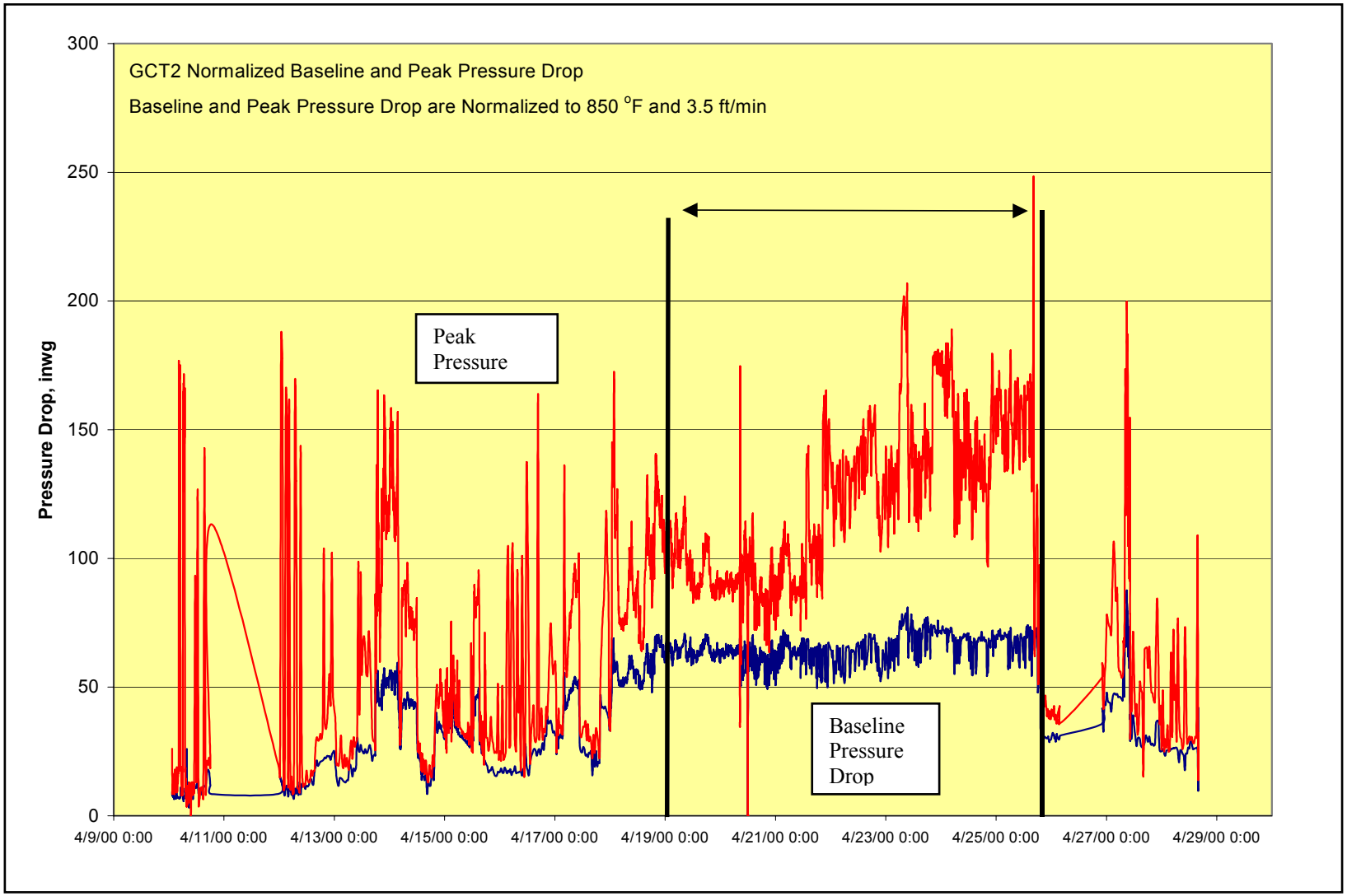

Figure 3.2-16 GCT2 Normalized Baseline and Peak Pressure Drop

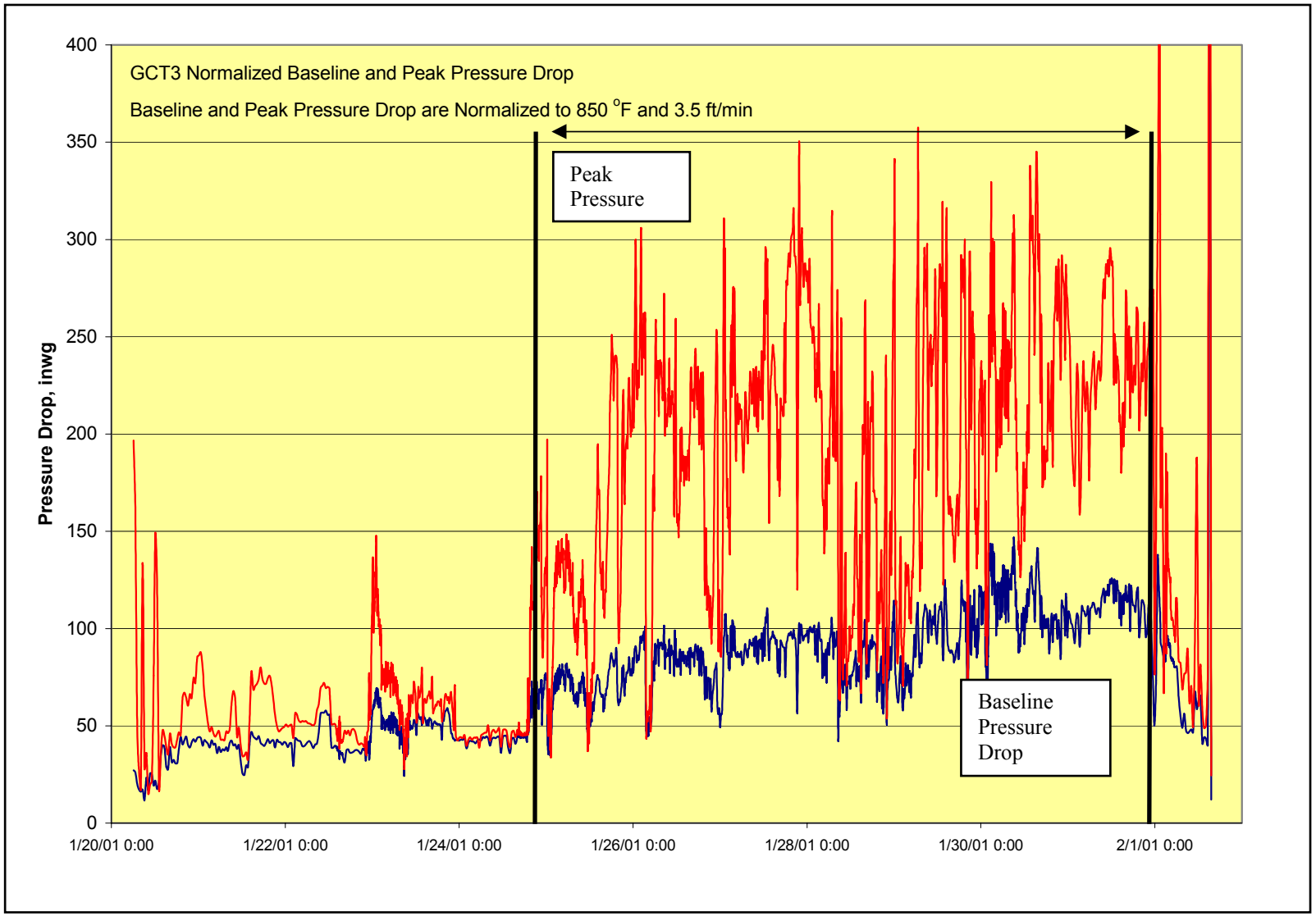

Figure 3.2-17 GCT3 Normalized Baseline and Peak Pressure Drop

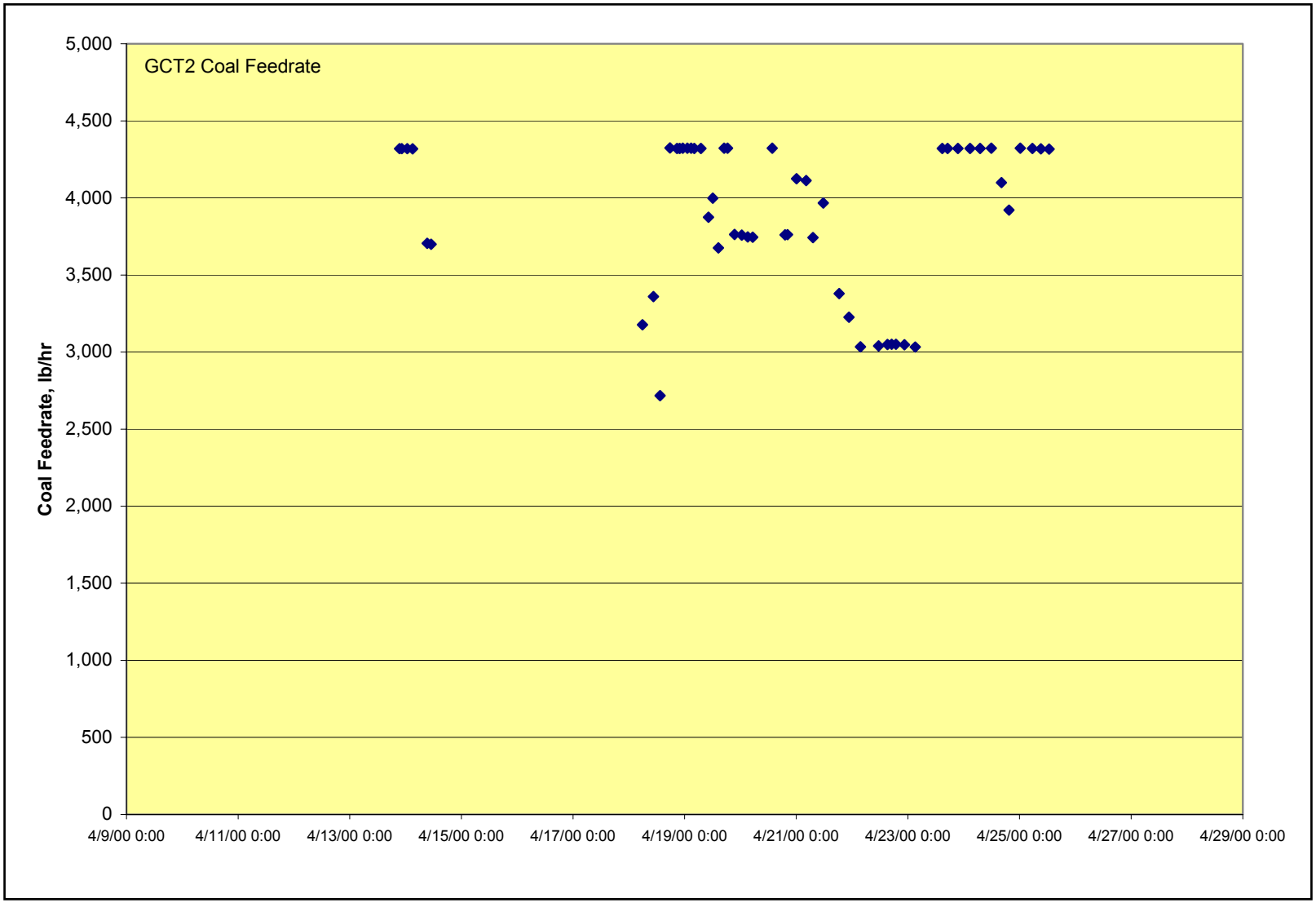

Figure 3.2-18 GCT2 Coal-Feed Rate

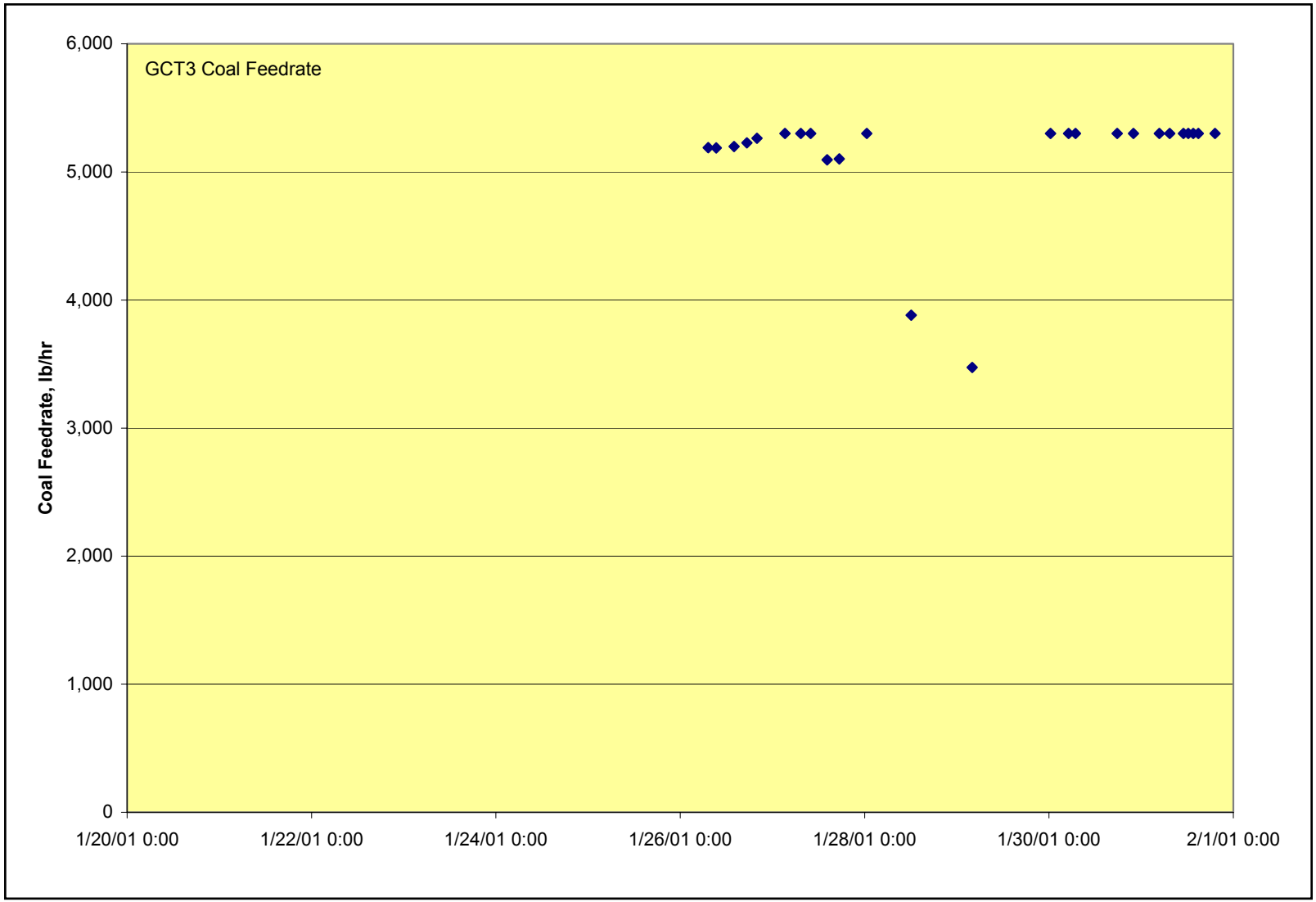

Figure 3.2-19 GCT3 Coal-Feed Rate

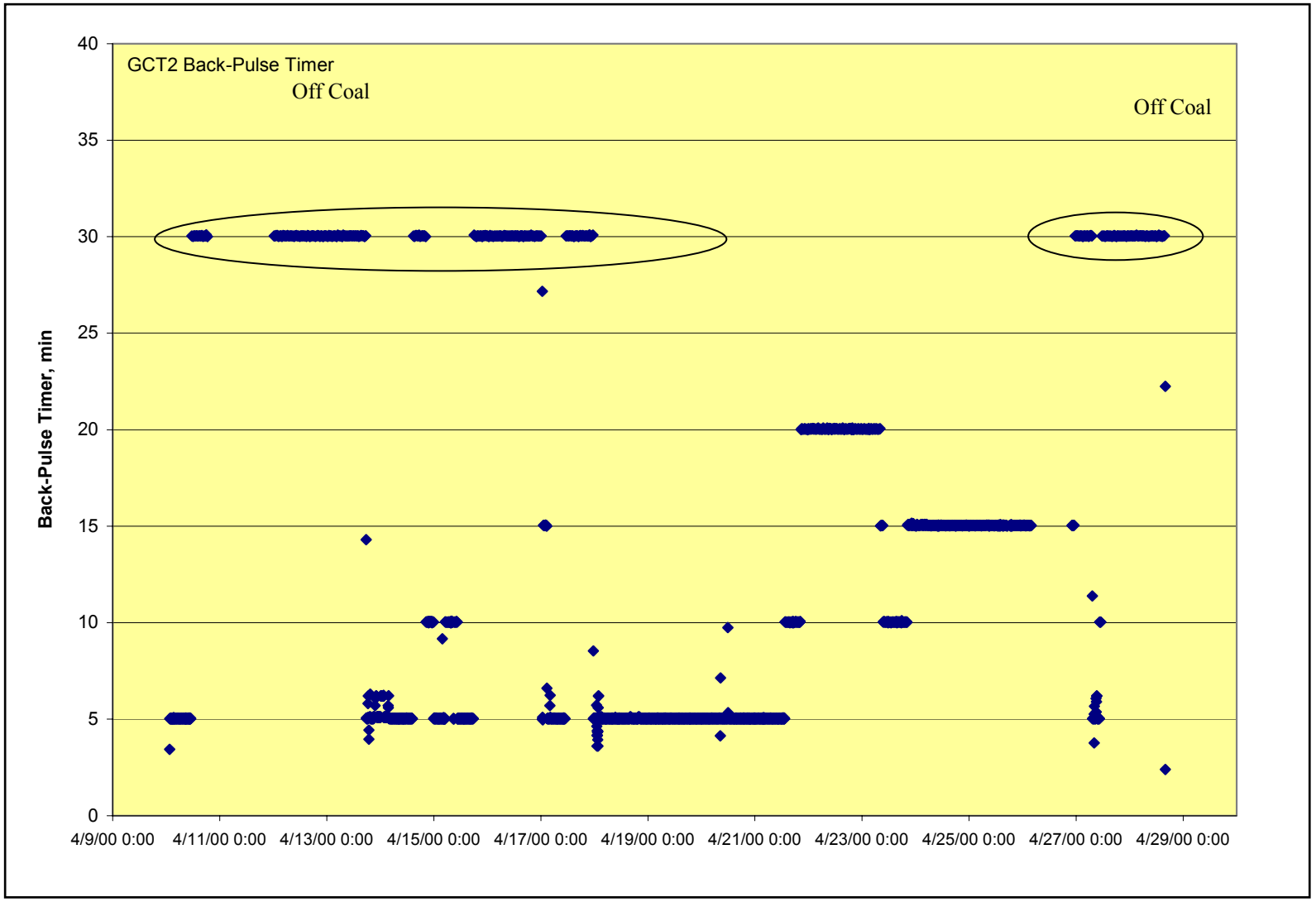

Figure 3.2-20 GCT2 Back-Pulse Timer

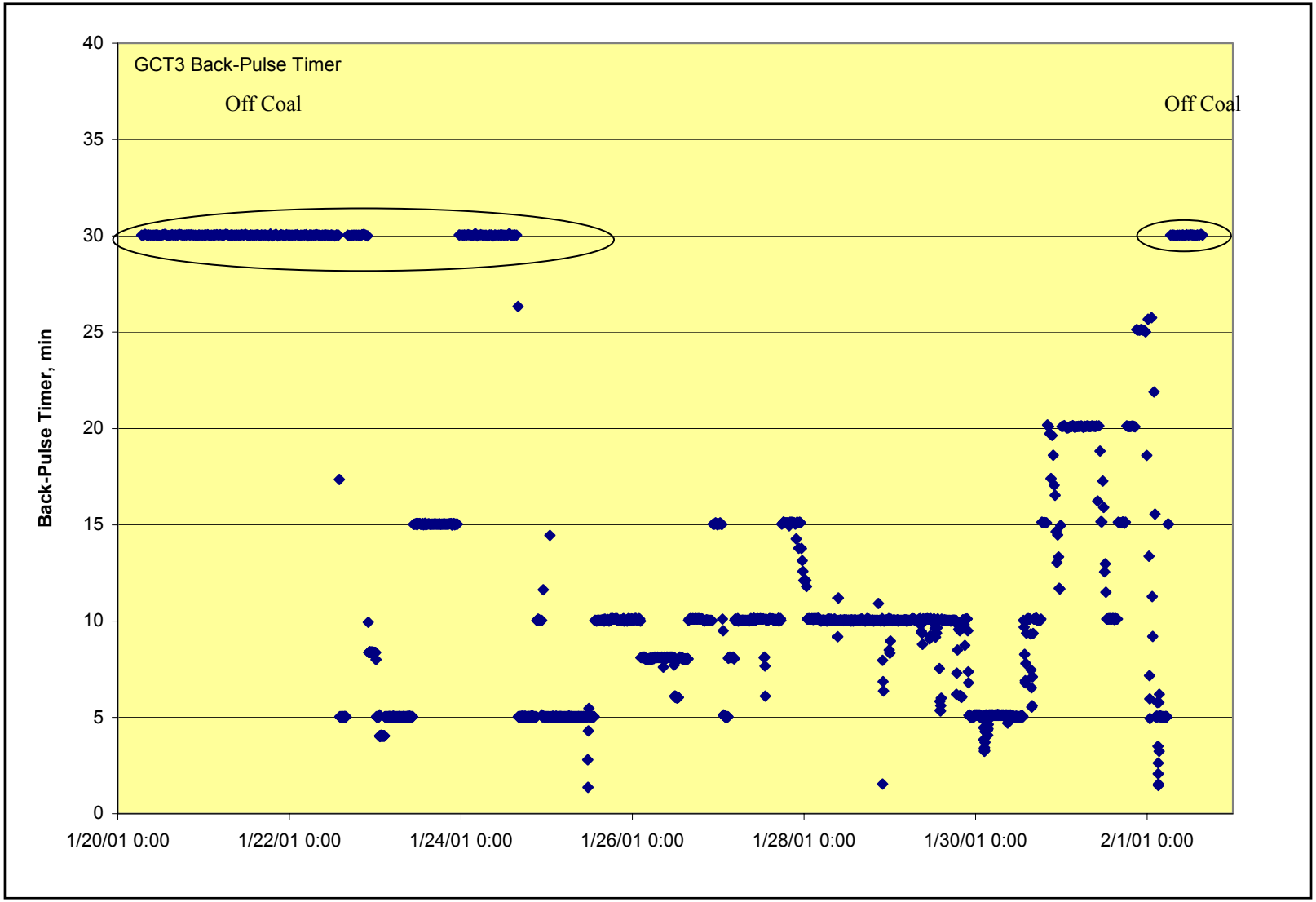

Figure 3.2-21 GCT3 Back-Pulse Timer

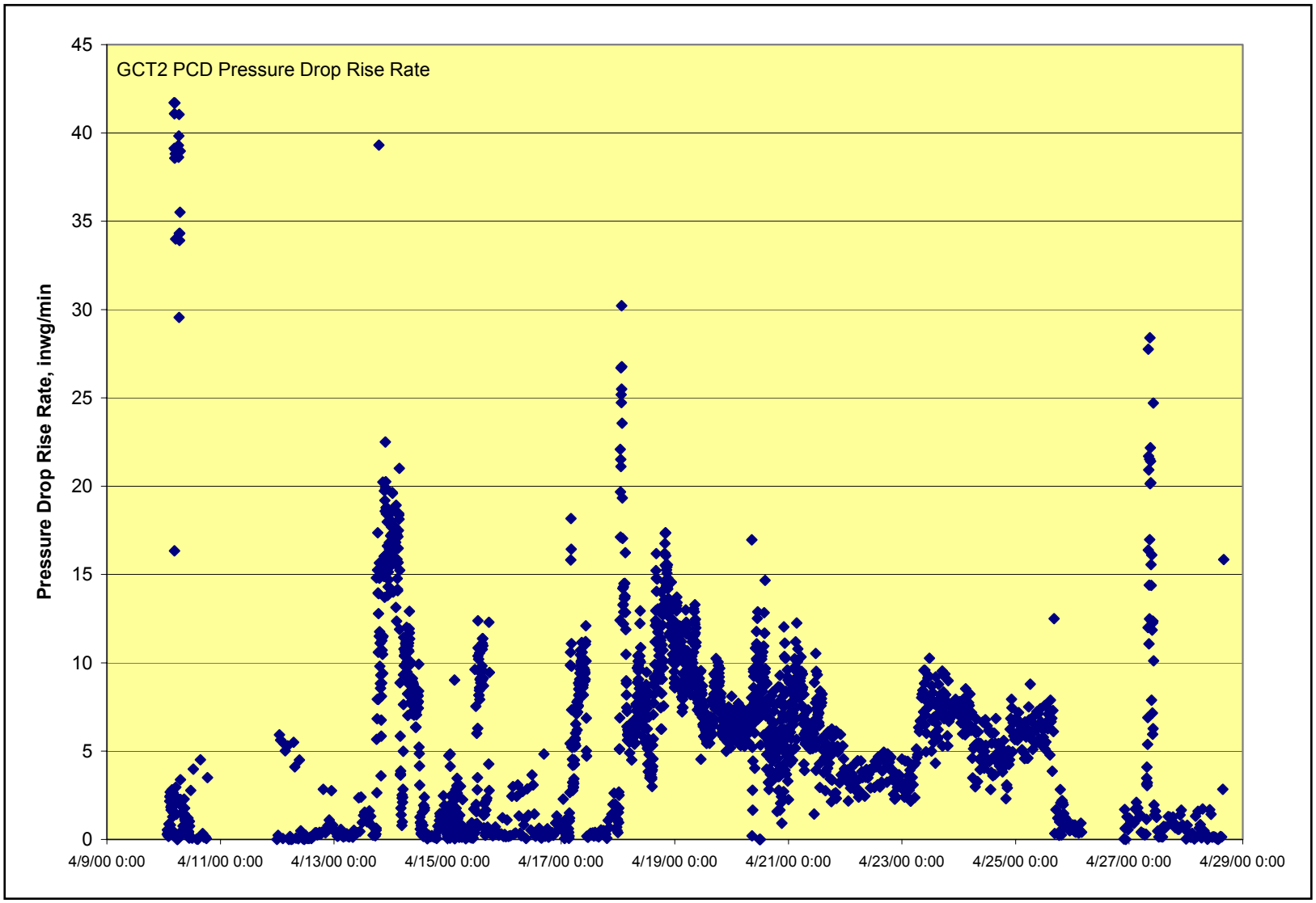

Figure 3.2-22 GCT2 PCD Normalized Pressure Drop Rise Rate

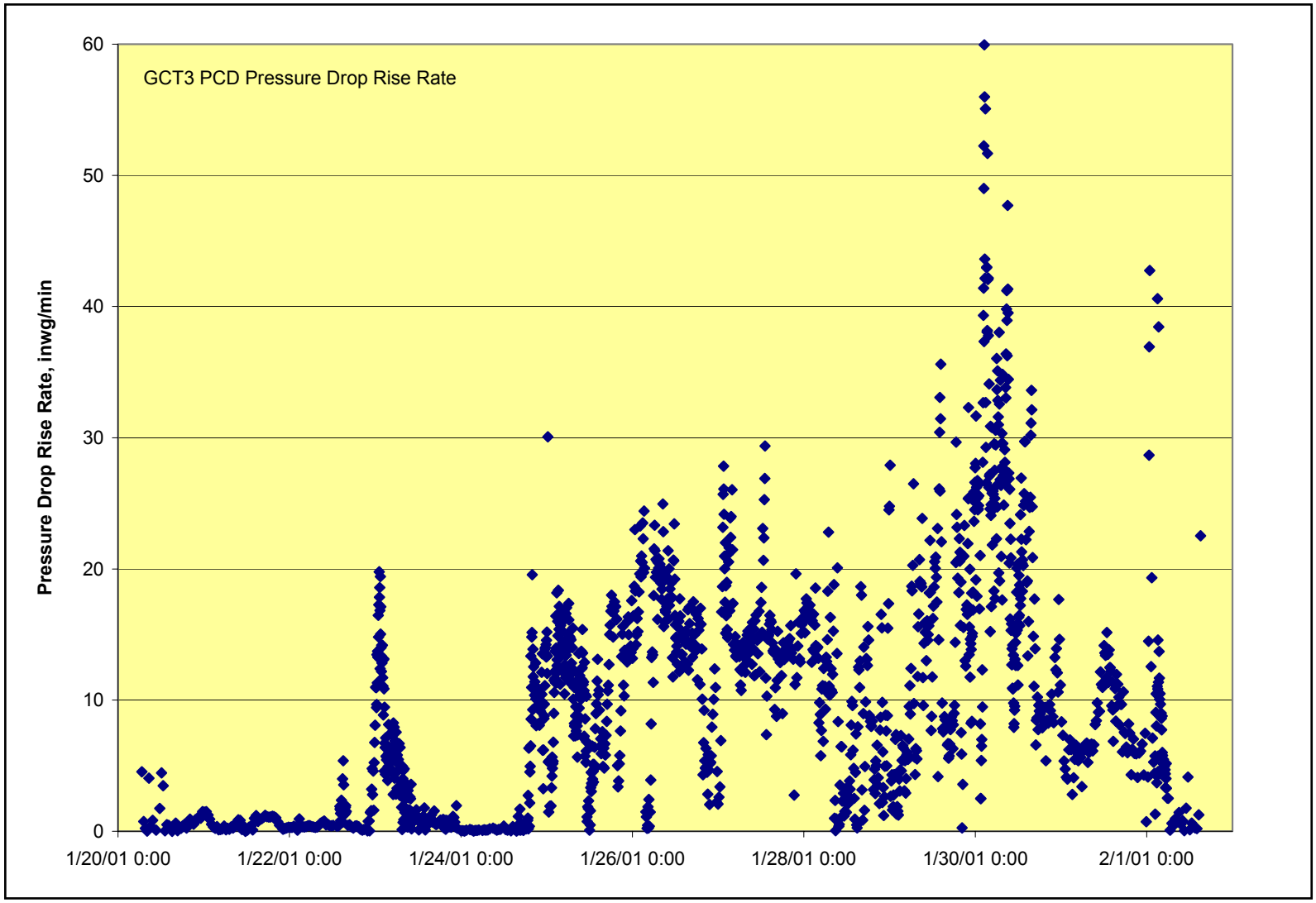

Figure 3.2-23 GCT3 Normalized PCD Pressure Drop Rise Rate

3.3 GCT3 INSPECTION REPORT

3.3.1 Introduction

The gasification portion of test run GCT3 started on January 20, 2001, (coal feed started on January 22, 2001) and ended on February 1, 2001. The PCD operating parameters are shown in Table 3.2-2. The PCD was inspected after the GCT3 run. In general, the inspection included 1) examinations of the filter elements and their fixtures to the plenums, 2) ash deposition, 3) filter element gaskets, and 4) auxiliary equipment. Following the inspection 33 silicon carbide and 4 iron aluminide filters were replaced.

3.3.2 Inspection

The PCD operated in gasification mode for a total of 184 on-coal hours during the GCT3 gasification run. The outlet loading from the PCD as measured by SRI was below 1 ppmw. The system was shut down due to the following reasons:

- The coal feeder (FD0210 system) spheri valve below the surge bin and above the lock vessel failed to close. During inspection it was discovered that one of the bags from the baghouse on the surge bin fell into the coal feeder and blocked the spheri valve, which prevented it from closing.

- The ash removal system (FD0520) below the PCD plugged. Ceramic filter pieces were found in the lock vessel and it was believed that a filter had failed.

The PCD was shut down in a clean state, which means the back-pulse system continued to cycle after the coal feed was stopped. The PCD vessel was opened on February 5, 2001, and the GCT3 inspection was performed during that week. There were no broken filter elements; however, there was some char bridging present as shown in Figures 3.3-1 and -2.

3.3.2.1 Char Deposition

The char bridging was isolated to the bottom plenum. Figure 3.3-3 shows where the char bridging was located on the bottom plenum. It was believed that the char bridging was due to tar condensing in the PCD and the mid-level support brackets on the filters. During the GCT3 run the coal feeder had problems maintaining steady-state operation. The reactor temperature would at times drop into a regime where it was believed tar was formed. If the tar condensed in the PCD the dustcake would become very sticky. This would explain the char bridging in the PCD. Also, it was believed that the brackets used to support the mid-section of the filters (See Figure 3.3-4) helped facilitate the char bridging, or acted as a platform for the char to grow. Before the next run all the brackets on the 1.5-meter filters are to be removed from the mid-section of the filters and all filters will be supported at the bottom support pins using bars and wing nuts as shown in Figure 3.3-5.

The residual char cake on the filter element was generally thin, approximately 0.02 inches thick (See Section 3.4). The char build-up on the top and bottom plenums was not severe. Just as in

GCT2, there were vertical paths in the accumulated char on the top ash shed (See Figure 3.3-6). There was very little char build-up on the inside wall of the shroud. Also, there was minimal char build-up on the liner sections (See Figure 3.3-7). Finally, the clean side of the tubesheet was clean with no apparent char penetration (See Figure 3.3-8). However, there was a shiny scale material on the top of the tubesheet that appeared to be tar deposition. This kind of material was also formed on the inside surfaces of the fail-safe and filter holders. No analysis was performed on the film at this time; additional information will be reported at a later date.

3.3.2.2 Filter Elements

During the GCT3 run, new monolithic silicon carbide (SiC) and iron aluminide (Fe_3Al) filters were installed in the PCD. Figure 3.2-1 is a filter element layout drawing (Layout 18).

The monolithic SiC elements performed well during GCT2 gasification run; therefore, it was determined to continue testing SiC filters. During the GCT3 run there was one major thermal event in the PCD. Figures 3.3-9 and -10 show the top and bottom plenum temperature response to the thermal event as provided by the thermocouples on the filters. The figures show that the filters experienced an approximately 300°F increase in temperature within 1 minute. This was reason for concern since there were 33 ceramic filter elements in the vessel. In an early combustion run a similar thermal transient resulted in failure of several types of ceramic filter elements. Fortunately, no apparent filter element failure was observed. The post-GCT3 inspection revealed that all the ceramic filter elements were intact. Since similar thermal transients are likely to occur in the next gasification run the decision was made to remove all the ceramic filter elements and replace them with Pall Fe_3Al filters. It was believed that over time, damage could accumulate and cause failure of the ceramic filters.

The Pall Fe_3Al filters performed well during the GCT3 gasification run. The elements were visibly inspected and no obvious damage was found. During the outage seven Fe_3Al filters were removed and inspected. There was no loose char inside any of the filter elements that were removed and there was no char accumulated on the inside walls of the elements.

3.3.2.3 Filter Element Fixtures

As mentioned in the GCT2 report, a modified filter holder was designed to address the problems with the original filter element holder. This new filter holder set includes a fail-safe holder and a modified filter nut. They performed well in GCT2, so as a continual evaluation they were also installed in GCT3. During the post-GCT3 inspection they were found to be in good condition.

During the inspection, torque was checked on three filter nuts and two fail-safe holders. The initial torque on the fail-safe holder was 120 in-lb on each bolt. The remaining torque after the run was in the range of 115 to 120 in-lb. The initial torque on the filter nuts was 70 in-lb for ceramic filters on each bolt. The remaining torque after the run ranged from 60 to 70 in-lb. The holder performance in the run indicated that the remaining torque was still sufficient to maintain adequate compression.

There was a coating inside many of the fail-safe holders and in the flange section of the fail-safe that could be flaked off in pieces. This material appeared to be similar to the shiny scale seen on the clean side of the tubesheet. It was suspected that this coating was caused by tar deposition that occurred during the many coal feeder trips. Once the process was restarted it was believed that the higher temperatures would volatilize the lighter hydrocarbons, leaving the heavier residue behind. This area will continue to be investigated.

3.3.2.4 Filter Element Gaskets

One of the objectives for the PCD during the GCT3 run was to continue evaluating the Siemens Westinghouse lapped-construction primary gaskets. Compared to the original fiberfrax ring gaskets used during GCT1A, these lapped-construction gaskets provided a better seal during the GCT1B through D and GCT2 runs. Therefore, the lapped-construction gaskets were installed with each filter element prior to the GCT3 run. The gasket types used during the GCT3 are:

Gasket Type	Gasket Location
Lapped-construction	Plenum-to-fail-safe (primary gasket)
Top donut	Fail-safe-to-fail-safe holder
Bottom donut (No. 1)	Fail-safe holder-to-element
Bottom donut (No. 2)	New filter nut-to-element
Sock gasket	Element-to-bottom donut gasket (No. 2)

In the post GCT3 outage only 37 filter elements and 23 fail-safes were removed. Therefore, the inspection of the gaskets was not extensive. However, the following observations were made based on the gaskets that were examined:

- There were no leak paths in the area of the new fail-safe holder flanges that would have indicated a leak past the primary gaskets.

- Some lapped-construction gaskets had broken fibers. This did not appear to affect the sealing capability of the gasket. The fibers could have been damaged when the fail-safes were removed from the plenum during disassembly.

- A small amount of loose char was found inside the fail-safe holder-to-element gaskets. The color of the gaskets had changed from white to light black. Some of the gaskets were cut to inspect the extent of char penetration. The gaskets were relatively clean on the inside with only small traces of char penetration. Some char penetration was expected since the gaskets are dust-tight, not gas-tight seals.

3.3.2.5 Fail-safes

Twenty-three fail-safes were removed during the GCT3 outage, with no evidence of fail-safe damage observed.

Ten prototype fail-safes designed by Siemens Westinghouse were continuously evaluated during the GCT3 run. Each prototype fail-safe contained metal fiber. The metal fiber is designed to allow free flow of clean process gas yet plug completely in the event of a filter failure, filter leak, and/or gasket leak. Two fiber fail-safes were removed, weighed, and flow tested during the GCT3 outage. Neither of these fail-safes had a significant weight change. The flow coefficients for the two fail-safes measured following the GCT3 run were 7 and 9 percent lower than the pretest values. Since there was no significant change in weight the increased flow resistance is thought to be due to settling of the fiber. These two fail-safes were reinstalled and all 10 will be further exposed during GCT4.

3.3.2.6 Auxiliary Equipment

Prior to the GCT3 run there were 14 thermocouples installed on individual filter elements to monitor the local temperatures. Among them there were seven thermocouples installed on the top plenum and seven on the bottom plenum. Starting with the GCT2 run the thermocouple wires were routed from the dirty side of the PCD directly to atmosphere through a nitrogen-purged flange on the PCD. The thermocouple wires were sealed using Conax fittings with Teflon sealant. For the GCT3 run the thermocouple wires were routed in the same manner as in GCT2. No leaks through the Conax fittings were noticed during the GCT3 run. Also, all 14 thermocouples gave accurate readings throughout the run.

There was tar accumulation on the back-pulse pipes, particularly in the area where the pipes enter the PCD head and the temperature is lower. The tar was cleaned off to verify that there was no corrosion in this area.

One final note with respect to the back-pulse pipes: after the sand circulation run of December 2000, when the back-pulse pipes were inspected after the sand circulation run, the inner liner of pulse pipe "A" was found to have cracked, rolled inward, and partially obstructed the gas path. The inner liner is a thin sheet metal tube inside the main pulse pipe. The purpose of the inner liner is to reduce the thermal stress on the main pipe when the back-pulse gas is injected. This inner liner has a longitudinal weld seam which had corroded, allowing the pulse gas to get behind the inner liner and roll it into the main gas stream. Material for a new liner could not be obtained on short notice; therefore, one of the pulse pipes from the Foster Wheeler PCD (FL0352) was removed, shortened to the correct length, and installed in the PCD (FL0301) on the Halliburton KBR gasification train.

3.3.3 GCT3 Inspection Summary

No major leakage through the PCD occurred during the GCT3 run and the outlet loading was very low. This is significant because the pressure drop during the GCT3 run was higher than during previous runs. This implies that the modified filter holders provided a better sealing effect on the gaskets than the previous sealing arrangement. The decision was made to continue using the modified filter holder in the GCT4 run.

As seen in GCT2, the Siemens Westinghouse lapped-construction primary gaskets provided good sealing during the GCT3 run. There were no obvious leak paths in the area of the modified filter holder that would indicate leakage past the primary or element flange gaskets.

Therefore, the lapped-construction gaskets will be used during the subsequent (GCT4) gasification run.

The Pall Fe_3Al filter elements performed well during the GCT3 gasification run. The filters were visually inspected and no obvious damage was found. Also, the monolithic SiC filter elements performed well during the run. These filters survived a relatively severe thermal transient event. During inspection, the SiC filters were visually inspected and no obvious damage was found. However, all the monolithic SiC filters were removed because of the likelihood of continued reliability problems with the coal feeder.

The filter element char cake was generally thin, approximately 0.02 in. thick (See Section 3.4). Char build-up on the non-filtration surfaces was not severe; however, char bridging was noted. It was suspected that the char bridging was a result of the filter element support brackets and tar formation during the startup periods.

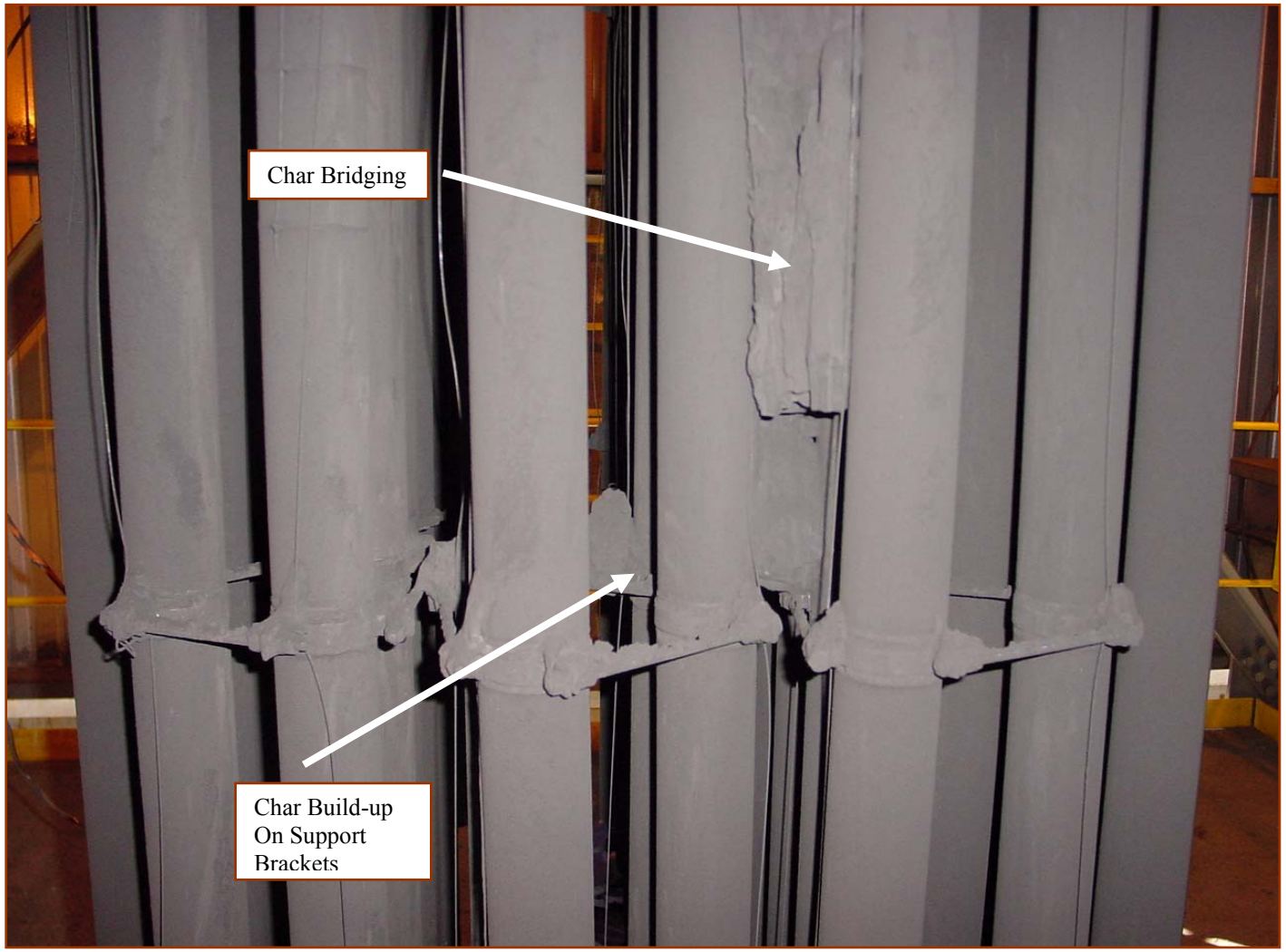

Figure 3.3-1 Char Bridging on the Bottom Plenum

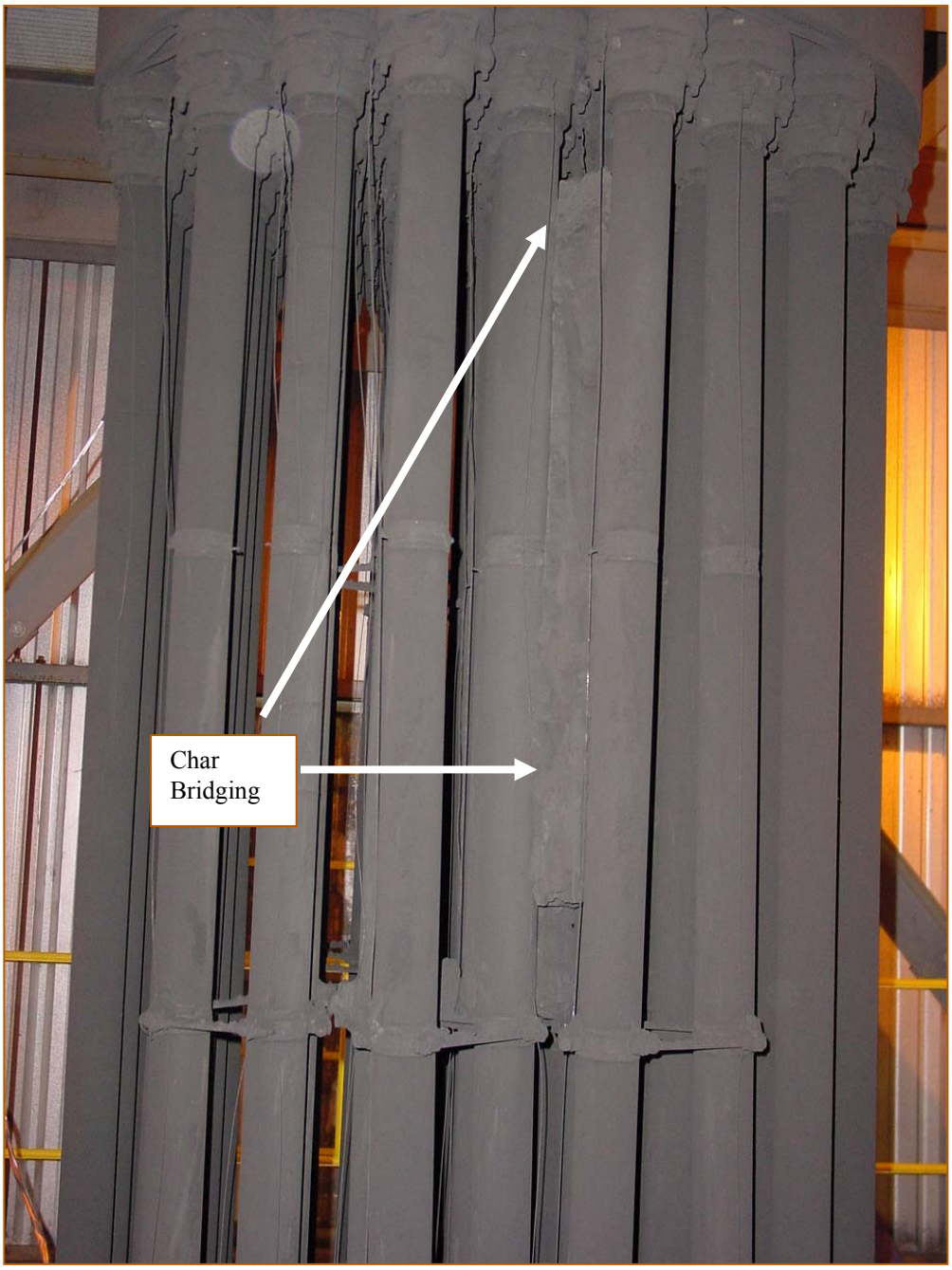

Figure 3.3-2 Char Bridging on the Bottom Plenum

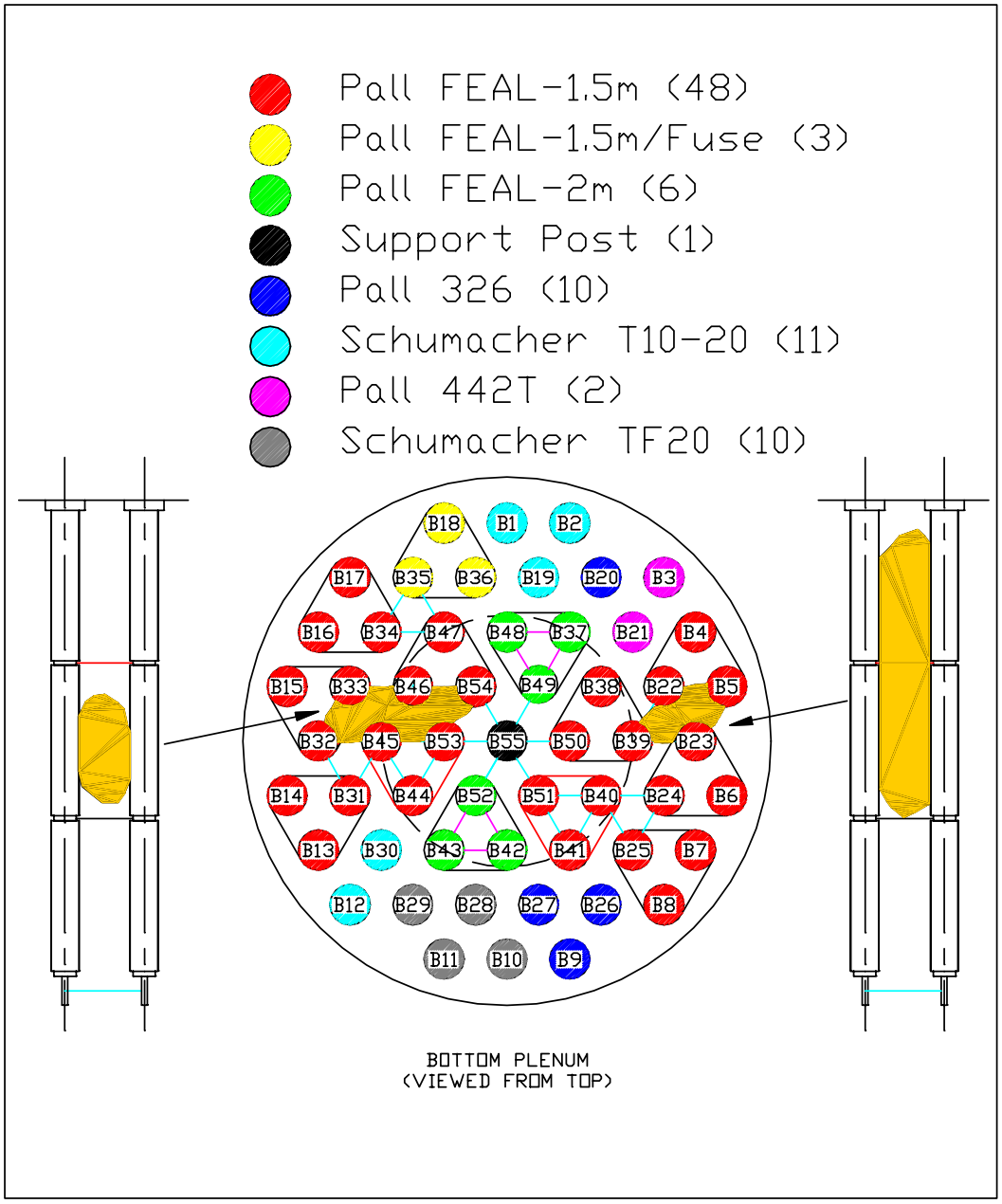

Figure 3.3-3 Location of Char Bridging on the Bottom Plenum

Figure 3.3-4 Mid-level Support Brackets

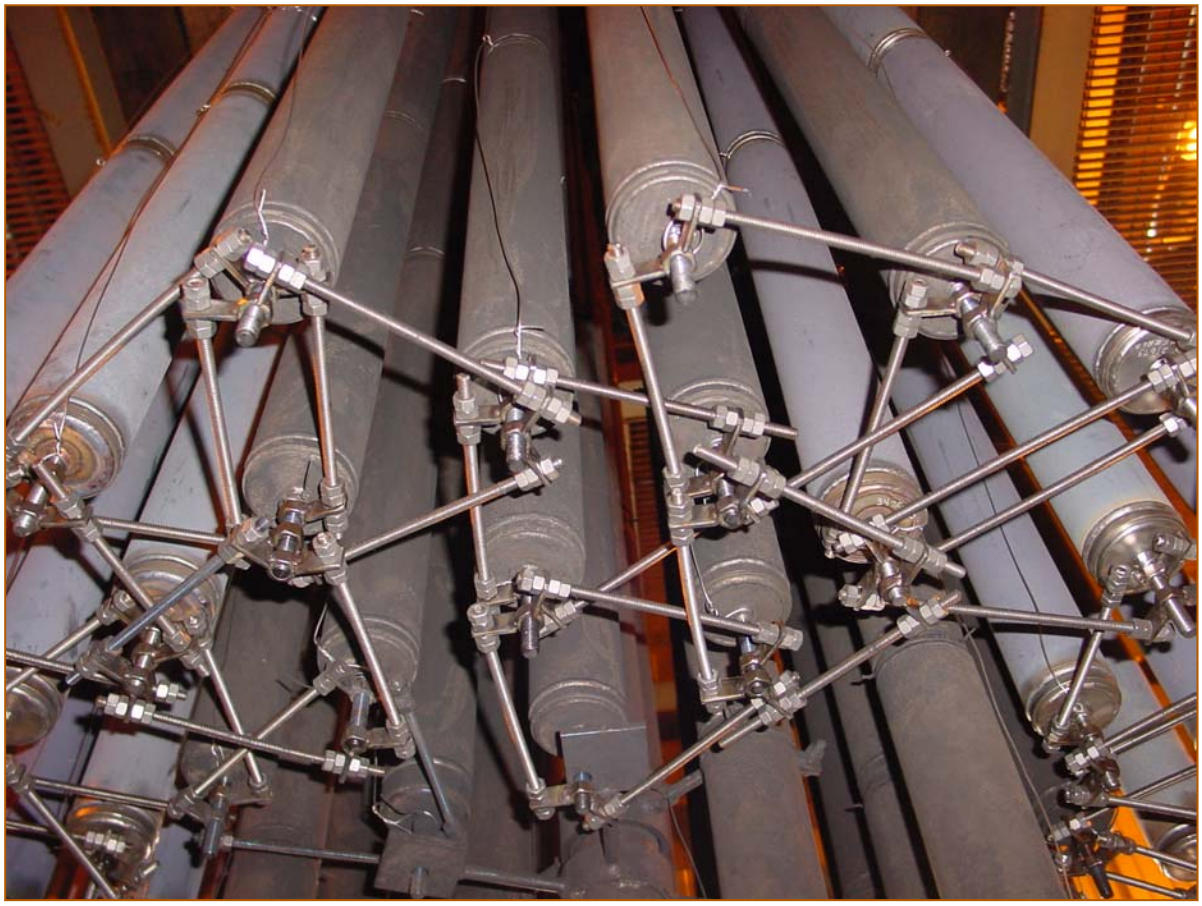

Figure 3.3-5 Bottom Level Support Brackets

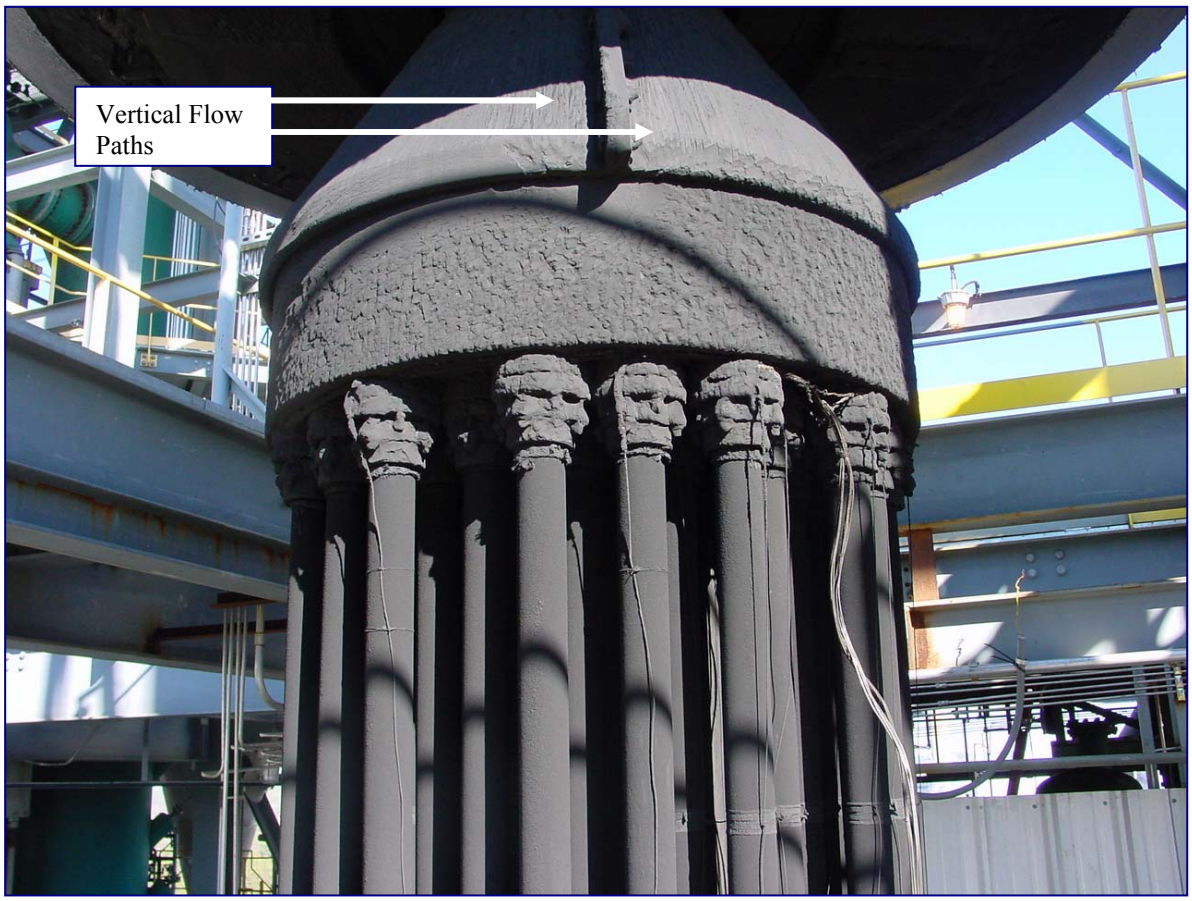

Figure 3.3-6 Flow Pattern on the Top Ash Shed

Figure 3.3-7 Char Accumulation on Shroud and Liner Section

Figure 3.3-8 Clean Side of Tubesheet

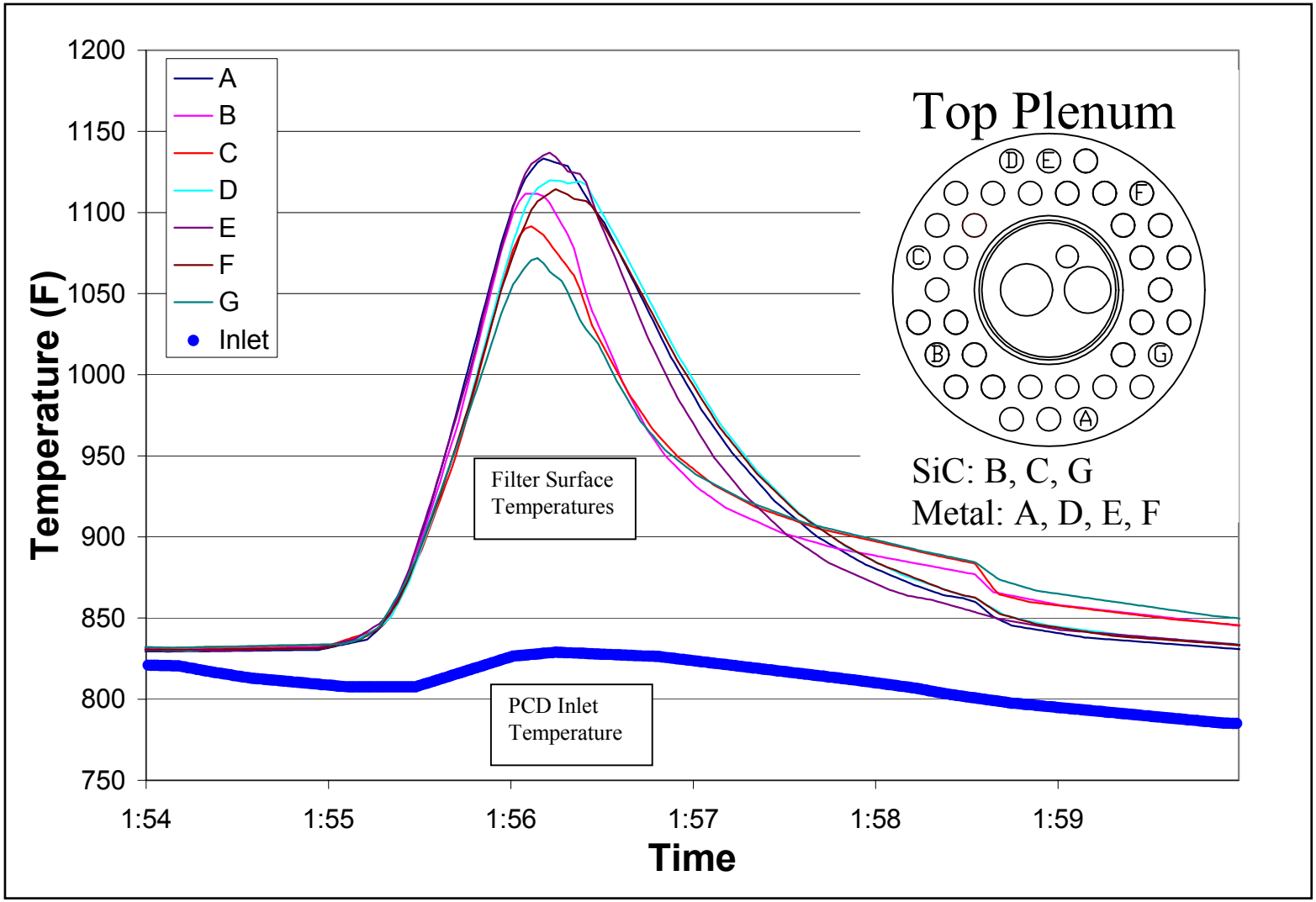

Figure 3.3-9 Thermal Transient Event on January 29, 2001, on the Top Plenum

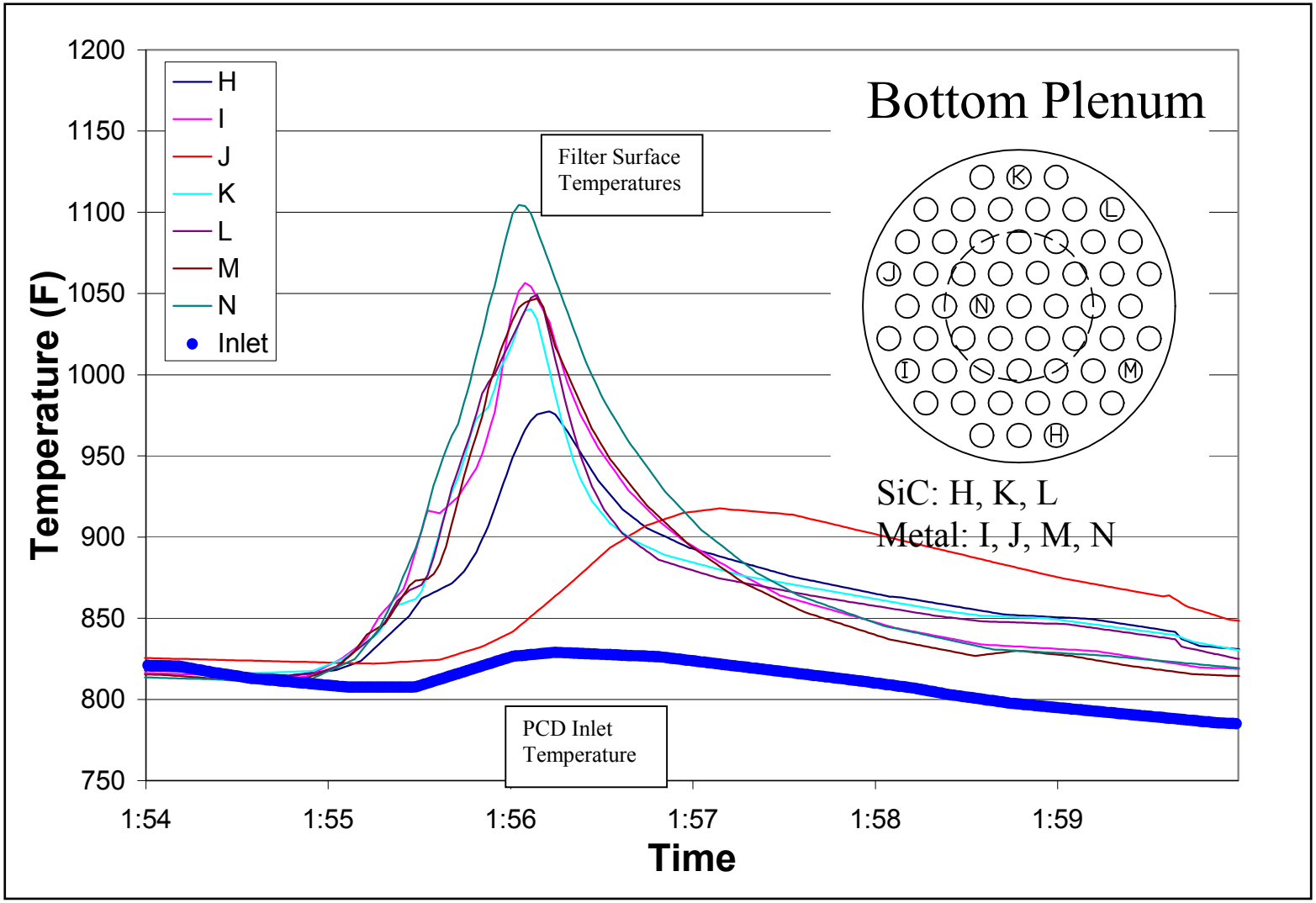

Figure 3.3-10 Thermal Transient Event on January 29, 2001, on the Bottom Plenum

3.4 FILTER ELEMENT TEST RESULTS

Property testing of filter elements continued during this test campaign. The IF&P REECER™, Pall 326 and 181, Schumacher TF20 and T10-20, Schumacher N10-20, and Pall iron aluminide (Fe_3Al) filter elements from GCT1A, GCT1B, and GCT2 operation were tested. Each type of element was tested previously in as-manufactured condition and each, except Pall 181 and Schumacher N10-20, was tested after combustion operation. Data tables shown in this section include the results obtained during only this reporting period on the elements from gasification operation. Previously reported results for as-manufactured elements are included in the graphs to compare properties of as-manufactured material versus properties after gasification. Where it is relevant, properties measured after combustion are also included in the property graphs. One Schumacher T05-20 filter element was also tested in as-manufactured condition to verify that this material is the same as Schumacher TF20 and T10-20 except for the outer membrane. The elements tested and the test matrices are summarized in Tables 3.4-1 through -4. Cutting plans for all elements tested in this test campaign are shown in Figures 3.4-1 through -4. Descriptions of these materials were provided in previous reports (See References 1 and 2) and are not repeated here. Several other types of composite and metal filter elements were used during operation in GCT1A, but property testing was not conducted because their continued use is uncertain in gasification at the PSDF.

3.4.1 Pall Iron Aluminide

Pall iron aluminide elements were not used during GCT2; therefore, one of the two elements from GCT1A, element 034H-004, was selected for property testing. Char was removed from the outside surface to help keep equipment clean during specimen machining and testing. The method used to clean this element was not documented but it was either brushed with a wire brush or pressure washed with water. The element was tested to determine if there was any strength degradation or decrease in ductility during 50 hours of gasification operation.

3.4.1.1 Density

Density was measured on the hoop tensile specimens from GCT1A before testing (See Table 3.4-5). The density ranged from 246 to 248 lbm/ft^3 and the average was 247 lbm/ft^3. The outside surface of the element was cleaned before testing but some char remained in the pores. These density values were calculated based on weights measured with char in the pores and, therefore, do not represent a material property. The values are for comparisons only.

3.4.1.2 Tensile Results

Axial tensile results are summarized in Table 3.4-6 and the stress-strain responses are shown in Figure 3.4-5. Previously reported stress-strain curves for virgin material are also included in this figure. Average tensile properties at room temperature were an ultimate strength of 17,900 psi, yield strength of 11,800 psi, Young's modulus of 5.6 msi, and strain-to-failure of 10.0 mils/inch. Average tensile properties at 1,400°F were an ultimate strength of 5,380 psi, yield strength of 3,200 psi, and Young's modulus of 2.9 msi. Strain-to-failure is not provided at elevated temperature because deformation continued at decreasing load levels well beyond the ultimate

strength. The yield strength was calculated based on a 0.05-percent offset (a line was drawn parallel to the initial slope of the stress-strain curve but offset by 0.0005 and the intersection of this line with the stress-strain curve is the 0.05-percent offset yield strength). These results are nearly the same as for virgin material. The strength was slightly lower (~ 5 percent at room temperature) for the element from GCT1A but the difference is likely due to element-to-element variability, not degradation during operation.

Hoop tensile results are summarized in Table 3.4-7 and the stress-strain responses are shown in Figure 3.4-6. Previously reported stress-strain curves for virgin material are included in this figure. Note that the endpoints of the hoop stress-strain curves are not ultimate strength and strain values. This is because the strain values shown were measured at the outside surface and the corresponding stress values were calculated at the outside surface; however, the maximum stress and strain values, as reported in Table 3.4-7, occur at the inside surface. The ultimate strength appeared unchanged after 50 hours of operation in GCT1A, ranging from ~ 16 to ~ 18 ksi (maximum hydrostatic pressure ranged from 1,060 to 1,100 psig). The stress-strain curves rolled over at a slightly lower stress and extended to a slightly higher maximum strain for the element from GCT1A than the virgin element. As with axial results, this difference in stress-strain response is likely due to element–to-element variability.

3.4.1.3 Flow Test Results

In support of efforts to evaluate the system pressure drop during GCT1A, flow testing of element 034H-003 was conducted. This element was flow tested dirty after removal from GCT1A and then flow tested again after char was removed from the outside surface. The resulting pressure drop versus face velocity curves are shown in Figure 3.4-7. At a face velocity of 5 ft/min (using air at ambient conditions), the pressure drop measured on the element as removed from GCT1A was 27 inH_2O. After cleaning by brushing the outside surface the pressure drop was 17 inH_2O. By comparison, the average pressure drop measured on virgin element Fe_3Al elements at 5 ft/min was 4 inH_2O. The pressure drop versus face velocity measured on element 034H-003 was affected by several factors that are unique to GCT1A, including the high pressure drop during operation and "back-side blinding" due to leaks. Therefore, these results are for use in evaluating the overall system pressure during GCT1A only, and should not be considered an indication of the performance of Fe_3Al elements under typical gasification operating conditions.

3.4.1.4 Summary

Tensile test results showed no evidence of property changes during 50 hours of operation during GCT1A. No conclusions can be drawn from the flow test results because the operating conditions in GCT1A are not typical of what is likely during future gasification operation at the PSDF. Pall Fe_3Al elements will be used extensively during future gasification runs and property evaluations will continue on some of these elements.

3.4.2 Pall 326

Testing was conducted on specimens from four filter elements. Two were tested as removed from GCT2 (char was brushed from the outside surface with a soft brush to help keep equipment clean during specimen machining and testing) to determine if any strength degradation occurred during 200 hours of gasification operation. One was removed from GCT2 and cleaned at Southern Metals Processing (SMP) before testing. One virgin element went through the cleaning process at SMP and was then tested. The two elements that were cleaned at SMP were tested to determine if the cleaning process degraded the elements.

3.4.2.1 Density

Density was measured on the tensile specimens before testing and the results are summarized in Table 3.4-8. The average density was 114 lbm/ft^3. Char may have remained in the pores when the specimens were weighed even though the outside surface was brushed before testing. These densities were calculated based on the measured weights and may have been affected by the char; therefore, the values are for comparisons only and do not represent a material property.

3.4.2.2 Tensile Results

Hoop tensile results are summarized in Table 3.4-9 and the strengths are shown as plotted versus hours in operation in Figure 3.4-8. Like the previous results for virgin elements and combustion elements, the strengths from any particular element were quite consistent but there was definite element-to-element variability. All of the strength values were in the range of 2,000 to 2,500 psi. There was no strength decrease during the 200 hours of operation in GCT2 or during cleaning at SMP. The two elements that were cleaned at SMP had slightly higher strengths than the other two elements from GCT2, but considering the element-to-element variability seen, the cleaning process at SMP appears to have no effect on strength.

3.4.2.3 Flow Test Results

Flow testing was conducted on two elements from GCT2, elements 1326-4 and 1331-1, and one element from GCT1B, element 1310-1. The outside surface of each element was cleaned by vacuuming before the flow test. The resulting pressure drop versus face velocity curves are shown in Figure 3.4-9. At a face velocity of 5 ft/min (using air at ambient conditions), the pressure drop measured on the element from GCT1B was 9.2 inH_2O and the pressure drop measured on the elements after GCT2 was 6.2 inH_2O. By comparison, the pressure drop measured on virgin material was 1.3 inH_2O at the same face velocity. The difference between the pressure drop after GCT1B and GCT2 may have been due to dust leakage past the elements in GCT1B that was eliminated in GCT2.

3.4.2.4 Summary

No degradation in strength was seen in 200 hours of operation in GCT2. The elements cleaned at SMP also showed no strength degradation; therefore, the remaining Pall elements from GCT2 will be sent there for cleaning.

3.4.3 Pall 181

Pall 181 elements were not used during GCT2, so an element from GCT1B was tested to determine if its strength degradation occurred during 160 hours of operation. The filter element was water washed before testing, but some char remained in the pores.

3.4.3.1 Density

Density was measured on the tensile specimens before testing and the results are summarized in Table 3.4-10. The average density was 113 lbm/ft^3, the same as previously measured for virgin material. These densities were calculated based on weights measured with char in the pores and, therefore, do not represent a material property. The values are for comparisons only.

3.4.3.2 Tensile Results

Hoop tensile results are summarized in Table 3.4-11. The average room temperature tensile strength after 160 hours of operation in GCT1B was 2,830 psi, which is the same nominal value as for virgin material.

3.4.3.3 Summary

No property degradation was seen after 160 hours in gasification operation at a nominal temperature of 1,000°F. There are no Pall 181 elements currently in the inventory at the PSDF, but more will be ordered and installed for use during gasification in the future.

3.4.4 Schumacher TF20, T10-20, and T05-20

Testing was conducted on specimens from one T10-20 and two TF20 elements from GCT2. The T10-20 and one of the TF20 elements were tested as removed from GCT2 (char was brushed from the outside surface with a soft brush to help keep equipment clean during testing) to determine if any strength degradation occurred during 200 hours of gasification operation. The other TF20 removed from GCT2 was cleaned at SMP before testing. One virgin T05-20 element was tested to determine if the structural support material (that is, all material except the outer membrane layer) is the same as found in TF20 and T10-20.

3.4.4.1 Density

Density was measured on the tensile specimens before testing; results are summarized in Table 3.4-12. The average density of all TF20 and T10-20 specimens from GCT2 was 120 lbm/ft^3. The TF20 element that was cleaned at SMP had the lowest density (118 lbm/ft^3); however, all

of the TF20 and T10-20 elements from GCT2 had a slightly lower density than virgin or combustion elements. Densities of the virgin and combustion elements ranged from 121 to 124 lbm/ft^3. The measured density values may have been affected by char remaining in the pores after operation, especially in the elements tested as removed from GCT2. The values are for comparisons only and do not represent a material property.

The average density of the virgin T05-20 element was 121 lbm/ft^3.

3.4.4.2 Tensile Results

Hoop tensile results are summarized in Table 3.4-13 and the strengths are shown as plotted versus hours in operation in Figure 3.4-10. Previously reported results for virgin elements and elements from operation in combustion at 1,400°F are included in this figure. The measured strength values ranged from 1,050 to 1,370 psi. This represents a decrease of ~ 30 percent compared to virgin strengths yet is within the range measured after combustion operation. The average strength measured on the TF20 element cleaned at SMP was 1,130 psi, slightly lower than the other two gasification elements, yet it is still within the range of values measured on elements after combustion operation.

The average strength of the virgin T05-20 element was 1,330 psi. While there has been some scatter in the previous virgin tensile strengths, this element has a lower strength than any tested so far. Optical microscopic examination of the test specimens indicated no differences from the previously tested T10-20 and TF20 specimens. SEM and chemical analysis might indicate differences between this T05-20 element and the T10-20 and TF20 elements; however, such analyses have not been conducted.

3.4.4.3 Thermal Expansion

Thermal expansion of one virgin T05-20 specimen is shown as plotted in Figure 3.4-11 along with the expansion of TF20. The average coefficient of thermal expansion from 500 to 1,500°F was 2.6×10^{-6}/°F. The expansion of T05-20 was the same as the expansion of TF20.

3.4.4.4 Flow Test Results

Flow testing was conducted on two TF20 and two T10-20 elements from GCT2. The outside surface of each element was cleaned by vacuuming before the flow test. The resulting pressure drop versus face velocity curves are shown in Figure 3.4-12. At a face velocity of 5 ft/min (using air at ambient conditions), the pressure drop measured on the elements from GCT2 was 6.1 inH_2O for TF20 and 9.4 inH_2O for T10-20. By comparison, the pressure drop measured on virgin material at the same face velocity was 2.1 inH_2O for TF20 and 4.4 inH_2O for T10-20. One virgin T05-20 element was flow tested and a pressure drop of 5.4 inH_2O at a face velocity of 5 ft/min was obtained (again using air at ambient conditions).

3.4.4.5 Summary

The hoop tensile strength of TF20 and T10-20 decreased by ~ 30 percent as compared to previously reported virgin strengths during 200 hours of operation at 1,000°F in GCT2. This is

about the same strength decrease as seen during the first 500 hours of operation at 1,400°F in combustion. Further testing following gasification operation in the future will determine if the strength levels off after this initial decrease as in combustion. The strength retained after 200 hours of operation is sufficient if no further decrease is seen. Since there was no strength degradation due to cleaning at SMP the remaining GCT2 elements will be sent for cleaning.

3.4.5 Schumacher N10-20

Testing was conducted on specimens from one Schumacher N10-20 filter element after operation in GCT2. The element was tested as removed from the PCD (char was brushed from the outside surface with a soft brush to help keep equipment clean during testing) to determine if any strength degradation occurred during 200 hours of gasification operation.

3.4.5.1 Density

Density was measured on the tensile specimens before testing and the results are summarized in Table 3.4-14. The average density was 122 lbm/ft^3, nearly unchanged from the virgin density. These densities may have been affected by char in the pores and, therefore, do not represent a material property. The values are for comparisons only.

3.4.5.2 Tensile Results

Hoop tensile results are summarized in Table 3.4-15 and the strength is shown as plotted versus hours in operation in Figure 3.4-13. Note that the x-axis in this figure (hours in operation) extends out to 3,000 although no N10-20 element has more than 200 hours in operation. This is to keep the scale on the x-axis the same for all materials. The average room temperature tensile strength after 200 hours of operation in GCT2 was 2,330 psi. This is slightly lower than the average strength of 2,530 psi previously reported for virgin material; however, the difference may be due to element-to-element variability rather than strength degradation during operation.

3.4.5.3 Summary

There was a small strength difference of ~ 8 percent between the N10-20 element from GCT2 and the virgin element, probably representative of element-to-element variability. Testing of these elements after more operation in gasification will help determine if the strength difference was due to element-to-element variability or to strength degradation during operation.

3.4.6 IF&P REECER™

Testing was conducted on specimens from one IF&P REECER™ filter element after operation in GCT1A. Char was removed from the outside surface to help keep equipment clean during specimen machining and testing. The method used to clean this element was not documented, but it was either brushed with a wire brush or was pressure washed with water. Hoop tensile strength was measured to determine if any strength degradation occurred during 50 hours of gasification operation. The filter element tested in this effort was from the same manufactured "batch" as the four elements previously tested, two virgin and two from combustion operation,

and the same manufacturer anomalies were seen. Wall thickness varied along the length of the elements by ~ 0.05 to 0.10 inch and "bubbles" up to ~ 1/8 inch in diameter were seen in the element walls. Some of these bubbles were internal and some extended to the inside surface. None extended to the outside surface. There was no evidence that these manufacturer anomalies have affected performance during operation; however, IF&P is working to prevent these anomalies in the future.

3.4.6.1 Density

Density was measured on the tensile specimens before testing and the results are summarized in Table 3.4-16. The average density was 150 lbm/ft^3, nearly the same as previously measured on these elements following combustion operation. These densities may have been affected by char in the pores and, therefore, do not represent a material property. The values are for comparisons only.

3.4.6.2 Tensile Results

Hoop tensile results are summarized in Table 3.4-17 and strength is shown as plotted versus hours in operation in Figure 3.4-14. Previously reported results for virgin as well as combustion elements are included for comparison in this figure. No change in strength was seen after 50 hours of operation at 1,000°F in GCT1A. All of these element specimens failed at the "bubble" as discussed above. Earlier test results for virgin and combustion elements indicate that these bubbles did not decrease strength; since these specimens had approximately the same strength as the virgin specimens the bubbles apparently did not cause a strength decrease in these specimens either.

3.4.6.3 Summary

The IF&P REECER™ elements that have been used so far during operation at the PSDF (four in combustion at 1,400°F and one in gasification at 1,000°F) have been successful. No evidence of strength degradation has been seen. During combustion operation these elements have survived thermal transients that led to failure of monolithic oxide and clay-bonded SiC elements. There have been some manufacturing anomalies seen, including the inconsistent wall thickness and "bubbles" mentioned above; however, these anomalies have not led to element failures. Future plans at the PSDF include more use of these elements and property measurements after operation to help predict long-term performance. There are no REECER™ elements currently in the inventory at the PSDF but more have been ordered.

3.4.7 References

1. "Technical Progress Report for Kellogg Brown & Root Transport Reactor Train With Siemens Westinghouse Particulate Control Device: TC04 Report, October 14 – 17, 1998, " Prepared by Southern Company Services, DOE Cooperative Agreement Number DE-FC21-90MC25140.

2. "Technical Progress for Kellogg Brown & Root Transport Reactor Train With Siemens Westinghouse Particulate Control Device: GCT2 Report, April 10 – April 27, 2000," Prepared by Southern Company Services, DOE Cooperative Agreement Number DE-FC21-90MC25140

Table 3.4-1

Filter Elements Tested

Material	Manufacturer Candle ID	Run	Operation Hours	Test Matrix
Pall Fe_3Al	034H-004	GCT1A	50	1
Pall 326	1318-1		virgin[1]	2
Pall 326	1322-2	GCT2	200	2
Pall 326	1316-6	GCT2	200	2
Pall 326	1339	GCT2	200[1]	2
Pall 181	1406H-2	GCT1B	160	2
Schumacher T05-20	324H21		virgin	3
Schumacher T10-20	335I297	GCT2	200	2
Schumacher TF20	326I121	GCT2	200	2
Schumacher TF20	326I126	GCT2	200[1]	2
Schumacher N10-20	354I39	GCT2	200	2
IF&P REECER™	FE98073104	GCT1A	50	2

Note: 1. Element was cleaned at Southern Metal Processing before testing.

Table 3.4-2

Test Matrix 1

Test	Direction	Number of Tests at Room Temperature
Tension	Hoop	6
Tension	Axial	5
Microstructure – optical, SEM, EDX, as required		Yes

Table 3.4-3

Test Matrix 2

Test	Direction	Number of Tests at Room Temperature
Tension	Hoop	6
Microstructure – optical, SEM, EDX, as required		Yes

Table 3.4-4

Test Matrix 3

Test	Direction	Number of Tests at Room Temperature	Number of Tests at 2,000°F
Tension	Hoop	6	
Thermal Expansion	Axial	1---------->	
Microstructure – optical, SEM, EDX, as required		Yes	

Table 3.4-5

Density of Pall Fe_3Al After Gasification Operation

Element	Specimen Number	Hours in Operation	I.D. (in.)	O.D. (in.)	Density (gr/cm^3)	Density (lb/ft^3)	Remarks
034H-004	Tn-Hoop-342	50	2.21	2.37	3.97	248	Notes 1,2
034H-004	Tn-Hoop-343	50	2.21	2.36	3.95	246	Notes 1,2
034H-004	Tn-Hoop-344	50	2.21	2.36	3.94	246	Notes 1,2
034H-004	Tn-Hoop-345	50	2.22	2.36	3.97	247	Notes 1,2
034H-004	Tn-Hoop-346	50	2.20	2.35	3.95	247	Notes 1,2
034H-004	Tn-Hoop-347	50	2.20	2.35	3.97	248	Notes 1,2
		Average			3.96	247	
		Standard Deviation			0.012	0.72	
		Coefficient of Variation (COV)			0.29%	0.29%	

Notes:
1. Elements were water washed before density measurements but some char remained in the pores. Density values were calculated based on weights measured with char in the pores and therefore do not represent a material property. The values are for comparison only.
2. All operation at SCS - PSDF in gasification mode at a nominal temperature of 1,000°F.

Table 3.4-6

Axial Tensile Results for Pall Fe_3Al After Gasification Operation

Candle	Specimen Number	Hours in Operation	Test Temperature (°F)	0.05% Yield Strength (psi)	Ultimate Strength (psi)	Young's Modulus (msi)	Strain-to-Failure[1] (mils/in.)	Remarks
034H-004	Tn-Ax-10	50	RT[2]	11390	17770	5.63	10.5	Note 3
034H-004	Tn-Ax-12	50	RT	12470	18010	5.45	9.50	Note 3
034H-004	Tn-Ax-14	50	RT	11460	17950	5.70	10.1	Note 3
			Average	11773	17910	5.59	10.0	
034H-004	Tn-Ax-11	50	1400		5200			Notes 3,4
034H-004	Tn-Ax-13	50	1400	3190	5320	3.30	>10.5	Note 3
034H-004	Tn-Ax-15	50	1400	3210	5610	2.58	>13.6	Note 3
			Average	3200	5377	2.94		

Notes:
1. The specimens tested at room temperature failed at this strain level. For the elevated temperature specimens, the > sign indicates that this value is the strain level at maximum stress. These specimens continued to deform beyond this point with decreasing load.
2. RT = Room Temperature
3. All operation at SCS - PSDF in gasification mode at a nominal temperature of 1000°F.
4. Strain measurements were not obtained because the extensometers slipped during the test.

Table 3.4-7

Hoop Tensile Results for Pall Fe_3Al After Gasification Operation

Candle	Specimen Number	Hours in Operation	Maximum Hydrostatic Pressure (psig)	Ultimate Strength (psi)	Young's Modulus (msi)	Maximum Strain at O.D. (mils/in.)	Remarks
034H-004	Tn-Hoop-342	50	1100	16700	5.34	5.97	Note 1
034H-004	Tn-Hoop-343	50	1120	16800	5.59	6.26	Note 1
034H-004	Tn-Hoop-344	50	1090	16210	5.46	5.51	Note 1
034H-004	Tn-Hoop-345	50	1070	17190	5.72	6.79	Note 1
034H-004	Tn-Hoop-346	50	1180	17680	5.74	7.6	Note 1
034H-004	Tn-Hoop-347	50	1140	17220	5.70	6.50	Note 1
Average			1117	16967	5.59	6.44	
Standard Deviation			36	464	0.15	0.66	
Coefficient of Variation (COV)			3%	3%	3%	10%	

Notes: 1. All operation at SCS - PSDF in gasification mode at a nominal operating temperature of 1000°F.

Table 3.4-8

Density of Pall 326

Element	Specimen Number	Hours in Operation	I.D. (in.)	O.D. (in.)	Density (gr/cm³)	Density (lb/ft³)	Remarks
1318-8	Tn-Hoop-461	Virgin	1.55	2.37	1.81	113	Note 1
1318-8	Tn-Hoop-462	Virgin	1.55	2.37	1.80	112	Note 1
1318-8	Tn-Hoop-463	Virgin	1.57	2.38	1.81	113	Note 1
1318-8	Tn-Hoop-464	Virgin	1.57	2.38	1.80	113	Note 1
1318-8	Tn-Hoop-465	Virgin	1.60	2.36	1.81	113	Note 1
1318-8	Tn-Hoop-466	Virgin	1.60	2.35	1.81	113	Note 1
		Average			1.81	113	
		Standard Deviation			0.003	0.17	
		Coefficient of Variation (COV)			0.15%	0.15%	
1322-2	Tn-Hoop-407	200	1.55	2.36	1.84	115	Notes 2,3
1322-2	Tn-Hoop-408	200	1.55	2.37	1.83	114	Notes 2,3
1322-2	Tn-Hoop-409	200	1.58	2.38	1.83	114	Notes 2,3
1322-2	Tn-Hoop-410	200	1.58	2.38	1.83	114	Notes 2,3
1322-2	Tn-Hoop-411	200	1.60	2.37	1.83	114	Notes 2,3
1322-2	Tn-Hoop-412	200	1.60	2.36	1.83	114	Notes 2,3
		Average			1.83	114	
		Standard Deviation			0.004	0.27	
		Coefficient of Variation (COV)			0.24%	0.24%	
1316-6	Tn-Hoop-413	200	1.55	2.36	1.84	115	Notes 2,3
1316-6	Tn-Hoop-414	200	1.55	2.36	1.83	114	Notes 2,3
1316-6	Tn-Hoop-415	200	1.58	2.37	1.83	114	Notes 2,3
1316-6	Tn-Hoop-416	200	1.58	2.37	1.83	114	Notes 2,3
1316-6	Tn-Hoop-417	200	1.60	2.37	1.83	114	Notes 2,3
1316-6	Tn-Hoop-418	200	1.60	2.36	1.83	114	Notes 2,3
		Average			1.83	114	
		Standard Deviation			0.004	0.27	
		Coefficient of Variation (COV)			0.24%	0.24%	
1339	Tn-Hoop-449	200	1.55	2.36	1.84	115	Notes 2,3,4
1339	Tn-Hoop-450	200	1.55	2.37	1.84	115	Notes 2,3,4
1339	Tn-Hoop-451	200	1.57	2.38	1.83	114	Notes 2,3,4
1339	Tn-Hoop-452	200	1.58	2.38	1.83	114	Notes 2,3,4
1339	Tn-Hoop-453	200	1.60	2.37	1.83	114	Notes 2,3,4
1339	Tn-Hoop-454	200	1.60	2.37	1.83	114	Notes 2,3,4
		Average			1.83	114	
		Standard Deviation			0.006	0.39	
		Coefficient of Variation (COV)			0.34%	0.34%	

1. Element went through cleaning process at Southern Metals Processing in virgin condition.
2. All operation at SCS - PSDF in gasification mode at a nominal temperature of 1000°F.
3. Char was brushed off the outside surface with a soft brush before density measurements but some char remained in the pores. Density values were calculated based on weights measured with char in the pores and therefore do not represent a material property. The values are for comparison only.
4. Elements were cleaned at Southern Metals Processing before density measurements but some char remained in the pores. Density values were calculated based on weights measured with char in the pores and therefore do not represent a material property. The values are for comparison only.

Table 3.4-9

Room Temperature Hoop Tensile Strength of Pall 326

Element	Specimen Number	Hours in Operation	Maximum Hydrostatic Pressure (psig)	Ultimate Strength (psi)	Remarks
1318-8	Tn-Hoop-461	virgin	930	2310	Note 1
1318-8	Tn-Hoop-462	virgin	900	2250	Note 1
1318-8	Tn-Hoop-463	virgin	910	2320	Note 1
1318-8	Tn-Hoop-464	virgin	880	2270	Note 1
1318-8	Tn-Hoop-465	virgin	820	2200	Note 1
1318-8	Tn-Hoop-466	virgin	850	2290	Note 1
	Average		882	2273	
	Standard Deviation		37	40	
	COV		4.2%	1.8%	
1322-2	Tn-Hoop-407	200	820	2070	Note 2
1322-2	Tn-Hoop-408	200	840	2120	Note 2
1322-2	Tn-Hoop-409	200	820	2100	Note 2
1322-2	Tn-Hoop-410	200	810	2080	Note 2
1322-2	Tn-Hoop-411	200	760	2050	Note 2
1322-2	Tn-Hoop-412	200	740	2010	Note 2
	Average		798	2072	
	Standard Deviation		36	35	
	COV		4.5%	1.7%	
1316-6	Tn-Hoop-413	200	870	2190	Note 2
1316-6	Tn-Hoop-414	200	850	2150	Note 2
1316-6	Tn-Hoop-415	200	790	2030	Note 2
1316-6	Tn-Hoop-416	200	770	1990	Note 2
1316-6	Tn-Hoop-417	200	800	2140	Note 2
1316-6	Tn-Hoop-418	200	790	2120	Note 2
	Average		812	2103	
	Standard Deviation		36	70	
	COV		4.4%	3.3%	
1339	Tn-Hoop-449	200	910	2270	Notes 1,2
1339	Tn-Hoop-450	200	1000	2510	Notes 1,2
1339	Tn-Hoop-451	200	900	2300	Notes 1,2
1339	Tn-Hoop-452	200	920	2360	Notes 1,2
1339	Tn-Hoop-453	200	920	2450	Notes 1,2
1339	Tn-Hoop-454	200	890	2410	Notes 1,2
	Average		923	2383	
	Standard Deviation		36	83	
	COV		3.9%	3.5%	

Notes:
1. Element went through cleaning process at Southern Metals Processing.
2. All operation at SCS - PSDF in gasification mode at a nominal operating temperature of 1000°F.

Table 3.4-10

Density of Pall 181

Element	Specimen Number	Hours in Operation	I.D. (in.)	O.D. (in.)	Density (gr/cm³)	Density (lb/ft³)	Remarks
1406H-2	Tn-Hoop-419	160	1.55	2.37	1.84	115	Notes 1,2
1406H-2	Tn-Hoop-420	160	1.55	2.36	1.84	115	Notes 1,2
1406H-2	Tn-Hoop-421	160	1.57	2.37	1.80	113	Notes 1,2
1406H-2	Tn-Hoop-422	160	1.57	2.36	1.80	112	Notes 1,2
1406H-2	Tn-Hoop-423	160	1.60	2.35	1.80	112	Notes 1,2
1406H-2	Tn-Hoop-424	160	1.60	2.34	1.80	112	Notes 1,2
		Average			1.81	113	
		Standard Deviation			0.020	1.23	
		Coefficient of Variation (COV)			1.08%	1.08%	

1. Elements were water washed before density measurements but some ash/char remained in the pores. Density values were calculated based on weights measured with ash/char in the pores and therefore do not represent a material property. The values are for comparison only.
2. All operation at SCS - PSDF in gasification mode at a nominal operating temperature of 1000°F.

Table 3.4-11

Room Temperature Hoop Tensile Strength of Pall 181

Element	Specimen Number	Hours in Operation	Maximum Hydrostatic Pressure (psig)	Ultimate Strength (psi)	Remarks
1406H-2	Tn-Hoop-419	160	1150	2880	Note 1
1406H-2	Tn-Hoop-420	160	1190	3000	Note 1
1406H-2	Tn-Hoop-421	160	1130	2920	Note 1
1406H-2	Tn-Hoop-422	160	1000	2610	Note 1
1406H-2	Tn-Hoop-423	160	1020	2780	Note 1
1406H-2	Tn-Hoop-424	160	1020	2780	Note 1
Average			1085	2828	
Standard Deviation			74	124	
Coefficient of Variation (COV)			7%	4%	

Notes: 1. All operation at SCS - PSDF in gasification mode at a nominal operating temperature of 1000°F.

Table 3.4-12

Density of Schumacher TF20, T10-20, and T05-20

Material	Element	Specimen Number	Hours in Operation	I.D. (in.)	O.D. (in.)	Density (gr/cm³)	Density (lb/ft³)	Remarks
T05-20	324H21	Tn-Hoop-1	Virgin	1.56	2.38	1.95	121	
T05-20	324H21	Tn-Hoop-2	Virgin	1.56	2.38	1.94	121	
T05-20	324H21	Tn-Hoop-3	Virgin	1.59	2.38	1.95	122	
T05-20	324H21	Tn-Hoop-4	Virgin	1.59	2.38	1.95	122	
T05-20	324H21	Tn-Hoop-5	Virgin	1.60	2.39	1.94	121	
T05-20	324H21	Tn-Hoop-6	Virgin	1.61	2.38	1.94	121	
	Average					1.94	121	
	Standard Deviation					0.006	0.35	
	Coefficient of Variation (COV)					0.29%	0.29%	
T10-20	335I297	Tn-Hoop-425	200	1.53	2.38	1.94	121	Notes 1,2
T10-20	335I297	Tn-Hoop-426	200	1.54	2.38	1.95	121	Notes 1,2
T10-20	335I297	Tn-Hoop-427	200	1.57	2.38	1.93	120	Notes 1,2
T10-20	335I297	Tn-Hoop-428	200	1.57	2.38	1.93	121	Notes 1,2
T10-20	335I297	Tn-Hoop-429	200	1.58	2.38	1.92	120	Notes 1,2
T10-20	335I297	Tn-Hoop-430	200	1.58	2.38	1.91	119	Notes 1,2
	Average					1.93	120	
	Standard Deviation					0.011	0.71	
	Coefficient of Variation (COV)					0.59%	0.59%	
TF20	326I121	Tn-Hoop-431	200	1.53	2.37	1.93	120	Notes 1,2
TF20	326I121	Tn-Hoop-432	200	1.55	2.37	1.94	121	Notes 1,2
TF20	326I121	Tn-Hoop-433	200	1.57	2.38	1.92	120	Notes 1,2
TF20	326I121	Tn-Hoop-434	200	1.58	2.38	1.92	120	Notes 1,2
TF20	326I121	Tn-Hoop-435	200	1.59	2.38	1.92	120	Notes 1,2
TF20	326I121	Tn-Hoop-436	200	1.59	2.38	1.92	120	Notes 1,2
	Average					1.92	120	
	Standard Deviation					0.008	0.48	
	Coefficient of Variation (COV)					0.40%	0.40%	
TF20	326I126	Tn-Hoop-455	200	1.53	2.38	1.90	118	Notes 1,3
TF20	326I126	Tn-Hoop-456	200	1.55	2.38	1.90	118	Notes 1,3
TF20	326I126	Tn-Hoop-457	200	1.57	2.38	1.89	118	Notes 1,3
TF20	326I126	Tn-Hoop-458	200	1.57	2.38	1.89	118	Notes 1,3
TF20	326I126	Tn-Hoop-459	200					Notes 1,3,4
TF20	326I126	Tn-Hoop-460	200					Notes 1,3,4
	Average					1.89	118	
	Standard Deviation					0.002	0.15	
	Coefficient of Variation (COV)					0.13%	0.13%	

Notes:
1. All operation at SCS - PSDF in gasification mode at a nominal temperature of 1000°F.
2. Char was brushed off the outside surface with a soft brush before density measurements but some char remained in the pores. Density values were calculated based on weights measured with char in the pores and therefore do not represent a material property. The values are for comparison only.
3. Element was cleaned at Southern Metals Processing before density measurements but some char remained in the pores. Density values were calculated based on weights measured with char in the pores and therefore do not represent a material property. The values are for comparison only.
4. Density was not measured.

Table 3.4-13

Hoop Tensile Strength of Schumacher TF20, T10-20, and T05-20

Material	Element	Specimen Number	Hours in Operation	Maximum Hydrostatic Pressure (psig)	Ultimate Strength (psi)	Remarks
T05-20	324H21	Tn-Hoop-1	Virgin	540	1350	
T05-20	324H21	Tn-Hoop-2	Virgin	540	1360	
T05-20	324H21	Tn-Hoop-3	Virgin	510	1340	
T05-20	324H21	Tn-Hoop-4	Virgin	520	1360	
T05-20	324H21	Tn-Hoop-5	Virgin	500	1330	
T05-20	324H21	Tn-Hoop-6	Virgin	460	1240	
	Average			512	1330	
	Standard Deviation			27	42	
	COV			5%	3%	
T10-20	335I297	Tn-Hoop-425	200	530	1270	Note 1
T10-20	335I297	Tn-Hoop-426	200	530	1290	Note 1
T10-20	335I297	Tn-Hoop-427	200	460	1160	Note 1
T10-20	335I297	Tn-Hoop-428	200	460	1160	Note 1
T10-20	335I297	Tn-Hoop-429	200	470	1220	Note 1
T10-20	335I297	Tn-Hoop-430	200	460	1180	Note 1
	Average			485	1213	
	Standard Deviation			32	52	
	COV			7%	4%	
TF20	326I121	Tn-Hoop-431	200	560	1370	Note 1
TF20	326I121	Tn-Hoop-432	200	510	1270	Note 1
TF20	326I121	Tn-Hoop-433	200	470	1210	Note 1
TF20	326I121	Tn-Hoop-434	200	480	1220	Note 1
TF20	326I121	Tn-Hoop-435	200	520	1360	Note 1
TF20	326I121	Tn-Hoop-436	200	460	1190	Note 1
	Average			500	1270	
	Standard Deviation			34	71	
	COV			7%	6%	
TF20	326I126	Tn-Hoop-455	200	510	1230	Notes 1,2
TF20	326I126	Tn-Hoop-456	200	490	1200	Notes 1,2
TF20	326I126	Tn-Hoop-457	200	430	1090	Notes 1,2
TF20	326I126	Tn-Hoop-458	200	440	1120	Notes 1,2
TF20	326I126	Tn-Hoop-459	200	410	1050	Notes 1,2
TF20	326I126	Tn-Hoop-460	200	420	1070	Notes 1,2
	Average			450	1127	
	Standard Deviation			37	66	
	COV			8%	6%	

Notes: 1. All operation at SCS - PSDF in gasification mode at a nominal operating temperature of 1000°F.
2. Element went through cleaning process at Southern Metals Processing.

Table 3.4-14

Density of Schumacher N10-20

Candle	Specimen Number	Hours in Operation	I.D. (in.)	O.D. (in.)	Density (gr/cm³)	Density (lb/ft³)	Remarks
354I39	Tn-Hoop-437	200	1.52	2.37	1.94	121	Notes 1,2
354I39	Tn-Hoop-438	200	1.53	2.37	1.95	122	Notes 1,2
354I39	Tn-Hoop-439	200	1.56	2.36	1.96	122	Notes 1,2
354I39	Tn-Hoop-440	200	1.57	2.37	1.95	122	Notes 1,2
354I39	Tn-Hoop-441	200	1.58	2.37	1.95	122	Notes 1,2
354I39	Tn-Hoop-442	200	1.58	2.37	1.95	122	Notes 1,2
		Average			1.95	122	
		Standard Deviation			0.004	0.28	
		Coefficient of Variation (COV)			0.23%	0.23%	

Notes: 1. All operation at SCS - PSDF in gasification mode at a nominal temperature of 1000°F.
2. Char was brushed off the outside surface with a soft brush before density measurements but some char remained in the pores. Density values were calculated based on weights measured with char in the pores and therefore do not represent a material property. The values are for comparison only.

Table 3.4-15

Room Temperature Hoop Tensile Results for Schumacher N10-20

Element	Specimen Number	Hours in Operation	Maximum Hydrostatic Pressure (psig)	Ultimate Strength (psi)	Remarks
354I39	Tn-Hoop-437	200	980	2350	Note 1
354I39	Tn-Hoop-438	200	1020	2500	Note 1
354I39	Tn-Hoop-439	200	940	2410	Note 1
354I39	Tn-Hoop-440	200	890	2270	Note 1
354I39	Tn-Hoop-441	200	830	2160	Note 1
354I39	Tn-Hoop-442	200	890	2300	Note 1
Average			925	2332	
Standard Deviation			63	107	
Coefficient of Variation (COV)			7%	5%	

Notes: 1. All operation at SCS - PSDF in gasification mode at a nominal temperature of 1000°F.

Table 3.4-16

Density of IF&P REECER™

Element	Specimen Number	Hours in Operation	I.D. (in.)	O.D. (in.)	Density (gr/cm³)	Density (lb/ft³)	Remarks
FE98073104	Tn-Hoop-443	50	1.58	2.40	2.39	149	Notes 1,2
FE98073104	Tn-Hoop-444	50	1.60	2.40	2.42	151	Notes 1,2
FE98073104	Tn-Hoop-445	50	1.67	2.40	2.39	149	Notes 1,2
FE98073104	Tn-Hoop-446	50	1.67	2.40	2.40	150	Notes 1,2
FE98073104	Tn-Hoop-447	50	1.75	2.40	2.43	152	Notes 1,2
FE98073104	Tn-Hoop-448	50					Notes 1,2,3
Average					2.41	150	
Standard Deviation					0.017	1.04	
Coefficient of Variation (COV)					0.70%	0.70%	

Notes:
1. All operation at SCS - PSDF in gasification mode at a nominal temperature of 1000°F.
2. Char was brushed off the outside surface with a soft brush before density measurements but some char remained in the pores. Density values were calculated based on weights measured with char in the pores and therefore do not represent a material property. The values are for comparison only.
3. Density not measured.

Table 3.4-17

Room Temperature Hoop Tensile Results for IF&P REECER™

Candle	Specimen Number	Hours in Operation	Maximum Hydrostatic Pressure (psig)	Ultimate Strength (psi)	Remarks
FE98073104	Tn-Hoop-443	50	760	1920	Notes 1,2
FE98073104	Tn-Hoop-444	50	690	1790	Notes 1,2
FE98073104	Tn-Hoop-445	50	790	2280	Notes 1,2
FE98073104	Tn-Hoop-446	50	760	2210	Notes 1,2
FE98073104	Tn-Hoop-447	50	700	2280	Notes 1,2
FE98073104	Tn-Hoop-448	50	670	2150	Notes 1,2
Average			728	2105	
Standard Deviation			44	186	
COV			6%	9%	

Notes:
1. All operation at SCS - PSDF in gasification mode at a nominal temperature of 1000°F.
2. Elements had "bubbles" up to ~1/8 inch diameter in the wall. All specimens failed at a bubble. All REECER elements tested so far had similar bubbles. There has been no evidence that these bubbles affected performance but the manufacturer is working to eliminate them.

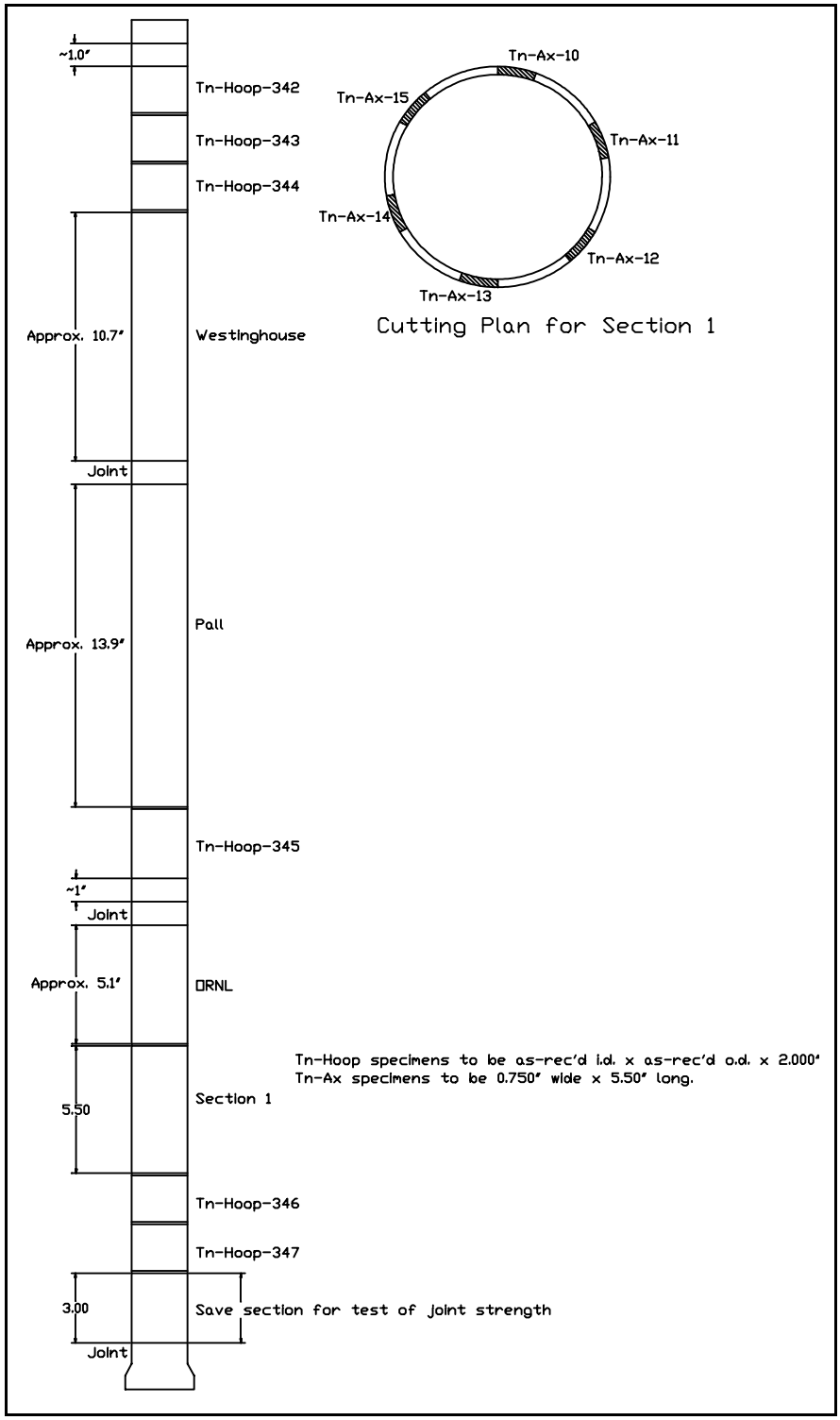

Figure 3.4-1 Cutting Plan for Pall Fe_3Al Element 034H-004

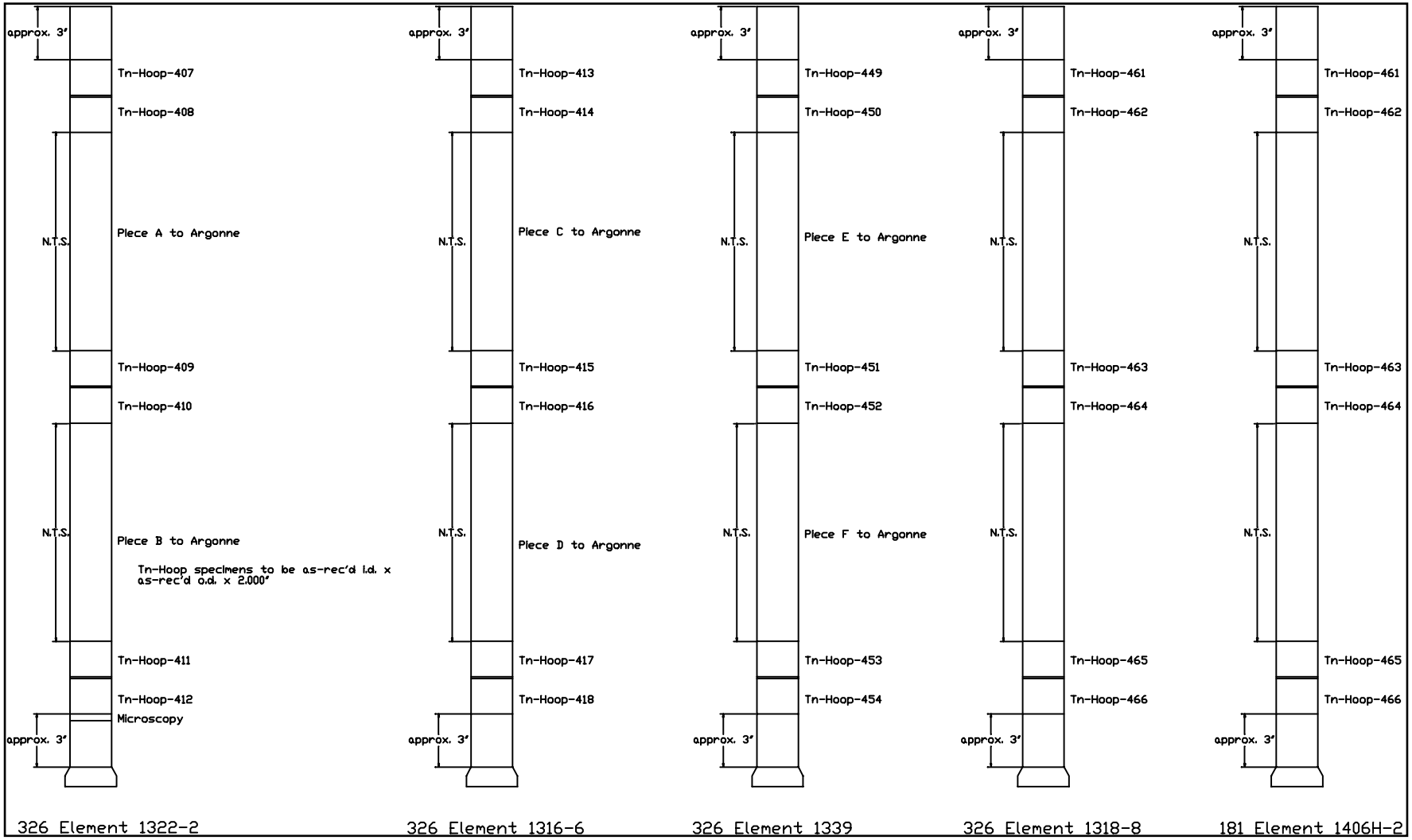

Figure 3.4-2 Cutting Plan for Pall 326 and 181 Clay-Bonded SiC Filter Elements

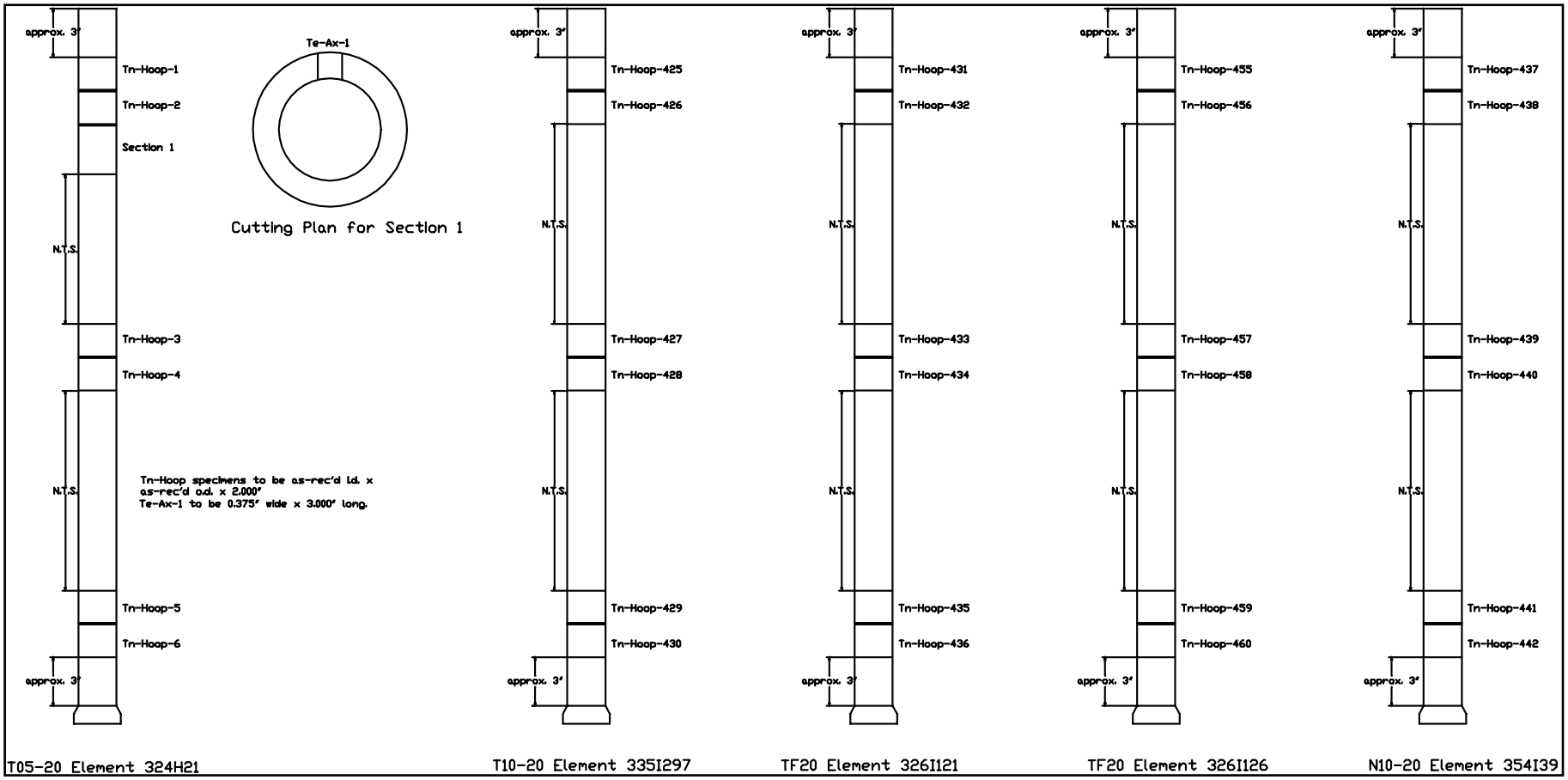

Figure 3.4-3 Cutting for Schumacher T05-20, T10-20, TF20, and N10-20 Ceramic Filter Elements

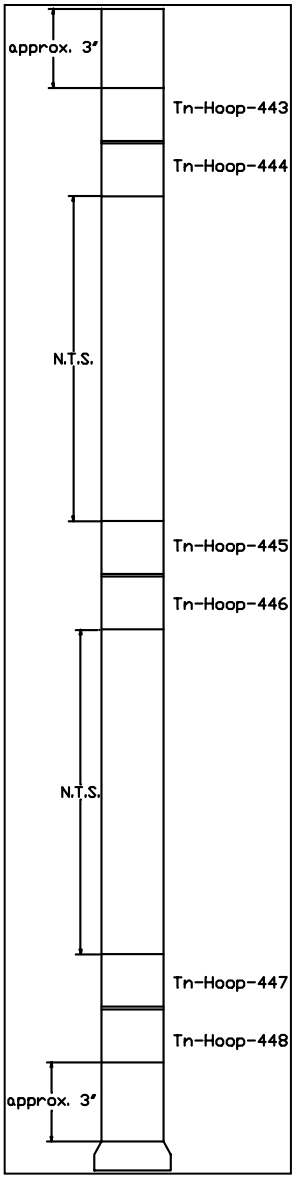

Figure 3.4-4 Cutting Plan for IF&P REECER™ Element FE98073104

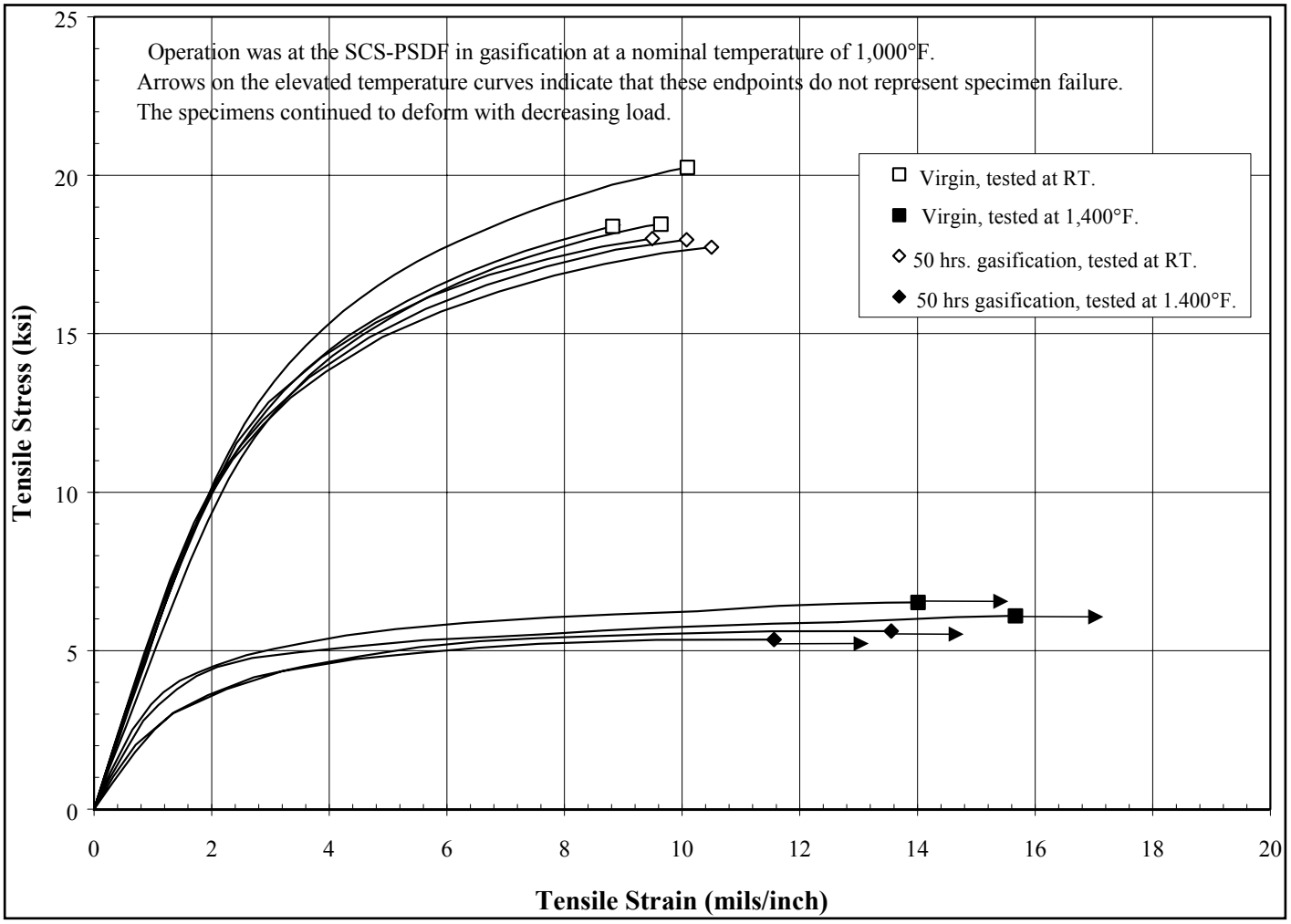

Figure 3.4-5 Axial Tensile Stress-Strain Responses for Pall Fe_3Al

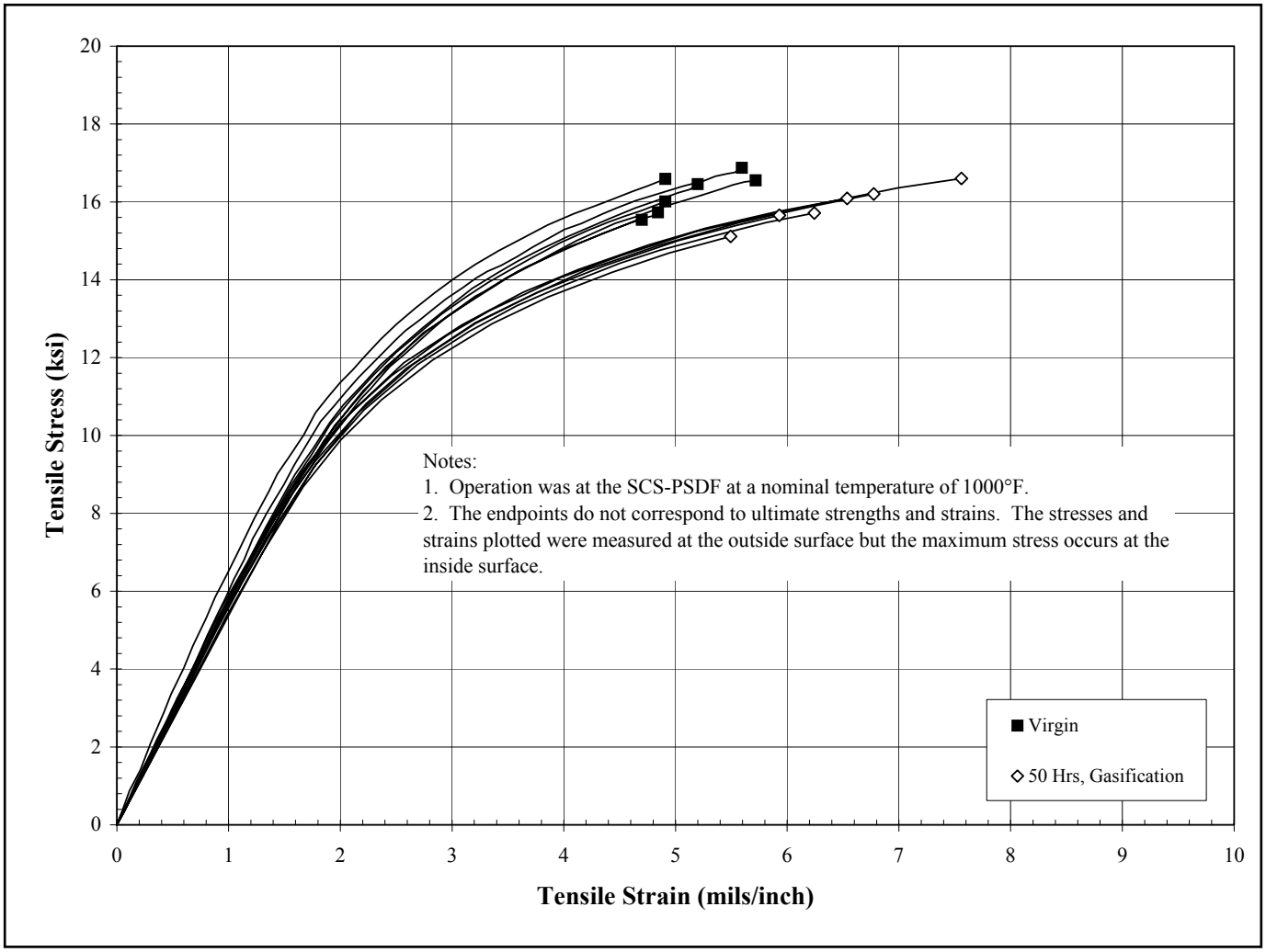

Figure 3.4-6 Room Temperature Hoop Tensile Stress-Strain Responses for Pall Fe_3Al

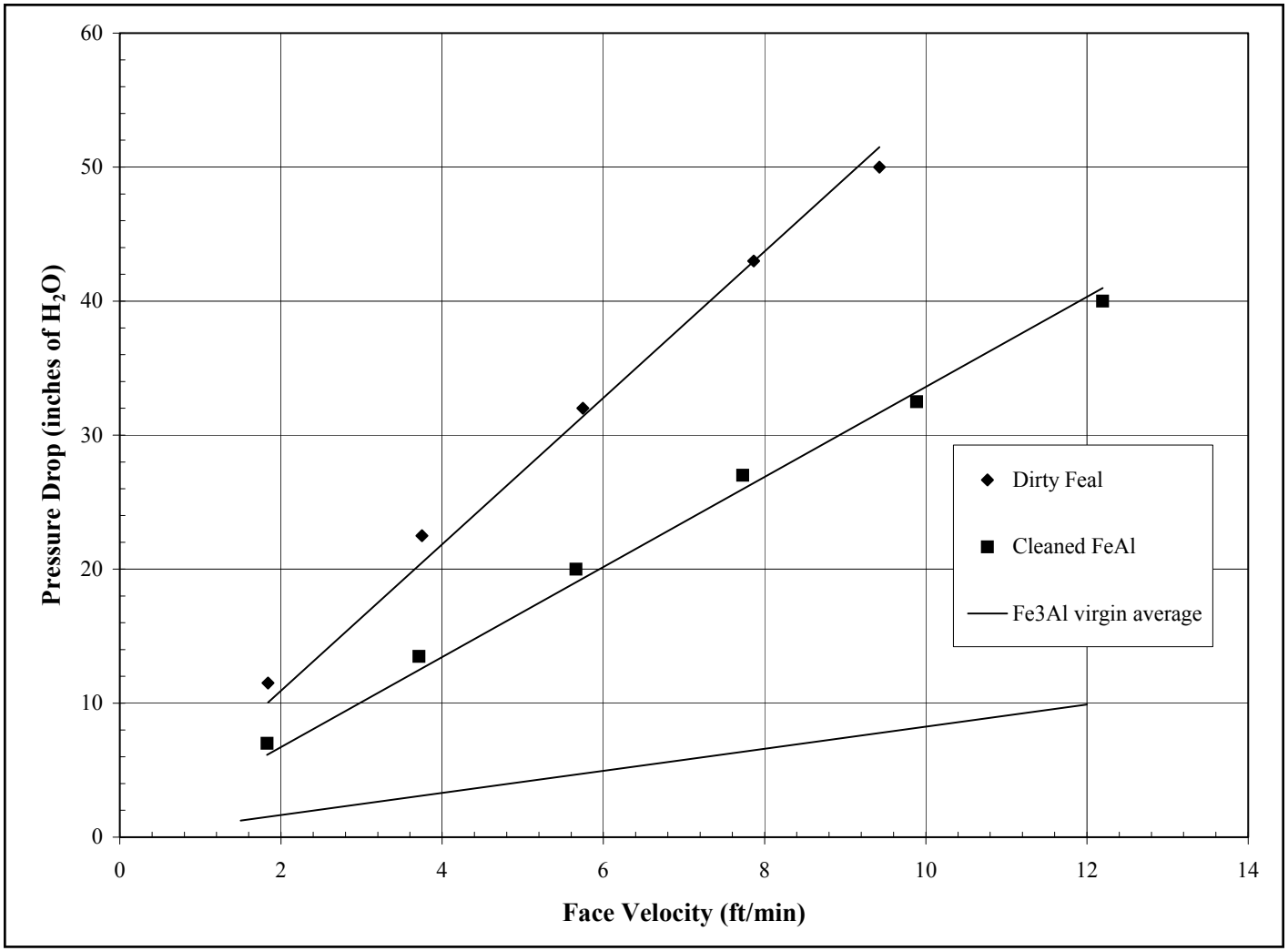

Figure 3.4-7 Pressure Drop Versus Face Velocity for Pall Fe_3Al

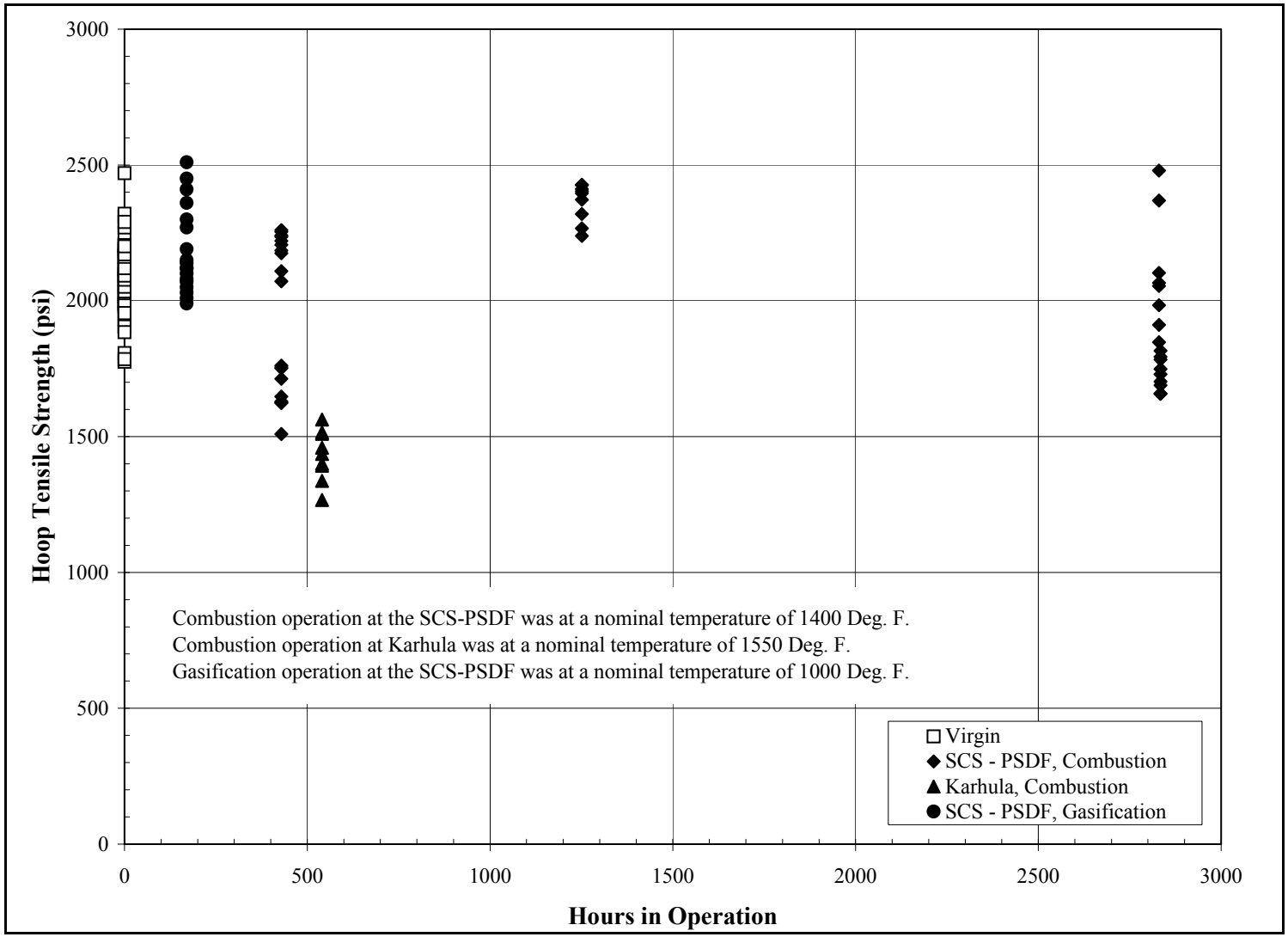

Figure 3.4-8 Room Temperature Hoop Tensile Strength of Pall 326

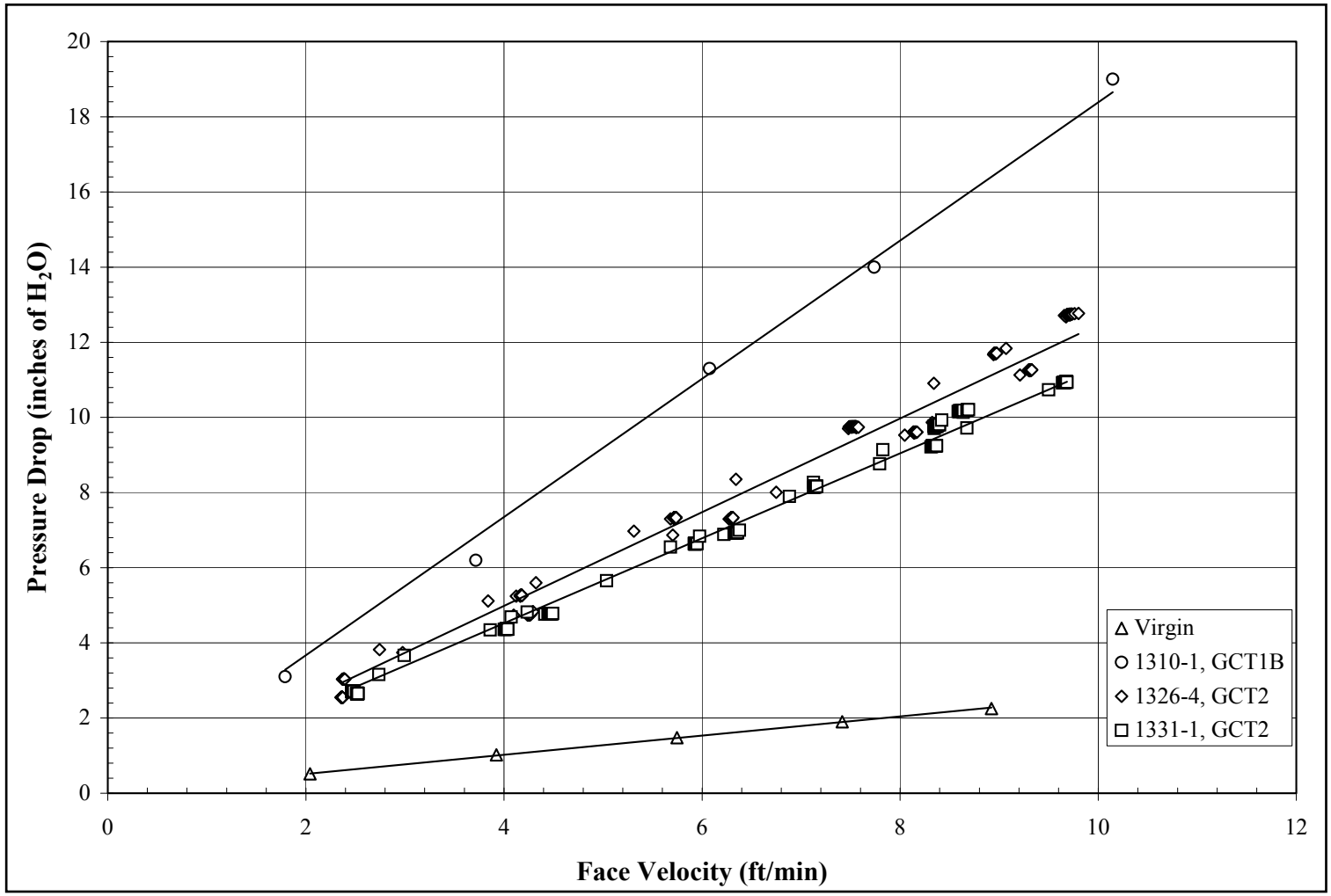

Figure 3.4-9 Pressure Drop Versus Face Velocity for Pall 326

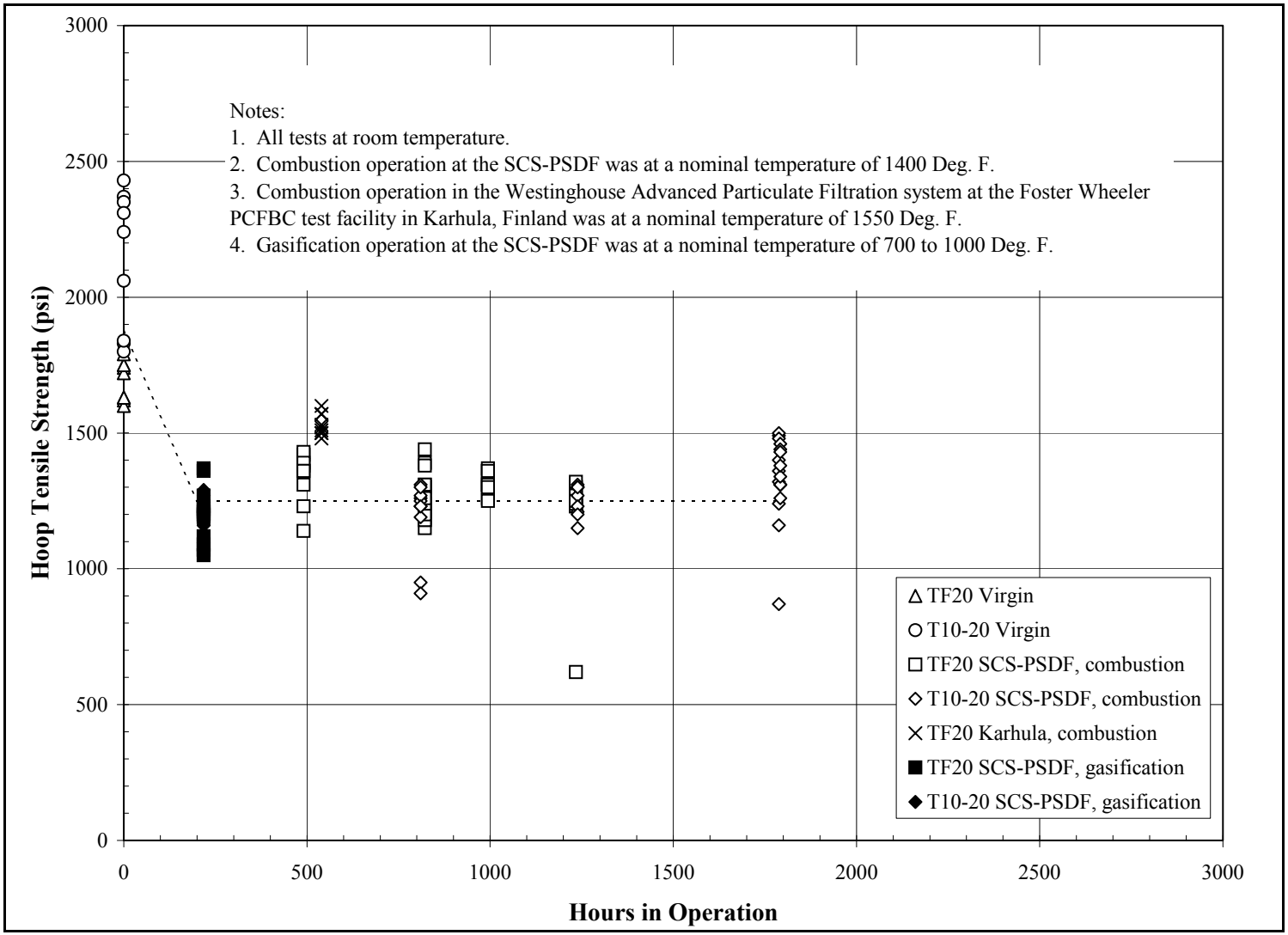

Figure 3.4-10 Room Temperature Hoop Tensile Strength of Schumacher TF20, T10-20, and T05-20

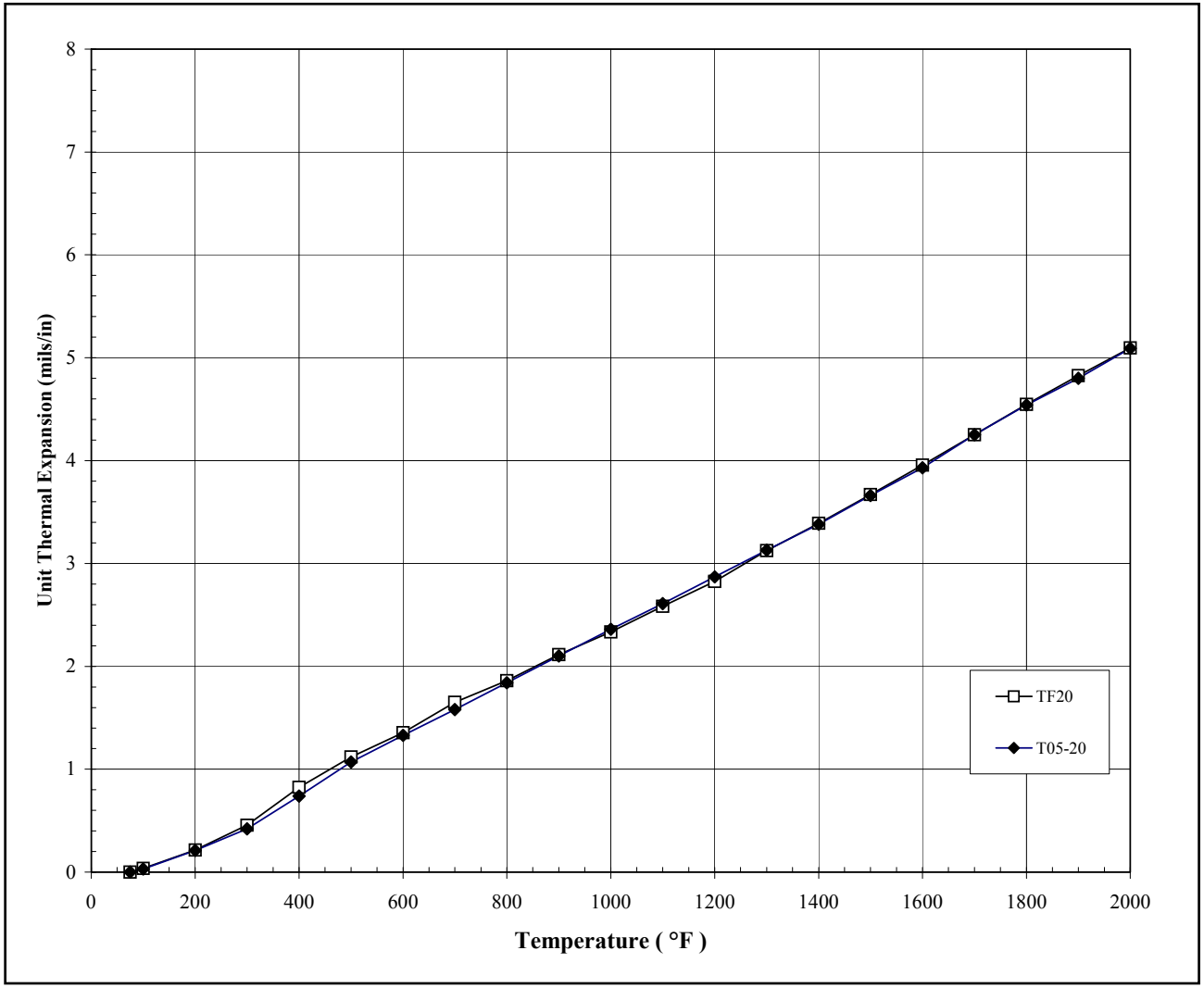

Figure 3.4-11 Unit Thermal Expansion of Schumacher T05-20

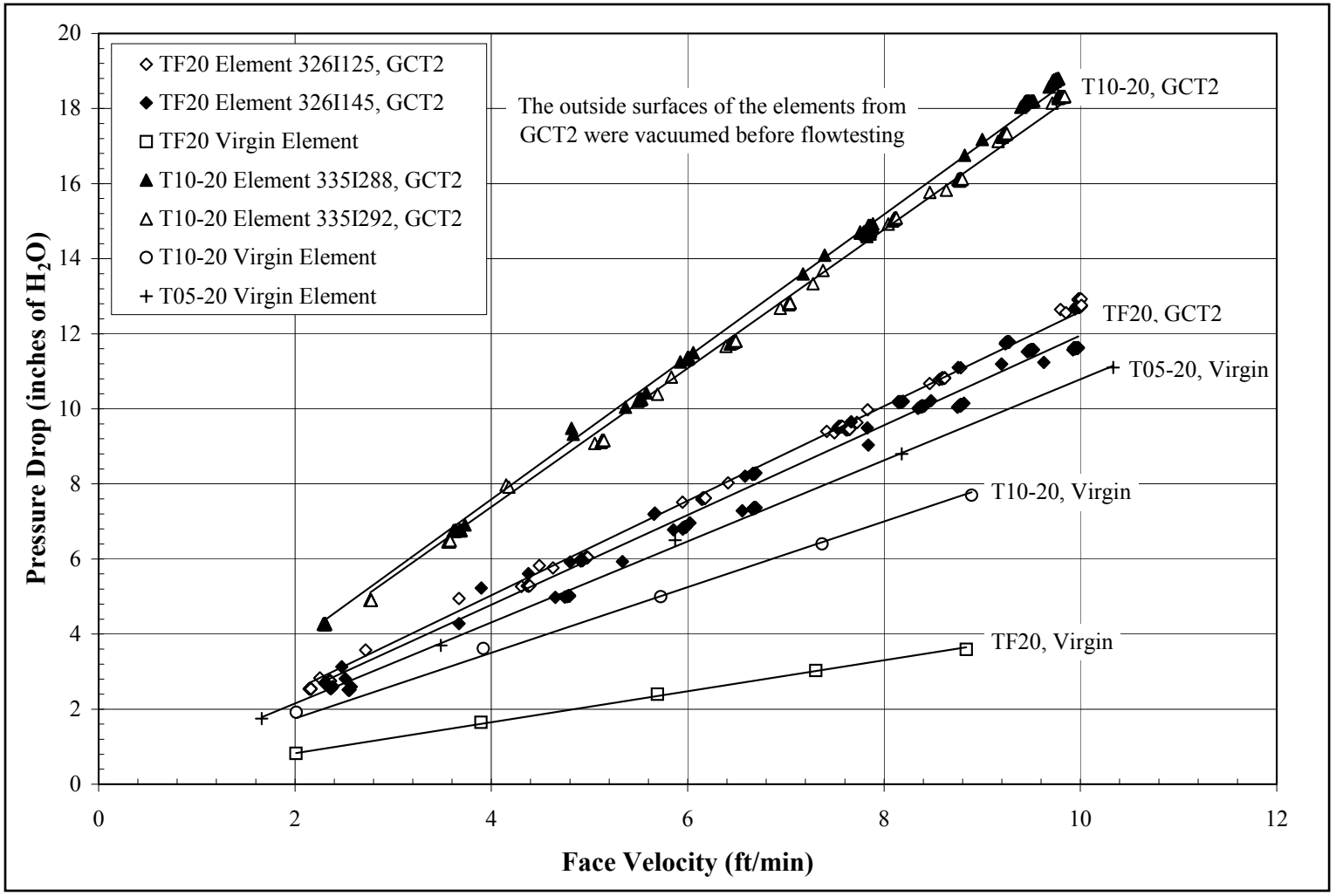

Figure 3.4-12 Pressure Drop Versus Face Velocity for Schumacher TF20, T10-20, and T05-20

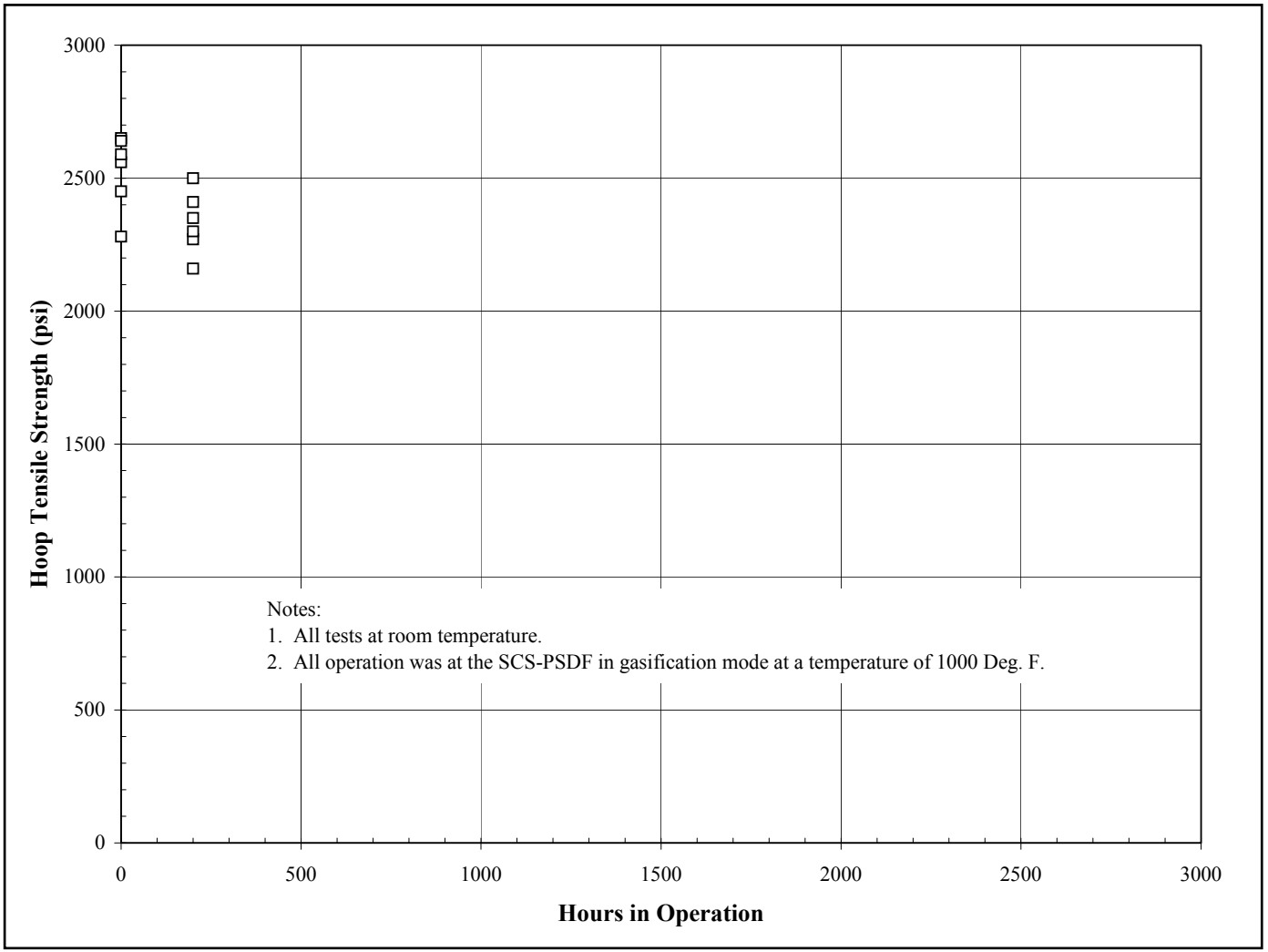

Figure 3.4-13 Hoop Tensile Strength of Schumacher N10-20

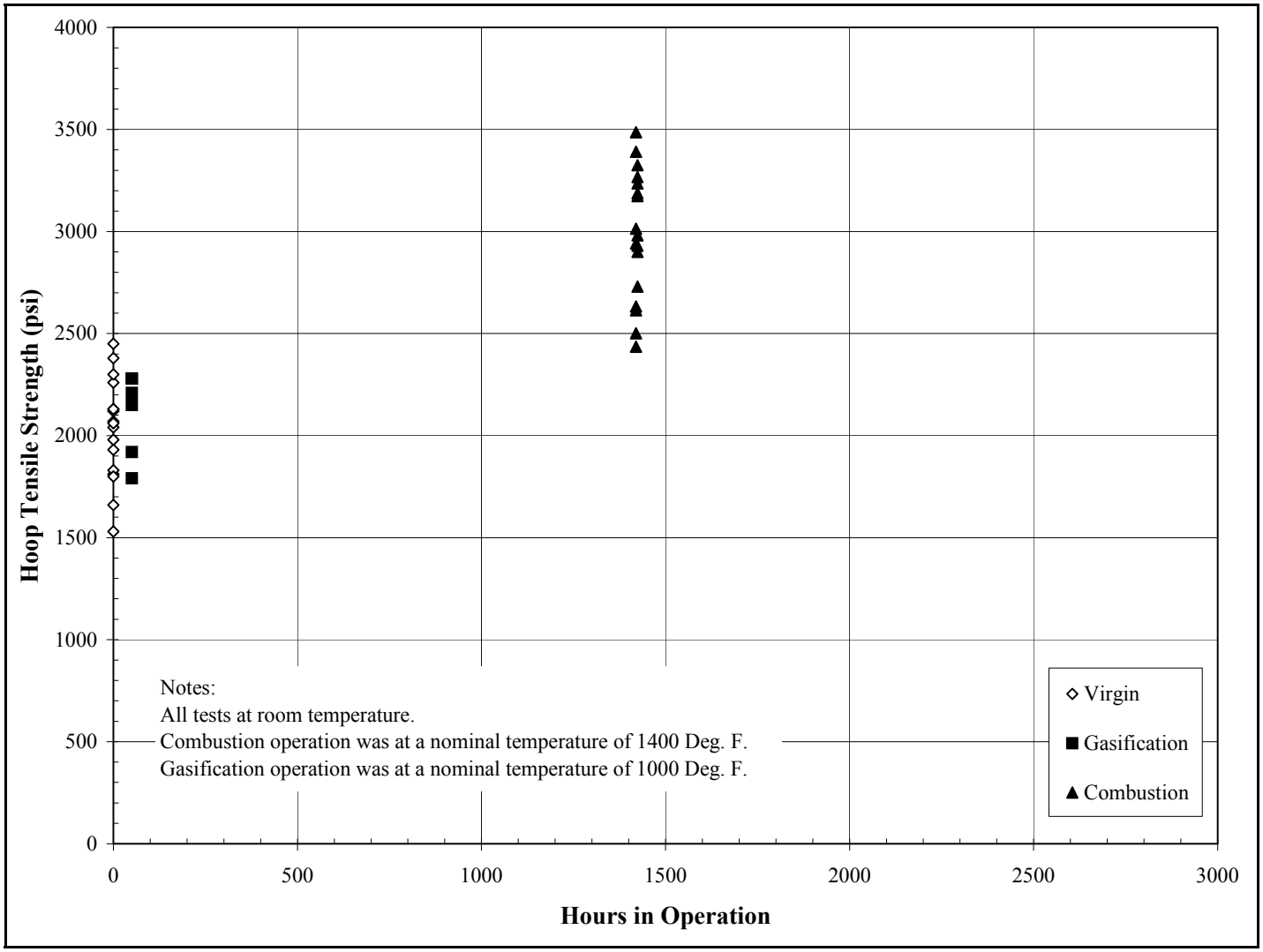

Figure 3.4-14 Hoop Tensile Strength of IF&P REECER™

3.5 FINES HANDLING SYSTEM

3.5.1 Operational Summary

The spent fines removal system performed well during the GCT3 run. However, the system did require some attention from the process engineers, operators, and maintenance personnel. Attention was required in the following areas: (1) spheri valve failure to close, (2) lock vessel pressurization valve failure to close, (3) frequent cycle timer changes, (4) gasket leak on the discharge conveying line, and (5) discharge conveying line plug. The screw cooler required minimal attention relative to the FD0520 system. The major problem associated with the screw cooler was occasional leakage through the seals.

A suitable level probe has still not been found for the FD0520 system; therefore, the FD0520 system had to operate on a timer. This required excessive attention from the operators and engineers to ensure that char was being removed from the PCD at a sufficient rate. At the same time, the timer had to be set at a rate that would not excessively cycle the valves. Between the GCT2 and GCT3 gasification runs a new level probe was tested. The level probe tested was a Delta M level probe, a device that detects the temperature differential between two resistive thermal detectors (RTD) when they are uncovered. When process material (ash, char, etc.) fills the vessel to the point of covering the RTDs, the material in contact with the heated RTD cools the RTD. This lessens the thermal differential between the RTDs, which gives a "covered" signal. A test rig was set up and the level probe initially showed "covered" when the solids in the test rig covered the RTDs; however, the "covered" indication began to change to "uncovered' within 30 seconds. It was believed that the RTDs heated the static solid material over time and increased the thermal differential back to a level that would trigger the level probe to send an "uncovered" signal. Based on the testing it was decided that the Delta M level probe would not work in the FD0520 application.

One of the reasons for ending the GCT3 gasification run was that the exit line of the dense-phase vessel plugged and tripped the spent fines handling system. Operators discovered ceramic filter pieces plugging the exit line. Initially, it was thought that a filter failure had occurred. However, upon inspection of the PCD it was discovered that none of the filters had failed. Therefore, there was suspicion that the ceramic filter pieces were from the filter that failed during the sand circulation run. For some reason the filter pieces must have dislodged, worked their way through the spent fines removal system, and plugged the exit line.

Attention to the screw cooler was mainly due to leakage through the seals. On several occasions the bolts on the packing follower had to be tightened. Modifications to the sealing arrangement are currently being explored.

3.5.2 Spent Fines Transport System (FD0520) – Observation and Events

A. January 20, 2001, at 01:00 – The lock vessel system was started.
B. January 20, 2001, at 18:00 – The fine ash handling system was tripped.
C. January 20, 2001, at 19:20 – The fine ash handling system was restarted.

D. January 22, 2001, at 00:08 – Pressure equalization valve failed to close. This resulted in higher pressures in the lock vessel, which tripped the conveying system. Operations found that the air line to the valve had come loose. The line was reconnected and the fine ash handling system was restarted.
E. January 23, 2001, at 08:50 – The fine ash handling system was tripped. The FD0530 system was experiencing trouble conveying solids to the sulfator. The fine ash handling system was shut down for maintenance to work on FD0530.
F. January 24, 2001, at 15:40 – The fine ash handling system was restarted.
G. January 24, 2001, at 23:45 – The dense-phase vessel was holding 15 psig pressure. The exit line was blown out by operations and the pressure resumed back to baseline.
H. January 26, 2001, at 22:00 – The spent fines handling system tripped because the top spheri valve failed to close.
I. January 26, 2001, at 22:15 – The spent fines handling system was restarted.
J. January 29, 2001, at 12:50 – The spent fines handling system was shut down due to a gasket leak on the conveying discharge line.
K. January 29, 2001, at 14:15 – The gasket leak was repaired and the spent fine handling system was restarted.
L. February 1, 2001, at 03:10 – The spent fines handling system tripped. The exit line of the dense-phase vessel was plugged. Operations found ceramic candle pieces in the dense-phase lock vessel.

3.5.3 Spent Fines Screw Cooler (FD0502) – Observations and Events

A. January 20, 2001, at 01:00 – The screw cooler was started.
B. January 20, 2001, at 18:00 – The screw cooler tripped.
C. January 20, 2001, at 19:20 – The screw cooler was restarted.
D. January 22, 2001, at 00:08 – The screw cooler tripped due to high pressure in the lock vessel.
E. January 23, 2001, at 08:50 – The screw cooler was tripped.
F. January 23, 2001, at 15:40 – The nondrive end of the screw cooler was leaking nitrogen between the packing follower and the flange. Maintenance adjusted the packing follower and sealed the leak.
G. January 24, 2001, at 15:40 – The screw cooler was restarted.
H. January 26, 2001, at 22:00 – The screw cooler tripped.
I. January 26, 2001, at 22:15 – The screw cooler was restarted.
J. January 29, 2001, at 03:05 – The drive end of the screw cooler had a small nitrogen leak. Maintenance adjusted the bolts on the packing follower and sealed the leak.
K. January 29, 2001, at 12:50 – The screw cooler was tripped.
L. January 29, 2001, at 14:15 – The screw cooler was restarted.
M. February 1, 2001, at 03:10 – The screw cooler tripped.

3.5.4 Fine Ash Removal System (FD0502/FD0520) Inspection

During the GCT3 outage the spent fines removal system was inspected. The screw cooler was disassembled and inspected. The packing rings appeared to be in good condition. However, the wear sleeve and stuffing box were severely scored (See Figures 3.5-1 and -2). Due to the scoring, the stuffing box was deformed, which prevented the spring retainer from being properly reinserted. Therefore, a new stuffing box was installed.

The FD0520 lock vessel system was thoroughly inspected. The dome valve and inflatable seal appeared to be in good condition and were reinstalled. However, the shuttle valves that control the inflatable seals on the upper and lower spheri valves were plugged with material of an unknown source. Any additional information learned about this material will be reported at a later date. Also, the seal on one of the vent valves was eroded and is to be replaced before the next gasification run.

Figure 3.5-1 FD0502 Wear Sleeve

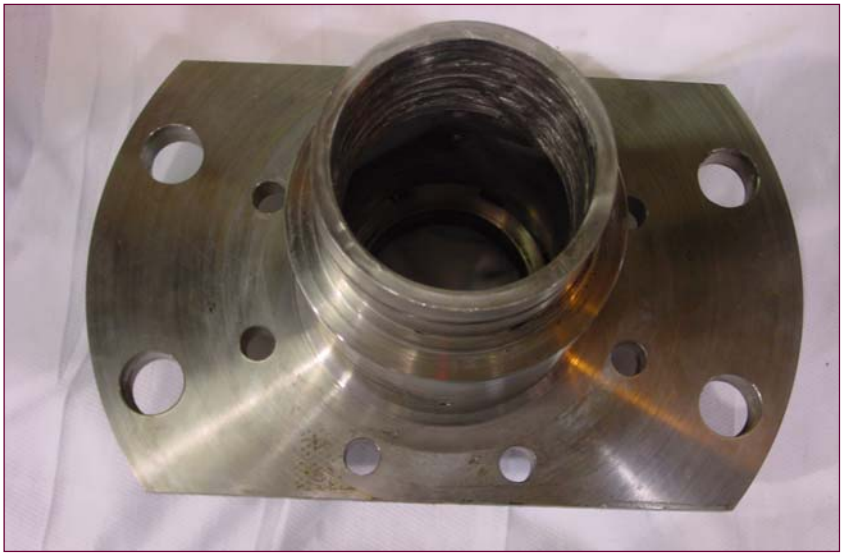

Figure 3.5-2 FD0502 Stuffing Box

3.6 CHAR CHARACTERISTICS AND PCD PERFORMANCE

Although most of this report deals with results collected during GCT3, this section will also include the results and analysis of data generated during the subsequent test program, GCT4. The reason for considering both data sets is that there were gaps in the GCT3 results that would have made analysis of that data, alone, misleading. Since the GCT4 data were available at the time this report was prepared, and since the operating conditions during GCT3 and GCT4 were essentially the same, considering them together gives a much more complete picture of PCD operation. The same analysis will be included with the GCT4 report.

This section addresses the characteristics of the gasification char produced during GCT3 and GCT4 and the relationship between the char characteristics and PCD performance. As in previous tests, in situ char samples and dustcake samples from GCT3 and GCT4 were thoroughly characterized in an effort to better understand the effects of the char characteristics on filter pressure drop and cleanability. In situ char samples were collected at both the PCD inlet and outlet throughout GCT3 and GCT4. Samples of residual dustcakes and bridged deposits that were trapped between the filter elements were also collected after both GCT3 and GCT4. Characterization of the in situ char samples and dustcake samples included chemical analysis, particle size analysis, laboratory drag measurements, and measurements of the true particle density, bulk density, uncompacted bulk porosity, and specific-surface area. As in GCT2, drag measurements were made on the GCT3 and GCT4 char samples using the resuspended ash permeability tester (RAPTOR). The design and operation of the RAPTOR system has been described in previous reports. For the measurements discussed in this section, the RAPTOR system was modified to include various combinations of cyclones between the fluidized-bed dust generator and the dustcake collection section. The modified system made it possible to obtain data on drag as a function of particle size, thereby allowing a more accurate simulation of hot-gas filter performance. These drag measurements were used to better understand the relative contribution of the dustcake to the total PCD pressure drop and to gain insight into the effect of particle size on drag.

3.6.1 In situ Sampling

As in previous test campaigns, in situ particulate sampling runs were performed on a regular basis at both the PCD inlet and outlet throughout GCT3 and GCT4. The system and procedures used for the in situ particulate sampling have been described in previous reports. During GCT3, seven particulate sampling runs were performed at the PCD inlet and eight at the PCD outlet. During GCT4, six particulate sampling runs were performed at the PCD inlet and seven at the PCD outlet. As in GCT2, all of the GCT3 and GCT4 samples were obtained during gasification of Powder River Basin (PRB) coal with the addition of Ohio (Bucyrus) limestone for in-bed sulfur capture.

3.6.1.1 PCD Inlet Particle Mass Concentrations

Table 3.6-1 provides a summary of the particulate loadings measured in the process gas stream during GCT3 and GCT4. Excluding startup and sand circulation periods, all of the GCT3 and

GCT4 mass loadings varied from 10,500 to 28,700 ppmw with a mean value of 18,400 ppmw and a standard deviation of 6,000 ppmw (coefficient of variation of 0.3). These values may be compared to the mass loadings obtained in GCT2, which varied from 25,700 to 34,000 ppmw, with a mean value of 31,100 ppmw and a standard deviation of 2,600 ppmw (coefficient of variation of 0.08). Thus, the mean mass loading measured during GCT3 and GCT4 was only about 59 percent of the mean mass loading measured during GCT2. The lower mass loadings obtained during GCT3 and GCT4 were produced with even higher coal-feed rates than those used in GCT2. Therefore, it is clear that the modifications made to the transport reactor cyclone/disengager system resulted in improved retention of char within the transport reactor loop and significantly reduced the particulate carryover to the PCD. The reduction in the total particulate mass entering the PCD was roughly 40 percent on average.

3.6.1.2 PCD Outlet Particle Mass Concentrations

Also shown in Table 3.6-1 are the particle concentrations measured at the outlet of the PCD, along with the PCD collection efficiency calculated from the corresponding inlet and outlet mass measurements. Except for the initial period of sand circulation at the beginning of GCT3, the PCD operated with very low outlet loadings, consistent with an absence of significant leaks. (The high loading obtained during the sand circulation period was caused by a broken filter element, which was replaced prior to the testing with coal feed.) The measured outlet char loading during all tests with coal feed was less than 0.10 ppmw, with an average collection efficiency exceeding 99.999 percent. These measurements were at the lower limit of resolution of the sampling system. As noted in the table, higher outlet loadings were measured on two runs (0.26 ppmw on GCT3OMT-3 and 38.6 ppmw on GCT4OMT-2), but these samples were contaminated with either a brown or black substance believed to be tar.

3.6.1.3 Tar Contamination

The inlet sample GCT4IMT-2 and the outlet sample GCT4OMT-2 were collected during a transition from propane to coal fire. During this period there was apparently a large carryover of poorly gasified coal, which produced an unusually high inlet loading (59,500 ppmw). The outlet sample collected during this time period (GCT4OMT-2) was contaminated with a black substance and the surface of the outlet sampler was coated with a black glaze. The deposition patterns on the sampler suggested that this material had impacted on the sampler surface in the form of liquid droplets. Thermogravimetric analysis of the black glaze showed that it lost only 30 to 35 percent of its weight when heated in nitrogen up to a temperature of 1,000°C, but it was completely burned away when heated in air up to 400°C. This result suggests that much of the tar that was originally present in the black glaze was cracked to carbon.

As discussed later in this report, evidence of partially cracked tar has also been found in the form of sticky residual dustcakes and in the form of condensed tar components found in the gas analysis system. The tar is apparently formed when coal is introduced into the transport reactor system while the temperatures in the system are too low to completely break down the tar components. It is generally believed that temperatures in excess of 1,600°F must be achieved in the transport reactor system to avoid tar formation. Since the propane start-up burner is only capable of producing temperatures of around 900°F, tar formation is unavoidable during the

transition from propane to coal feed. Similarly, tar production can be expected whenever coal is reintroduced into the transport reactor system after a temporary loss of coal feed with a concomitant drop in transport reactor temperatures below the level required for tar cracking.

3.6.1.4 Syngas Moisture Content

As in previous tests, measurements of the syngas moisture content were made in conjunction with the outlet particulate sampling runs. The water vapor content of the syngas was determined by collecting the condensate from the syngas in an ice-bath condenser and calculating the vapor concentration from the volume of gas sampled and the volume of condensate collected. The values determined for individual runs are included in Table 3.6-1.

3.6.2 PCD Dustcakes and Consolidated Deposits

Samples were collected of the dustcakes and deposits remaining in the PCD following each test program. At the end of GCT3 the PCD was back-pulsed extensively during shutdown, resulting in a very thin residual dustcake on the filter elements. While there was no transient dustcake remaining on the elements after GCT3, there was one area that contained a bridged deposit that was trapped between filter elements. Samples of the bridged deposit and of the residual dustcake were taken and measurements were made of the residual dustcake thickness and areal loading.

To allow characterization of both the residual and transient dustcakes formed during GCT4, a dirty shutdown of the PCD was attempted at the end of that run. Unfortunately, the coal feeder tripped midway through the last filtration cycle, resulting in an unusually slow rate of pressure drop increase during the last filtration cycle. As discussed later in this report, the properties of the transient dustcake that was produced during this problematic shutdown differ considerably from the properties of the GCT4 in situ samples and hopper samples. Analytical results and physical properties, which are discussed in detail later in this report, suggest that this particular transient dustcake sample may not be representative of the transient dustcake that was collected during normal operations. Nevertheless, samples of the transient dustcake were collected from various elements and the thickness and areal loading of the transient cake were estimated using procedures documented in previous reports. Residual dustcake samples were taken from several elements and the areal loadings of the residual dustcakes were determined by removing and weighing all of the residual dustcake on the elements. As in GCT3, samples were also taken of bridged deposits that were trapped between filter elements. (As mentioned in the section on PCD operations and inspection, the bridging found following GCT4 was much more extensive than found following GCT3.)

To investigate the differences between the residual and transient cakes and the bridged material, all samples were thoroughly characterized to evaluate their physical properties, chemistry, and potential contribution to PCD pressure drop. In a subsequent section of this report the dustcake drag measured in the laboratory is compared to the dustcake drag estimated from PCD pressure drop.

3.6.2.1 Residual Dustcake Observations

The GCT3 residual dustcake was extremely thin, making it difficult to obtain accurate measurements of the dustcake thickness and areal loading. Nevertheless, multi-point measurements of the dustcake thickness were made on four selected filter elements; the areal loadings of dustcake on these elements were determined by scraping off all of the dustcake within a specific area of the element surface. Based on these measurements, the residual dustcake thickness was estimated to be about 0.02 in. and the residual dustcake areal loading was estimated to be about 0.04 lb/ft^2. Dustcake porosity determined from these values of thickness and areal loading was 83 percent. This value of dustcake porosity was in reasonable agreement with the dustcake porosity determined from RAPTOR tests on the GCT3 residual char (83 percent measured on the filter element vs. 81 percent determined by RAPTOR). While slightly gummy feeling and tightly adhered to the elements, once removed the GCT3 residual dustcake was fluffy with no lumps or flakes.

The GCT4 residual dustcake was considerably thicker than the GCT3 residual dustcake and was crusty. The GCT4 residual dustcake thickness was estimated to be 0.1 in. and the areal loading was estimated to be 0.2 lb/ft^2. Dustcake porosity determined from these values of thickness and areal loading was 83 percent, the same value determined for the GCT3 residual dustcake.

As mentioned above, the GCT3 residual dustcake was fluffy after removal, whereas when the GCT4 dustcake was removed from the elements it came off in flakes that could be handled without breaking. After air blowing the flakes, the pore structure shown in Figure 3.6-1 was observed. The pores or holes through the residual dustcake flake are approximately 0.2 mm in diameter. These holes were apparently formed during back-pulsing and give the appearance that the dustcake was somewhat fluid or wet at the time. Figure 3.6-2 is a SEM photo of the char particles in the solid portion (between the 0.2-mm pores) of the GCT4 residual dustcake at a magnification of 5000x. The SEM indicates that the particles are significantly consolidated, which accounts for the high strength of the deposits. Presumably, the consolidating material is tar collected during the numerous coal restarts that occurred during GCT4.

After observing the substantial differences between the GCT3 and GCT4 dustcakes, the GCT2 samples were re-evaluated. Visual and microscopic inspection indicated that the GCT2 residual dustcake was also crusty and produced flakes that could be readily handled. However, the degree of consolidation was not as great as that observed for GCT4 and the pore structure was not well developed.

The following listing compares the dustcake thicknesses, areal loadings, and porosities determined for GCT2, GCT3, and GCT4. Because of the pores and the consolidation these porosity values should be used with caution. In the case of GCT2 and GCT4 the average and local values of porosity may be considerably different.

	Residual Dustcake			Transient
	GCT2	GCT3	GCT4	GCT4
Avg thickness (in.)	0.05	0.02	0.1	0.3
Avg areal loading (lb/ft^2)	0.09	0.04	0.2	0.6
Avg porosity (%)	84	83	83	83
RAPTOR porosity (%)	81	81	84	84

3.6.3 Chemical Analysis of In situ Samples and Dustcakes

As in previous test runs, chemical analyses were performed on the in situ particulate samples and on the dustcake/bridging samples from GCT3 and GCT4. The samples were analyzed for carbon, hydrogen, nitrogen, sulfur, and ash; ashes from the ignited samples were subjected to a standard ash mineral analysis. The standard ash mineral analysis included aluminum, calcium, iron, magnesium, phosphorous, potassium, silicon, sodium, and titanium. Only the results for aluminum, calcium, iron, magnesium, and silicon are reported here since the concentrations of the other elements were generally less than 0.5 wt percent in the original sample. The elemental analyses reported here are expressed as weight percent of the element in the original sample on an as-received basis.

Using the elemental analyses along with an analysis of CO_2 content, the chemical composition of each sample was calculated as follows:

- $CaCO_3$ content was calculated assuming that all of the CO_2 originated from $CaCO_3$.
- CaS content was calculated assuming that all of the sulfur was present as CaS.
- Any remaining Ca was assumed to take the form of CaO.
- All carbon not accounted for in $CaCO_3$ was assumed to be present as elemental carbon.
- All metals were assumed to be present as the oxides.

The justification for the assumptions used in these calculations are discussed in detail in the GCT2 report and will not be repeated here.

3.6.3.1 In situ Samples

Tables 3.6-2 and -3 provide the analytical results for the in situ particulate samples obtained during GCT3 and GCT4. The listing below provides a summary of the average values of carbon, sulfur, calcium, magnesium, and silicon for each run.

	GCT2	GCT3	GCT4
Average carbon (wt %)	39.7	40.6	40.4
Average sulfur (wt %)	0.5	1.0	1.0
Average calcium (wt %)	14.3	16.2	10.0
Average magnesium (wt %)	2.0	2.8	1.8
Average silicon (wt %)	8.3	7.6	9.0

Comparing these major elements, the most striking difference is in sulfur content, with the GCT3 and GCT4 char samples containing twice as much sulfur as the GCT2 char samples. There was no significant difference in coal sulfur content between GCT2 and GCT3 and GCT4, and the difference in the calcium content of the char does not appear to be significant. Therefore, the higher sulfur content of the GCT3 and GCT4 char is almost certainly attributable to improved sorbent utilization. This assertion seems reasonable since the modifications made to the transport reactor loop between GCT2 and GCT3 would tend to improve the solids retention within the loop, resulting in longer solids residence times for sulfidation of the sorbent. Solids compositions that were calculated from the foregoing analytical results are summarized below.

	GCT2	GCT3	GCT4
Average elemental carbon (wt %)	35.7	N.D.	44.9
Average $CaCO_3$ (wt %)	13.7	N.D.	11.3
Average free lime (CaO) (wt %)	11.5	N.D.	6.2
Average CaS (wt %)	1.1	2.3	2.2
Average inerts (wt %)	38.0	31.8	35.4

The designation N.D. indicates that a component could not be determined because the sample size was insufficient for the CO_2 analysis. While this prevented the determination of elemental carbon, $CaCO_3$, and CaO in the GCT3 in situ samples, it was still possible to determine CaS for these samples. As shown in the listing above, the GCT3 and GCT4 chars contain more CaS than the GCT2 char, which again reflects the improved conversion of the $CaCO_3$ to CaS as a result of the increased residence time of the solids within the reactor loop.

It should be noted that the higher carbon content of the GCT4 sample does not contradict the assertion that the carbon conversion was higher in GCT4 than it was in GCT2. The average particulate loading exiting the transport reactor during GCT4 was only 18,000 ppmw compared to 31,000 ppmw during GCT2. Therefore, the total mass flow of carbon from the reactor during GCT4 was only about 70 percent of the carbon mass flow during GCT2. Since the coal-feed rate was higher during GCT4 than it was during GCT2, it is clear that there was much better carbon conversion during GCT4.

3.6.3.2 Dustcake Samples

Following GCT3, one bulk residual dustcake sample was obtained by scraping the dustcakes from all of the accessible filter elements in the top and bottom plenums and a bulk sample of the bridged material was obtained by removing the bridged material between certain elements in the bottom plenum. (The exact locations of the bridged material are described in Section 3.3, GCT3 PCD Inspection Report.) Following GCT4, residual and transient dustcake samples were taken from individual filter elements, and a bulk sample of the bridged deposit was also collected. (Again, the exact locations of the bridged deposits are described in the section on the GCT4 PCD inspection.)

Tables 3.6-4 and -5 summarize the analytical results obtained on the residual dustcake samples and the samples of transient dustcake and bridged material removed during the post-GCT3 and

the post-GCT4 PCD inspections. The listing below compares the average values of the major elements in the residual dustcake samples and bridged deposits.

	Residual Dustcake			Bridged Deposits	
	GCT2	GCT3	GCT4	GCT3	GCT4
Average carbon (wt %)	39.0	44.7	56.1	37.0	58.5
Average sulfur (wt %)	0.7	1.1	1.0	0.8	1.0
Average calcium (wt %)	11.8	13.5	9.3	16.8	11.1
Average magnesium (wt %)	1.8	2.7	1.4	2.9	2.4
Average silicon (wt %)	7.5	4.6	5.1	7.0	8.0
Calcium utilization (%)	7.4	10.2	13.4	6.0	9.0

The calcium utilization values shown above were calculated as follows:

$$CalciumUtilization,\% = 100\% \bullet \frac{\frac{AvgSulfur,Wt\%}{32}}{\frac{AvgCalcium,Wt\%}{40}}$$

The term "calcium utilization" is used here instead of "sorbent utilization" because about half of the calcium comes from the coal. Since only about half of the calcium is derived from the sorbent, sorbent utilization values would be considerably higher than the calcium utilization values shown here. Assuming that half of the calcium originated from the sorbent, actual sorbent utilization is estimated to be 12 to 18 percent in the bridged deposits and 14 to 27 percent in the residual dustcakes. These sorbent utilizations are relatively low, as expected, because of the low sulfur content of the PRB coal and the equilibrium limitations on H_2S removal.

In terms of the elemental analyses, the GCT3 residual dustcake appears to contain more sulfur and less calcium than does the bridged material. The GCT4 residual dustcake contains the same amount of sulfur as the bridged deposit, but with less calcium. When the sulfur and calcium results are expressed in terms of calcium utilization, as defined above, it can be seen that these differences in sulfur and calcium reflect a significant increase in the conversion of the calcium in the residual cake. For GCT3 this effect amounts to a 70-percent increase in calcium utilization. For GCT4, the additional sulfidation in the cake results in a 49-percent increase in calcium utilization. This increase in calcium utilization in the residual cake is not surprising since the residual cake was exposed to H_2S over a longer time period than was the bridged deposit.

The following table summarizes the chemical compositions calculated from the analytical results on the residual dustcakes and bridged deposits. As noted previously, the designation N.D. indicates that elemental carbon, $CaCO_3$, and CaO were not determined for the GCT3 residual dustcake and bridged deposits because no CO_2 analysis was done on these samples.

	Residual Dustcake			Bridged Deposit	
	GCT2	GCT3	GCT4	GCT3	GCT4
Average elemental carbon (wt %)	38.7	N.D.	54.7	N.D.	57.0
Average $CaCO_3$ (wt %)	2.0	N.D.	11.9	N.D.	12.7
Average free lime (CaO) (wt %)	14.2	N.D.	4.5	N.D.	6.8
Average CaS wt (%)	1.5	2.6	2.3	1.7	2.2
Average inerts wt (%)	43.6	35.1	26.6	38.6	21.3

It is apparent from the compositions summarized above that the GCT4 residual dustcake and bridged deposit contain significantly more CaS and $CaCO_3$ and significantly less free lime (CaO) than the GCT2 residual dustcake. As noted earlier, this difference is a reflection of the additional sulfidation that has occurred in the residual dustcake as a result of the prolonged exposure of the residual cake to syngas.

The analytical results for the GCT3 and GCT4 dustcake samples are compared below to those of the in situ samples.

	GCT3			GCT4		
	In situ	Residual	Bridging	In situ	Residual	Bridging
Average carbon (wt %)	40.6	44.7	37.0	40.4	56.1	58.5
Average sulfur (wt %)	1.0	1.1	0.8	1.0	1.0	1.0
Average calcium (wt %)	16.2	13.5	16.8	10.0	9.3	11.1
Average magnesium (wt %)	2.8	2.7	2.9	1.8	1.4	2.4
Average silicon (wt %)	7.6	4.6	7.0	9.0	5.1	8.0

There appears to be a significant difference in calcium content between the GCT3 and GCT4 samples, which can be seen in the in situ samples (16 percent in GCT3 vs. 10 percent in GCT4), in the residual dustcake samples (13 percent in GCT3 vs. 9 percent in GCT4) and in the bridged deposits (17 percent in GCT3 vs. 11 percent in GCT4). This comparison suggests that the GCT3 samples contain more sorbent than do the GCT4 samples.

The listing below compares the calculated chemical compositions for the GCT3 and GCT4 dustcake samples and the corresponding in situ samples. (Again, these compositions were calculated from the analytical data shown above using the procedures and assumptions discussed previously.)

	GCT3			GCT4		
	In situ	Residual	Bridging	In situ	Residual	Bridging
Average elemental carbon (wt %)	N.D.	N.D.	N.D.	44.9	54.7	57.0
Average $CaCO_3$ (wt %)	N.D.	N.D.	N.D.	11.3	11.9	12.7
Average free lime (CaO) (wt %)	N.D.	N.D.	N.D.	6.2	4.5	6.8
Average CaS (wt %)	2.3	2.6	1.7	2.2	2.3	2.2
Average inerts (wt %)	31.8	35.1	38.6	35.4	26.6	21.3

These results suggest that the GCT3 residual dustcake contains more CaS than the GCT3 in situ samples and bridged deposits (2.6 percent in the residual dustcake vs. 2.3 percent in the in situ sample and 1.7 percent in the bridged deposit). As suggested earlier, this difference can probably be explained in terms of the additional sulfidation of the calcium in the residual cake. In the case of the GCT4 samples this difference is less pronounced (2.3 percent in the residual cake vs. 2.2 percent in the in situ sample and in the bridged material). However, as indicated earlier, there is a significant difference in calcium utilization that supports the contention that there was significant additional sulfidation in the residual dustcakes in both GCT3 and GCT4.

3.6.4 Physical Properties of In situ Samples and Dustcakes

As in previous tests, the GCT3 and GCT4 in situ particulate samples and dustcake samples were subjected to the standard suite of physical measurements, including true (skeletal) particle density, bulk density, uncompacted bulk porosity, specific-surface area, and particle size analysis. The instruments and procedures used for making these measurements are described in previous reports.

3.6.4.1 In situ Particulate Samples

Physical properties of the in situ particulate samples from GCT3 and GCT4 are presented in detail in Table 3.6-6. Listed below is a comparison of the average in situ physical properties for all three runs (GCT2, GCT3, and GCT4).

	GCT2	GCT3	GCT4
Average bulk density (g/cc)	0.36	0.37	0.27
Average skeletal particle density (g/cc)	2.24	2.28	2.29
Average uncompacted bulk porosity (%)	83.9	83.8	88.2
Average specific surface area (m^2/g)	93.4	128	197
Average mass-median diameter (μm)	17.9	14.2	15.9

Based on the above comparison, the chars produced from GCT3 and GCT4 appear to be somewhat finer than the char produced in GCT2. This is, of course, an expected result of the increased cyclone collection efficiency and the improved carbon conversion in the transport reactor loop. The GCT3 and GCT4 chars also appear to have significantly higher specific-surface areas than GCT2 char. This difference in surface area is not completely understood, but it may be associated with the improved solids retention and enhanced carbon conversion (that is, better gasification) attained in the transport reactor. Again, it should be noted that all three of these chars were produced from the same PRB coal and the same Ohio (Bucyrus) limestone.

Compared to PRB combustion ashes produced in the transport reactor system in earlier runs, it is now clear that the PRB gasification chars have relatively low bulk density, relatively high bulk porosity, and relatively high specific-surface area. As discussed in more detail later, the specific-surface area of the char is believed to be a significant contributing factor in the high flow resistance of this material, but differences in particle size and surface area alone do not completely explain the high drag of the gasification char. The role of these properties in

determining dustcake drag will be discussed in more detail in the section on drag measurements. A more detailed comparison of the particle size distributions of the GCT2, GCT3, and GCT4 chars will be presented in a subsequent section of this report.

3.6.4.2 Dustcake Samples

The physical properties of the residual and transient dustcake samples and bridged deposits from GCT3 and GCT4 are presented in detail in Table 3.6-7 and summarized below.

	Residual Dustcakes			Bridged Char	
	GCT2	GCT3	GCT4	GCT3	GCT4
Average bulk density (g/cc)	0.43	0.36	0.34	0.37	0.34
Average skeletal particle density (g/cc)	2.15	2.37	1.91	2.40	2.21
Average uncompacted bulk porosity (%)	80.0	84.8	82.2	84.6	84.6
Average specific surface area (m^2/g)	23.9	44.0	8.0	127	173
Average mass-median diameter (μm)	7.4	4.3	8.4	12.0	12.7

The properties of the transient dustcake collected at the end of GCT4 are included in Table 3.6-7, but are not included in the summary above because the transient cake was clearly not representative of normal operation (such as, specific-surface area = 28 to 37 m^2/g vs. 105 to 265 m^2/g for the in situ samples and 151 to 194 m^2/g for the bridged material). As discussed later in this report, the transient cake also had lower drag than the bridged material and hopper samples (in situ samples were not tested due to insufficient sample size). The relatively low drag, low surface area, and low carbon content of the transient cake sample, coupled with the low rate of ΔP increase during the last filtration cycle, suggest that the transient dustcake sample collected at the end of GCT4 was not representative of the transient dustcakes formed during normal operations.

In comparing all of the residual dustcakes from the three runs, it is the GCT3 residual dustcake that appears to be unusual in terms of the relatively small mean particle size (MMD of 4 μm vs. 7 to 8 μm for GCT2 and GCT4) and in terms of the relatively large specific-surface area (44 m^2/g vs. 8 to 24 m^2/g for GCT2 and GCT4). However, as mentioned previously, the GCT3 residual dustcake was the only one of the three that did not appear to undergo some degree of consolidation, presumably caused by collection of tar within the dustcake. This consolidation would prevent the individual particles from being separated and sized correctly, resulting in a larger indicated particle size. Also, the tar would reduce the particle specific-surface area by coating and plugging the pore structure of the particles. This is not to suggest that no tar was present during GCT3. The fairly low surface area of the GCT3 residual dustcake compared to the in situ samples and bridged deposits suggest that some pore plugging occurred because of tar collection or due to reaction with other chemical components of the gas stream. However, it appears that this effect was much less with GCT3 than during the other test programs.

The listing below compares the average properties of the in situ samples, bridged deposits, and residual dustcakes from GCT3 and GCT4. From this comparison it is clear that the in situ samples and bridging material from GCT3 and GCT4 have much larger mean particle sizes

(MMDs) than those of the residual dustcakes from these runs. In the past this difference in mean particle size has been blamed on inertial removal of large particles by the cyclonic action of the PCD system. (During combustion operation this was a demonstrated effect.) However, the data compiled above suggest that this explanation does not apply for char. Comparing the in situ samples to the bridged deposits, it can be seen that only a small amount of particle dropout has apparently occurred (that is, the mean particle size has been reduced from 14 to16 to 12 to 13 μm). In the absence of significant dropout, alternative explanations for the finer size of the residual dustcakes could include fine-particle enrichment with time or the possibility that a finer dust size was generated during initial startup and this material stayed in place throughout the run.

	GCT3			GCT4		
	In situ	Residual	Bridging	In situ	Residual	Bridging
Avg bulk density (g/cc)	0.37	0.36	0.37	0.27	0.34	0.34
Avg particle density (g)/cc	2.28	2.37	2.40	2.29	1.91	2.21
Avg bulk porosity (%)	83.8	84.8	84.6	88.2	82.2	84.6
Avg surface area (m^2/g)	128	44.0	127	197	8.0	173
Avg MMD, (μm)	14.2	4.3	12.0	15.9	8.4	12.7

The similarity of the specific-surface area values between the in situ and bridged samples suggests that although the bridging may have been caused by tar the bridged deposit was not highly affected by the tar. If the bridged deposit had be subjected to extensive tar deposition it would have presumably been more agglomerated like the residual dustcake. Since this was not the case it may be inferred that the GCT4 bridging must have occurred near the end of the test program (probably on March 27, 2001, when there was an abrupt change in the baseline ΔP), after which there were no more episodes of tar formation and deposition.

3.6.5 Particle Size Analysis of In situ Samples and Dustcakes

The size distribution of the particles that make up the PCD dustcake is a critical factor in determining the drag properties of the dustcake. In addition, knowledge of the size distribution of particles leaving the transport reactor system can aid in understanding the operating characteristics of the system. As in previous tests, particle size distribution measurements were made using a Leeds & Northrup Microtrac X-100 particle size analyzer on the samples collected in situ in the gas stream at the inlet of the PCD and on the bridged deposits and dustcake samples removed from the filter elements at the end of each test program.

The average particle size distributions of the GCT3 and GCT4 in situ samples collected at the inlet of the PCD are shown in Figure 3.6-3. The distributions for these two gasification runs after modification of the transport reactor loop are almost identical. The average particle size distribution of the GCT2 in situ samples is shown for comparison. This comparison shows that the changes made in the transport reactor loop resulted in a reduction in the mass concentration of particles over a wide range of particle sizes from a few microns up to the largest particle sizes detected. For the smaller particle sizes, the reduction in mass concentration diminishes with decreasing particle size to a point where there is virtually no reduction at particle sizes below

1 μm. This result is consistent with more efficient particle collection in the disengager/cyclone system and improved carbon retention and gasification in the reactor loop.

Figure 3.6-4 is a comparison of the particle size distributions of the various samples collected during and following GCT3. The distributions shown include samples from the inlet gas stream, the PCD hopper, the bridged deposit, and the residual dustcake. The bridged deposits removed from the PCD are assumed to represent the transient dustcake. Interestingly, all of the distributions except for the residual dustcake are essentially identical. This suggests that little if any dropout or inertial collection is occurring in the PCD as was observed previously during combustion runs. As discussed in the previous section, the residual dustcake is much finer than the incoming dust for reasons that are not understood at this time.

The GCT4 particle size distributions are shown in Figure 3.6-5. Although there is a little more scatter in the data there is little real difference between the PCD inlet samples, the bridged deposit (transient dustcake), and the hopper samples. With the exception of the residual dustcakes, the GCT4 particle size distributions are not significantly different from the particle size distributions obtained for GCT3. As discussed previously, the apparent difference in the residual dustcakes is believed to be related to tar deposition in the cake, which makes it difficult to obtain accurate particle size data. The GCT4 residual dustcake, which was bonded together with tar, was probably not sized correctly by the Microtrac particle size analyzer, because the particle dispersion techniques used with this instrument are probably not adequate to break apart particles that are bonded together with condensed tar. Consequently, the Microtrac instrument was probably measuring clumps of consolidated particles rather than individual particles in the residual dustcake sample.

In the absence of the tar deposition there is no reason to believe that the residual dustcake from GCT4 would have been significantly different from the GCT3 residual dustcake. In future tests the transport reactor will be started on coke breeze in an effort to attain higher temperatures in the gasifier before coal is introduced. If this modification of the start-up procedures is successful in eliminating tar formation in the reactor the tar-related problems encountered with the particle size analysis should also be eliminated. Of course, it is also possible that the char produced from the coke may differ from the char produced from coal in terms of particle size and other characteristics.

3.6.6 Drag Characteristics of Dustcakes and Size-Segregated Hopper Samples

The normalized drag of a dust sample, R, provides a very valuable indication of the pressure drop, ΔP, that can be expected with a given areal loading of the dust, AL, at a given face velocity, FV, in accordance with the following simple relationship.

$$R = \frac{\Delta P}{AL \bullet FV}$$

Previous work has demonstrated a good correlation between PCD pressure drop and normalized drag measurements made using the resuspended ash permeability tester (RAPTOR),

which has been described in previous reports. For the drag measurements discussed here, the RAPTOR apparatus was modified by adding various combinations of cyclones between the fluidized-bed dust feeder and the dust dispersion and collection sections. This modification made it possible to make drag measurements as a function of the mean particle size collected on the filter, thus providing valuable information on the effect of particle size on drag and on the ability of the modified RAPTOR system to accurately simulate the performance of the PCD. The drag measurements with the modified RAPTOR system were made on bulk residual dustcake samples from GCT2, GCT3, and GCT4, on bulk samples of the bridged material from GCT3 and GCT4, and on PCD hopper samples collected during all three runs.

Figure 3.6-6 shows the results of the modified RAPTOR measurements of drag vs. mass median particle diameter (MMD). These data were obtained on samples that were size classified using various combinations of cyclones in the modified RAPTOR system. The cyclones used in making these measurements were cyclone Nos. 1, 2, and 3 from SRI's five-stage cascade cyclone sampling assembly. In order to obtain data with successively decreasing MMDs, drag measurements were made with no cyclones, with cyclone 1, with cyclone 2, and with cyclones 2 and 3 in series. The measurements of drag vs. MMD made on the redispersed samples of bridged deposits from GCT3 and GCT4 fell on the same trend line as the measurements made on the PCD hopper samples from these runs, so all of these data were grouped together for the regression analysis. As shown in the plot of drag vs. MMD, the data for the GCT2 samples and for the GCT3 and GCT4 samples fell on two different straight lines in logarithmic space. These lines were of the form:

$$R_{RAPTOR} = 10^{[m \bullet log(MMD) + b]}$$

in which R_{RAPTOR} is the drag measured using the modified RAPTOR apparatus in units of inWC/(lb/ft^2)/(ft/min), *MMD* is the mass median diameter of the dustcake collected in the RAPTOR apparatus in μm, m is the slope of the regression line, and b is the intercept of the regression line. The best-fit values of m and b and the coefficient of regression (r^2) for each straight-line fit are:

	GCT2	GCT3 and GCT4
m	-1.135	-0.982
b	2.740	2.997
r^2	0.91	0.90

The relatively high values of r^2 shown above indicate that the straight line fits are reasonably good representations of the data, and there is a good correlation between drag and particle size for the hopper/bridged samples. These results clearly demonstrate that drag is a strong function of particle size and that there is a definite difference between the GCT2 char and the GCT3 and GCT4 char. At any given particle size the GCT3 and GCT4 char has significantly higher flow resistance than the GCT2 char. This result suggests that particle size is not the only significant

factor affecting the drag. It seems intuitive that the surface roughness, or external surface area, of the particles could also have a strong influence on drag.

To examine the effect of roughness/surface area on drag, measurements were made of the specific-surface area of the various size-classified samples collected in the RAPTOR apparatus. The measurements of specific-surface area were made with a Micromeritics FlowSorb II surface-area analyzer, which utilizes the Brunauer-Emmett-Teller (BET) nitrogen-adsorption technique. Unfortunately, the BET technique measures the total surface area and cannot distinguish between external surface area that affects drag and internal surface area that does not affect drag. Nevertheless, it was hoped that these measurements might provide some insight into the role that surface area has in determining the drag of the char.

Figure 3.6-7 shows how the BET specific-surface area varied with MMD of the RAPTOR filter catches. This plot shows that the GCT3 and GCT4 hopper samples and the GCT3 and GCT4 bridged deposits fall on two distinctly different lines (even though these two groups of samples fall on the same trend line of drag vs. MMD). At a given particle size, the specific-surface areas of the GCT3 and GCT4 samples differ by as much as a factor of two (such as, from about 150 to about 300 m^2/g at an MMD of 10 μm), even though all of these samples fell on the same line of drag vs. MMD. In other words, substantially different surface areas were measured on samples that have about the same MMD and drag. One way of explaining this result is to postulate that some of the measured surface area is in the form of internal pores that do not contribute to flow resistance. In fact, since all of the GCT3 and GCT4 hopper samples and bridged deposits have surface areas in excess of 150 m^2/g, and all of these samples fall on the same line of drag vs. MMD, it can be reasonably concluded that surface areas in excess of 150 m^2/g do not affect drag. For these particular samples, most of the additional surface area beyond 150 m^2/g appears to be in the form of internal surface area that does not affect drag. Since the GCT2 samples fall on a different line of drag vs. MMD, and since the GCT2 samples all have surface areas of less than 70 m^2/g, it can be further inferred that the cutoff point for surface area that affects drag must be somewhere between 70 and 150 m^2/g, with these particular samples.

As shown in the previous plot of surface area vs. MMD, the bridged deposits from both GCT3 and GCT4 have lower surface areas than the hopper samples from the same tests. This result suggests that some of the pores in the bridged deposits may have been blocked by tar deposition, sulfidation, or some type of consolidation. Because of the Kelvin effect, tar vapors would tend to first condense in the smallest pores, which would not contribute to drag. This could explain why the surface area of the bridged deposits has been decreased without a commensurate reduction in drag. Sulfidation could also result in the preferential closure of the smallest pores, but the chemical analyses discussed earlier show that the bridged deposits contain no more CaS than the in situ samples. Since the GCT3 and GCT4 bridged deposits were formed at relatively low temperatures (700 to 900°F), it seems unlikely that there could have been any type of consolidation that would require the formation of molten phases or eutectics. Therefore, tar deposition seems to be the most likely explanation for the lower surface areas of the bridged deposits.

The effect of tar deposition on surface area can be seen even more dramatically in the residual dustcake samples, as shown below.

	GCT2	GCT3	GCT4
Mean surface area of in situ samples (m^2/g)	93	128	197
Mean surface area of bridged material (m^2/g)	----	127	173
Mean surface area of residual dustcake (m^2/g)	24	44	13

The surface area values shown above suggest that the residual dustcakes were subjected to even greater degrees of pore closure by tar deposition. This result is consistent with the SEM photographs discussed previously that show the char particles in the residual dustcakes bonded together with tar.

Referring back to Figure 3.6-6, it is also clear that the GCT3 and GCT4 residual dustcakes have much lower measured drag values than do the GCT3 and GCT4 hopper samples and bridged deposits. The drag data for the residual dustcakes are single-point measurements that were made using the residual dustcake samples without any cyclones to adjust the particle size distribution reaching the RAPTOR filter. For these measurements the cyclones were deemed to be unnecessary since the purpose of these measurements was to determine whether the drag of the bulk residual dustcake was similar to the drag of the hopper samples and the bridged deposits. Also, the residual dustcake samples had MMDs that were smaller than or equal to the cutpoint of cyclone 1. As indicated in the plot, good agreement between the residual dustcake measurement and the size-segregated hopper measurement was achieved for GCT2, but not for GCT3 or for GCT4.

As mentioned previously, the residual dustcakes from GCT2 and GCT4 contained flakes that presumably consisted of char particles that were "glued" together with tar and the average MMDs of these dustcakes were about 7 to 8 μm. The GCT3 residual dustcake did not contain these "glued-together" flakes and the MMD of the GCT3 residual dustcake was about 4 μm. As discussed previously in the section on particle size analysis, this apparent difference in MMD was attributed to the inability of the dispersion techniques used with the Microtrac particle size analyzer to break apart the agglomerates of tar-bonded char particles. If the residual dustcakes are held together tightly enough to prevent their complete dispersion in the Microtrac sample preparation procedures, then it seems unlikely that they would be broken apart completely in the RAPTOR apparatus. Because of this incomplete dispersion, the dustcake formed in the RAPTOR apparatus is probably comprised of particle agglomerates that are larger than the individual char particles. This effect probably explains why the porosity of the RAPTOR dustcake was 83 percent, while the porosity of agglomerated flakes taken from the residual dustcake ranged from 72 to 75 percent. Because of this large difference in porosity the RAPTOR dustcake would be expected to have a lower drag than one that was formed from the individual char particles and then glued together with tar. Therefore, the RAPTOR measurements on the residual dustcakes probably do not accurately reflect the true drag of the tar-bonded dustcake as it resided on the filter elements during the runs. This validity of this assertion will be tested later in the analysis of PCD pressure drop.

The foregoing discussion examined the relationship between drag and particle size, the relationship between specific-surface area and particle size, and the effects of tar deposition on specific-surface area and drag but the relationship between drag and surface area has not been explicitly investigated. Efforts to develop correlations between specific-surface area and drag have failed to yield a simple, direct correlation between these parameters. Yet it seems reasonable that the flow resistance of a particle should be related to the surface area of the particle, or at least to a portion of the surface area. To investigate this possibility further, the particle surface area (SA_p) was calculated for all of the GCT2, GCT3, and GCT4 char samples using the following equation:

$$SA_p = BET \bullet \rho_{true} \bullet \frac{\pi}{6} \bullet (MMD)^3 \bullet 10^{-12}$$

in which SA_p is the surface area of the mass-median particle in m^2, BET is the specific-surface area of the sample at the mass median particle size in m^2/g, ρ_{true} is the true particle density in g/cm^3, and MMD is the mass median particle diameter in μm. Using a typical value of true density of 2.2 g/cm^3, this equation simplifies to

$$SA_p = 1.15x10^{-12} \bullet BET \bullet (MMD)^3$$

In Figure 3.6-8 the calculated values of SA_p are plotted against the drag values determined for the same samples. The regression fit shows that the drag-vs.-SA_p provides a better correlation than the drag-vs.-MMD regression presented earlier. For the GCT3 and GCT4 data, the regression coefficient for the drag-vs.-SA_p correlation is 0.93, compared to only 0.90 for the drag-vs.-MMD correlation. This difference in regression coefficients represents a 30-percent reduction in the uncertainty of the correlation. One way of interpreting this result is that a better correlation with drag can be obtained by incorporating the BET surface area along with the MMD rather than using the MMD alone. This improvement was not achieved with the GCT2 data, presumably because there was little variation in the BET surface areas for these samples.

Even with the improved correlation obtained using the SA_p, there are still two distinctly different regression lines for GCT2 and for GCT3 and GCT4. This result suggests that the combined effects of surface area and MMD still do not explain the substantial difference between these two data sets. The failure of the drag-SA_p correlation to collapse both sets of data onto one line may indicate that there are other factors affecting drag that are not being taken into account with this correlation. The quality of the correlation could probably be improved substantially by using only the surface area that contributes to drag, as opposed to the total (BET) surface area; however, existing data are not adequate to define precisely the fraction of the surface area that influences drag. To address this shortcoming, efforts are underway to measure the distribution of surface area as a function of pore size. There is hope that these measurements will provide insight into the fraction of the surface area that is contained in pores large enough to affect drag. By subtracting out the contribution of the smaller pores to the surface area, it may be possible to

achieve a better correlation with drag and a better understanding of how surface area affects drag.

3.6.7 Analysis of PCD Pressure Drop

For the purposes of this discussion, it is convenient to consider the PCD pressure drop (ΔP) in two separate parts: 1) the transient ΔP, which is the pressure drop that accumulates during each filtration cycle and 2) the baseline ΔP, which is the pressure drop that remains after the filter elements are back-pulsed. Transient ΔP is a function of the concentration and flow resistance (drag) of the dust reaching the filter elements, the gas flow, the length of the filtration cycle (time between back-pulses), and the total filter surface area. In addition to such factors as coal-feed rate and operating conditions, particle dropout in the filter vessel can also affect the particulate concentration reaching the filter elements and, thereby, influence the transient ΔP. According to conventional wisdom, baseline ΔP is not a function of the particulate concentration, or at least not a strong function. This assertion seems reasonable when the baseline ΔP is maintained at a stable value for prolonged periods of PCD operation, but it may be called into question when the baseline ΔP increases over time. In addition to the flow resistance of the residual dustcake, the baseline ΔP is also influenced by vessel losses and any irrecoverable changes that may occur in the flow resistance of the filter elements or fail-safes (such as changes caused by backside blinding or fail-safe plugging). Based on flow tests that were performed on filter elements and fail-safes that were used in the various gasification runs it can be assumed that backside blinding and fail-safe plugging were negligible during GCT2, GCT3, and GCT4.

In the following sections, the contributions of the transient and residual dustcakes to PCD ΔP are examined by comparing dustcake drag values calculated from the PCD ΔP to dustcake drag values measured by RAPTOR. This is a very valuable comparison because mismatches between these two methods of determining drag can indicate that other factors (such as tar deposition) may be influencing the PCD ΔP.

3.6.7.1 Transient ΔP

The following analysis was used to assess the portion of the PCD ΔP that was contributed by the transient dustcake accumulated during each filtration cycle. First, data from the Plant Information (PI) system were used to determine the average rate of PCD ΔP rise ($\Delta P/\Delta t$) during each of the in situ particulate sampling runs. The rate of increase in the dustcake areal loading during each sampling run [$\Delta\ (AL)/\ \Delta t$] was then calculated as follows:

$$\frac{\Delta(AL)}{\Delta t} = \frac{ML \bullet W}{1{,}000{,}000 \bullet 60 \bullet A}$$

in which $\Delta(AL)/\Delta t$ is the rate of increase in the dustcake areal loading in lb/ft^2/min, ML is the inlet particulate mass loading in ppmw, W is the process gas mass-flow rate in lb/hr, and A is the total active surface area of the filter elements in ft^2. The values of $\Delta P/\Delta t$ and $\Delta\ (AL)/\ \Delta t$ determined for each sampling run may be used to calculate a corresponding value of PCD

transient drag, *R*, using the same basic equation used in determining normalized drag from the RAPTOR data:

$$R = \frac{\Delta P}{AL \bullet FV} = \frac{\frac{\Delta P}{\Delta t}}{\frac{\Delta (AL)}{\Delta t} \bullet FV}$$

in which *R* is the PCD transient drag in inWC/(lb/ft^2)/(ft/min), $\Delta P/\Delta t$ is the average rate of pressure drop increase during the sampling run in inWC/min, $\Delta(AL)/\Delta t$ is the rate of increase in the dustcake areal loading in lb/ft^2/min, and *FV* is the average PCD face velocity in ft/min. To allow direct comparison of this PCD drag value with the RAPTOR drag measurements, the dustcake drag obtained in this manner must be adjusted to the RAPTOR conditions using the ratio of the syngas viscosity at process temperature to the viscosity of air at laboratory room temperature, according to the following equation:

$$R_{normalized} = R \bullet \frac{\mu_{air}}{\mu_{syngas}} = \frac{\Delta P}{AL \bullet FV} \bullet \frac{\mu_{air}}{\mu_{syngas}} = \frac{\frac{\Delta P}{\Delta t}}{\frac{\Delta (AL)}{\Delta t} \bullet FV} \bullet \frac{\mu_{air}}{\mu_{syngas}}$$

in which $R_{normalized}$ is the PCD transient drag normalized to the same gas viscosity as the RAPTOR measurements (air at room temperature), μ_{air} is the viscosity of air at room temperature (77°F) in ΔP, and μ_{syngas} is the viscosity of the syngas at the process gas temperature in ΔP.

The RAPTOR drag value for each particulate sampling run was taken from the plot of drag vs. MMD, shown previously in Figure 3.6-6, using the MMD values determined by Microtrac analysis for each sampling run. Since it was difficult to accurately interpolate values directly from the drag-vs.-MMD plot, the drag data were obtained from the regression equations describing the best straight-line fits to the drag-vs.-MMD data in logarithmic space. These equations were provided in the section on the laboratory drag measurements. Table 3.6-8 provides the laboratory drag values determined from the regression fits of the RAPTOR data and the PCD transient drag values determined from the rate of ΔP increase during the sampling runs. From the tabulated drag values it is obvious that the data for runs GCT3IMT-2 and GCT4IMT-1 are outliers. Average values of drag determined by the two different approaches, excluding the outliers, are shown below. The drag values are in units of inWC/(lb/ft^2)/(ft/min) and are on the viscosity basis of air at 77°F.

	GCT2	GCT3	GCT4
Average drag from PCD ΔP rise	29	93	66
Average drag from RAPTOR data	21	70	70

This summary shows that there is fairly good overall agreement between the PCD calculations and the RAPTOR measurements. This agreement can also be seen by plotting the individual values of PCD drag and RAPTOR drag determined for each sampling run, as shown in Figure 3.6-9. The outliers mentioned above are the two data points that fall well below the perfect-agreement line on the plot. Ignoring these outliers, the plot clearly shows that the RAPTOR drag values track the PCD transient drag values reasonably well. This result suggests that the flow resistance of the char is high enough to account for all of the transient ΔP and that the transient dustcake drag was not affected by tar deposition or other anomalies during the in situ particulate sampling runs. As shown in the following section, this was not the case with the residual dustcake drag, which was increasing as shown by the creeping baseline ΔP. The difference between the measurements of transient and residual drag is attributable to the fact that the transient sampling avoided the few tar deposition events that occurred, while the residual dustacke was unavoidably exposed to all tar events.

3.6.7.2 Baseline ΔP

In order to facilitate the direct comparison of the baseline pressure drops during GCT2, GCT3, and GCT4, the baseline ΔP data from all three runs were first normalized to the same temperature (850°F) and the same face velocity (3.5 ft/min). Figure 3.6-10 shows a plot of the normalized baseline ΔP as a function of time throughout all of the gasification runs. As shown in the plot, both GCT3 and GCT4 were characterized by increasing baseline pressure drop, with the normalized baseline ΔP achieving values as high as 150 inWC in GCT3 and values of over 200 inWC in GCT4. This behavior may be contrasted with the baseline pressure drop performance during GCT2, in which the normalized baseline ΔP increased initially and then stabilized at about 70 inWC. Unlike GCT2, a stable baseline ΔP was never achieved in GCT3 or GCT4.

As discussed previously, one of the possible explanations for the observed increase in PCD baseline ΔP is tar deposition within the residual dustcake. It is also possible that some of the observed increase in baseline ΔP could be caused by a reduction in the effective filtration area as a result of bridged deposits. The deposition of tar on char particles could make the particles sticky, thereby contributing to the formation of the bridged deposits. The presence of agglomerated flakes in the GCT2 and GCT4 residual dustcakes suggests that these cakes may have been substantially affected by tar deposition. Although these flakes were not seen in the GCT3 residual dustcake the presence of bridged deposits within the PCD after GCT3 suggests that tar could have also had some effect on the PCD pressure drop during GCT3. Also, it was observed during both GCT3 and GCT4 that the coal restarts (when tar was formed due to low gasification temperatures) were frequently followed by increases in baseline ΔP.

These effects complicate the analysis of PCD baseline ΔP and make it difficult to rationalize the baseline ΔP in terms of laboratory drag measurements. Nevertheless, comparison of residual dustcake drag values determined from the PCD baseline ΔP and from the RAPTOR measurements can help to provide better understanding of the magnitude of the effect of tar deposition on the residual dustcake drag. Therefore, the remainder of this section will focus on attempting to quantify the contribution of the residual dustcake to the PCD baseline ΔP.

As shown in previous reports, the contribution of the residual dustcake to the baseline ΔP can be estimated by subtracting the contributions of the vessel losses and any irreversible increases in the filter element ΔP and the fail-safe ΔP. For GCT2, GCT3, and GCT4, vessel losses were estimated from the baseline ΔP recorded during the startups prior to the initiation of coal feed. To put both the final baseline ΔP and the startup baseline ΔP on the same basis, startup ΔPs were also normalized to a temperature of 850°F and to a face velocity of 3.5 ft/min. The changes in filter element and fail-safe ΔPs were assumed to be negligible for all of these runs since there was no potential for backside blinding and flow tests performed on the used filter elements and fail-safes did not show any irrecoverable change in ΔP.

After establishing the pressure drop attributable to the residual dustcake ($\Delta P_{residual}$) (as discussed above), the residual dustcake drag ($R_{residual}$) can then be calculated using the same basic formula used in reducing the RAPTOR data and in calculating the transient dustcake drag:

$$R_{residual} = \frac{\Delta P_{residual}}{AL_{residual} \bullet FV}$$

in which $R_{residual}$ is the residual dustcake drag in inWC/(lb/ft^2)/(ft/min), $\Delta P_{residual}$ is the residual dustcake pressure drop in inWC, $AL_{residual}$ is the residual dustcake areal loading in lb/ft^2, and FV is the face velocity in ft/min. The values of FV recorded during GCT3 and GCT4 were adjusted to account for the fraction of the filter surface that was blocked by bridged deposits. Based on the observations of the bridging after GCT3 and GCT4, it was estimated that about 10 percent of the filter surface was blocked in GCT3 and about 30 percent in GCT4. Therefore, the face velocities recorded by PI were increased by 10 percent for GCT3 and by 30 percent for GCT4. (Of course, it is possible that the blockage of the filter surface was actually higher than 10 percent and 30 percent, since some of the bridged deposits may have fallen out after shutdown. Nevertheless, the values of 10 percent and 30 percent will be used here, since there is no rational basis for specifying an alternative degree of blockage.)

To allow direct comparison of the PCD residual dustcake drag values with the RAPTOR drag measurements, the PCD residual dustcake drags were adjusted to laboratory conditions using the same viscosity correction technique applied in the transient drag analysis. The results of these calculations are summarized in the following table.

	GCT2	GCT3	GCT4
1. Final baseline ΔP normalized to 850°F and 3.5 ft/min (inWC)	70	180	200
2. Vessel losses (startup ΔP normalized to same conditions) (inWC)	30	30	30
3. Residual dustcake ΔP (item 1 – item 2) (inWC)	40	150	170
4. Residual dustcake areal loading (lb/ft^2)	0.09	0.04	0.2
5. Adjusted face velocity (ft/min)	3.5	3.9	4.6
6. PCD dustcake drag (item 3/item 4/item 5) (inWC/(lb/ft^2)/(ft/min))	130	960	185
7. PCD dustcake drag at room temp (item 5/1.74)	73	550	110

The PCD residual dustcake drag values calculated above may now be compared with the RAPTOR measurements made on the residual dustcake samples. However, as discussed previously, the residual dustcake samples were apparently agglomerated with tar. Since this agglomeration prevented the complete dispersion of the residual dustcake samples for particle size analysis, it is also very likely that the residual dustcake samples were not dispersed into their constituent char particles in the RAPTOR apparatus. Because of this effect, the RAPTOR measurements made on the residual dustcake samples are probably unrealistically low. It may be possible to obtain a better estimate of the true residual dustcake drag by using the drag-vs.-MMD regression fit to the RAPTOR measurements made on the hopper samples and bridged deposits, while using the MMDs of the respective residual dustcake samples in the regression equation. Therefore, the comparisons given here will include both the RAPTOR measurements made on the residual dustcake samples and the RAPTOR drag values obtained from the hopper and bridging regression fits at the residual dustcake MMDs. The following listing shows a comparison of all of these values.

Normalized drag, $\frac{\text{inWC}}{(\text{lb}/\text{ft}^2)(\text{ft}/\text{min})}$

	GCT2	GCT3	GCT4
Calculated from PCD baseline ΔP	73	550	110
RAPTOR on residual dustcake	60	85	42
RAPTOR on hopper/bridged samples	57	240	130

This comparison shows that the RAPTOR measurements on the samples collected from the residual dustcakes tend to underpredict the actual residual dustcake drag. However, much better agreement is achieved by using the drag values obtained from the regression fits on the hopper/bridging samples at the actual MMDs of the residual dustcake. This result suggests that the drag of the char, alone, may be sufficient to explain much of the PCD baseline ΔP, at least in the case of GCT2 and GCT4. This comparison also demonstrates that it may be dangerous to rely on RAPTOR measurements made on agglomerated samples that cannot be completely redispersed.

The very high drag value calculated for the PCD residual dustcake during GCT3 may be partially caused by a dustcake areal loading that is not representative. After both GCT2 and GCT3 the PCD was back-pulsed repeatedly to remove as much dust as possible. After GCT4, the PCD was not back-pulsed to preserve the dustcakes. As discussed in a previous section, the residual dustcake after GCT2 was crusty, while after GCT3 the residual layer was fluffy. It is possible that the back-pulsing after shutdown was more effective at the end of the GCT3 test program, resulting in an unrealistically low areal loading and an unrealistically high drag.

It could also be argued that some of the disagreement between the RAPTOR measurements and the actual residual dustcake drag could be attributed to a failure to accurately take into account the degree of bridging within the PCD during operation. If some of the bridged deposits fell out while removing the internals or during the system shutdown and cooling, then the blockage of the filter surface area may have actually been more extensive than the 10- and 30-percent blockages used in this analysis. This would have the effect of increasing the effective face velocities in GCT3 and GCT4, resulting in lower values of PCD residual dustcake drag for these runs. However, the effect of the bridging cannot completely explain the difference between the actual PCD and the RAPTOR measurements made on the residual dustcakes. In order to bring these values into agreement, it would be necessary to have over 85 percent blockage of the surface area in GCT3 and over 70 percent blockage in GCT4, which seems unlikely. Therefore, it seems improbable that bridging can completely explain the discrepancy between the actual baseline ΔP and the RAPTOR measurements of residual dustcake drag.

3.6.8 Real-Time Particulate Monitor Evaluation

Protection of the combustion turbine located downstream of the PCD is of paramount importance. Accordingly, an instrument that could provide real-time particle concentration monitoring at the exit of the PCD is desirable to minimize turbine damage resulting from a filter failure or other high-mass emission event. During GCT3 and GCT4 the ongoing evaluation of real-time particulate monitors was continued with testing of the PCME DustAlert 90 Emissions Monitoring System. This instrument is manufactured by Pollution Control & Measurement (Europe) of Cambridgeshire, England.

The DustAlert 90 determines particle concentration by detecting the naturally occurring electrical charge on the suspended particles in the gas stream as they flow past the probe. This type of probe differs from the triboelectric probes that measure the charge generated when a particle impacts on the surface of the probe. Triboelectric probes typically do not measure very small particles well because those particles tend to follow the gas-flow stream lines around the probe and fail to impact. Since the goal is to detect particle sizes and concentrations that are quite low, the PCME technique was considered to be a promising approach.

Previous tests of the PCME probe had not successfully demonstrated that it could detect particles at the low concentrations required for turbine protection. To enhance the detection capabilities of the probe, modifications were made to improve the electrical insulators and to increase the electrical sensitivity of the probe. The modified probe was installed prior to GCT3, but the insulators were fouled with tar during startup of the transport reactor. The fouling effectively shorted the probe signal to ground and no signal could be detected from the unit for the remainder of GCT3. Although there was a nitrogen purge system on the PCME that was intended to prevent insulator contamination, it was not adequate for the high-tar concentrations encountered. After completion of GCT3 the insulators were cleaned and the normal response of the probe returned.

Prior to GCT4, an improved purge system was installed on the PCME port to shield the insulators from the gas stream and to prevent tar contamination. The modified purge system worked as planned and signal output from the PCME was maintained for the duration of GCT4.

During normal operation the PCME generally indicated a very low reading that appeared to be in the noise range of the instrument. This response was consistent with the actual mass concentration at the outlet of the PCD, which was determined by in situ batch measurements to be less than 0.1 ppmw. Thus, from observation of the instrument during normal operation, the lower limit of resolution appears to be above 0.1 ppmw. This result was not surprising since this instrument was not expected to detect such low concentrations.

Since the PCD outlet particulate concentration was too low to test the PCME under normal operating conditions, a brief period of comparative tests was conducted with dust injected into the PCD outlet stream. The dust injection system used for these tests is described in previous reports. Although current operation is in gasification mode, combustion ash particles were used for the test because the behavior of the injection system with combustion ash has been thoroughly characterized. Figure 3.6-11 shows the output of the PCME over a 1.5-hour period with various injected dust concentrations. The vertical scale of the chart is zero to 100 percent of full-scale output (the PCME will not provide absolute concentration data unless it can be calibrated to known conditions). In the chart, the background reading with no dust injected (zero ppmw) can be compared to three injected concentrations. The three concentrations of 8, 12, and 30 ppmw are estimated values taken from the calibration curve of the dust injection system. The test was to be repeated the next day using the in situ batch sampling system to substantiate the injected concentrations, but problems with the coal feeder terminated the test program before those data could be collected. Nevertheless, it is clear that the PCME responded to the injected dust in a definite and repeatable way.

In addition to the uncertainty as to the exact injected concentrations, there are several other caveats that must be considered in evaluation of these results. Since the instrument does not actually detect particles, but instead measures the charge on the particles, char particles may produce a different response than the combustion ash used in these tests. The dust injection system will be modified before the next test program to allow these tests to be repeated with char injection upstream of the PCME. Even then, all of the questions regarding the response of this measurement system will not be answered with injected char because char exiting the transport reactor may have a different charge-to-mass ratio than the particles blown out of the dust injection system. If elevated PCD outlet concentrations are encountered in the future the batch sampling system will be used to calibrate the output of the PCME. In the meantime the results presented here indicate that the PCME output should be monitored as an early warning of PCD leakage problems.

3.6.9 Conclusions

The GCT3 and GCT4 test programs successfully demonstrated that very low levels of particulate emissions (< 1 ppmw) can be achieved during operation of the PCD on gasification char. All of the outlet loadings were below the limit of resolution of the measurements (<0.1 ppmw) except for two measurements in which it appears that tar penetrated through the PCD as a vapor and was subsequently collected as tar droplets.

Inlet particulate loadings and particle size distributions measured during GCT3 and GCT4 confirmed that the modifications made to the transport reactor loop had the expected effect on

the mass concentration and size distribution of dust entering the PCD. On average, the particulate loading entering the PCD was reduced by about 40 percent compared to GCT2, even though the coal-feed rate was typically higher in GCT3 and GCT4 than in GCT2.

Contrary to the results obtained in GCT2, stable PCD operation at an acceptable baseline ΔP was not achieved in either GCT3 or GCT4. There were several episodes of significant baseline ΔP creep during both GCT3 and GCT4 that are believed to be associated with tar deposition and the formation of bridged deposits caused by sticky char particles.

Based on a comparison of RAPTOR drag measurements with transient drag values calculated from the rate of PCD ΔP rise, the drag of the char appears to be high enough to account for all of the observed ΔP rise during filtration. Tar deposition or other anomalies apparently did not have any significant effect on the PCD transient ΔP.

The residual dustcake drag measured by RAPTOR appears to be far too low to explain the observed baseline ΔP. Much better agreement with the baseline ΔP was obtained by using the MMDs of the residual dustcake samples in the regression fits of the drag-vs.-MMD data for the hopper samples and bridged deposits. This result suggests that the RAPTOR apparatus may not accurately simulate the formation of residual cakes that are stuck together with tar.

Correlations of the drag with MMD and surface area demonstrate that these parameters are not sufficient to completely explain the char drag observed in all three gasification tests, even though these parameters can separately correlate the data from GCT2 and from GCT3 and GCT4. In an effort to investigate the other factors that may be contributing to the observed variation in drag, further studies are planned to investigate the distribution of surface area as a function of pore size. There is hope that from these studies a better understanding may be gained of the fraction of the particle-surface area that contributes to drag, making it possible to develop more reliable correlations between char drag and physical properties.

A preliminary evaluation of the PCME real-time particulate monitor with injected combustion ash yielded promising results, but additional testing is needed to determine whether this instrument will reliably detect char particles from coal gasification.

Table 3.6-1

PCD Inlet and Outlet Particulate Measurements From GCT3 and GCT4

Test Date	PCD Inlet				PCD Outlet					PCD Collection Efficiency (%)
	SRI Run No.	Start Time	End Time	Particle Loading (ppmw)	SRI Run No.	Start Time	End Time	H_2O Vapor (vol. %)	Particle Loading (ppmw)	
GCT3										
12/15/00	1	09:35	10:35	1,700[1]	1	09:30	11:30	6.4	16.87	99.01
12/15/00	--	--	--	--	2	14:45	16:15	3.0	15.92	--
1/25/01	2	10:45	11:02	11,000	3	10:30	11:16	4.4	0.26[2]	--
1/26/01	3	09:30	09:39	25,900	4	08:50	10:20	5.6	< 0.1	> 99.9996
1/27/01	4	08:25	08:40	20,700	5	08:05	11:05	6.8	< 0.1	> 99.9995
1/29/01	5	10:30	10:45	19,300	6	10:22	11:25	8.1	< 0.1	> 99.9995
1/30/01	6	09:35	09:50	28,700	7	09:20	12:20	6.8	< 0.1	> 99.9997
1/31/01	7	09:27	09:37	15,500	8	09:15	12:15	9.2	< 0.1	> 99.9994
GCT4										
3/09/01	1	09:00	09:15	23,300	1	09:30	11:30	4.9	< 0.1	> 99.9996
3/10/01	2	13:40	13:48	59,500[3]	2	12:45	13:50	9.4	38.6[4]	------
3/25/01	--	--	--	--	3	15:50	17:20	4.6	< 0.1	------
3/26/01	3	09:45	09:55	14,800	4	09:35	10:45	8.7	< 0.1	> 99.9993
3/27/01	4	12:15	12:25	19,800	5	09:10	12:40	8.0	< 0.1	> 99.9995
3/28/01	5	09:50	10:00	10,500	6	09:30	13:30	10.2	< 0.1	> 99.9990
3/29/01	6	12:20	12:35	12,600	7	10:55	13:55	10.3	< 0.1	> 99.9992

Notes:
1. Sample collected during circulation of bed material only without any coal feed.
2. Sample contaminated with brown substance (possibly tar) – no visible char on sampling filter.
3. Sampling performed during start of coal feed.
4. Sampling filter covered with black substance assumed to be tar.

Table 3.6-2

Analytical Results on In situ Particulate Samples From GCT3

Elemental Analysis (As-Received Basis)

Lab ID	SRI Run No.	Date	C	H	N	S	Al	Ca	Fe	Mg	Si
AB07661	GCT3IMT-2	01/25/01	42.59	0.57	0.36	1.31	3.84	15.14	2.09	2.70	7.47
AB07684	GCT3IMT-3	01/26/01	43.64	0.56	0.40	1.06	3.22	16.34	1.85	2.74	6.55
AB07835	GCT3IMT-4	01/27/01	41.16	0.55	0.33	0.96	3.05	17.38	1.84	2.92	6.50
AB07836	GCT3IMT-5	01/29/01	41.65	0.59	0.32	1.02	3.47	16.39	1.95	2.83	6.68
AB07837	GCT3IMT-6	01/30/01	50.36	0.64	0.41	1.04	3.40	12.76	1.72	2.13	6.54
AB07838	GCT3IMT-7	01/31/01	24.31	0.35	0.15	0.83	5.37	19.17	2.74	3.33	11.58
Average			40.62	0.54	0.33	1.04	3.72	16.20	2.03	2.78	7.55

Chemical Composition Calculated from Elemental Analysis*

Lab ID	SRI Run No.	Date	CO_2	$CaCO_3$	CaS	CaO	Al_2O_3	Fe_2O_3	MgO	SiO_2	Elem C**
AB06811	GCT2IMT-2	04/19/00	N.M.	######	2.95	#####	7.25	2.99	4.51	16.01	#####
AB06812	GCT2IMT-3	04/20/00	N.M.	######	2.39	#####	6.08	2.64	4.56	14.04	#####
AB06813	GCT2IMT-4	04/21/00	N.M.	######	2.16	#####	5.76	2.63	4.87	13.92	#####
AB06814	GCT2IMT-5	04/22/00	N.M.	######	2.30	#####	6.55	2.79	4.71	14.32	#####
AB06815	GCT2IMT-6	04/24/00	N.M.	######	2.34	#####	6.42	2.46	3.55	14.01	#####
AB06816	GCT2IMT-7	04/25/00	N.M.	######	1.87	#####	10.14	3.92	5.56	24.82	#####
Average			####	######	2.33	#####	7.03	2.90	4.63	16.19	#####

* Assumes that all CO_2 is present as $CaCO_3$, all sulfur is present as CaS, and remaining calcium is present as CaO.

** Assumes that all carbon not accounted for as $CaCO_3$ is in the form of elemental carbon.

N.M. = Not measured due to insufficient sample size.

= Could not be determined since CO_2 was not measured.

Table 3.6-3

Analytical Results on Dustcake Samples From GCT3

Elemental Analysis (As-Received Basis)

Lab ID	Description	Date	C	H	N	S	Al	Ca	Fe	Mg	Si
AB07857	Transient/bridging	02/06/01	36.96	0.54	0.25	0.77	3.86	16.76	2.16	2.89	6.99
AB07858	Residual dustcake	02/06/01	44.70	0.86	0.53	1.14	3.14	13.47	2.11	2.65	4.60
AB07859	FD0520 Hopper	02/02/01	34.14	0.49	0.25	0.71	3.90	16.58	2.14	2.84	9.42

Chemical Composition Calculated from Elemental Analysis*

Lab ID	Description	Date	CO_2	$CaCO_3$	CaS	CaO	Al_2O_3	Fe_2O_3	MgO	SiO_2	Elem C**
AB07857	Transient/bridging	02/06/01	N.M.	######	1.73	#####	7.29	3.09	4.81	14.99	#####
AB07858	Residual dustcake	02/06/01	N.M.	######	2.57	#####	5.93	3.01	4.41	9.86	#####
AB07859	FD0520 Hopper	02/02/01	N.M.	######	1.60	#####	7.36	3.06	4.73	20.19	#####

* Assumes that all CO_2 is present as $CaCO_3$, all sulfur is present as CaS, and remaining calcium is present as CaO.

** Assumes that all carbon not accounted for as $CaCO_3$ is in the form of elemental carbon.

N.M. = Not measured due to insufficient sample size.

= Could not be determined since CO_2 was not measured.

Table 3.6-4

Analytical Results on In situ Particulate Samples From GCT4

Elemental Analysis (As-Received Basis)

Lab ID	SRI Run No.	Date	C	H	N	S	Al	Ca	Fe	Mg	Si
AB08051	GCT4IMT-1	03/09/01	52.87	0.61	0.01	1.87	3.44	12.05	1.86	2.12	5.38
AB08052	GCT4IMT-2	03/10/01	40.36	0.27	0.01	0.60	3.00	9.73	1.59	1.69	12.11
AB08233	GCT4IMT-3	03/26/01	35.12	0.37	0.01	N.M.	N.M.	N.M.	N.M.	N.M.	N.M.
AB08234	GCT4IMT-4	03/27/01	45.18	0.58	0.01	0.84	5.34	8.20	2.53	1.63	9.63
AB08235	GCT4IMT-5	03/28/01	34.79	0.40	0.01	N.M.	N.M.	N.M.	N.M.	N.M.	N.M.
AB08236	GCT4IMT-6	03/29/01	33.93	0.43	0.01	0.65	N.M.	N.M.	N.M.	N.M.	N.M.
Average			40.38	0.44	0.01	0.99	3.93	9.99	1.99	1.81	9.04

Chemical Composition Calculated from Elemental Analysis*

Lab ID	SRI Run No.	Date	CO_2	$CaCO_3$	CaS	CaO	Al_2O_3	Fe_2O_3	MgO	SiO_2	Elem C**
AB08051	GCT4IMT-1	03/09/01	5.41	12.30	4.22	6.70	6.50	2.65	3.53	11.53	51.39
AB08052	GCT4IMT-2	03/10/01	5.69	12.93	1.36	5.33	5.67	2.27	2.82	25.96	38.81
AB08233	GCT4IMT-3	03/26/01	N.M.	####	####	####	####	####	####	####	#####
AB08234	GCT4IMT-4	03/27/01	2.63	5.98	1.90	6.66	10.08	3.61	2.71	20.65	44.46
AB08235	GCT4IMT-5	03/28/01	N.M.	####	####	####	####	####	####	####	#####
AB08236	GCT4IMT-6	03/29/01	6.08	13.82	1.46	####	####	####	####	####	#####
Average			4.95	11.26	2.23	6.23	7.42	2.84	3.02	19.38	44.89

* Assumes that all CO_2 is present as $CaCO_3$, all sulfur is present as CaS, and remaining calcium is present as CaO.
** Assumes that all carbon not accounted for as $CaCO_3$ is in the form of elemental carbon.
N.M. = Not measured due to insufficient sample size.
= Could not be determined since CO_2 was not measured.

Table 3.6-5

Analytical Results on Dustcake Samples From GCT4

Elemental Analysis (As-Received Basis)

Lab ID	Description	Date	C	H	N	S	Al	Ca	Fe	Mg	Si
AB08248	Transient, Candle T-6	04/06/01	32.27	1.11	0.19	0.91	4.82	16.90	2.33	4.20	6.43
AB08249	Transient, Candle T-8	04/06/01	30.15	0.98	0.13	0.90	4.29	18.14	2.39	4.56	6.40
AB08250	Transient, Candle T-9	04/06/01	30.69	0.98	0.18	0.94	4.16	17.95	2.38	4.47	6.65
AB08251	Transient, Candle T-14	04/06/01	32.69	1.08	0.18	1.32	4.44	17.49	2.78	4.11	7.03
AB08252	Residual, Top Plenum	04/06/01	57.19	1.16	0.75	1.02	2.87	9.06	1.44	1.70	4.77
AB08253	Residual, Top Plenum	04/06/01	55.06	1.07	0.62	1.01	3.22	9.46	1.27	1.62	5.48
AB08254	Bridging, Top Plenum	04/06/01	73.21	4.70	1.42	0.99	3.62	10.93	2.16	2.30	7.85
AB08255	Bridging, Bottom Plenum	04/06/01	43.74	0.26	0.32	0.92	3.81	11.31	2.20	2.48	8.22

Chemical Composition Calculated from Elemental Analysis*

Lab ID	Description	Date	CO_2	$CaCO_3$	CaS	CaO	Al_2O_3	Fe_2O_3	MgO	SiO_2	Elem C**
AB08248	Transient, Candle T-6	04/06/01	4.81	10.93	2.05	15.95	9.11	3.33	7.00	13.78	30.96
AB08249	Transient, Candle T-8	04/06/01	4.78	10.86	2.03	17.73	8.10	3.42	7.59	13.71	28.85
AB08250	Transient, Candle T-9	04/06/01	4.76	10.82	2.12	17.42	7.86	3.39	7.45	14.26	29.39
AB08251	Transient, Candle T-14	04/06/01	4.74	10.77	2.97	16.14	8.39	3.97	6.85	15.06	31.40
AB08252	Residual, Top Plenum	04/06/01	5.07	11.52	2.30	4.43	5.42	2.06	2.84	10.22	55.81
AB08253	Residual, Top Plenum	04/06/01	5.40	12.27	2.28	4.60	6.09	1.82	2.70	11.75	53.59
AB08254	Bridging, Top Plenum	04/06/01	5.62	12.77	2.23	6.42	6.84	3.09	3.83	16.82	71.68
AB08255	Bridging, Bottom Plenum	04/06/01	5.55	12.61	2.08	7.16	7.20	3.15	4.14	17.62	42.23

* Assumes that all CO_2 is present as $CaCO_3$, all sulfur is present as CaS, and remaining calcium is present as CaO.

** Assumes that all carbon not accounted for as $CaCO_3$ is in the form of elemental carbon.

Table 3.6-6

Physical Properties of GCT3 and GCT4 In situ Samples

Lab ID	SRI Run No.	Date	Bulk Density, g/cm^3	True Density, g/cm^3	Uncompacted Bulk Porosity, %	BET Surface Area, m^2/g	Mass-Median Diameter, μm
GCT-3							
AB07834	GCT3IMT-1	12/15/00	0.89	2.61	65.9	2.2	22.0
AB07661	GCT3IMT-2	01/25/01	0.32	2.23	85.7	96.7	14.9
AB07684	GCT3IMT-3	01/26/01	0.39	2.26	82.7	118.0	13.8
AB07835	GCT3IMT-4	01/27/01	0.37	2.28	83.8	100.0	12.9
AB07836	GCT3IMT-5	01/29/01	0.41	2.22	81.5	81.6	13.0
AB07837	GCT3IMT-6	01/30/01	0.32	2.15	85.1	181.0	14.3
AB07838	GCT3IMT-7	01/31/01	0.38	2.54	85.0	188.0	16.1
GCT-3 Average[1]			0.37	2.28	84.0	127.6	14.2
GCT-4							
AB08051	GCT4IMT-1	03/09/01	0.31	2.25	86.2	132.0	16.9
AB08052	GCT4IMT-2	03/10/01	0.54	2.28	76.3	105.0	13.2
AB08233	GCT4IMT-3	03/26/01	0.22	2.28	90.4	265.0	16.4
AB08234	GCT4IMT-4	03/27/01	0.26	2.21	88.2	198.0	12.1
AB08235	GCT4IMT-5	03/28/01	0.27	2.35	88.5	204.0	15.9
AB08236	GCT4IMT-6	03/29/01	0.31	2.34	86.8	188.0	18.3
GCT-4 Average[2]			0.27	2.29	88.0	197.4	15.9

1. GCT3IMT-1 excluded from average since it was done with sand circulation only.
2. GCT4IMT-2 excluded from average due to high bulk density and low surface area.

Table 3.6-7

Physical Properties of GCT3 and GCT4 Dustcake Samples

Type of Sample	Plenum or Element	Date	Bulk Density, g/cc	Particle Density, g/cc	Uncompacted Bulk Porosity, %	Specific Surface Area, m^2/g	Mass-Median Diameter, μm
GCT-3							
Bridged Material	Various	02/06/01	0.37	2.40	84.6	127	12.0
Residual Dustcake	Various	02/06/01	0.36	2.37	84.8	44.0	4.3
GCT-4							
Bridged Material	Top	04/06/01	0.31	2.21	86.0	194	11.9
Bridged Material	Bottom	04/06/01	0.36	2.21	83.7	151	13.5
Residual Dustcake	Top	04/06/01	0.32	2.00	84.0	8.0	8.0
Residual Dustcake	B-8	04/10/01	0.35	1.82	80.8	N.M.	8.7
Residual Dustcake	Top	04/06/01	0.33	2.02	83.7	16.9	7.8
Residual Dustcake	B-17	04/10/01	0.30	1.81	83.4	N.M.	7.8
Transient Dustcake	T-6	04/06/01	0.31	2.36	86.9	36.8	11.8
Transient Dustcake	T-8	04/06/01	0.35	2.33	85.0	32.4	11.0
Transient Dustcake	T-9	04/06/01	0.34	2.35	85.5	27.7	11.9
Transient Dustcake	T-14	04/06/01	0.32	2.34	86.3	35.9	11.6

Table 3.6-8

Transient Drag Determined From PCD ΔP and From RAPTOR

Sampling Run No.	ΔP/Δt (inWC/min)	Δ (AL)/Δt (lb/ft²/min)	FV (ft/min)	MMD (μm)	Drag (R), inWC/(lb/ft²)/(ft/min)		
					PCD	PCD @ RT	RAPTOR
GCT-2							
GCT2IMT-1	14.16	0.0540	4.86	17.4	54	29	21
GCT2IMT-2	9.33	0.0340	3.84	17.6	72	39	21
GCT2IMT-3	8.27	0.0448	3.34	16.3	55	31	23
GCT2IMT-4	6.09	0.0376	3.16	15.8	51	29	24
GCT2IMT-5	3.40	0.0294	2.73	19.9	42	24	18
GCT2IMT-6	5.38	0.0396	3.10	19.3	44	24	19
GCT2IMT-7	6.20	0.0408	2.84	18.6	53	29	20
Average for GCT-2					53	29	21
GCT3							
GCT3IMT-1	0.51	0.0012	3.36	22.0	126	95	68
GCT3IMT-2	9.49	0.0103	3.07	14.9	301	178	92
GCT3IMT-3	14.67	0.0405	3.13	13.8	116	69	98
GCT3IMT-4	10.97	0.0304	2.90	12.9	125	74	104
GCT3IMT-5	12.37	0.0292	3.06	13.0	138	82	103
GCT3IMT-6	19.92	0.0376	3.00	14.3	177	106	96
GCT3IMT-7	6.45	0.0229	3.07	16.1	92	55	87
Average for GCT3 (1)					129	80	70
GCT4							
GCT4IMT-1	21.96	0.0344	3.12	16.9	205	116	49
GCT4IMT-2	44.67	0.0873	4.71	13.2	109	60	65
GCT4IMT-3	5.82	0.0208	3.03	16.4	92	51	51
GCT4IMT-4	15.03	0.0305	3.27	12.1	151	88	71
GCT4IMT-5	3.79	0.0126	2.42	15.9	124	75	53
GCT4IMT-6	3.64	0.0153	2.47	18.3	96	58	45
Average for GCT4 (2)					114	66	70

1. Excluding Run No. GCT3IMT-2.
2. Excluding Run No. GCT4IMT-1.

Figure 3.6-1 GCT4 Residual Dustcake at 30x Magnification

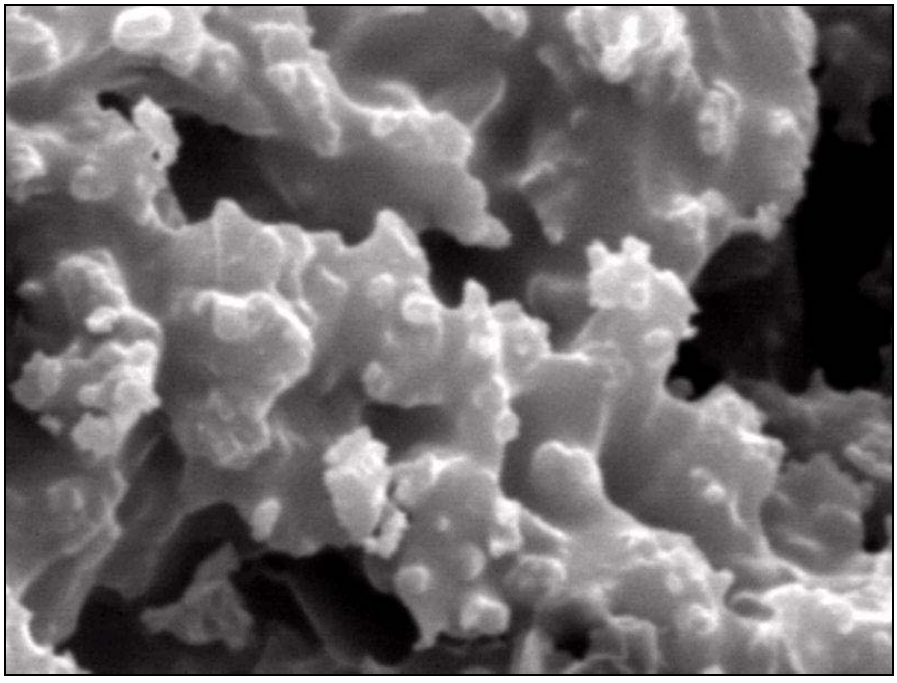

Figure 3.6-2 GCT4 Residual Dustcake at 5000x Magnification

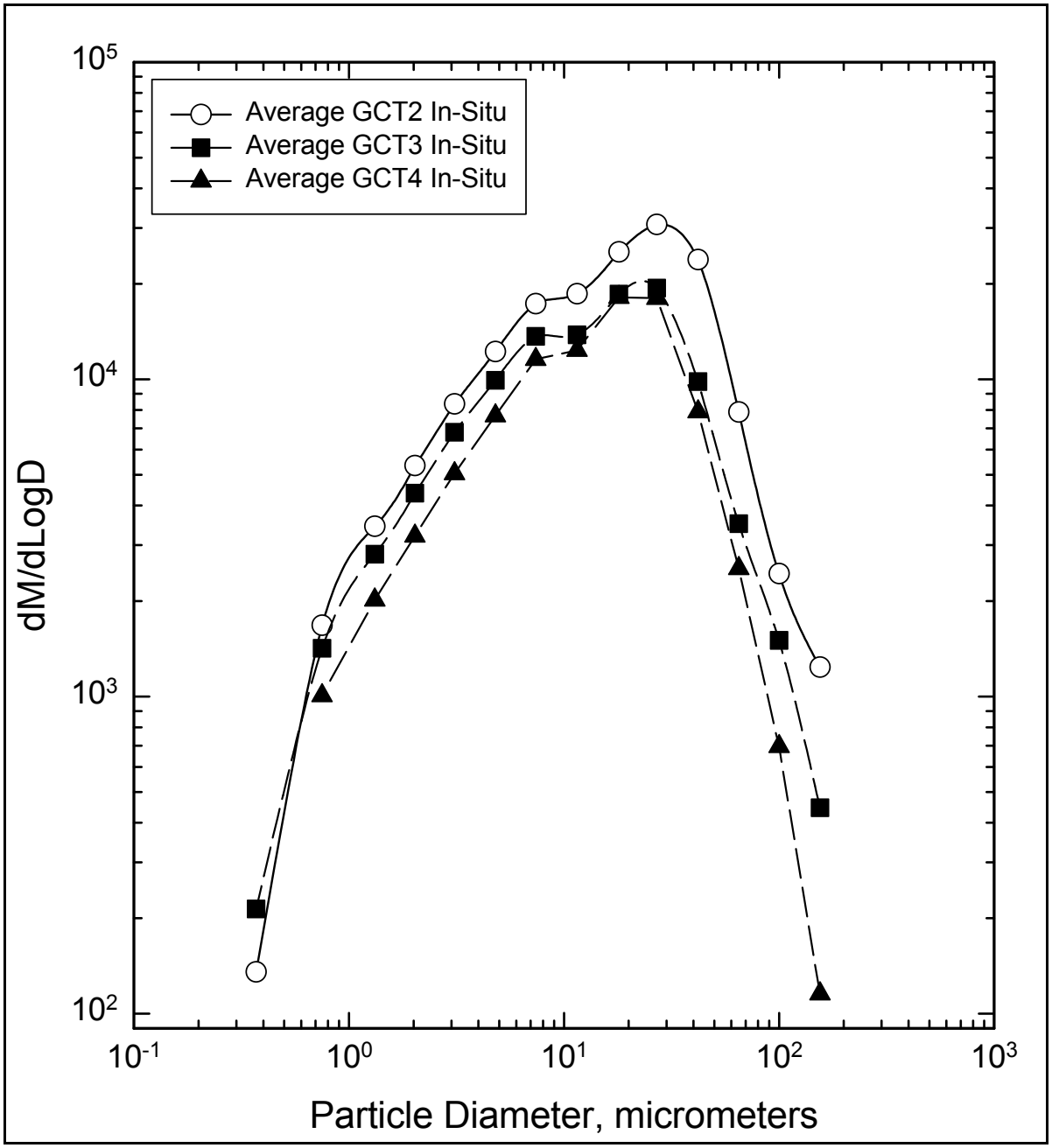

Figure 3.6-3 PCD Inlet Particle Size Distributions

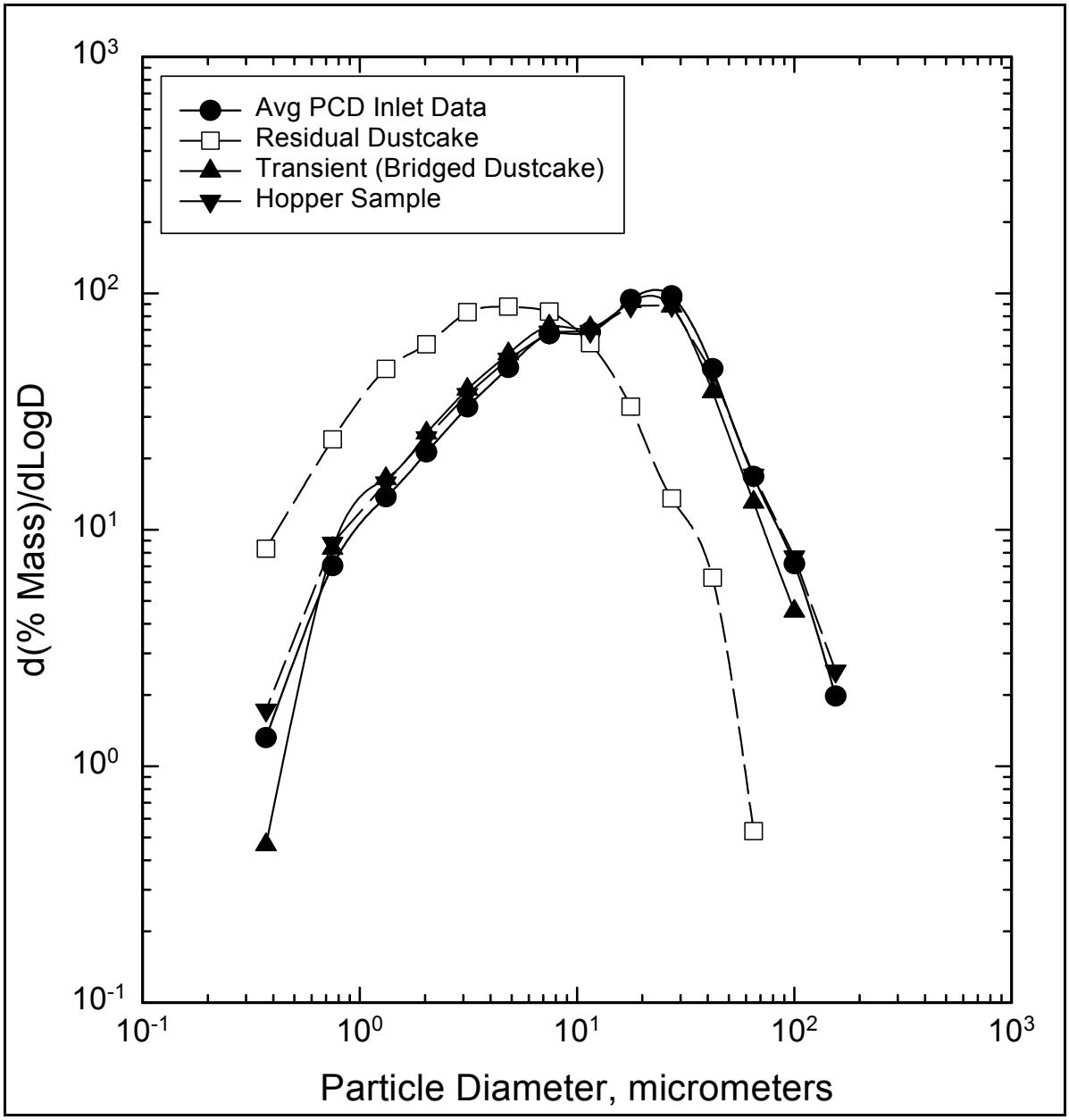

Figure 3.6-4 Particle Size Distributions for GCT3 Char

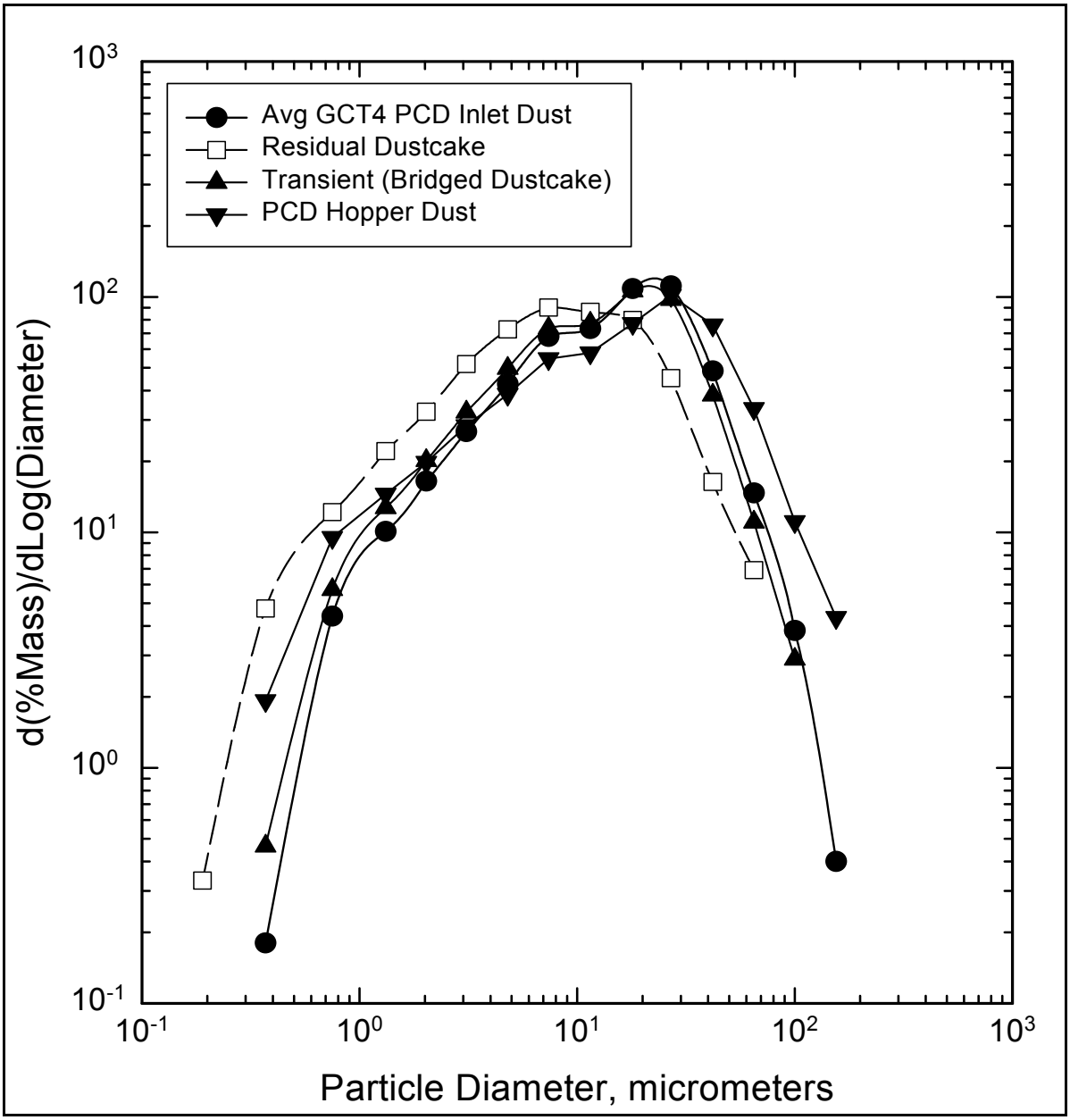

Figure 3.6-5 Particle Size Distributions for GCT4 Char

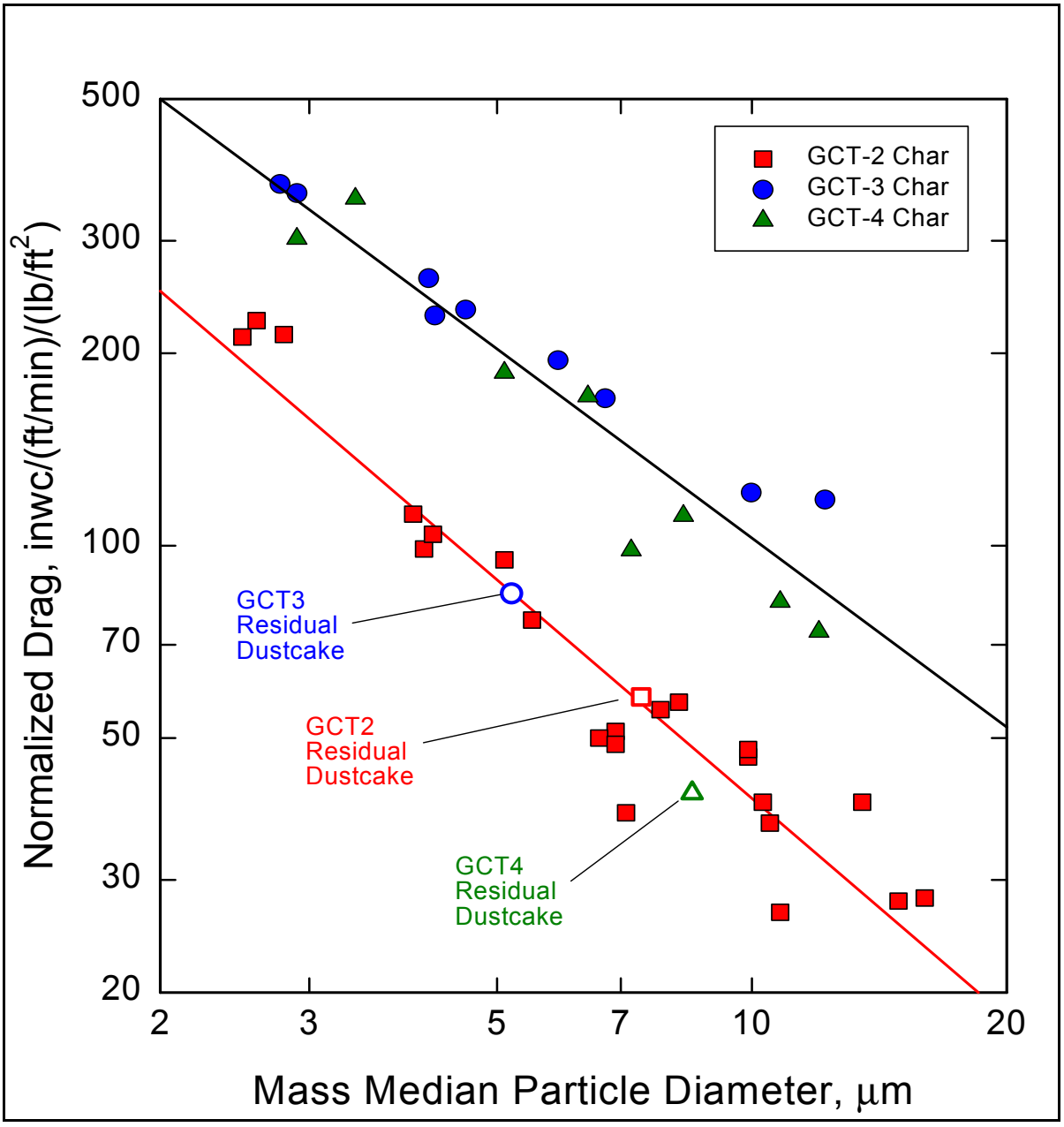

Figure 3.6-6 RAPTOR Drag Vs. Particle Size

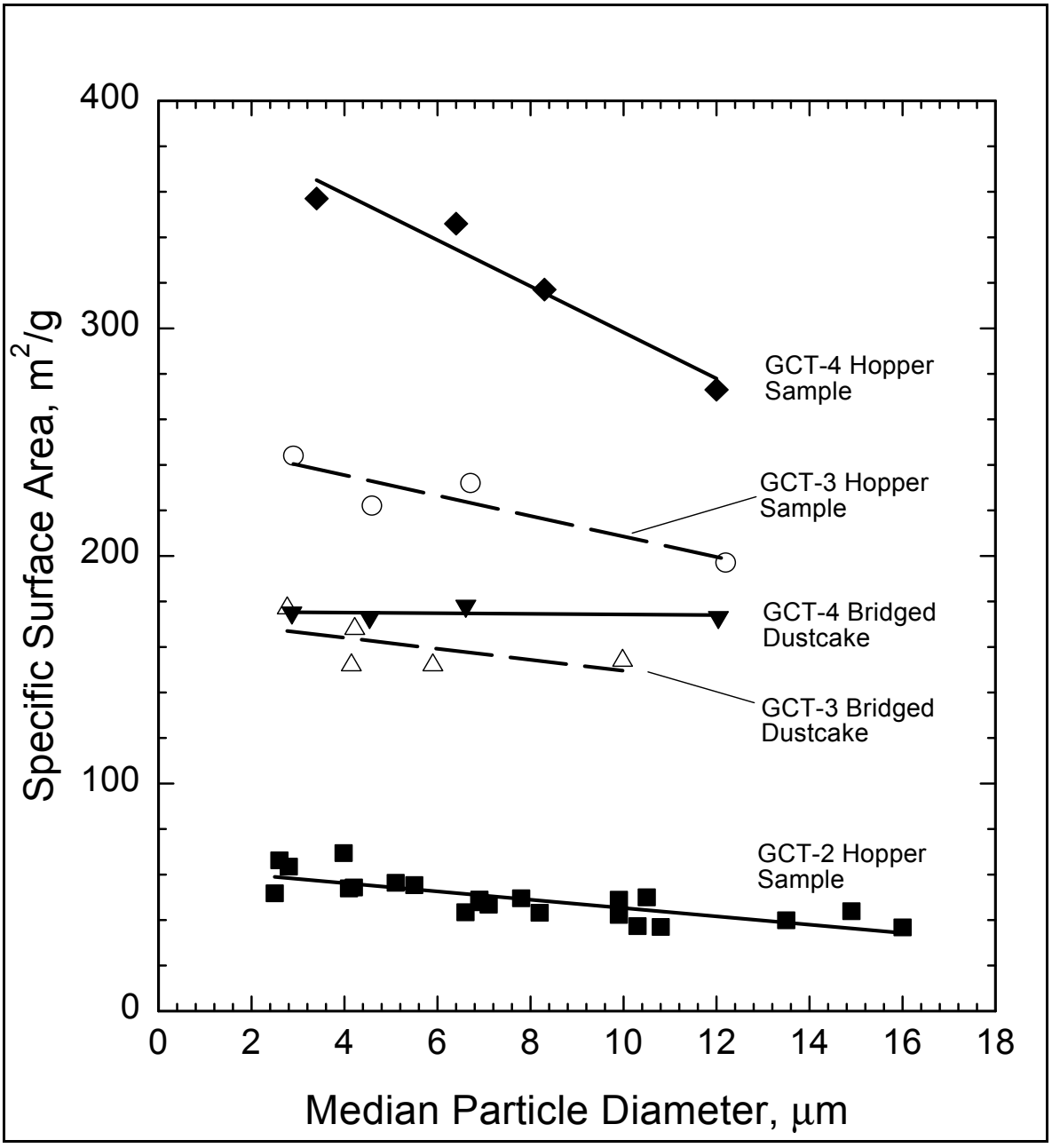

Figure 3.6-7 Specific-Surface Area of PSDF Char Vs. Particle Size

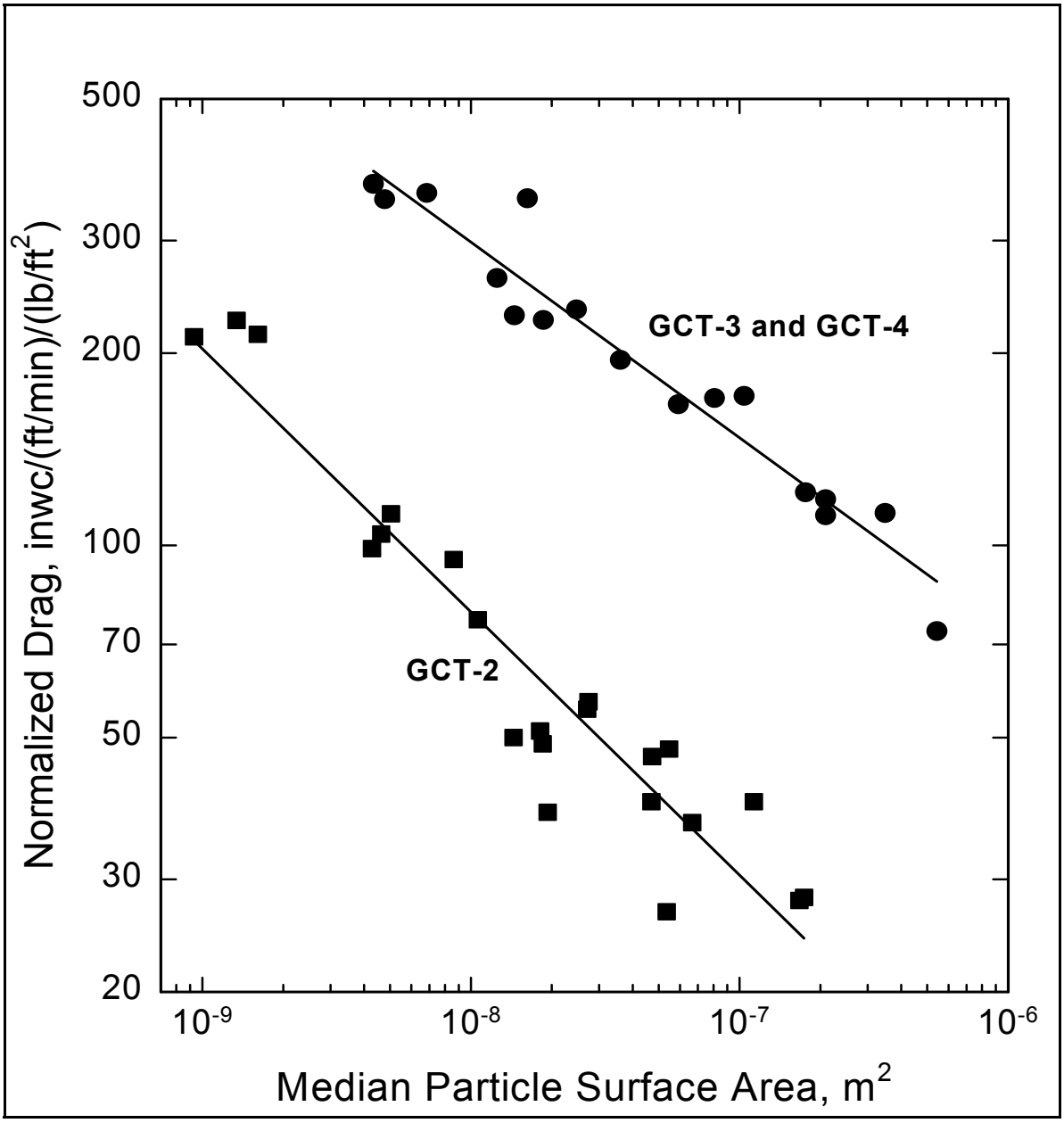

Figure 3.6-8 Normalized Drag Vs. Median Particle Surface Area

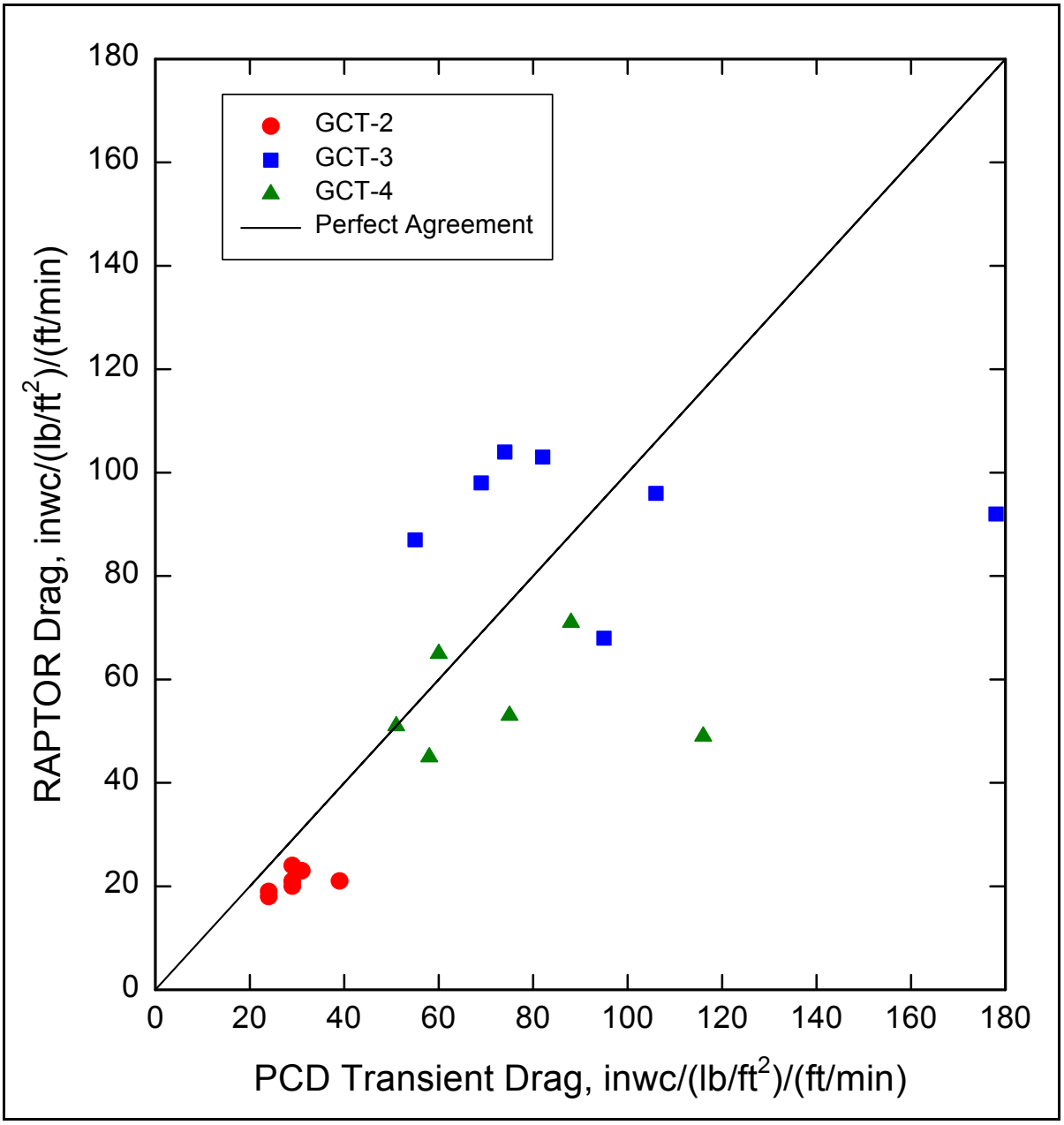

Figure 3.6-9 Comparison of Laboratory and Actual PCD Drag

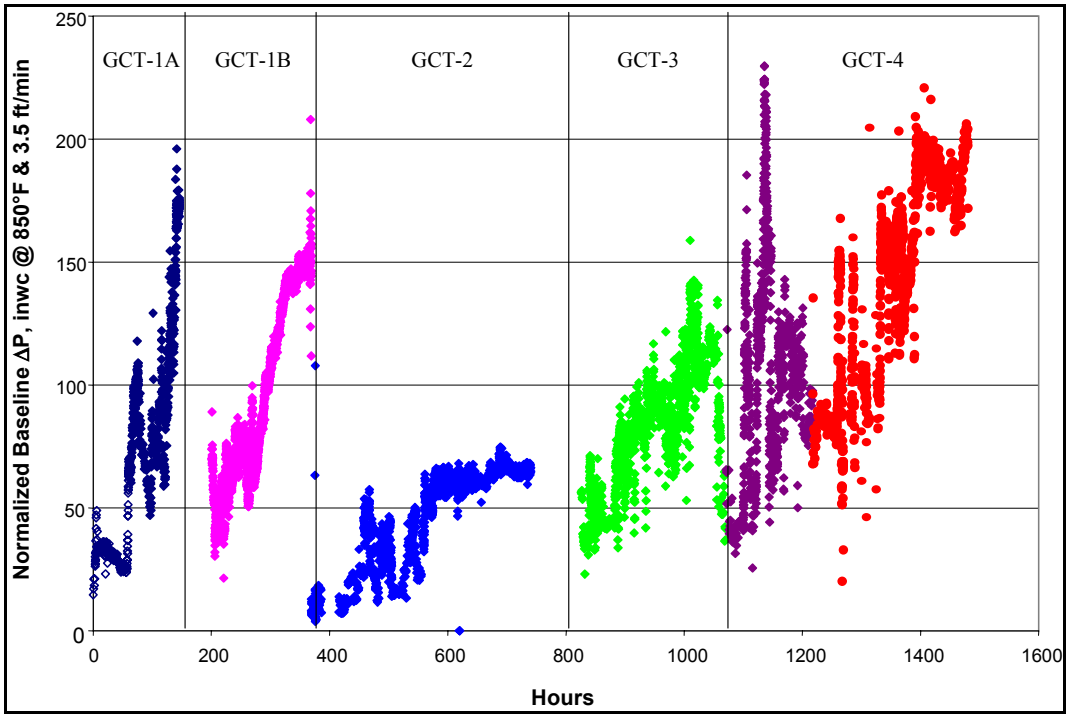

Figure 3.6-10 Normalized PCD Baseline ΔP During GCT 1 Through GCT 4

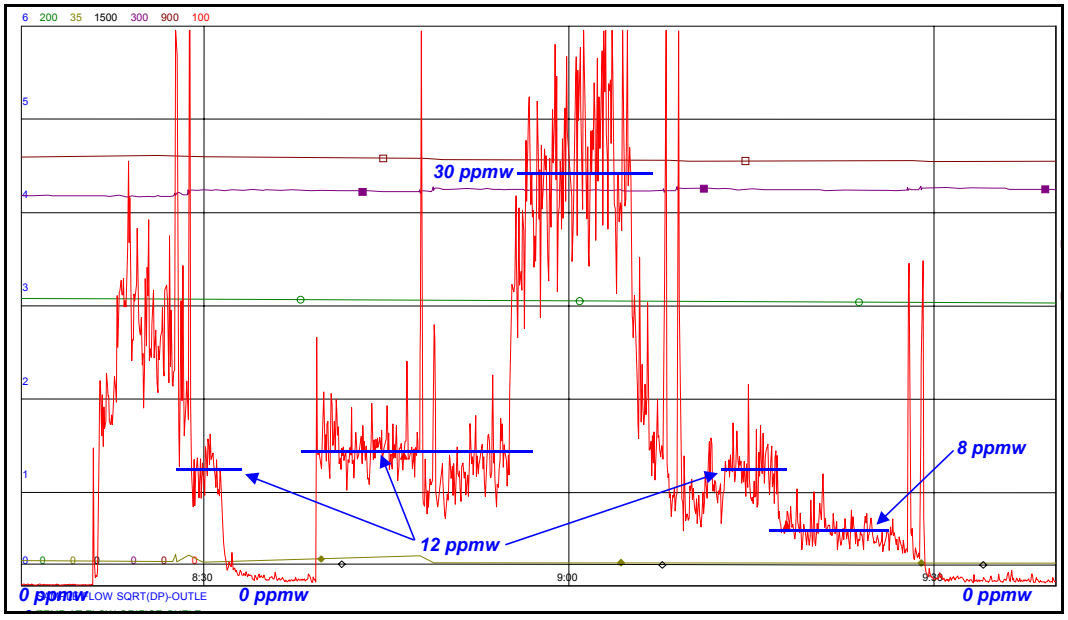

Figure 3.6-11 PCME Real-Time Particulate Monitor Output During Duct Injection

4.0 TRANSPORT REACTOR

4.1 GCT3 RUN SUMMARY

GCT3 began on December 1, 2000, with startup of the thermal oxidizer fan. The new loop seal arrangement was commissioned in the first portion of test run GCT3, with only sand circulation. The second portion of the test run was the actual gasification testing. On December 8, 2000, the start-up burner was started to heat and cure reactor refractory. Sand was added for preliminary testing of the new loop seal from December 13 until December 15. Aeration rates and solids circulation rates were varied in successfully commissioning the new loop seal.

In the gasification portion of this test run, the PCD warm up was started on January 20, 2001. Coal feed was started on January 22, 2001, at 21:55 and stopped on January 23, 2001, at 08:42 due to a plug in the char/ash vessel (FD0530 surge bin) feeding the sulfator. The reactor was restarted on coal feed for 3 hours on January 24 at 18:54 when the steam drum level went low, tripping the reactor. Feed resumed at 22:56. Coal feed was lost for 26 minutes on January 25, 34 minutes on January 26, and 21 minutes on January 28. The run ended on February 1 at 01:31 due to a filter bag and cage stuck in the coal feed lock vessel valves.

Total time on coal was 184 hours, and 386 tons of PRB coal was processed. The limestone for the run was Ohio Bucyrus.

Primary objectives of test run GCT3 are as follows:

- Commission loop seal – Evaluate operational stability of loop seal, with sand and limestone as bed material, at different solids-circulation rates. Establish maximum solids-circulation rate through loop seal with inert bed.

- Loop seal operations – Evaluate loop seal operational stability during coal feed operations and establish maximum solids-circulation rate.

Secondary objectives include the continuation of reactor characterizations:

- Operational stability – Characterize reactor loop and PCD operations with short-term tests by varying coal feed, air/coal ratio, riser velocity, solids-circulation rate, system pressure, and air distribution.

- Reactor operations – Devolatilization and tar cracking effects from transient conditions during transition from start-up burner to coal; effect of process operations on heat release; heat transfer and accelerated fuel particle heat-up rates; and effect of changes in reactor conditions on transient temperature profiles, pressure balance, and product gas composition.

- Effects of reactor conditions on syngas composition – Vary air distribution, steam/coal ratio, and solids-circulation rate. Effect of reactor temperature on CO/CO_2 ratio, gasification rates, carbon conversion, and cold and hot gas efficiencies.

Activities during the outage preceding test run GCT3 included 62 equipment revisions. Those affecting the process the most were installations and modifications listed below:

- Loop seal installed under the primary cyclone, disengager lengthened, and refractory replaced in the primary and disengager cyclones.
- Solids sampler on the standpipe replaced.
- Economizer installed after thermal oxidizer and sulfator for temperature control to the baghouse.
- Modifications made to raise the sulfator steam coil outlet temperature and to use the super-heated steam from the sulfator.
- Modified the gas sample systems for tar removal.
- Revised logic, motor, and purges to allow faster cycle on the coal feeder.

The lock vessel on the coal feeder was the cause of several upsets. (The bag falling from the baghouse into the surge bin, where it plugged the knife gate valve, caused the problem. The knife gate valve is usually throttled to a 1-in. opening to reduce the coal-flow rate so that it does not overfill the lock vessel. When the coal becomes too packed, the coal bridges and does not fall.) During the run, the knife gate had to be opened much larger, causing the lock vessel to become overfilled.

The December 1 to December 15, 2000, period was used to test the new loop seal and to cure new refractory in the reactor loop and sulfator. The new loop seal performed much better than the previous slant leg, and little material was lost during circulation.

The coal gasification section of GCT3 was started on January 20, 2001, with a PCD warmup preceding the start-up burner firing to bring the reactor to temperature. Several nozzles in the loop seal became plugged, were then unplugged, and heating of the sulfator was started. Due to several small problems the coal was finally started at 21:55 on January 22, 2001. Coal continued until 08:42 when char could not be removed from FD0530 (char from reactor to sulfator). The surge drum had become plugged with hardened ash. After repairs, coal was restarted at 18:54 on January 24. At 22:49, the steam drum was at low level due to high economizer exit temperatures tripping the coal feeder and the thermal oxidizer, causing the main air compressor to unload. Coal feed was restarted at 22:56. The main air compressor tripped again at 00:23 on January 25 causing a coal outage until 01:20. Reactor pressure was increased to 235 psig on January 26, 2001. Tests were conducted from January 26 through 31, with brief interruptions in coal feed. The run ended at 01:31 on February 1, 2001, when the baghouse bag became stuck in the coal feeder spheri valves.

The following gasification test periods were selected (see Table 4.1-4 for more details):

GCT3-1 First steady-state period.

GCT3-2 Recovery after temperature swing of ~40°F.

GCT3-3 Increased sorbent feed, decreased steam flow, lowered standpipe level.

GCT3-4 Increased air flow, higher temperature.

GCT3-5 Higher temperature.

GCT3-6 Steady state after upset, low temperature operation.

GCT3-7 Riser inlet controlled at higher setpoint, but air was less and coal was higher.

GCT3-8 Increased steam flow from 58 to 62 percent, ~150 lb/hr, lower temperature.

GCT3-9 Increased sorbent feed, decreased coal feeder speed.

GCT3-10 Increased steam flow, increased air, higher temperature.

GCT3-11 Decreased steam flow, then recovery from upsets.

GCT3-12 Recovery after low coal feed.

GCT3-13 Recovery after large temperature swings.

GCT3-14 Recovery after low coal feed.

GCT3-15 Recovery after low coal feed.

GCT3-16 Decreased coal feeder speed, increased air, lower temperature.

GCT3-17 Recovery after low coal feed.

GCT3-18 Increased air, increased steam flow, higher temperature.

GCT3-19 Increased SP level, steam flow increased.

GCT3-20 Decreased sorbent feed to 5 percent.

GCT3-21 Recovery after small temperature swings.

GCT3-22 Increased air flow.

GCT3-23 Increased sorbent feed, increased air flow.

GCT3-24 Increased air flow, higher temperature.

GCT3-25 Decreased air flow, lower temperature.

Table 4.1-1

GCT3 Operating Conditions for Transport Reactor

Start-up Bed Material	Sand (~ 120 μm)
Fuel Type	Powder River Basin
Fuel Particle Size (mmd)	250 to 350 μm
Average Fuel-Feed Rate	Maximum possible without accumulating ash/char in PCD cone (5,000 lb/hr)
Sorbent Type	Ohio Bucyrus Limestone
Sorbent Particle Size	20 μm
Sorbent-Feed Rate	125 to 300 lb/hr (Ca/S molar ratio (2:1 to 5:1)
Mixing Zone Temperature	1,725 to 1,775°F
Reactor Pressure	225 psig
Riser Gas Velocity (fps)	Minimum to 45 ft/s
Solids Circulation Rate (lb/hr)	Maximum possible without overloading loop seal or accumulating ash/char in PCD cone
Primary Gas Cooler Bypass	0%
PCD Temperature	750 to 800°F
Total Gas Flow Rate	19,000 to 28,000 lb/hr
Air/Coal Ratio	3.0 (As needed to control reactor temperature)
Primary Air Split ($1^{st}/2^{nd}$ levels)	50/50 to 90/10
Steam/Coal Ratio	0.0 to 0.5
Sulfator Operating Temperature	1,500 to 1,600°F
Planned Duration of Coal Feed	Nominally 250 hr

Table 4.1-2

Coal Analyses as Fed

	PRB
Moisture	17.7
Ash	5.6
Sulfur	0.3
C	58.3
H	4.0
N	0.7
O	13.3
Vol	35.7
Fix C	41.0
Heating Value(Btu/lb)	9,747

Table 4.1-3

Sorbent Analyses

	Bucyrus Limestone From Ohio
$CaCO_3$ (wt %)	77.6
$MgCO_3$ (wt %)	16.5
Inerts (wt %)	5.9

Table 4.1-4

Operating Periods

Test No.	Start	End	MZ Temp (°F)	Riser Temp (°F)	Pres psig	Coal-Feed Rate lb/hr	Air Flow lb/hr	Air/ Coal Ratio	Air/C Ratio	Steam Flow lb/hr	Steam/Coal Ratio
GCT3-1	1/26/01 06:45	1/26/01 07:45	1733	1743	227	5110	14866	2.91	5.29		
GCT3-2	1/26/01 08:53	1/26/01 09:53	1729	1741	227	5109	14616	2.86	5.20	80	0.02
GCT3-3	1/26/01 12:30	1/26/01 15:30	1726	1741	227	5115	14502	2.84	5.15	1320	0.26
GCT3-4	1/26/01 15:45	1/26/01 19:00	1740	1763	227	5130	14876	2.90	5.27	1373	0.27
GCT3-5	1/26/01 19:30	1/26/01 20:30	1785	1817	227	5148	14625	2.84	5.17	1371	0.27
GCT3-6	1/27/01 02:45	1/27/01 03:45	1694	1717	227	5471	14953	2.73	4.97	1127	0.21
GCT3-7	1/27/01 06:45	1/27/01 08:00	1740	1758	227	5023	13882	2.76	5.03	1041	0.21
GCT3-8	1/27/01 08:05	1/27/01 11:45	1721	1738	227	5023	13852	2.76	5.01	1122	0.22
GCT3-9	1/27/01 13:45	1/27/01 14:45	1719	1737	227	5058	13692	2.71	4.92	1389	0.27
GCT3-10	1/27/01 16:05	1/27/01 18:45	1726	1748	227	5062	14043	2.77	5.04	1368	0.27
GCT3-11	1/27/01 23:15	1/28/01 01:55	1746	1778	227	5355	15273	2.85	5.19	702	0.13
GCT3-12	1/28/01 11:30	1/28/01 12:45	1722	1756	227	4104	11900	2.90	5.27	1026	0.25
GCT3-13	1/29/01 03:30	1/29/01 04:30	1661	1666	227	3660	9355	2.56	4.65	1151	0.31
GCT3-14	1/29/01 23:45	1/30/01 01:00	1678	1702	209	5022	14043	2.80	5.08	22	0.00
GCT3-15	1/30/01 04:30	1/30/01 05:45	1677	1697	225	5482	13788	2.52	4.57	22	0.00
GCT3-16	1/30/01 06:00	1/30/01 07:45	1667	1689	225	5413	13914	2.57	4.67	22	0.00
GCT3-17	1/30/01 16:45	1/30/01 18:45	1765	1805	225	5021	14465	2.88	5.24	22	0.00
GCT3-18	1/30/01 20:15	1/30/01 23:45	1766	1810	225	5019	15062	3.00	5.46	22	0.00
GCT3-19	1/31/01 04:00	1/31/01 05:25	1756	1803	225	5020	15353	3.06	5.56	22	0.00
GCT3-20	1/31/01 06:05	1/31/01 08:45	1756	1804	225	5017	14771	2.94	5.35	22	0.00
GCT3-21	1/31/01 10:15	1/31/01 11:45	1750	1804	225	5015	14842	2.96	5.38	22	0.00
GCT3-22	1/31/01 11:45	1/31/01 12:45	1749	1803	225	5016	15195	3.03	5.51	22	0.00
GCT3-23	1/31/01 12:50	1/31/01 14:15	1750	1803	225	5016	15311	3.05	5.55	22	0.00
GCT3-24	1/31/01 14:15	1/31/01 15:30	1764	1820	225	5016	15761	3.14	5.71	22	0.00
GCT3-25	1/31/01 17:15	1/31/01 21:15	1753	1808	225	5016	15029	3.00	5.45	22	0.00

4.2 GAS ANALYSIS

During GCT3, synthesis gas and synthesis gas combustor outlet analyzers were continuously monitored and recorded by the plant information (PI) system. Several in situ grab samples of synthesis gas moisture were measured during the PCD outlet loading sampling. This section will use the gas analyzer data to show:

- Synthesis gas heating value.
- Synthesis gas molecular weight.
- Synthesis gas compositions for CO, H_2, CO_2, H_2O, N_2, CH_4, $C_2H_6^+$, and total reduced sulfur (H_2S, COS, and CS_2).
- Sulfur removal and emissions.

Run GCT3 coal feed began on January 22, 2001, and ended on February 1, 2001. Run GCT3 consisted of two periods of operation. The first period was very short, lasting only about 10 hours. Since there were no steady periods of operation during this period, no data from this period will be analyzed. This section will concentrate on the long-term operation from January 24 to February 1. The only fuel used during GCT3 was Powder River Basin coal, a mixture of four different coals. The sorbent used was Ohio Bucyrus limestone.

Hourly averages for the mixing zone temperatures, PCD (particulate control device, FL0301) temperatures, and reactor pressures are shown on Figure 4.2-1. The reactor mixing zone temperature was quickly increased to 1,750°F a few hours after startup and was maintained between 1,725 and 1,775°F for the first 4 days. Between 07:00 on January 28 to 19:00 on January 30 there were numerous coal feed trips and the reactor temperature was maintained at around 1,650°F between coal trips. Periods of low temperatures indicate coal feeder trips. The reactor pressure was increased in several increments from 190 to 225 psig, with the majority of the run at 225 psig. The PCD inlet was maintained at about 775°F for nearly the entire run except for slight excursions during coal feed trips.

Hourly averages for the coal-feed and air rate are provided in Figure 4.2-2. The coal-feed rate was calculated from a correlation using the coal feeder speed and the FD0210 weight cell data (see Section 4.4). The coal rate correlation indicated that the maximum coal rate was 5,300 lb/hr for feeder speeds above 36.0 rpm. The air rate was obtained from FI205. The air rate followed the coal rate to maintain an approximate air/coal ratio of about 2.8, which was required to maintain the reactor temperature. The numerous low excursions of the air rates also emphasize the numerous coal feeder trips during GCT3. Note the unsteady air rate due to the numerous coal trips from 07:00 on January 28 to 19:00 on January 30.

A plot of the hourly synthesis gas (FI465_COMP) and aeration instrument nitrogen (FI609) is shown in Figure 4.2-3. The synthesis gas rate was usually from 25,000 to 28,000 lb/hr except during the period of numerous coal trips from January 28 to 30. The nitrogen rate slowly decreased during the run from 9,300 to 6,500 lb/hr. It is estimated that about 1,000 lb/hr from FI609 does not enter the process but is used to seal valves, for pressurized-depressurized feed and ash lock hopper systems, and in the seals for the screw coolers. Future calculations will assume that about 1,000 lb/hr of nitrogen from FI609 does not enter the synthesis gas.

The plant gas analyzer system analyzed synthesis gas, as listed below, during GCT3, using the associated analyzers also shown below:

CO	AI425, AI434B, AI453G, AI464C
CO_2	AI434C, AI464D
CH_4	AI464E
$C_2H_6^+$	AI464F
H_2	AI464G
H_2O	AI448, AI7510
N_2	AI464B

The AI464B through G analyzers use a gas chromatograph and typically have about a 6-minute delay. The other three CO analyzers (AI425, AI434B, and AI464C) and CO_2 analyzer (AI434C) are IR-based and give more real-time measurements. All analyzers (except for the H_2O analyzer) require that the gas sample is conditioned to remove water vapor; therefore, all these analyzers report gas compositions on a dry basis. During the run, the gas analyzer conditioning system frequently plugged with tar and naphthalene, which required the analyzer technicians to clean the gas analyzer conditioning systems. There was more gas analyzer plugging in GCT3 than in GCT2, probably due to the increased number of coal feed trips. The gas combustor (GC) analyzers were not in operation from 23:00 on January 25 to 10:00 on January 30, and in the last several hours of the run. Therefore, there was very little H_2, N_2, CH_4, and $C_2H_6^+$ analyzer data obtained.

The raw synthesis gas analyzer data was adjusted to produce the best estimate of the actual gas composition by:

1. Choice of CO and CO_2 analyzers.

2. Normalization of dry gas compositions (force to 100-percent total).

3. Conversion of dry compositions to wet compositions.

With four CO analyzers there is a measure of self-consistency when all or several of the four analyzers read the same value. When the CO analyzers do not agree there is the choice of which CO analyzer(s) to use in further analyses. The raw data hourly averages for the four CO analyzers are provided in Figure 4.2-4. Three of the CO analyzers (AI464C, AI434B, and AI425) were reading zero (out-of-operation) for periods during GCT3. All zero analyzer data is excluded from the plots shown in Figure 4.2-4. During most of GCT3, CO analyzers AI425 and AI434B agreed very well with each other. The low CO measurements are either periods when the gas analyzers were calibrated or during coal feeder trips. The CO compositions used in calculations were interpolated for the times when gas analyzers were being calibrated.

Data from both of the CO_2 analyzers are shown on Figure 4.2-5. There was good agreement between the two analyzers when the GC CO_2 analyzer (AI464D) was operating. The CO_2 analyzer (AI464D) was reading zero (out-of-operation) for periods during GCT3. Analyzer data plots for these periods is not used Figure 4.2-5.

The water analyzer data in Figure 4.2-6 is shown compared with the in situ synthesis gas moisture measurement made during PCD outlet particulate sampling. The data is also compared with the synthesis gas-steam rate. The in situ moisture data compares well with the moisture analyzer data, showing moisture was constant during the periods of 200 to 400 lb/hr steam operation, and tracked the increase in steam rate to 1,200 lb/hr on January 31.

Figure 4.2-7 provides gas analyzer data for H_2, CH_4, and $C_2H_6^+$ for GCT3. The GC H_2 analyzer seems to have given reasonable results on the first day of operation and for the period of 13:00, January 30 to 03:00, January 31. The CH_4 seemed to be giving reasonable results for the first 24 hours of operation, and then from 03:00, January 30 to 03:00, January 31. The $C_2H_6^+$ data was much higher than GCT2 $C_2H_6^+$ data. The $C_2H_6^+$ data was not used for the balance of the analysis. A plot similar to that shown in Figure 4.2-7 could also be made for the N_2 data, showing when the GC was off-line and not available.

Since there is no H_2 gas analyzer data for most of GCT3, the H_2 concentration was estimated using the water-gas shift equilibrium at the riser temperature (TI360) and the measured H_2O, CO_2, and CO concentration. The water-gas shift reaction and equilibrium constant is:

$$CO + H_2O \leftrightarrow H_2 + CO_2 \quad (1)$$

$$Kp = \frac{(H_2)(CO_2)}{(H_2O)(CO)} \quad (2)$$

This was similar to estimating the moisture content in GCT2 using the water-gas shift equilibrium at the riser temperature and the measured H_2, CO_2, and CO concentrations. Figure 4.2-8 shows the comparison between the measured H_2 during test periods GCT3-1, -17, -18, -19, and -20 and the results from the water-gas shift equilibrium constant at the riser temperature, as well as the measured CO, CO_2, and H_2O concentrations. The H_2 concentrations for GCT3-1, -17, -18, -19, and -20 agreed best when an approach temperature of -50°F was used.

The results of these calculations are shown in Figure 4.2-8 and Table 4.2-1 for the steady operating periods defined in Section 4.1. The H_2 analyzer data was only used during test periods GCT3-1, -17, -18, -19, and -20. For the other 20 test periods, H_2 was estimated from water-gas shift equilibrium constant at the riser temperature minus 50°F and the measured CO, CO_2, and H_2O concentrations.

The CH_4 concentrations seemed reasonable only for operating periods GCT3-17, -18, and -20 (see Figure 4.2-9 and Table 4.2-1). A value of 1.4 mole-percent CH_4 was estimated from preliminary TC06 data and is used in Figure 4.2-9 and Table 4.2-1 for the other 22 operating periods. None of the $C_2H_6^+$ data taken during the steady operating periods was consistent with previous data, so a value of 0.0-mole percent (dry) was used for all of the steady operating periods that were consistent with preliminary TC06 data.

The N_2 concentrations shown in Table 4.2-1 are taken from the N_2 analyzer only for steady periods of operation (GCT3-1, -17, -18, -19, and -20). For these periods, all gas compositions were normalized by dividing each gas composition by the sum of the mole fractions. Prior to

normalization the gas compositions were 98 to 104 percent. The N_2 concentration was estimated by difference for the other 20 periods.

The CO/CO_2 ratio is shown in Table 4.2-1. The CO/CO_2 ratio varied from 0.8 to 1.5, but was usually 1.0 to 1.3.

The synthesis gas lower gas heating value (LHV) is used in the plot shown in Figure 4.2-10 and Table 4.2-1. The synthesis gas heating value varied from 49 to 71 Btu/SCF. The LHV value was calculated using the formula:

$$\mathrm{LHV(Btu/SCF)} = \left\{ \begin{matrix} 275\times(\mathrm{H_2\%}) + 322\times(\mathrm{CO\%}) + \\ 913\times(\mathrm{CH_4\%}) + 1641\times(\mathrm{C_2H_6^+\%}) \end{matrix} \right\} / 100 \qquad (3)$$

The PSDF transport reactor adds more N_2 per pound to synthesis gas than a commercial reactor because of the additional PSDF sampling and instrument purges, and the need to aerate the lower portion of the reactor. Instrument purges would be proportionally smaller in a commercial design due to the scale factor (instruments stay the same size as plant size increases). Any additional N_2 added to the riser also requires additional fuel to bring the additional N_2 up to operating temperatures. This additional fuel then requires additional air, which then adds more N_2 from air to the reactor and further dilutes the synthesis gas. In a commercial reactor aeration N_2 would be used only for startup. To determine a commercial synthesis LHV, the following gas components are deleted from the raw synthesis gas:

- Nitrogen added through FI609.
- Nitrogen added with the air necessary to burn coal required to heat FI609 nitrogen to reactor process temperature.
- Carbon dioxide from burning the coal required for heating FI609 nitrogen.
- Water vapor resulting from burning the coal required for heating FI609 nitrogen.

A plot showing the raw synthesis gas LHV and N_2-corrected LHV are shown in Figure 4.2-10. The N_2-corrected LHV was between 84 and 112 Btu/SCF. The N_2 correction adds about 40 Btu/SCF to the raw LHV. The N_2-corrected gas compositions and LHV are shown in Table 4.2-2. Since the correction removes CO_2 and H_2O from the synthesis gas, the corrected water gas-shift equilibrium and CO/CO_2 ratio are also shown in Table 4.2-2. The N_2 correction increases the CO/CO_2 ratio and decreases the water-gas shift equilibrium constant.

The heating values calculated from the measured and assumed gas analyses can be checked by the synthesis gas combustor energy balance (BR0401). The gas compositions can be checked by oxygen balance around the synthesis gas combustor since the synthesis gas combustor exit oxygen is measured by AIT8775. Synthesis gas combustor energy balance and oxygen balance were calculated by using the following thermal oxidizer process tags:

Primary air flow	FI8773
Secondary air flow	FFIC8772MEAS
Quench air flow	FI8771

Propane flow	FI8753
Oxygen concentration	AIT8775

The measured and mass balance calculated oxygen values are shown in Figure 4.2-11 and Table 4.2-3. The measured and calculated oxygen concentrations agreed well with each other except for GCT3-2, -11, and -14. The agreement was excellent for the last nine operating periods (GCT3-17 to -25). The earlier operating periods generally had higher calculated oxygen concentrations than measured, which would indicate that the assumed gas compositions had less combustible compounds than the actual synthesis gas composition. The earlier operating periods then had an actual higher heating value than the assumed gas compositions indicated. The agreement is consistent with GCT2 results when there was much more reliable N_2, H_2, CH_4, and $C_2H_6^+$ gas analyzer data, and this provides confidence in the synthesis gas-flow and synthesis gas combustor-flow rate measurements.

The synthesis gas combustor energy balance is calculated by assuming a synthesis gas combustor heat loss, to make the synthesis gas LHV calculated by the synthesis gas combustor energy balance agree with LHV calculated from the synthesis gas analyzer data. In GCT2, the synthesis gas combustor heat loss was usually between 1.5 and 4.0 x 10^6 Btu/hr to get agreement. In GCT3, the best fit was 1.0 x 10^6 Btu/hr. The calculated synthesis gas combustor heat loss is quite reasonable.

The comparison between the LHV of the synthesis gas calculated by the synthesis gas combustor energy balance and LHV calculated from the gas analyzers is shown in Figure 4.2-12 and Table 4.2-3. All comparisons for the operating periods are within 9 Btu/SCF of each other except operating period GCT3-2, which provides more assurance the assumptions for the synthesis gas compositions were not too far off, and are consistent with the thermal oxidizer data.

Since the transport reactor H_2S analyzer was not working during GCT3 the H_2S concentration and sulfur emissions from the transport reactor were not directly measured. The synthesis gas combustor SO_2 analyzer (A1534A) measures the total sulfur emissions from the transport reactor. The total sulfur emissions would consist of primarily of H_2S, COS, and CS_2. The main sulfur species in coal gasification are considered to be H_2S and carbon oxysulfide (COS). There should also be only a minor amount of carbon disulfide (CS_2). Waltz Mills KRW gasifier data indicates that the majority of the gaseous sulfur is present as H_2S, with the balance as COS. KRW typically measured concentrations of 100 to 200 ppm COS for 0.6- to 1.0-percent sulfur fuels.

The sulfur emissions expressed as total reduced sulfur (TRS) from the transport reactor are provided in Figure 4.2-13 and Table 4.2-3. Since the synthesis gas combustor exit gas-flow rate is about twice that of the synthesis gas rate, the synthesis gas total reduced-sulfur concentration is about twice that of the measured synthesis gas combustor SO_2 concentration. The synthesis gas combustor SO_2 concentrations from A1534A are provided in Table 4.2-3. The maximum sulfur emissions possible are shown in the plot in Figure 4.2-13. The maximum sulfur emissions were calculated from the coal-feed rate, coal sulfur level, and synthesis gas rate, assuming that all of the coal sulfur left the system with the synthesis gas (zero-percent sulfur removal). Coal-feed rate will be discussed in Section 4.4 and the coal sulfur levels will be discussed in Section 4.3.

The sulfur emissions in pounds sulfur dioxide (per MBtu coal fed) are provided in Figure 4.2-14 and Table 4.2-3. The SO_2 emissions varied from 0.136 to 0.318 lb SO_2 per MBtu coal fired (higher coal-heating value used).

The equilibrium H_2S concentration in coal gasification using limestone is governed by three reversible reactions:

$$CaCO_3 \leftrightarrow CaO + CO_2 \tag{4}$$

$$H_2S + CaO \leftrightarrow CaS + H_2O \tag{5}$$

$$H_2S + CaCO_3 \leftrightarrow CaS + H_2O + CO_2 \tag{6}$$

Reaction (4) is the limestone calcination reaction. At thermodynamic equilibrium, the CO_2 partial pressure should be a function of only the system temperature as long as there are both $CaCO_3$ and CaO present according to the equilibrium constant:

$$K_1 = P^O_{CO_2} \tag{7}$$

where $P^O_{CO_2}$ is the partial pressure of CO_2. A plot of the partial pressure of CO_2 and temperature is provided in Figure 4.2-15 of the GCT1 report. At thermodynamic equilibrium, $CaCO_3$ and CaO coexist only on the equilibrium curve, while above the curve only $CaCO_3$ exists, and below the curve only CaO exists. Typically, there are both $CaCO_3$ and CaO present in the PCD solids. This is because of kinetic limitations and the quick cooling down of the solids in the fuel gas from the reactor temperatures to PCD temperatures. This quick cooling down tends to 'freeze' reactions at higher equilibrium temperatures than would be indicated by the actual system exit temperature.

The H_2S equilibrium is governed by reactions shown in Equations (8) and (9), with the associated equilibrium constants:

$$K_2 = \frac{P^O_{H_2O}}{P^O_{H_2S}} \tag{8}$$

$$K_3 = \frac{P^O_{H_2O} P^O_{CO_2}}{P^O_{H_2S}} \tag{9}$$

Equations (8) and (9) state that the equilibrium H_2S concentrations in the $CaCO_3$-CaO-CaS system is a function of the system temperature and the CO_2 and H_2O partial pressures. As the CO_2 and H_2O partial pressures increase, so would H_2S partial pressures. The equilibrium constants are all functions of temperature and can be determined using thermodynamic data with Aspen simulations.

The GCT3-25 H_2S equilibrium concentrations, as a function of temperature, are shown in Figure 4.2-15. The H_2S equilibrium curve was determined from Aspen simulations. The average partial pressure of CO_2 was 23 psia, which means that the CO_2 partial pressure crosses the CO_2 equilibrium partial pressure curve at 1,683°F. This means that at equilibrium for 23 psia CO_2 partial pressure, the temperature of 1,683°F is the only temperature at which CaO and $CaCO_3$ can coexist. At equilibrium, calcium is only present as CaO, or CaS above 1,683°F, and below 1,683°F all calcium is present as $CaCO_3$ or CaS. In Figure 4.2-15, a heavy vertical line divides the figure into $CaCO_3$ and CaO regions, left and right-hand columns, respectively.

The temperature dictates which H_2S reaction will be used for sulfur removal (see either Equation (5) or (6), since (5) contains CaO and (6) contains $CaCO_3$). Thermodynamic data for Equation (6) indicates that H_2S concentration decreases with a temperature increase, while thermodynamic data for Equation (5) indicates that H_2S concentration increases as temperature increases. Both curves meet at the equilibrium temperature for $CaCO_3$ calcination (1,683°F, determined by the CO_2 partial pressure and 230 ppm H_2S concentration), the temperature which determines the minimum equilibrium H_2S concentration possible for the measured partial pressures of H_2O and CO_2. This minimum equilibrium concentration is independent of the amount of excess sorbent that is added to the system.

The measured TRS concentrations and the maximum coal TRS concentration (calculated from the coal sulfur, assuming that all coal sulfur is released as sulfur to the fuel gas) are shown as horizontal lines in Figure 4.2-15. The measured TRS and coal TRS indicate 44-percent sulfur capture. This data indicates that if all the coal sulfur was present as H_2S, the transport reactor achieved 88 percent of the theoretically possible H_2S removal.

The minimum thermodynamic H_2S concentrations are provided in Table 4.2-3 for the 25 operating periods. The measured total reduced sulfur and minimum H_2S concentrations are compared in Figure 4.2-16. The minimum H_2S and measured reactor total reduced sulfur points are centered around the equilibrium line, which implies that the transport reactor is operating close to the minimum theoretical H_2S emissions and minimal CS_2 and COS emissions.

Seven of the 25 points on Figure 4.2-16 have measured total reduced sulfur less than the minimum theoretical H_2S concentration. All of these points have measured total reduced sulfur less than 200 ppm. These observations are consistent with observations from operation at Beijing Research Institute of Coal Chemistry in the early 1990's (Guohai Liu, personal communications). It is possible that the synthesis gas combustor SO_2 analyzer is less accurate at lower SO_2 concentrations or that the thermodynamic equilibrium data is less accurate at lower SO_2 concentrations.

Table 4.2-1

Gas Compositions, Molecular Weight, and Heating Value

Operating Period	H_2O Mole %	CO Mole %	H_2 Mole %	CO_2 Mole %	CH_4 Mole %	$C_2H_6^+$ Mole %	N_2 Mole %	Total Mole %	Measured WGS K_p	Equilibrium Temp ^OF	Riser TI360 ^OF	Calculated WGS K_p -50^OF	Syngas MW lb./Mole	Syngas CO/CO_2 Ratio	Syngas LHV Btu/SCF
GCT3-1	6.5	10.7	5.8	7.0	0.8	0.0	69.2	100.0	0.59	1,820	1,660	0.80	26.9	1.5	57
GCT3-2	6.6	11.7	7.5	8.3	1.3	0.0	64.6	100.0			1,665	0.80	26.6	1.4	70
GCT3-3	9.4	9.3	7.9	9.1	1.3	0.0	63.0	100.0			1,649	0.82	26.3	1.0	63
GCT3-4	9.3	9.2	7.5	9.0	1.3	0.0	63.7	100.0			1,669	0.79	26.4	1.0	62
GCT3-5	8.9	8.8	6.1	8.9	1.3	0.0	65.9	100.0			1,758	0.69	26.8	1.0	57
GCT3-6	8.3	9.9	8.0	8.6	1.3	0.0	64.0	100.0			1,632	0.84	26.3	1.1	66
GCT3-7	7.2	10.4	6.9	8.6	1.3	0.0	65.7	100.0			1,671	0.79	26.7	1.2	64
GCT3-8	7.1	10.6	7.0	8.7	1.3	0.0	65.4	100.0			1,660	0.80	26.7	1.2	65
GCT3-9	7.6	10.0	7.0	8.7	1.3	0.0	65.4	100.0			1,655	0.81	26.6	1.1	63
GCT3-10	9.0	8.9	7.0	9.1	1.3	0.0	64.8	100.0			1,665	0.80	26.6	1.0	59
GCT3-11	8.0	11.1	7.6	9.0	1.3	0.0	62.9	100.0			1,689	0.77	26.5	1.2	68
GCT3-12	6.4	9.5	5.4	8.4	1.3	0.0	68.9	100.0			1,704	0.75	27.1	1.1	58
GCT3-13	7.0	7.0	5.2	8.4	1.3	0.0	71.1	100.0			1,594	0.90	27.1	0.8	49
GCT3-14	7.1	10.7	7.9	8.1	1.3	0.0	64.9	100.0			1,632	0.84	26.4	1.3	68
GCT3-15	7.1	10.7	7.7	8.4	1.3	0.0	64.8	100.0			1,629	0.85	26.5	1.3	68
GCT3-16	7.0	11.2	8.0	8.4	1.3	0.0	64.2	100.0			1,626	0.85	26.4	1.3	70
GCT3-17	7.7	10.7	7.2	8.6	1.6	0.0	64.2	100.0	0.75	1,651	1,729	0.72	26.6	1.2	69
GCT3-18	7.7	11.3	6.9	8.8	1.9	0.0	63.3	100.0	0.70	1,694	1,736	0.71	26.6	1.3	73
GCT3-19	9.9	8.8	6.9	8.8	1.2	0.0	64.4	100.0	0.70	1,700	1,766	0.68	26.5	1.0	58
GCT3-20	9.8	9.1	8.3	9.2	1.3	0.0	62.4	100.0	0.85	1,579	1,769	0.68	26.2	1.0	64
GCT3-21	9.1	10.2	7.1	9.2	1.7	0.0	62.8	100.0			1,749	0.70	26.5	1.1	68
GCT3-22	9.1	10.4	7.3	9.2	1.6	0.0	62.5	100.0			1,742	0.71	26.5	1.1	68
GCT3-23	9.3	10.3	7.3	9.3	1.6	0.0	62.3	100.0			1,742	0.71	26.5	1.1	67
GCT3-24	9.3	10.9	7.7	9.1	1.7	0.0	61.4	100.0			1,764	0.68	26.3	1.2	71
GCT3-25	9.9	9.7	6.9	9.4	1.5	0.0	62.6	100.0			1,768	0.68	26.5	1.0	64

Notes:

1. Except for GCT3-1, -17, -18, -19, and -20, H_2 was estimated from water-gas shift equilibrium constant and measured CO, CO_2, and H_2 concentrations.
2. Except for GCT3-1, -17, -18, and -20 to -25, CH_4 was estimated from preliminary TC06 data.
3. All $C_2H_6^+$ values were estimated from preliminary TC06 data.
4. Except for GCT3-1, -17, -18, -19, and -20, N_2 was estimated by difference.

Table 4.2-2

N_2-Corrected Gas Composition, Molecular Weight, and Heating Value

Operating Period	H_2O Mole %	CO Mole %	H_2 Mole %	CO_2 Mole %	CH_4 Mole %	$C_2H_6^+$ Mole %	N_2 Mole %	Total Mole %	Syngas MW lb./Mole	Syngas CO/CO_2 Ratio	Syngas WGS K_p	Syngas LHV Btu/SCF
GCT3-1	9.1	17.9	9.7	8.9	1.3	0.0	53.1	100.0	25.8	2.0	0.53	96
GCT3-2	9.0	18.7	12.0	10.6	2.1	0.0	47.6	100.0	25.4	1.8	0.76	112
GCT3-3	13.5	14.9	12.6	12.0	2.0	0.0	45.0	100.0	25.0	1.2	0.76	101
GCT3-4	13.2	14.6	11.9	11.8	2.0	0.0	46.5	100.0	25.2	1.2	0.73	98
GCT3-5	12.9	14.6	10.1	11.9	2.1	0.0	48.5	100.0	25.7	1.2	0.63	94
GCT3-6	11.6	15.6	12.7	11.2	2.0	0.0	47.0	100.0	25.1	1.4	0.78	104
GCT3-7	10.0	16.8	11.2	11.2	2.1	0.0	48.6	100.0	25.6	1.5	0.74	104
GCT3-8	9.6	16.7	10.9	11.1	2.0	0.0	49.7	100.0	25.7	1.5	0.76	102
GCT3-9	10.5	16.0	11.2	11.4	2.1	0.0	48.8	100.0	25.6	1.4	0.76	101
GCT3-10	12.7	14.1	11.1	12.0	2.0	0.0	48.1	100.0	25.5	1.2	0.74	94
GCT3-11	10.7	16.6	11.3	11.3	1.9	0.0	48.2	100.0	25.6	1.5	0.72	102
GCT3-12	9.6	17.6	10.0	11.9	2.4	0.0	48.4	100.0	26.1	1.5	0.71	106
GCT3-13	12.0	14.7	11.0	13.3	2.8	0.0	46.2	100.0	25.7	1.1	0.83	103
GCT3-14	9.5	16.5	12.1	10.3	2.0	0.0	49.6	100.0	25.3	1.6	0.79	104
GCT3-15	9.5	16.3	11.7	10.6	2.0	0.0	49.9	100.0	25.5	1.5	0.80	103
GCT3-16	9.3	16.8	12.0	10.5	2.0	0.0	49.4	100.0	25.4	1.6	0.81	105
GCT3-17	10.2	15.9	10.7	10.8	2.4	0.0	50.0	100.0	25.6	1.5	0.71	103
GCT3-18	10.0	16.5	10.1	10.9	2.8	0.0	49.7	100.0	25.8	1.5	0.67	106
GCT3-19	13.0	12.7	9.9	10.8	1.7	0.0	51.8	100.0	25.6	1.2	0.65	84
GCT3-20	13.1	13.3	12.1	11.4	1.9	0.0	48.3	100.0	25.1	1.2	0.79	93
GCT3-21	11.8	14.7	10.1	11.3	2.4	0.0	49.6	100.0	25.7	1.3	0.66	97
GCT3-22	11.7	14.8	10.3	11.2	2.2	0.0	49.7	100.0	25.7	1.3	0.67	96
GCT3-23	12.1	14.7	10.4	11.5	2.3	0.0	49.1	100.0	25.7	1.3	0.67	96
GCT3-24	12.0	15.3	10.8	11.0	2.3	0.0	48.6	100.0	25.5	1.4	0.64	100
GCT3-25	13.1	14.0	10.0	11.7	2.1	0.0	49.1	100.0	25.7	1.2	0.64	92

Note: See Table 4.2-1 for assumptions in gas compositions.

Table 4.2-3

Synthesis Gas Combustor Calculations

Operating Period	Calculated SGC[2] Exit H_2O M %	AIT8775 SGC Exit O_2 M %	Calculated SGC Exit O_2 M %	Energy Balance LHV[3] Btu/SCF	Gas Analyzer LHV Btu/SCF	Syngas TRS[4] Coal Max. ppm	Combustor SO_2 AI534A ppm	Syngas TRS SGC SO2 ppm	Syngas SO_2 Emissions lb. SO_2/ 10^6 Btu coal	Thermo. Equlibrium H_2S ppm
GCT3-1	8.0	5.8	6.8	64	57	465	67	144	0.185	134
GCT3-2	10.4	5.4	3.5	59	70	492	67	125	0.159	146
GCT3-3	11.3	4.7	5.3	66	63	476	112	226	0.300	216
GCT3-4	11.0	4.9	5.4	66	62	471	97	196	0.261	213
GCT3-5	10.7	4.8	4.7	57	57	475	109	205	0.255	203
GCT3-6	10.5	5.1	5.6	68	66	450	99	206	0.263	186
GCT3-7	9.5	5.0	5.8	68	64	568	71	150	0.172	161
GCT3-8	9.3	5.1	6.0	70	65	514	82	176	0.199	159
GCT3-9	9.6	5.0	6.0	70	63	475	107	229	0.271	170
GCT3-10	10.3	5.0	6.1	68	59	448	82	172	0.209	205
GCT3-11	10.6	6.1	4.7	65	68	414	57	111	0.136	183
GCT3-12	8.6	5.8	5.7	57	58	364	54	111	0.153	142
GCT3-13	9.2	5.4	5.5	51	49	361	64	124	0.163	156
GCT3-14	10.0	6.6	5.4	64	68	413	82	170	0.202	152
GCT3-15	9.4	5.5	6.4	72	68	421	97	215	0.250	157
GCT3-16	9.6	5.6	6.1	71	70	419	99	218	0.256	156
GCT3-17	10.2	5.4	5.3	67	69	417	80	167	0.196	173
GCT3-18	10.0	5.6	5.6	70	73	400	81	174	0.213	174
GCT3-19	10.9	5.4	5.8	63	58	387	117	237	0.302	224
GCT3-20	11.5	5.9	5.6	62	64	465	125	257	0.318	225
GCT3-21	10.6	5.6	5.7	67	68	465	116	245	0.300	208
GCT3-22	10.8	4.9	5.4	69	68	456	113	235	0.293	208
GCT3-23	11.0	4.8	5.3	70	67	452	102	210	0.265	214
GCT3-24	11.3	4.9	4.9	69	71	445	116	237	0.305	213
GCT3-25	11.4	5.0	4.9	64	64	462	131	258	0.317	230

Notes:

1. See Table 4.2-1 for assumptions in synthesis gas compositions.
2. SGC = Synthesis gas combustor.
3. Energy balance LHV assumed a SGC heat loss of 1 X 10^6 Btu/hr.
4. TRS = Total reduced sulfur (H_2S + COS + CS_2).

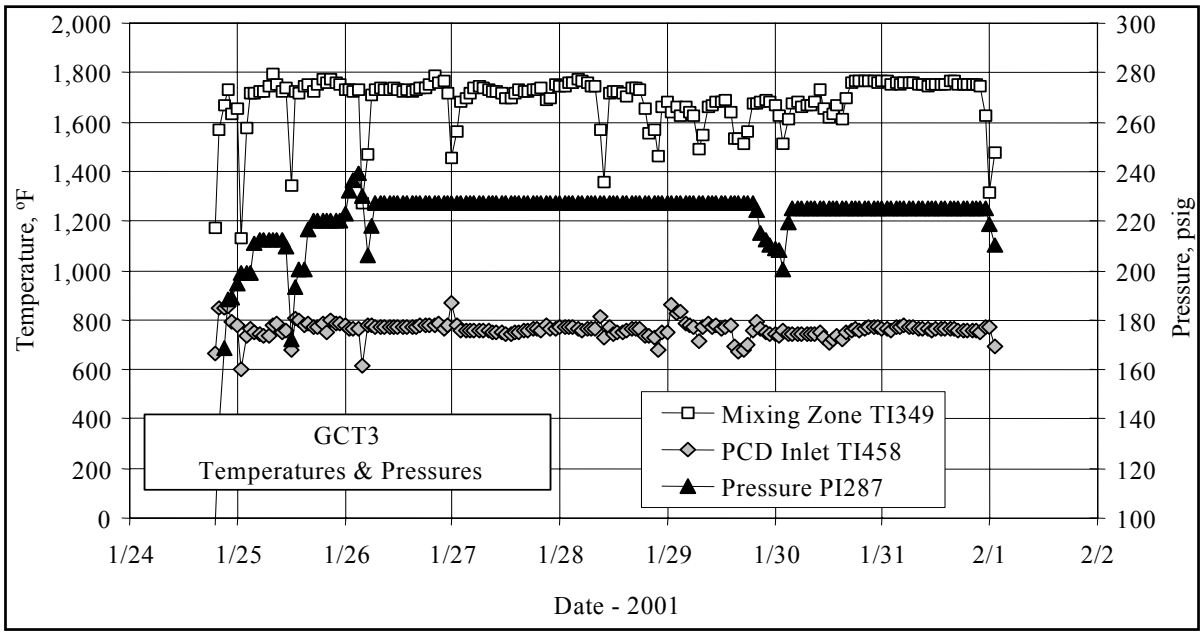

Figure 4.2-1 Temperature and Pressures

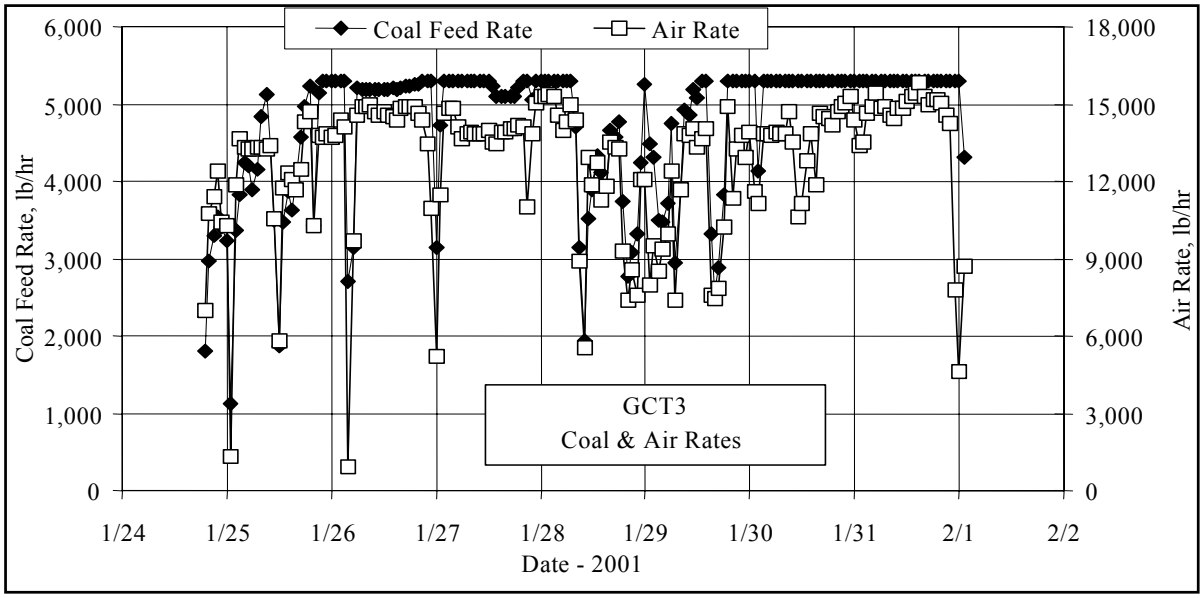

Figure 4.2-2 Coal and Air Rates

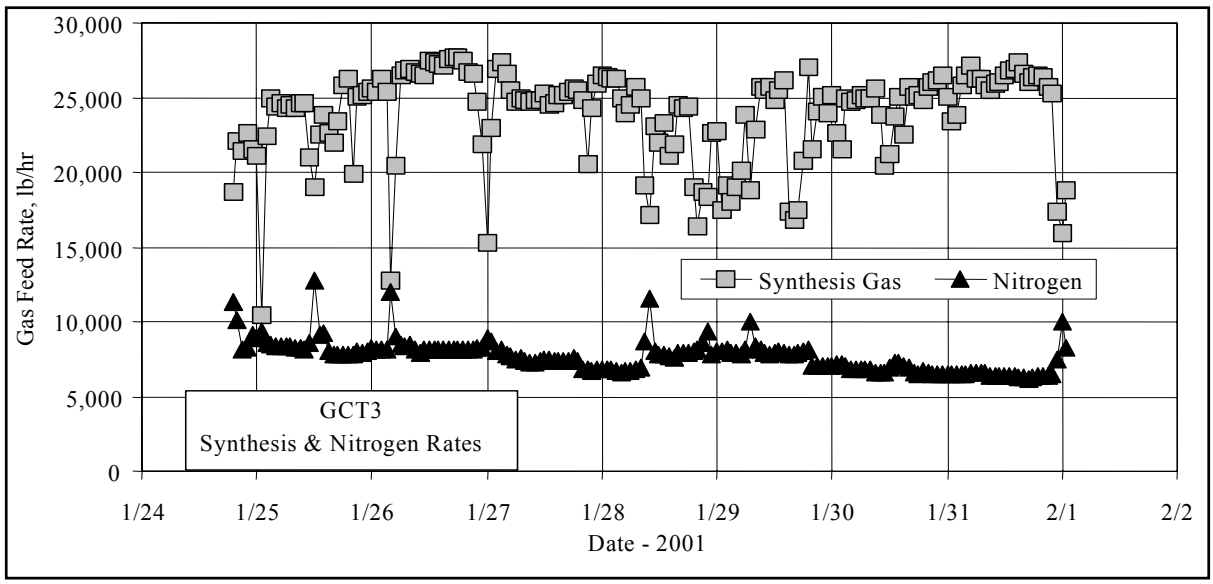

Figure 4.2-3 Synthesis Gas and Nitrogen Rates

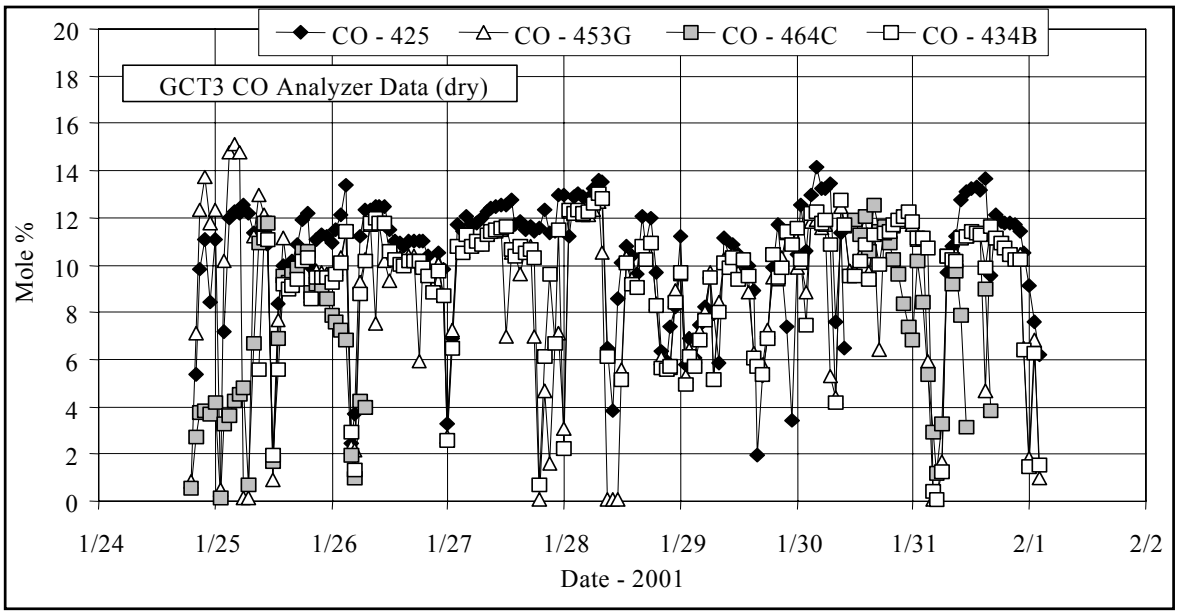

Figure 4.2-4 Analyzer CO Concentrations

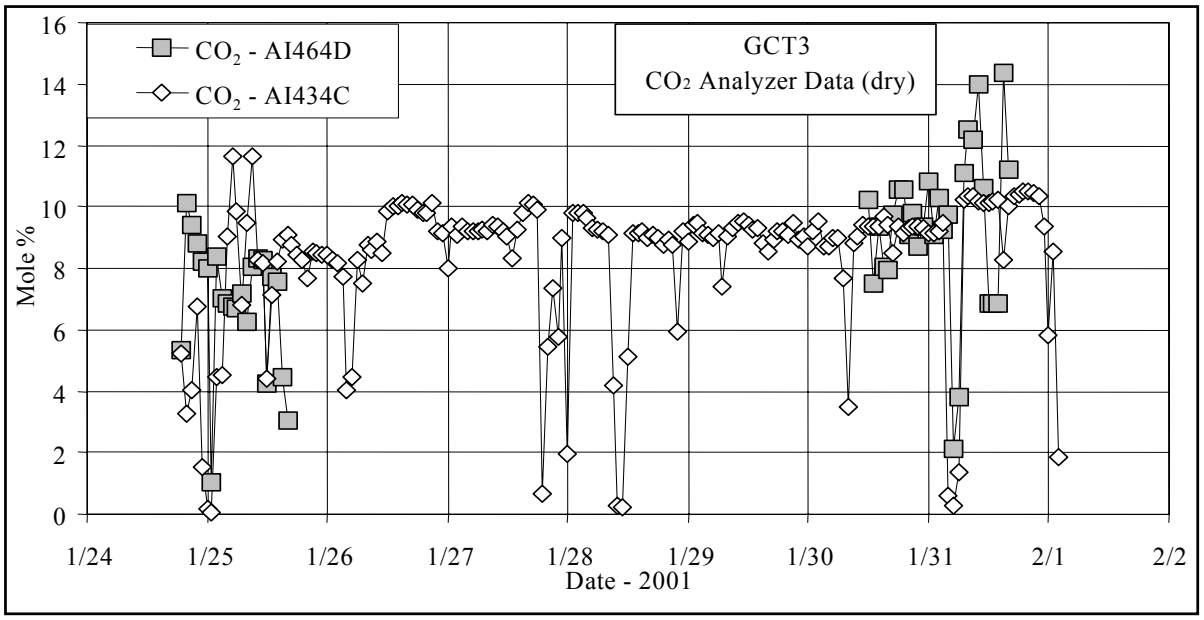

Figure 4.2-5 Analyzer CO_2 Concentrations

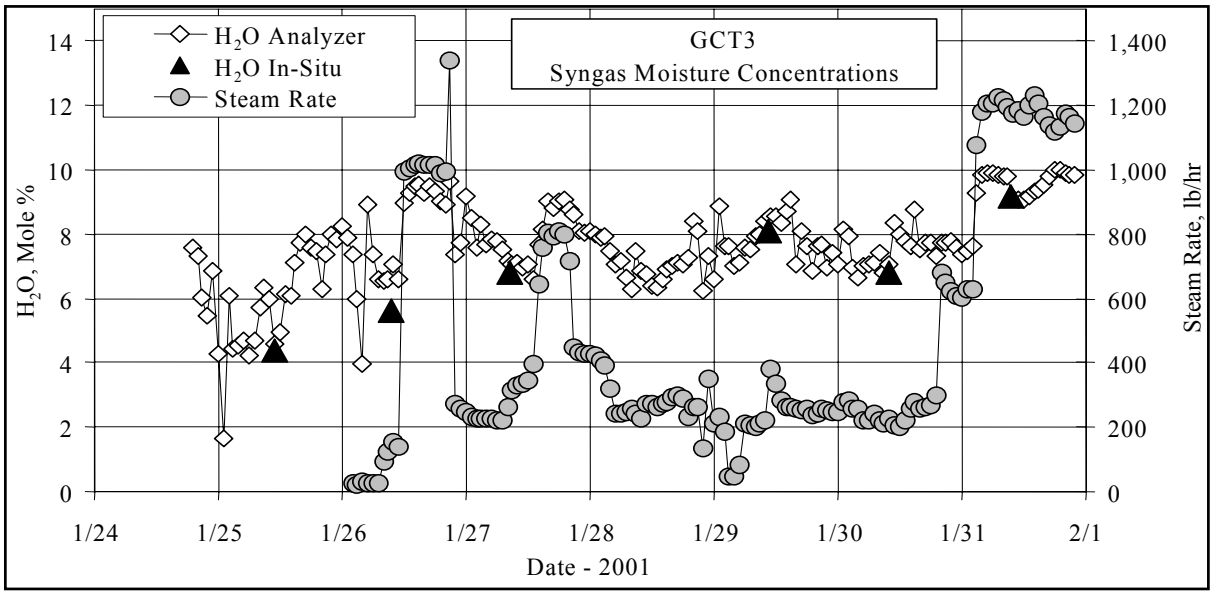

Figure 4.2-6 Analyzer H_2O Concentrations and Steam Rate

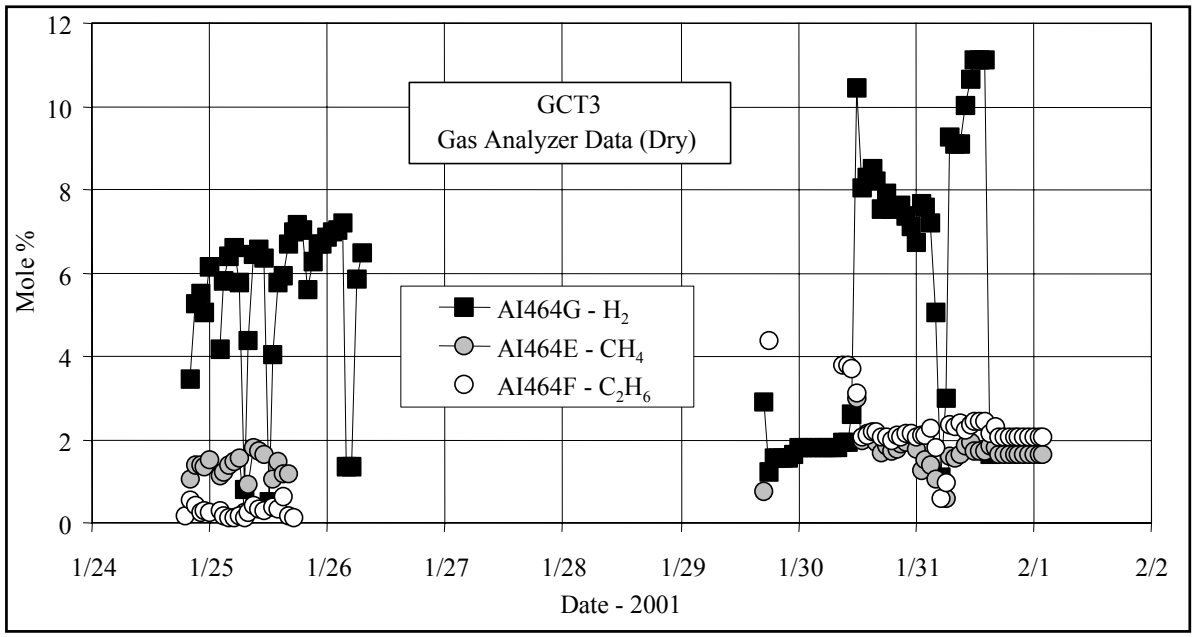

Figure 4.2-7 Analyzer H_2, CH_4, and $C_2H_6^+$ Concentrations

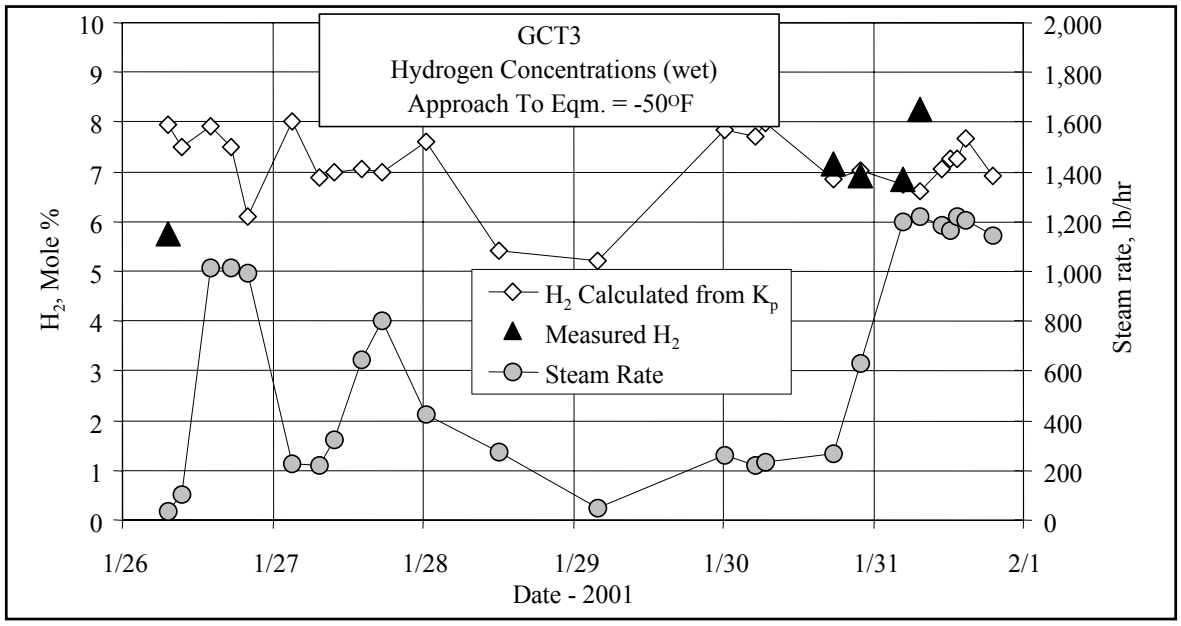

Figure 4.2-8 Analyzer and Calculated Equilibrium H_2 Concentrations

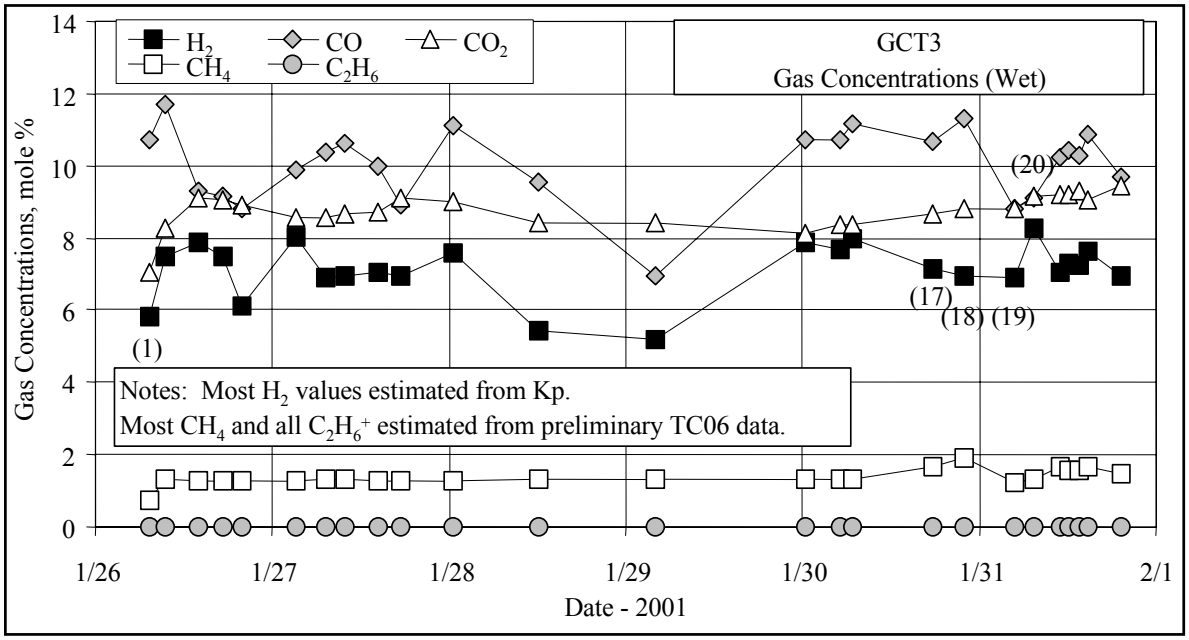

Figure 4.2-9 Wet CO, CO_2, H_2, CH_4, and $C_2H_6^+$ Concentrations

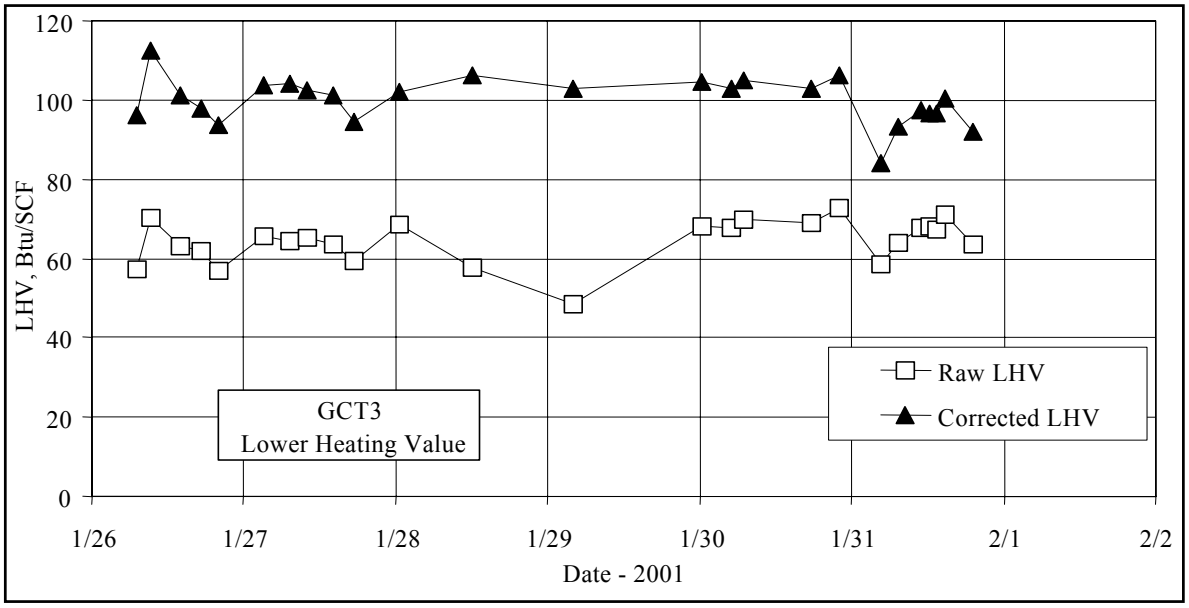

Figure 4.2-10 Raw and Corrected Lower Heating Values

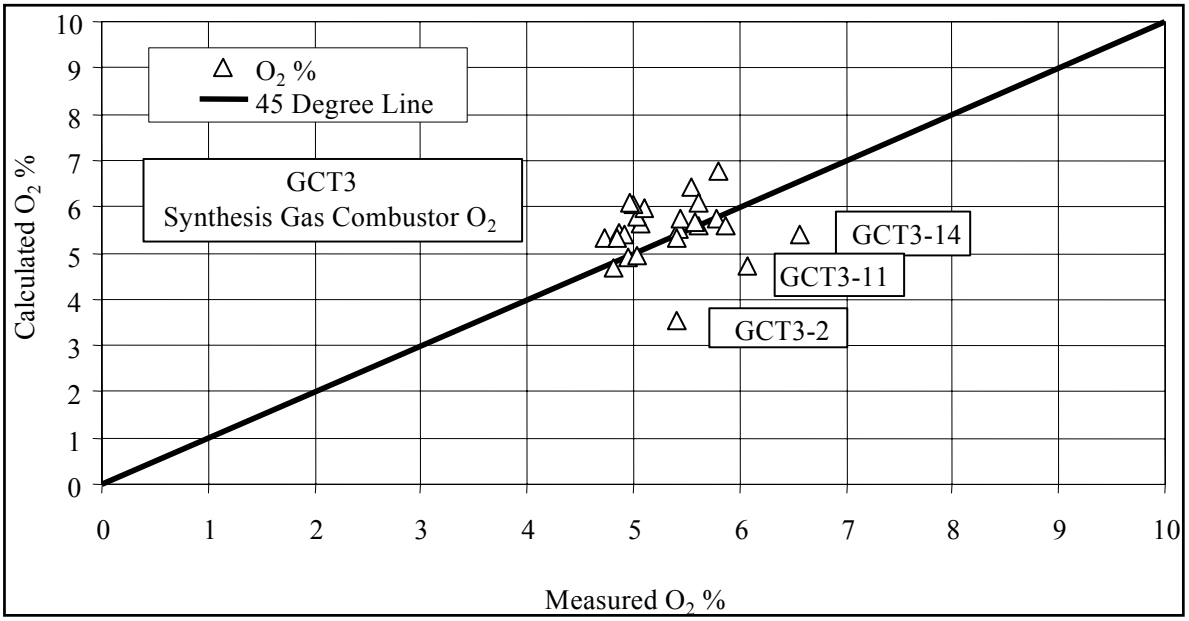

Figure 4.2-11 Synthesis Gas Combustor Exit Oxygen

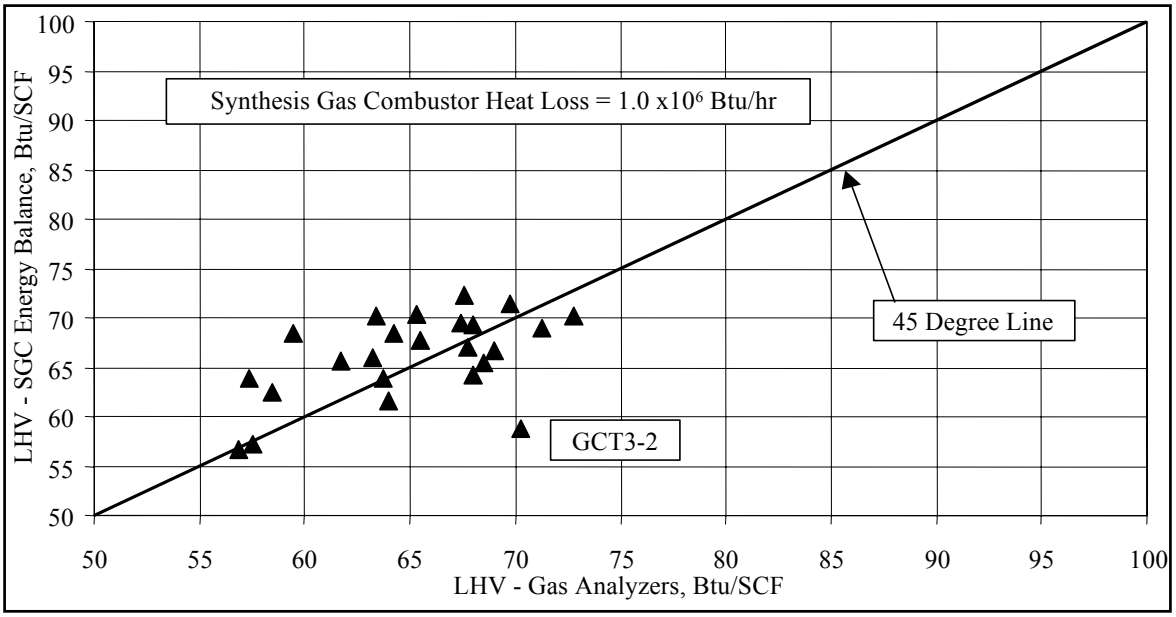

Figure 4.2-12 LHV - Gas Analyzers and Synthesis Gas Combustor Energy Balance

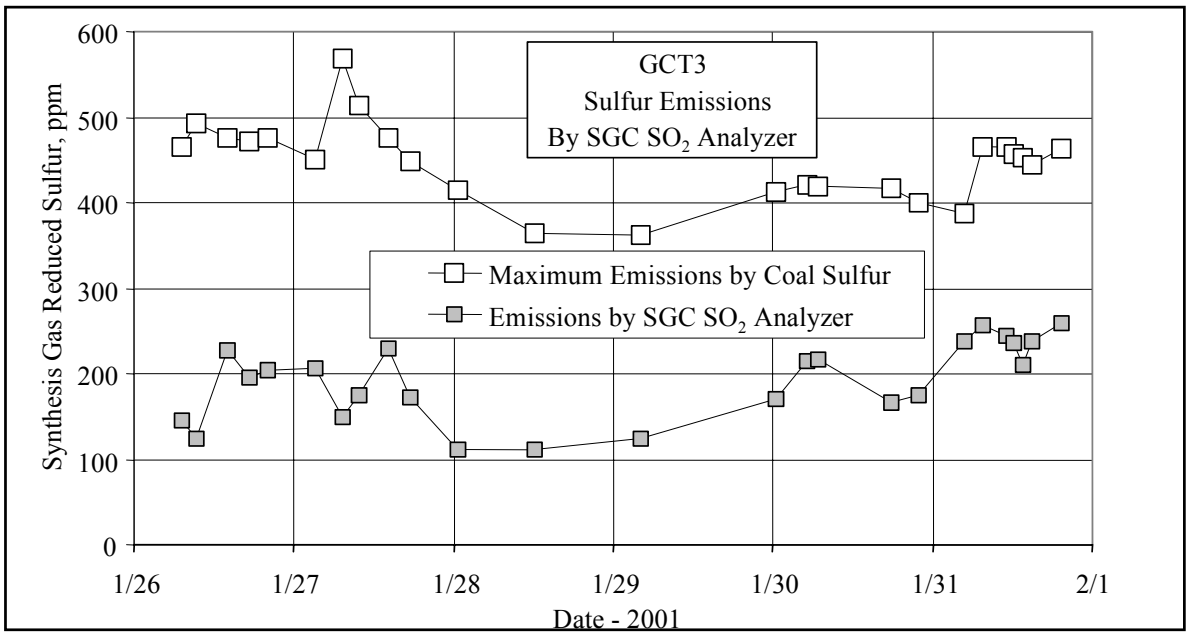

Figure 4.2-13 Transport Reactor Sulfur Emissions

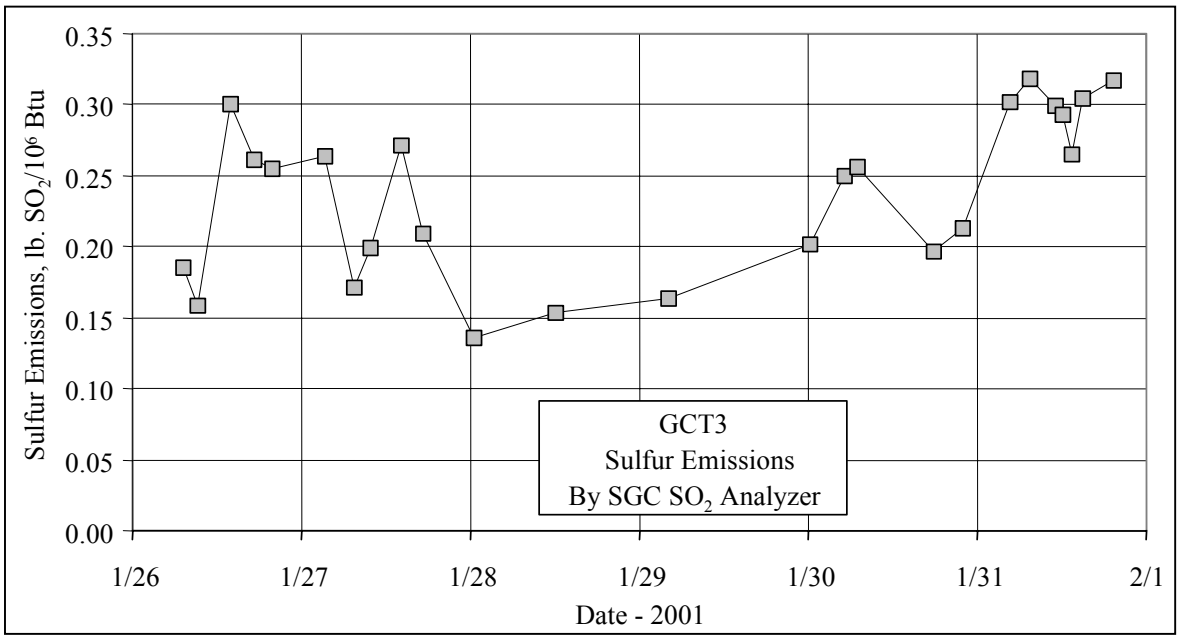

Figure 4.2-14 Transport Reactor Sulfur Emissions

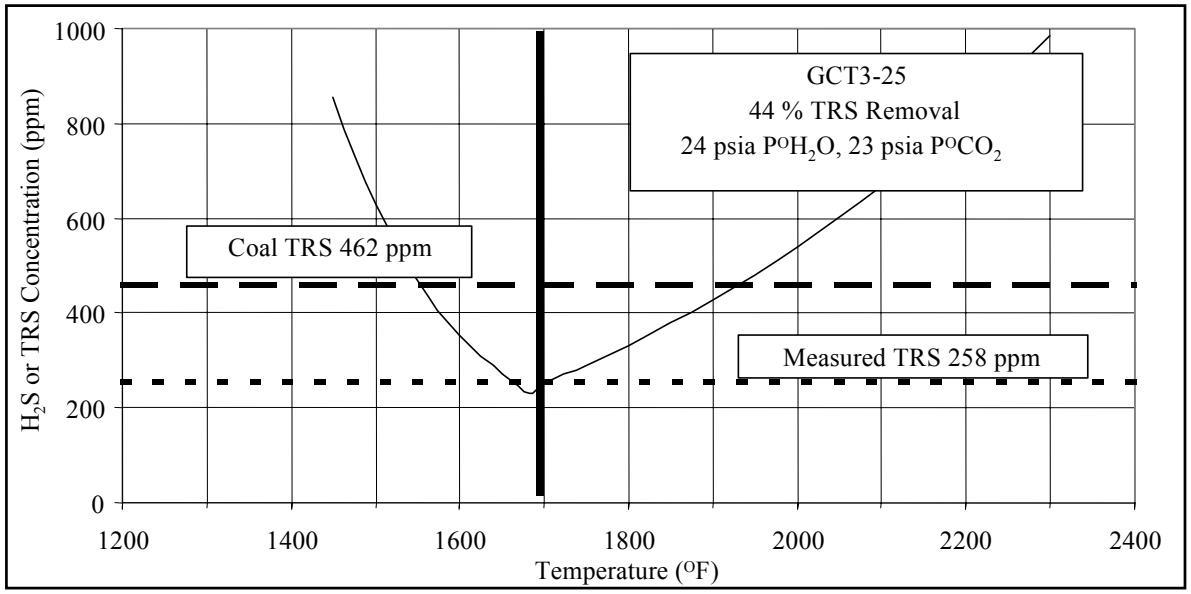

Figure 4.2-15 GCT3-25 Equilibrium H_2S Concentration

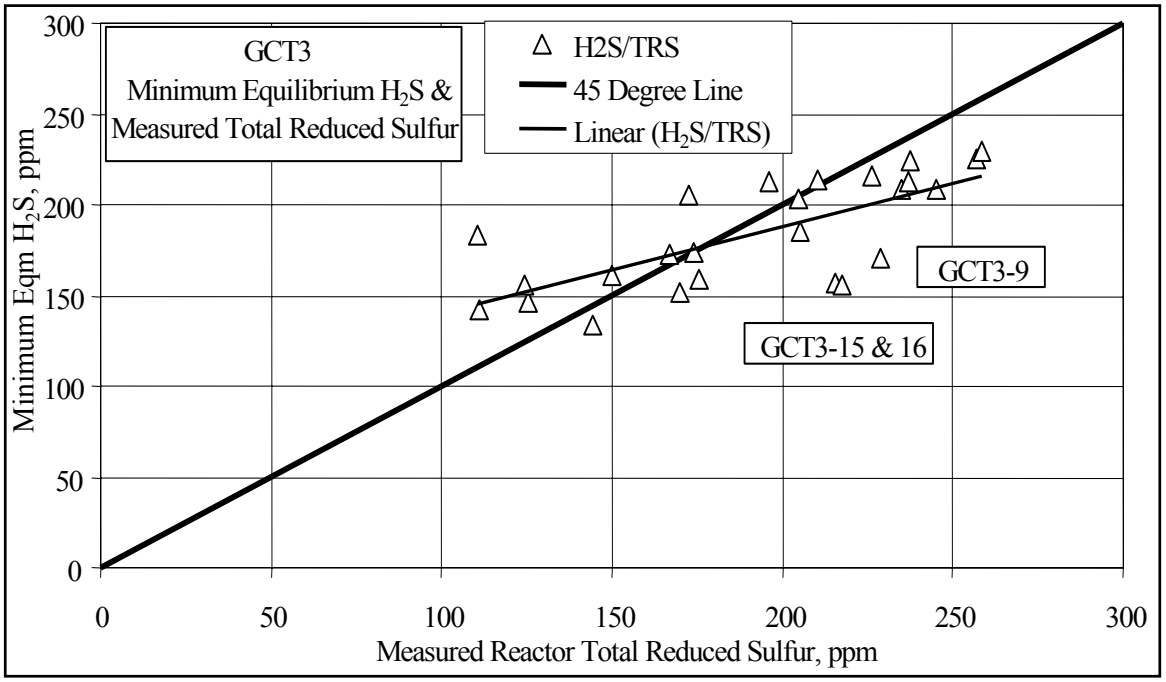

Figure 4.2-16 GCT3-25 Equilibrium H_2S and Measured Total Reduced Sulfur Concentration

4.3 SOLIDS ANALYSES

Solids were collected during the GCT3 test run from the fuel feed system (FD0210), the sorbent feed system (FD0220), the standpipe spent solids transport system (FD0510), and the PCD fine solids transport system (FD0520). In situ solids samples were also collected from the PCD inlet. These solids were analyzed for chemical composition and particle size. This section will utilize the chemical analysis data to show:

- Chemical composition changes.
- Particle size and bulk density changes.
- PCD solids calcination.
- PCD solids sulfation.

Figure 4.3-1 shows the coal sulfur and ash as sampled from the fuel feed system during GCT3. The Powder River Basin (PRB) coal had from 0.23- to 0.38-percent sulfur and from 5- to 8-percent ash. The ash was constant during the test, except for the first sample analyzed. The PRB sulfur and ash levels were lower in GCT3 than in GCT2. Also shown in Figure 4.3-1 are the interpolated sulfur levels for each test period used for the sulfur removal calculations found in Section 4.2 and the sulfur mass balance calculations in Section 4.4.

The coal carbon and hydrogen content as sampled from FD0210 are shown in Figure 4.3-2. The carbon was between 57- and 59-weight percent. Also shown in Figure 4.3-2 are the interpolated carbon levels for each test period used for the carbon conversion and carbon mass balance calculations found in Section 4.4. The hydrogen content was steady at about 6.0-weight percent, except for the first sample on January 25 (5.6 percent). The hydrogen is measured dry and reported as received, and does not include the hydrogen in the coal moisture. Also shown in Figure 4.3-2 are the interpolated hydrogen levels for each test period used for the hydrogen mass balance calculations found in Section 4.4.

The coal oxygen and moisture contents as sampled from FD0210 are shown in Figure 4.3-3. The coal oxygen was constant during GCT3 at 13-weight percent. The oxygen is reported as received, and does not include the oxygen in the coal-free moisture. Oxygen is also not directly measured, but is the value required to make the elemental analysis add up to 100 percent. Therefore, it is the least accurate of the coal elemental analyses. The coal moisture was between 15- and 18-weight percent for GCT3. Also shown in Figure 4.3-3 are the interpolated coal moisture levels for each test period used for the hydrogen and oxygen mass balance calculations found in Section 4.4.

The coal higher heating value (HHV) and lower heating value (LHV) are shown in Figure 4.3-4. Also shown in Figure 4.3-4 are the interpolated HHV levels for each test period used for the sulfur emission calculations shown in Section 4.2. The LHV was determined from HHV by reducing the heating value to account for the coal moisture and hydrogen. Also shown in Figure 4.3-4 are the interpolated LHV levels for each test period used for the energy balances and gasification efficiencies reported in Section 4.4.

A plot showing the Sauter mean diameter (SMD) and mass mean diameter (D_{50}) particle size of the coal feed to the transport reactor in GCT3 are shown in Figure 4.3-5. The coal SMD was usually between 275 to 425 μm during GCT3. The D_{50} was about 300 μm during the test, with two excursions that were up to 400 μm.

A measure of the amount of fines would be the percent of the smallest size fraction. To show the level of fines in the coal feed, the percent of ground coal less than 45 μm is shown in Figure 4.3-6. The fines percent was usually below 10 percent. Two samples around January 30 had fines percents greater than 14 percent. One of the probable causes of coal feeder trips is excessive fines in the coal. Periods of minimal coal feeder trips on January 26, 27, and 31 show less than 10-percent fines in the coal. Periods of numerous coal feeder trips on January 29 and 30 show higher fines in the coal feed.

The average mass mean particle sizes (D_{50}) for GCT3 measured at the coal feed system (FD0210) is shown in Table 4.3-1. The D_{50} standard deviation is also shown, to give an estimate of the variation in D_{50} during the testing. The GCT3 coal feed system mass mean particle sizes were finer than seen in the GCT2 coal feed system by about 38 μm, which was about 1 standard deviation of both sample sets.

FD0220 was used during GCT3 to feed Ohio Bucyrus limestone into the transport reactor. The compositions of the samples taken during GCT3 did not vary during the run. Average limestone compositions are provided in Table 4.3-2.

A plot of the SMD and D_{50} of the solids sampled from the sorbent feeder (FD0220) are shown in Figure 4.3-7. The SMD varied from 12 to 32 μm, and was usually 14 and 22 μm. The D_{50} varied from 7 to 18 μm, but was usually between 8 and 12 μm.

A plot of the SMD, D_{50}, and bulk density for the PCD solids sampled from FD0520 is shown in Figure 4.3-8. The SMD was fairly constant from January 25 to 30 at 8 to 13 μm. On January 31, the SMD increased from 10 to about 13 μm. The D_{50} at the start of the test was at about 20 μm on January 25, decreased to 15 μm, then increased to 18 μm, and then was steady at about 15 μm until January 31. On January 31, as with the SMD, the D_{50} increased up to 18 μm. A comparison of the D_{50} between GCT2 and GCT3, shown in Table 4.3-1, reveals that GCT3 PCD fine solids had a smaller D_{50} than found in GCT2. This was due to the changes made to the disengager, cyclone, and cyclone dipleg, which helped capture a larger amount of finer particulates and recycled them to the standpipe and mixing zone.

The bulk density varied between 10 and 20 lb/ft^3 for the entire run with a few outliers. The bulk density was increasing at the end of the run as the SMD and D_{50} particle sizes were also increasing.

The solids compounds produced by the transport reactor were determined using the solids analysis and the following assumptions:

1. All carbon dioxide measured came from $CaCO_3$, hence moles CO_2 = moles $CaCO_3$.

2. All sulfide sulfur measured came from CaS.

3. All sulfate sulfur measured came from $CaSO_4$.

4. All calcium not taken by CaS, $CaSO_4$, and $CaCO_3$ came from CaO.

5. All magnesium came from MgO.

6. Total carbon is measured, which is the sum of organic and inorganic (CO_2) carbon. The organic carbon is the total carbon minus the CO_2 carbon.

7. Inerts are the sum of the Al_2O_3, Fe_2O_3, P_2O_5, K_2O, SiO_2, Na_2O, and TiO_2 contents.

FD0510 was not run much during GCT3 and no samples were taken from the FD0510 sampling location. Two standpipe samples were taken using the new standpipe sampler. The compound breakdown for the two samples is provided in Table 4.3-3. The January 27 sample had an extremely high carbon content, which may include left-over material from startup. The January 29 sample is reasonable.

Figure 4.3-9 shows a plot of the organic carbon (total carbon minus CO_2 carbon) and the inerts (ash not containing calcium, magnesium, or sulfur compounds) for the PCD solids sampled from FD0520. Since FD0520 ran continuously during GCT3, solid samples were taken often, the goal being one sample every 2 hours. About half of the GCT3 PCD solids that were sampled were analyzed. Also shown in Figure 4.3-9 are the interpolated carbon levels for each test period used for the carbon mass balance calculations seen in Section 4.4. Figure 4.3-9 also shows the interpolated inerts levels for each test period used for the inerts mass balance calculations provided in Section 4.4. Solids recovered in situ during the PCD inlet particulate sampling were also analyzed. The in situ carbon and inerts are shown in Figure 4.3-9. The in situ solids compared well with the FD0520 solids, except for the January 25 carbon analyses.

The total carbon decreased on January 26 from 50 percent to 35 to 40 percent, where it leveled off for a few days. During the periods of numerous coal trips, the carbon content rose to 50 percent, but then decreased to 15 to 20 percent for the last day of operation. The inerts content was very steady at 20 to 30 percent for most of the run. During the last day of operation the inerts rose to 45 percent, while the carbon content decreased. A lower carbon content results in higher carbon conversions.

Figure 4.3-10 provides the amounts of $CaCO_3$, CaS, CaO, and $CaSO_4$ in the PCD solids as sampled from FD0520. The CaO at the start of the run was at 7-weight percent and then rose to 22-weight percent on January 28. The CaO dropped to 10 percent during the numerous coal trips and then rose to 25 percent by the end of the run. The $CaCO_3$ at the start of the run was at 10 percent, then increased to 20 on January 28. During the numerous coal trips, the $CaCO_3$ and CaO leveled off at 10 percent. On January 30, the $CaCO_3$ dropped to 5 percent. The CaO and $CaCO_3$ tracked each other for the first 5 days of operation, indicating a constant limestone calcination. The calcination increased for the last day of operation as the CaO content increased and the $CaCO_3$ content decreased.

The CaS had very low levels (less than 4 percent), indicating poor reactor sulfur capture. During the reactor coal trips there was more sulfur in the solids than during the rest of the run. The low

levels of $CaSO_4$ indicate that there was no $CaSO_4$ in the PCD solids, as expected. Table 4.3-4 provides the PCD fines compositions for the samples collected in FD0520. The consistency, seen in these totals that add up to 98.3 to 101.9 percent, is excellent for solids composition data. Note that it is organic carbon shown in Table 4.3-4, not the total carbon as seen in the plot in Figure 4.3-9. Organic carbon is the difference between the total carbon and the $CaCO_3$ carbon.

Figure 4.3-11 shows a plot of the CO_2 partial pressure and percent limestone calcination for GCT3. The CO_2 partial pressure is the system pressure times the mole fraction CO_2. The percent limestone calcination is the mole percent CaO divided by the sum of the mole percents of CaO and $CaCO_3$, or

$$\% \text{ Calcination} = \frac{\text{M\% CaO}}{\text{M\% CaO} + \text{M\% CaCO}_3} \quad (1)$$

The percent calcination was between 50 and 70 percent for the first 6 days of operation (minus the first sample on January 29), then increased to 80 to 90 percent during the last day of operation. For all of the test periods except two, the CO_2 partial pressure was 20 to 23 psia. The high calcination was at the end of the run, when the coal-feed rate was steady. Limestone calcination is complicated by the high calcium content of PRB coal, where typically the calcium fed with the coal is approximately equal to the calcium fed by limestone (see Table 4.4-3, Section 4.4). The calcium in the PCD solids is, therefore, one-half from limestone and one-half from PRB coal ash. Coal ash calcium is probably not present as calcite ($CaCO_3$), but might be present as a number of mineral carbonates or sulfate, including gypsum, dolomite, or ankerite {(Ca, Fe, Mg)CO_3)}. Equation (1) assumes that calcium is only present as CaO or $CaCO_3$. The calcination percent might be different for operation with coals that have a low calcium content.

The PCD solids nitrogen and hydrogen concentrations are shown in the plot of Figure 4.3-12. As expected, the fines hydrogen contents are lower than the coal hydrogen contents (see Figure 4.3-2). The PCD solids hydrogen was typically about 10 percent of the coal hydrogen.

A plot of the PCD solids LHV are shown in Figure 4.3-13. The LHV of the PCD solids at the start of GCT3 were about 7,500 Btu/lb and then decreased to between 5,000 and 5,500 Btu/lb. On January 29, the LHV rose from 5,000 to about 7,000 Btu/lb. After the coal-feed rate was held constant the LHV decreased to between 2,000 and 3,500 Btu/hr. Since there is very little hydrogen or moisture in the PCD solids the LHV is essentially equal to the HHV. The char fines LHV tracks the char fines carbon content, as expected.

The percent calcium sulfation, calculated as the mole percent of calcium compounds containing sulfur, are shown in the plot seen in Figure 4.3-14, as is sulfur removal calculated from the coal-feed rate, coal sulfur, and thermal oxidizer data.

The percent sulfation is defined as:

$$\%\ Sulfation = \frac{M\%\ CaS + M\%\ CaSO_4}{M\%\ CaO + M\%\ CaCO_3 + M\%\ CaS + M\%\ CaCO_3} \quad (2)$$

There seems to be no relationship between the percent sulfation and the percent sulfur removal, indicating that there would be a poor sulfur balance (see Section 4.4).

Table 4.3-1

Coal and PCD Solids Particle Sizes

Test		GCT3		GCT2	
		D_{50}	Standard Deviation	D_{50}	Standard Deviation
Location	Description	microns	microns	microns	microns
FD0210	Coal Feed	316	42	354	42
FD0520	Fine Solids	15.7	1.8	21.5	3.8

Table 4.3-2

Limestone Analysis

Compound	Weight %
$CaCO_3$	76.7
$MgCO_3$	16.5
$CaSO_4$	1.3
Inerts	3.3
H_2O	0.1
Total	97.9

Table 4.3-3

Standpipe Analysis

Sample Number	Sample Date & Time	Inerts Wt. %	$CaCO_3$ Wt. %	CaS Wt. %	$CaSO_4$ Wt. %	CaO Wt. %	MgO Wt. %	Organic C Wt. %	Total Wt. %
AB07686	1/27/01 2:00	64.2	2.0	0.2	0.3	9.5	1.9	25.6	103.7
AB07687	1/29/01 10:00	87.8	1.0	0.0	0.0	7.7	1.4	2.0	99.9

Table 4.3-4

PCD Fines From FD0520

Sample Number	Sample Date & Time	Inerts Wt. %	$CaCO_3$ Wt. %	CaS Wt. %	$CaSO_4$ Wt. %	CaO Wt. %	MgO Wt. %	Organic C ($C-CO_2$) Wt. %	Total Wt. %
AB07659	1/25/01 8:00	27.5	10.5	3.0	0.3	7.1	3.6	49.7	101.6
AB07675	1/26/01 0:00	28.4	8.2	2.7	0.2	10.1	3.4	48.9	101.9
AB07711	1/26/01 12:00	27.3	14.5	1.3	0.2	12.9	4.5	40.2	100.9
AB07712	1/26/01 20:00	29.3	13.1	1.3	0.2	15.1	4.8	36.6	100.4
AB07718	1/27/01 12:00	25.4	18.5	0.7	0.1	13.5	5.0	36.0	99.4
AB07720	1/27/01 18:00	25.4	18.4	0.3	0.1	19.5	6.0	28.0	97.8
AB07722	1/27/01 22:00	21.7	20.4	1.3	0.1	12.6	4.8	37.5	98.3
AB07734	1/28/01 2:00	23.4	17.2	0.4	0.2	19.1	5.8	33.3	99.4
AB07735	1/28/01 4:00	24.9	13.2	0.4	0.2	22.5	5.9	32.0	99.2
AB07747	1/29/01 8:00	18.8	32.6	0.7	0.1	8.6	5.2	32.6	98.7
AB07769	1/29/01 18:00	27.3	9.1	2.4	0.3	10.2	3.3	46.3	98.8
AB07771	1/29/01 22:00	24.2	12.0	2.7	0.1	10.4	3.7	45.3	98.5
AB07776	1/30/01 8:00	23.1	11.6	2.0	0.1	8.8	3.4	51.1	100.0
AB07805	1/30/01 12:00	24.7	9.2	3.1	0.2	9.4	3.3	50.3	100.2
AB07807	1/30/01 16:00	27.2	13.6	2.7	0.3	16.0	5.2	34.8	99.8
AB07809	1/30/01 20:00	32.9	9.8	1.6	0.2	24.6	6.5	24.5	100.1
AB07811	1/31/01 0:00	36.7	9.6	1.2	0.2	24.2	6.4	22.5	100.7
AB07813	1/31/01 4:00	35.8	9.3	1.0	0.2	27.3	7.0	20.2	100.7
AB07814	1/31/01 8:00	47.4	5.3	0.8	0.2	28.9	6.3	12.9	101.7
AB07818	1/31/01 12:00	42.0	6.8	1.9	0.2	22.8	5.6	21.8	101.2
AB07820	1/31/01 16:00	44.2	6.3	0.6	0.2	23.7	5.8	17.8	98.8
AB07822	1/31/01 20:00	42.8	6.5	0.8	0.1	27.1	6.3	14.8	98.3

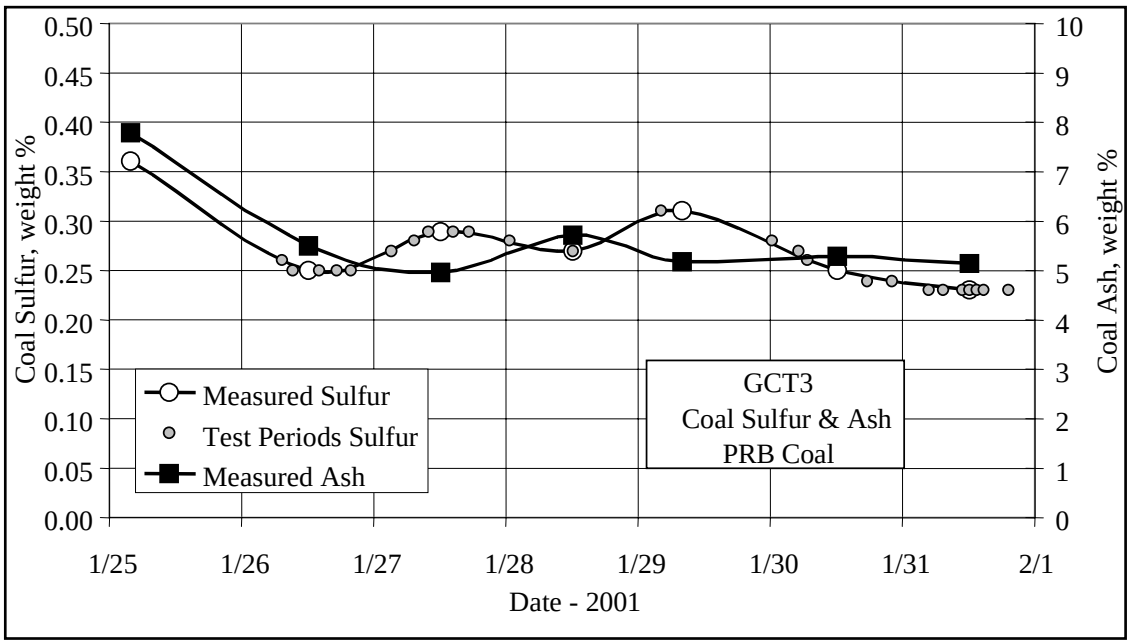

Figure 4.3-1 Coal Sulfur and Ash

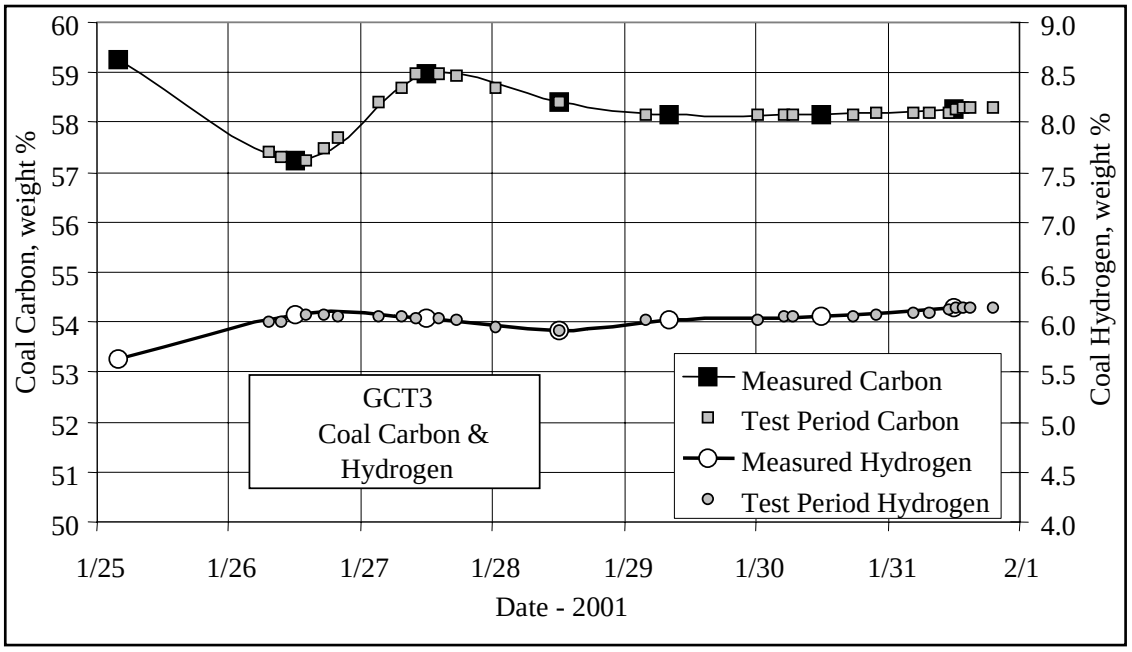

Figure 4.3-2 Coal Carbon and Hydrogen

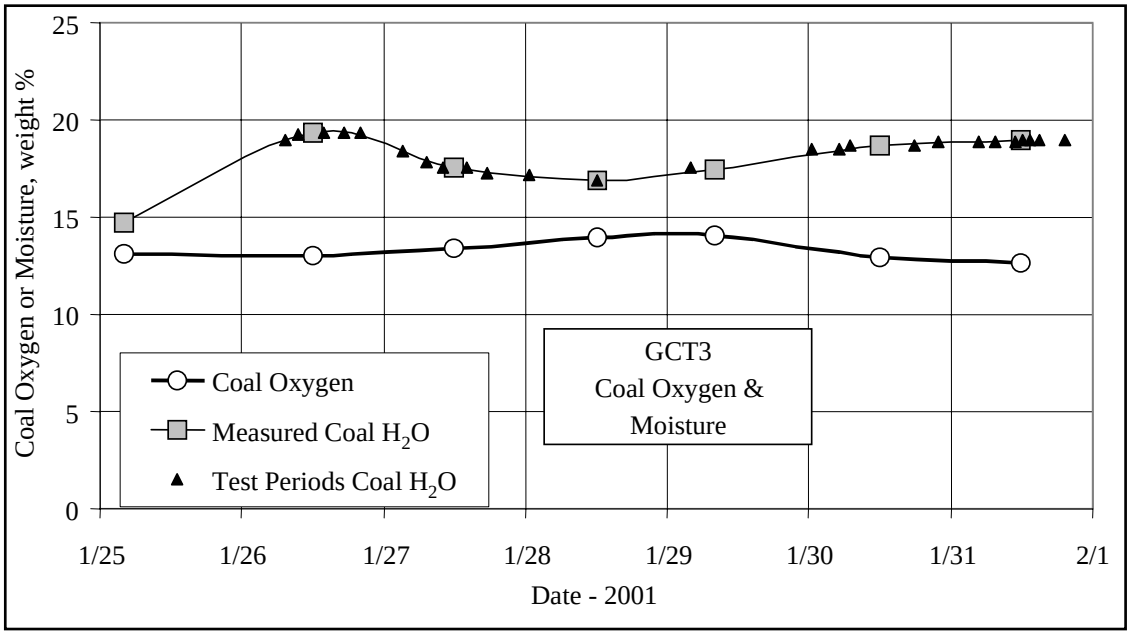

Figure 4.3-3 Coal Oxygen and Moisture

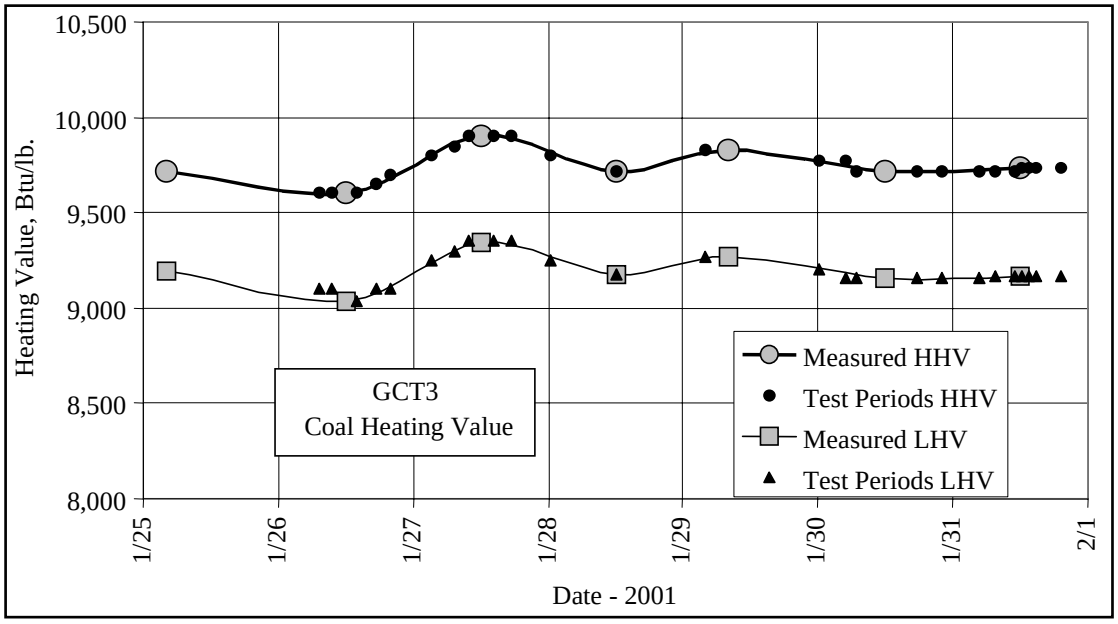

Figure 4.3-4 Coal Heating Value

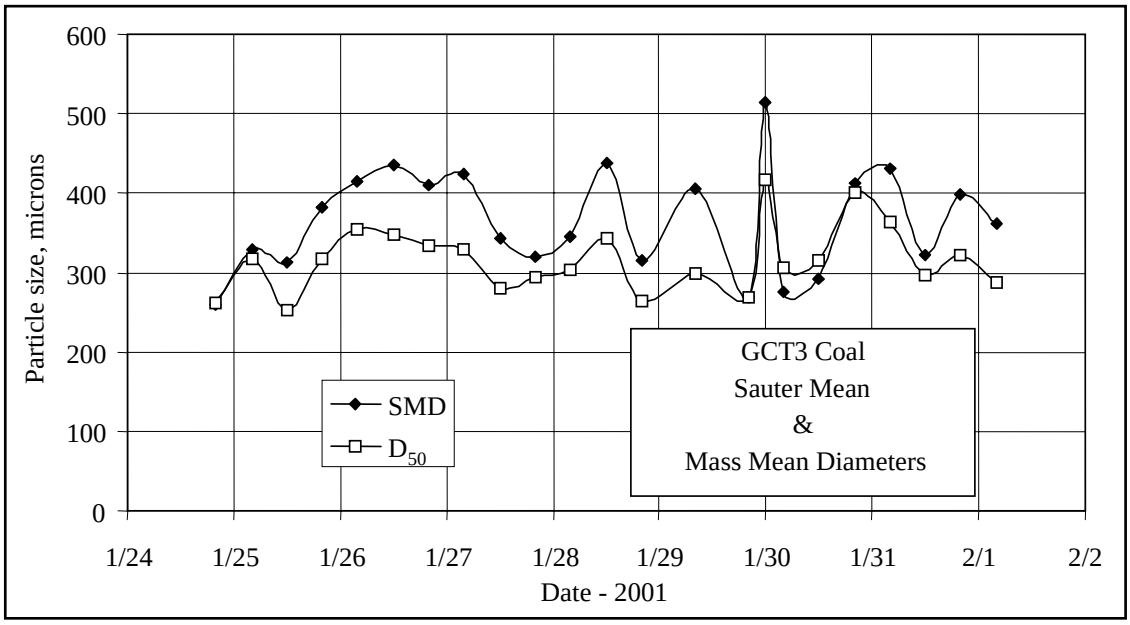

Figure 4.3-5 Coal Mass Mean and Sauter Mean Diameters

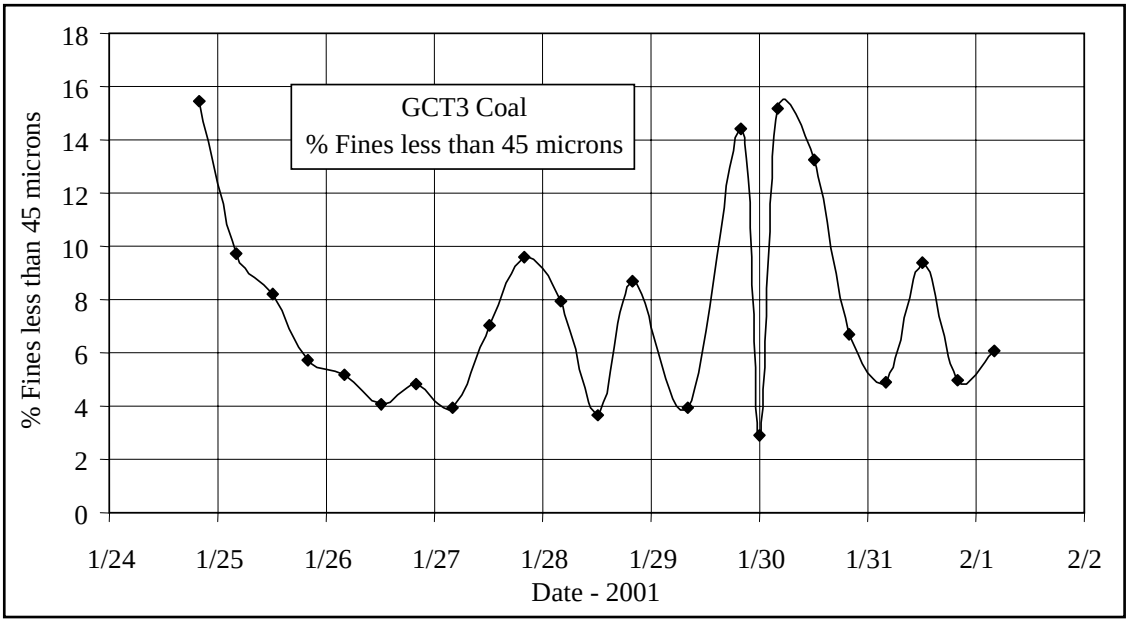

Figure 4.3-6 Percent Coal Fines

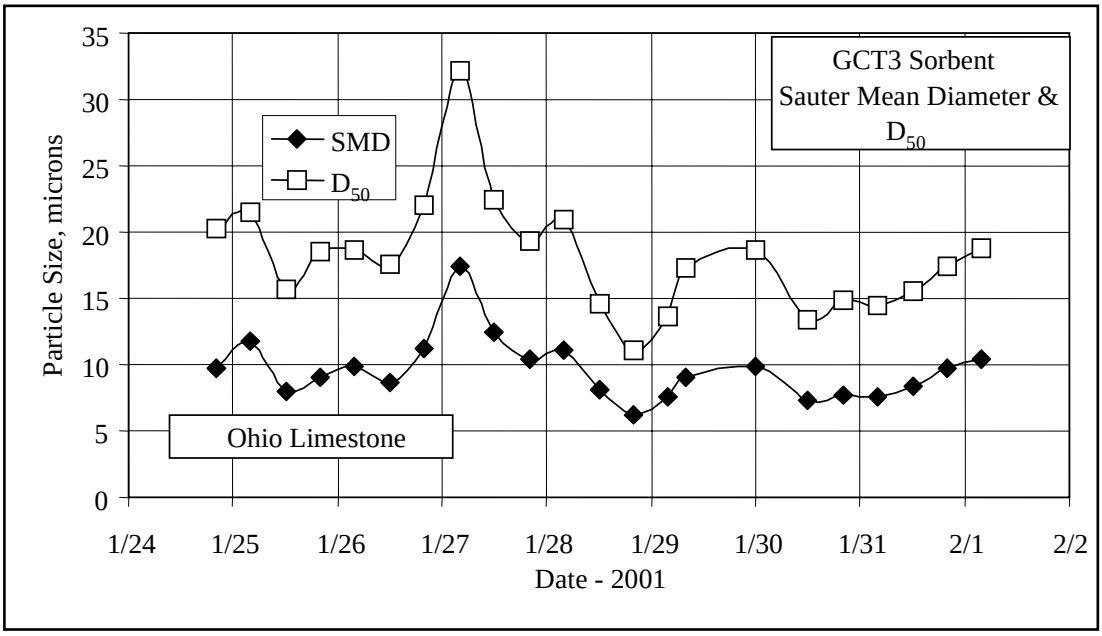

Figure 4.3-7 Sorbent Particle Size

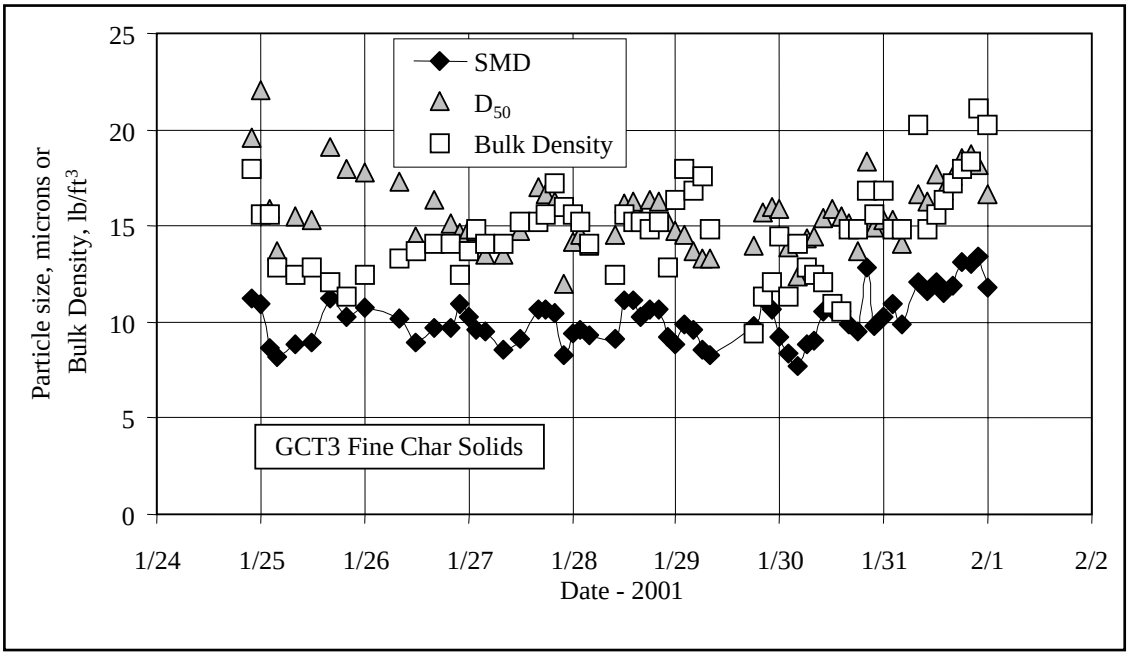

Figure 4.3-8 PCD Fine Solids Particle Size and Bulk Density

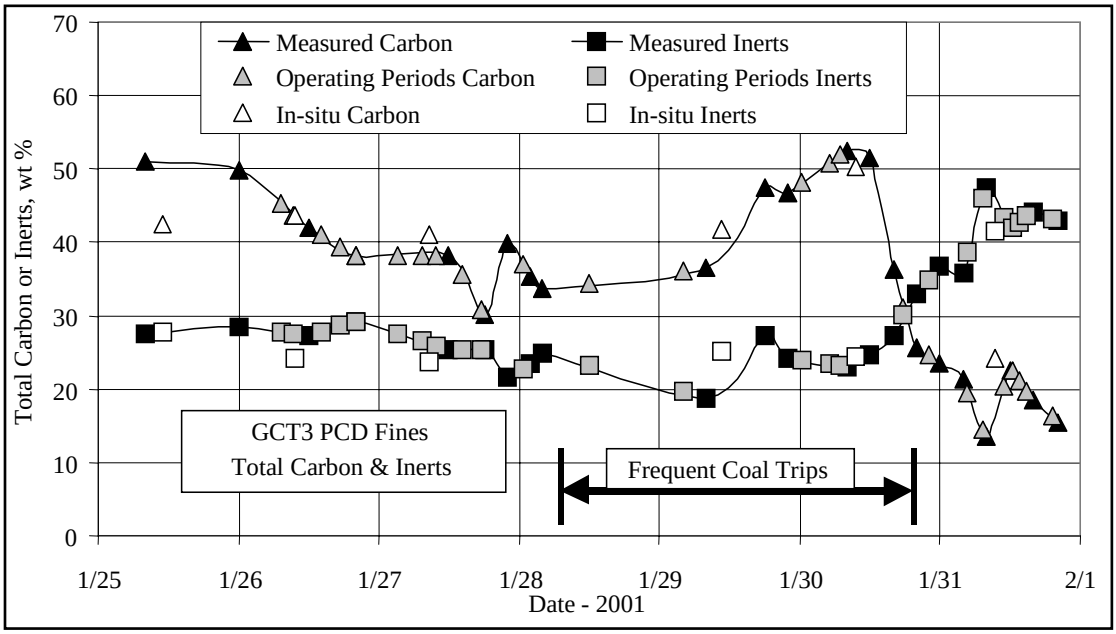

Figure 4.3-9 PCD Fines Total Carbon and Inerts

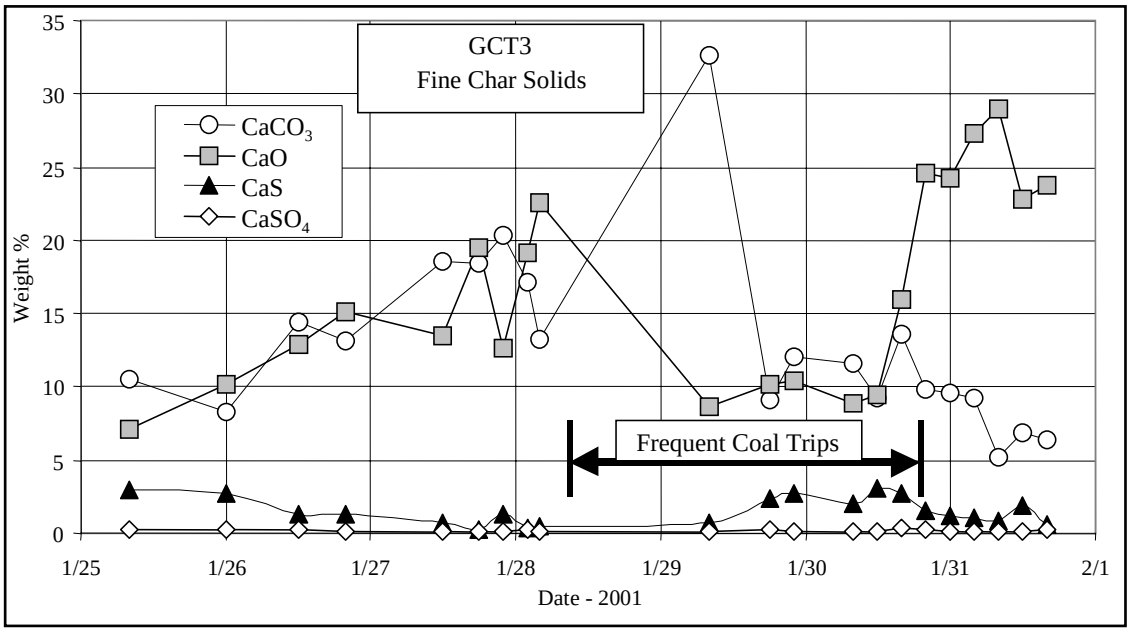

Figure 4.3-10 PCD Fines $CaCO_3$, CaO, CaS, $CaSO_4$

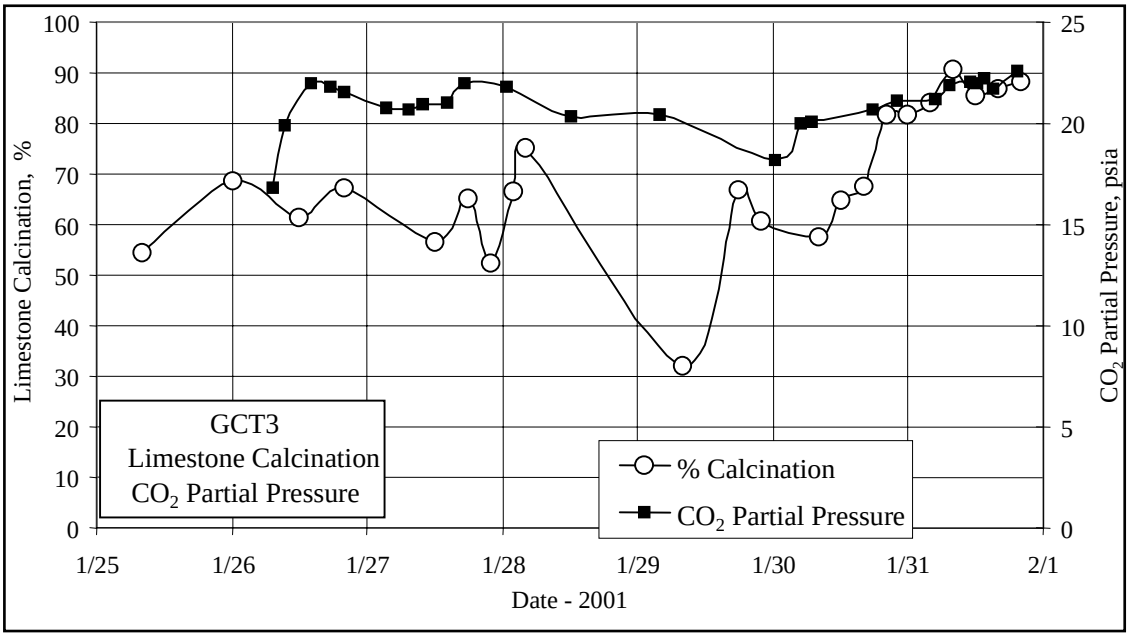

Figure 4.3-11 PCD Fines Calcination and CO_2 Partial Pressure

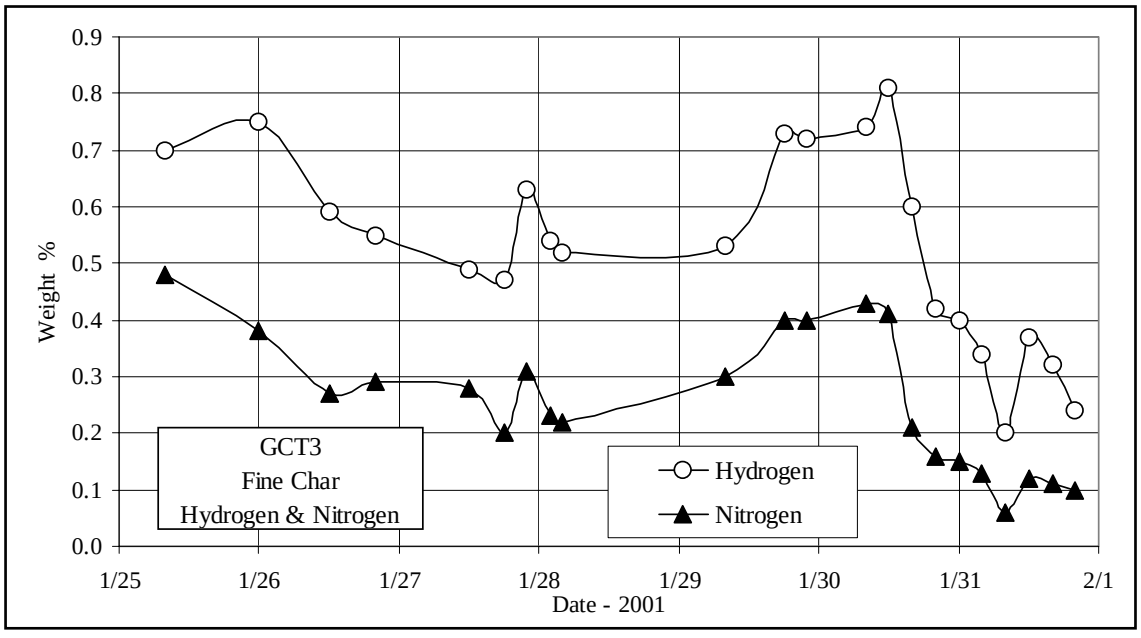

Figure 4.3-12 PCD Fines Nitrogen and Hydrogen

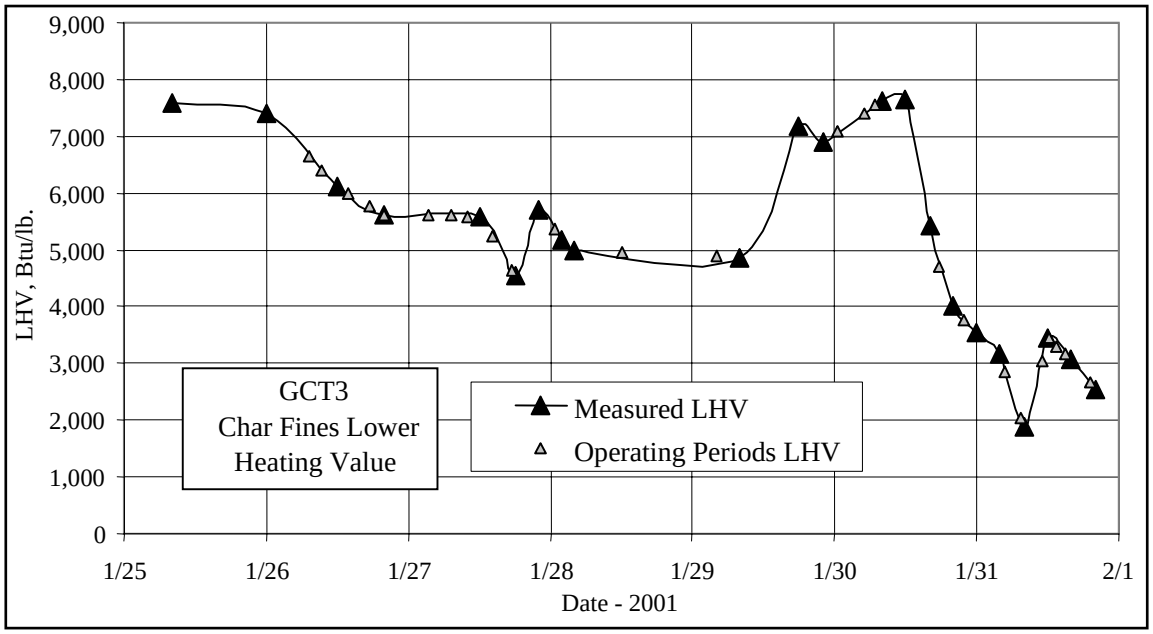

Figure 4.3-13 PCD Fines Lower Heating Value

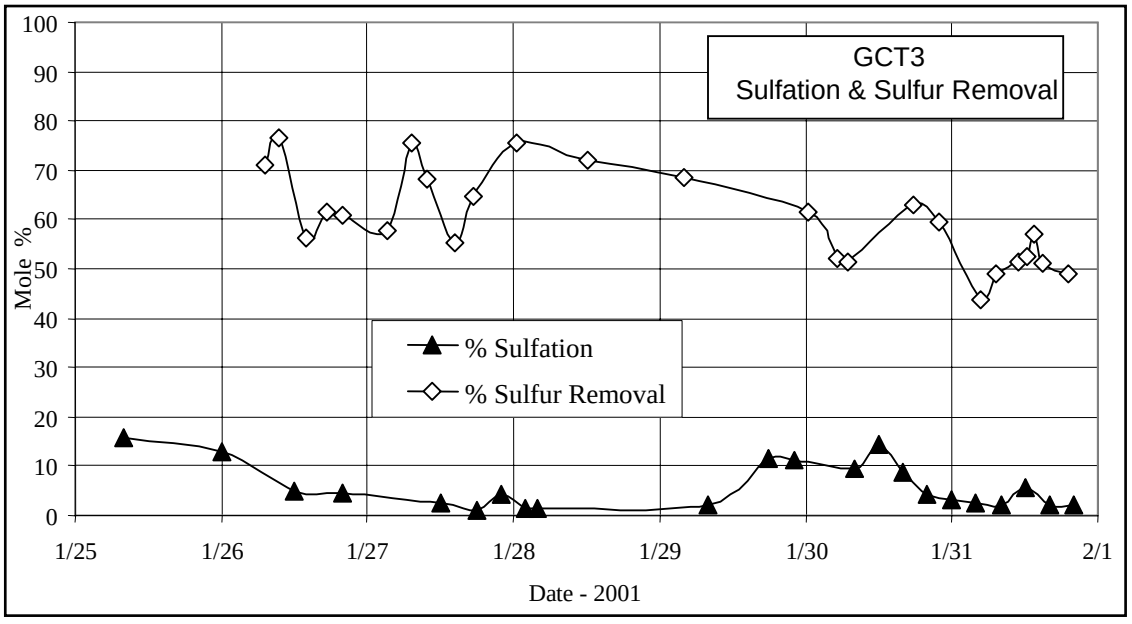

Figure 4.3-14 PCD Fines Sulfation Gas Sulfur Removal

4.4 MASS AND ENERGY BALANCES

Using the gas analyses, solids analyses, and process flows entering and leaving the KBR transport reactor, the following were determined:

- Overall mass balance.
- Carbon balance.
- Nitrogen balance.
- Oxygen balance.
- Sulfur balance.
- Calcium balance.
- Sulfur capture dependence on calcium to sulfur ratio.
- Inerts balance.
- Carbon conversion.
- Energy balance.
- Gasification efficiencies (hot gas and cold gas).

The process flows into the KBR transport reactor are:

- Coal flow through FD0210.
- Sorbent flow through FD0220.
- Air flow measured by FI205.
- Nitrogen flow measured by FI609.
- Steam flow measured by FIC204.

The process flows from the KBR transport reactor are:

- Synthesis gas flow rate from the PCD measured by FI465.
- PCD solids flow through FD0520.
- Reactor solids flow through FD0510.

The coal flow through FD0210 was determined from a correlation between feeder speed and total coal dumps from the FD0210 surge bin between fills. This correlation is shown in Figure 4.4-1. The coal rate data falls in a straight line up to about 36 rpm, then levels off at around 5,300 lb per hour. The correlation below a feeder speed of 36 rpm is:

$$\text{Coal rate} = 101.65\ (\text{rpm}) + 623.5\ (\text{rpm} < 36) \qquad (1)$$

There is an average of 25-percent variation in coal-feed rate for a given rpm. The hourly average coal and air flows are shown in Figure 4.2-2 (See Section 4.2, Gas Analyses). Table 4.4-1 shows the coal and air rates for the operating periods.

The sorbent flow through FD0220 was determined from a correlation between feeder speed and total sorbent dumps from the FD0220 storage bin between fills. This sorbent fill feeder speed data and correlation is shown in Figure 4.4-2. The correlation for the sorbent feeder is:

$$\text{Sorbent rate} = 37.596\ (\text{rpm}) + 65.422 \qquad (2)$$

The hourly average synthesis gas- and nitrogen-flow rates are shown in Figure 4.2-3. Table 4.4-1 shows the synthesis gas and nitrogen operating period flow rates. The synthesis gas rate was checked for all the operating periods using an oxygen balance around the synthesis gas combustor and found to be in excellent agreement with the synthesis gas combustor data.

The steam rate to the reactor was determined from FIC289, which measures the steam flow to the reactor J-leg rather than the FI204, which measures the total steam flow to the reactor. FI204 was not reading correctly for most of GCT3, and the mixing zone steam nozzles were plugged for most of the run. The steam nozzles to the reactor J-leg were generally less plugged during GCT3, so most of the steam entering the reactor entered through FIC289. The hourly average steam rate is shown in Figure 4.2-6. The steam rate for the operating periods is shown in Table 4.4-1.

Since FD0510 was rarely used during GCT3, this data is not used in determining mass balances and carbon conversion.

The solids flow from the PCD can be determined from two different methods by using:

1. In situ particulate sampling data upstream of the PCD.

2. FD0530 weight cell data.

The best measurement of the solids flow to the PCD is the in situ PCD inlet particulate determination. Using the synthesis gas flow rate, the solids flow to the PCD can be determined since the PCD captures all of the solids.

The FD0530 weight cell data can be used to determine the PCD solids flow only if both the FD0530 feeder and the FD0510 feeder (standpipe solids) are off because the FD0520 and FD0510 both feed into FD0530 and FD0530 feeds the sulfator. This method assumes that the PCD solids level in the PCD and FD0502 screw cooler are constant, that the PCD solids level is neither increasing nor decreasing. The results for the first two methods are compared in Figure 4.4-3. The rates used for the test periods in mass balance and carbon conversion calculations are shown in Figure 4.4-3 and Table 4.4-1.

The in situ particulate and weigh cell data generally compare well. The FD0530 weigh cell data was scattered on the first 2 days of operation. The steady periods rate was interpolated for the second through the fourth in situ particulate samples. On the last day of operation the weight cell was consistently giving about 200 lb per hour as opposed to the in situ sample at 400 lb per hour.

Material balances are useful in checking the accuracy and consistency of the data obtained, as well as determining periods of operation where the data is suitable for model development or commercial plant design.

Material balances for each operating period are provided in Figure 4.4-4 showing the relative difference (relative error) of transport reactor feeds-in minus products-out divided by the feeds ({in-out}/in) and the absolute difference (absolute error) of the feeds and the products (in-out). The overall material balance was excellent, within ± 4.0 percent for the relative difference (± 1,000 lb per hour for the absolute difference). There is a positive bias for most of the steady periods material balance at about 500 lb per hour. If the 1,000 lb per hour of feed nitrogen that does not enter the transport reactor is not considered, the high bias would have been larger. The numerous assumptions on gas compositions in Section 4.2 have no effect on the overall mass balance.

The transport reactor feed and products-flow rates are shown in Table 4.4-1 for all the operating periods. The air, nitrogen, and fuel rate dominate the "in" streams, while the synthesis gas dominates the "out" streams.

Test period nitrogen balances are shown in a plot seen in Figure 4.4-5 and listed in Table 4.4-2. Typical nitrogen flows for GCT-18 are shown in Table 4.4-3. The nitrogen balance is excellent for GCT3-2 to -13 at less than 2.3 percent relative error, with no positive or negative bias. The last 12 operating periods show a negative bias of about -4 percent (-750 lb per hour). The numbered points in Figure 4.4-5 are the operating periods when the synthesis gas nitrogen compositions was measured; the unnumbered points are the operating periods when the nitrogen was determined by difference from the other synthesis gas compositions. The same data in Figure 4.4-5 is shown in tabular form in Table 4.4-2. Operating period GCT3-1 had the worst nitrogen balance for the first 15 operating periods, even though the nitrogen was measured. Similarly GCT3-19 had the poorest nitrogen balance of the last 10 operating periods even though the nitrogen was measured. The last 10 operating periods would have been in excellent balance if the feed nitrogen had been reduced 250 lb per hour rather than 1,000 lb per hour. It is possible that the amount of N_2 lost through seals and lock hopper vents decreased during the last 10 operating periods of GCT3.

A plot of test period carbon balances are shown in Figure 4.4-6 and Table 4.4-4. The overall carbon balance is not very good, with the relative difference between inlet and outlet carbon usually at about a + 15-percent bias (+ 450 lb carbon per hour absolute difference). This lack of carbon balance produces large errors in carbon conversions and gasification efficiencies. The coal and synthesis gas rates dominate the carbon balance. Since there were only two standpipe solids composition data, the carbon and other solids standpipe accumulation term could not be calculated. The synthesis gas CH_4 and $C_2H_6^+$ were not measured during GCT3, so the synthesis gas CH_4 and $C_2H_6^+$ compositions were estimated from preliminary TC06 data. The mass balance shows that there was either 15 percent more carbon leaving the system than measured or 15 percent less carbon entering the system. Since the major components (CO and CO_2) in the synthesis gas were measured and the synthesis gas flow rate is consistent with synthesis gas combustor data it is unlikely that the actual CH_4 and $C_2H_6^+$ compositions could change the synthesis gas carbon by 15 percent. It is more likely that the actual coal rate was 15 percent lower than the measured coal rate.

Carbon conversion is defined as the percent fuel carbon that is gasified to CO, CO_2, CH_4, C_2H_6, and higher hydrocarbons. The commercial goal is 90 percent or greater carbon conversion. Carbon utilization is important because carbon conversion is the measure of how much carbon is rejected by the gasifier with the PCD solids. This rejected carbon is typically burned in a less efficient combustor and results in a less efficient use of the fuel. Carbon conversion can be calculated three ways:

1. From gas analysis (using the synthesis gas rate and synthesis gas composition) and the carbon-feed rate (using the coal-feed rate and coal carbon content). (Gas analyses)

2. From PCD solids data (using the PCD solids-flow rate and PCD solids carbon content) and the carbon-feed rate. (Solids analyses)

3. From the product analysis using the gas analysis data and the PCD solids data. (Product analyses)

The operating period results for the three carbon conversions are shown in Figure 4.4-7 and Table 4.4-4. The gas compositions used are determined by procedures described in Section 4.2. Solids compositions are shown in Section 4.3.

The carbon conversions calculated from the solids balance show little scatter during the test period and slowly rose from 90 to 97 percent during the first 3 days of operation. The solids carbon conversion dropped back down to 90 percent on January 30. For the last day of operation the solids carbon conversion increased to nearly 99 percent. If the higher PCD solids rate of 400 lb per hour was used rather than the PCD solids rate of 200 lb per hour (see Figure 4.4-3), the carbon conversion would have only decreased by about 1 percent. The products carbon conversions track the solids carbon conversions and are between 1 to 4 percent lower than the solids carbon conversions. The carbon conversions from the gas analyses were more scattered than the carbon conversions from the solids and products analyses. The gas carbon conversion was also consistently lower than the solids-based carbon conversions. The gas analyses-based carbon conversions started the test run at 75 to 85 percent and then decreased to 75 percent the next day. For the rest of the run the gas analyzer carbon conversion seemed to be scattered around 80 percent. The actual carbon conversions are probably closer to the solids analyses-based carbon conversions due to the inaccuracies in the gas measurements.

Sulfur balances for the GCT3 operating periods are shown in Figure 4.4-8, with typical values shown in Table 4.4-3. Table 4.4-2 shows the results of the sulfur balances for the operating periods. The sulfur balances are not good in that there is a consistent high bias of about 40 percent or 5 lb of sulfur per hour, except for the three operating periods early on January 30 (GCT3-14, -15, and -16). This means that there was either twice as much sulfur leaving the system as measured or half as much sulfur entering the system as measured. Of the three sulfur measurements, the sulfur in PCD solids is the least accurate measurement (PCD solids sulfur content, PCD solids rate) and the gaseous sulfur measurement the most accurate (synthesis gas-flow rate, synthesis gas combustor-flow rate, synthesis gas combustor-exit SO_2 concentration). It is possible that there was an accumulation of sulfur-containing solids in the reactor during GCT3, which would explain the high sulfur-balance bias. This can be verified by standpipe or

FD0510 reactor samples. The sulfur mass balance is also difficult to close due to the low sulfur flows and compositions as a result of using low sulfur Powder River Basin coal. As a result, the synthesis gas combustor SO_2 concentration was used for the sulfur emissions in Section 4.2.

Operating period hydrogen balances are shown in Figure 4.4-9, with typical values shown in Table 4.4-3. Table 4.4-2 shows the results of the hydrogen balances for all of the operating periods. The hydrogen balance was poor, with a low bias of -10 to -30 percent (-20 to -60 lb per hour hydrogen). The coal, steam, and synthesis gas streams dominate the hydrogen balance. The hydrogen in the coal is usually larger than the hydrogen in the steam added. Since the hydrogen out is larger than the hydrogen in, a hydrogen balance would calculate a larger steam rate than measured. The operating period hydrogen balances show no difference between the operating periods when the hydrogen was measured and periods when the hydrogen was calculated from the water-gas shift equilibrium and the measured synthesis gas H_2O, CO_2, and CO concentrations.

Operating period oxygen balances are shown in Figure 4.4-10, with typical values shown in Table 4.4-3. Table 4.4-2 shows the results of the oxygen balances for all of the operating periods. The oxygen balance was generally quite good at ± 10 percent (± 600 lb per hour) for the entire run, with most operating periods ± 6 percent (± 400 lb per hour). There was a slight low bias of only a few percent (-100 lb). Note the large oxygen contribution of the feed coal since PRB has a high oxygen content (moisture plus elemental oxygen). The coal and PCD solids oxygen concentration is determined by difference, so it is typically a less accurate value than the other elemental analyses values.

Operating period calcium balances are shown in Figure 4.4-11, with typical values shown in Table 4.4-3. Table 4.4-2 shows the results of the calcium balances for all of the operating periods. The PRB operation is characterized by low required-sorbent feed rates because of low sulfur in the PRB coal. Note the low total calcium rates, with about half of the inlet calcium coming from fuel and half from sorbent. The calcium balance at the start of the run was in balance, then increased to + 40 percent (+ 40 lb calcium per hour). The same three operating periods early on January 30 (GCT3-14, -15, and -16) that were in good sulfur balance were also in good calcium balance. Like the sulfur, it appears that calcium is accumulating in the reactor during the run.

Figure 4.4-12 shows a plot of GCT3 sulfur emissions (expressed as pounds SO_2 emitted per MBtu coal fed) and sulfur removal as a function of calcium-to-sulfur ratio (Ca/S) based on the coal and sorbent fed to the transport reactor. The expected trend lines of increasing sulfur removal with increasing Ca/S and decreasing sulfur emissions with increasing Ca/S removal are seen, but both trends are very weak. The sulfur emissions and removals are based on the synthesis gas combustor SO_2 analyzer (See Table 4.2-3, Section 4.2). The feed Ca/S ratios are shown in Table 4.4-2 for each operating period.

Figure 4.4-13 is a plot of GCT3 sulfur emissions (expressed as pounds SO_2 emitted per MBtu coal fed) and sulfur removal as a function of calcium-to-sulfur ratio (Ca/S) measured in the PCD solids samples from FD0520. The measured PCD solids Ca/S ratio is much higher than the feed Ca/S based on the sorbent calcium because the Powder River Basin coal has a high

calcium content. Again, the expected trend lines of increasing sulfur removal with increasing Ca/S and decreasing sulfur emissions with increasing Ca/S removal are seen, but both trends are very weak. A comparison of Figures 4.4-12 and -13 shows that the calcium from the PRB coal has less effect on the sulfur removal than the calcium in the limestone. It is probable that the coal calcium is not present in as reactive a compound as $CaCO_3$, which is the main calcium compound in limestone

Operating period inerts balances are shown in Figure 4.4-14, with typical values shown in Table 4.4-3. Table 4.4-2 shows the results of the inerts balances for all of the operating periods. The inerts are all the solid compounds that do not have carbon, calcium, magnesium, sulfur, oxygen, or hydrogen. The inerts balance mainly reflects the coal and PCD solids rates since the limestone sorbent typically had 3.3-percent inerts. The inerts balance is similar to the calcium balance since both are dominated by the coal and PCD solids rates and compositions. The inerts balance started the run in balance, then increased up to + 60 percent (+ 90 lb inerts per hour). The same three operating periods early on January 30 (GCT3-14, -15, and -16) that were in sulfur and calcium balance were also in inerts balance. The last 10 operating periods inerts balance had a + 50-percent bias (+ 80 lb per hour inerts). As with the calcium and sulfur, it appears that inerts accumulated in the reactor. Total solids are <u>not</u> accumulating in the reactor since the standpipe level was generally constant and minimal solids were not being withdrawn from the reactor.

The gas-flow rates were self consistent, as shown by the excellent overall mass balance that is dominated by the gas-flow rate measurements (± 4.0 percent for the operating periods). The carbon balance was not very good (+ 15-percent bias), possibly due to measuring the coal-feed rate too high. The hydrogen balance was not very good (- 20-percent bias), possibly due to errors in measuring the inlet steam rate too low. The oxygen balances were acceptable (± 10 percent). Elements dominated by the solids-flow rates (sulfur, calcium, and inerts) were not good (+ 40 percent bias) for most operating periods.

The transport reactor energy balance for the GCT3 test run is shown in Figure 4.4-15, with standard conditions chosen to be one atmosphere pressure and 100°F. Table 4.4-5 shows a breakdown of the individual components of the energy balance. The "energy in" consisted of the coal, air, and steam fed to the transport reactor. The nitrogen and sorbent fed to the reactor were considered to be at ambient conditions and hence have zero enthalpy. The energy to calcine the sorbent limestone was not considered. "Energy out" consisted of the synthesis gas and PCD solids. The lower heating value of the coal and PCD solids was used in order to be consistent with the lower heating value of the synthesis gas. The energy of the synthesis gas and PCD solids was determined at the transport reactor cyclone exit. Sensible enthalpy of the synthesis gas was determined by calculating an overall gas heat capacity from the synthesis gas composition and the individual gas heat capacities. The synthesis gas and PCD solids energy consists of both latent and sensible heat. The heat loss in the reactor was estimated to be 1.5 x 10^6 Btu/hr, as measured during a previous combustion transport reactor test. The GCT3 energy balance was biased high by 10 to 25 percent (5 to 13 MBtu/hr), a consequence of the carbon balance being biased high by 15 percent.

Similar to carbon conversion, the cold gas efficiency can be calculated at least three different ways, and since the energy balance is off by 10 to 25 percent, each result should be different. If there was a good energy balance, all three calculations would produce the same result. Three calculation methods were performed for cold gasification efficiencies consistent with the three methods of carbon conversion:

1. Based on the feed coal heat and the latent heat of the synthesis gas. This assumes that the feed coal heat and the synthesis gas latent heat are correct. (Gas analyses)

2. Based on the feed coal heat and the latent heat of the synthesis gas determined by a transport reactor energy balance, not the gas analyses. This assumes that the synthesis gas latent heat is incorrect. (Solids analyses)

3. Based on the synthesis gas latent heat and the feed coal heat determined by transport reactor energy balance. This assumes that the coal-feed rate is an error. (Products analyses)

These three calculation methods are consistent with the three methods of calculating carbon conversion and each makes a choice of which part of the energy balance is incorrect. The second and third methods assume a transport reactor heat loss of 1.5×10^6 Btu/hr.

The cold gas gasification efficiencies for the three calculation methods are shown in the plot in Figure 4.4-16 and in Table 4.4-6. The gas analysis cold gasification efficiencies were between 45 to 57 percent, except for GCT3-13. The solids analysis cold gasification efficiencies are between 64 to 75 percent. The product analysis cold gasification efficiencies were between 55 to 68 percent. As before with the carbon conversions, the gas analysis gasification efficiency was the lowest, the solids analysis the highest, and the products analysis was between the gas and solids analysis. Since both the synthesis gas rate and the PCD solids rates are independently checked, it is most likely that coal-feed rate errors are producing the error in the energy and carbon balances. Therefore the best estimate of the cold gas efficiency is by the products.

The hot gasification efficiency is the amount of coal energy that is available to a gas turbine plus a heat recovery steam generator. The hot gas efficiency counts both the latent and sensible heat of the synthesis gas. Similar to the cold gasification efficiency and carbon conversion, the hot gas efficiency can be calculated at least three different ways. Since the energy balance is off by about 10 to 25 percent, each efficiency will be different. The three calculation methods for hot gasification, which are consistent with the three methods of carbon conversion, are:

1. Based on the coal feed heat and the latent heat and sensible heat of the synthesis gas. This assumes that the coal feed heat and the synthesis gas latent heat are correct. (Gas analyses)

2. Based on the coal feed heat and the latent heat of the synthesis gas, of the synthesis gas determined by transport reactor energy balance plus the sensible heat of the synthesis gas. This assumes that the synthesis gas latent heat is incorrect. (Solids analyses)

3. Based on the synthesis gas latent and sensible heat and the coal feed heat determined by a transport reactor energy balance. This assumes that the coal feed is in error. (Products analyses)

These three calculation methods are consistent with the three methods of calculating carbon conversion and cold gasification efficiency and make a choice of which parts of the energy balance are correct.

The hot gasification efficiency assumes that the sensible heat of the synthesis gas can be recovered in a heat recovery steam generator, so the hot gasification efficiency is always higher than the cold gasification efficiency. The three gasification calculation methods are shown in the plot in Figure 4.4-17 and in Table 4.4-6. The hot gasification efficiency by the products increased from 85 percent to slightly over 100 percent during the last day of operation. Such high efficiencies highlight the errors in the energy balance since the heat loss and heat content of the PCD solids cannot be less than zero percent. These high efficiencies are a result of the low PCD fines carbon content and low PCD fines rates. As with the cold gasification efficiencies, the hot gasification efficiency by products should be more accurate than the hot gasification efficiencies by the gas and solids.

Gasification efficiencies can be calculated from the nitrogen-corrected gas heating values determined in Section 4.2. The nitrogen-corrected hot and cold gasification efficiencies are shown in the plot in Figure 4.4-18 and listed in Table 4.4-6 for all of the operating periods. Only the gasification efficiencies based on the products are shown in Figure 4.4-18 and Table 4.4-6 because they are the most representative of the actual gasification efficiencies. The nitrogen corrected increases the cold gasification efficiencies by about 7 percent for most of the operating periods. The nitrogen correction does not increase the hot gasification efficiency because the deleted nitrogen lowers the synthesis gas sensible heat, and hence changes the hot gasification efficiency by a small percentage.

Two main sources of losses in efficiency are 1) the reactor heat loss and 2) the latent heat of the PCD solids. The reactor heat loss of 1.5×10^6 Btu/hr is about 3.0 percent of the feed coal energy, while the total energy of the PCD solids is about 5.5 percent of the feed coal energy. The heat loss percentage will decrease as the reactor size is increased. While the transport reactor does not recover the latent heat of the PCD solids, this latent heat could be recovered in a combustor. The latent heat of the PCD solids can be decreased by decreasing both the PCD solids carbon content (heating value) and the PCD solids rate.

Table 4.4-1

Feed Rates, Product Rates, and Mass Balance

	Feeds (In)						Products (Out)				
Operating Period	Coal FD0210 lb/hr	Sorbent FD0220 lb/hr	Air FI205 lb/hr	Nitrogen FI609[1] lb/hr	Steam FIC298[2] lb/hr	Total lb/hr	Syngas FI465 lb/hr	PCD Solids FD0520 lb/hr	Total lb/hr	In - Out lb/hr	(In- Out)/In %
GCT3-1	5,189	131	14,866	7,400	35	27,621	26,863	634	27,497	124	0.4
GCT3-2	5,188	131	14,616	7,015	101	27,052	26,264	672	26,936	116	0.4
GCT3-3	5,199	185	14,502	7,126	1,013	28,024	27,235	650	27,885	139	0.5
GCT3-4	5,227	185	14,876	7,104	1,011	28,403	27,655	625	28,280	123	0.4
GCT3-5	5,263	186	14,625	7,106	993	28,173	26,653	606	27,259	914	3.2
GCT3-6	5,300	185	14,953	7,049	225	27,712	27,352	554	27,906	-194	-0.7
GCT3-7	5,300	185	13,882	6,479	220	26,066	24,879	521	25,400	666	2.6
GCT3-8	5,300	186	13,852	6,279	324	25,940	24,823	509	25,332	608	2.3
GCT3-9	5,094	187	13,692	6,368	643	25,984	24,883	491	25,374	610	2.3
GCT3-10	5,101	289	14,043	6,468	801	26,701	25,456	478	25,934	768	2.9
GCT3-11	5,300	289	15,273	5,861	422	27,145	26,400	440	26,840	305	1.1
GCT3-12	3,881	133	11,900	6,778	272	22,965	21,998	225	22,223	743	3.2
GCT3-13	3,473	316	9,355	6,858	47	20,049	18,995	372	19,367	682	3.4
GCT3-14	5,300	131	14,043	6,071	260	25,804	25,372	622	25,994	-190	-0.7
GCT3-15	5,300	131	13,788	5,841	220	25,280	24,863	666	25,529	-248	-1.0
GCT3-16	5,300	131	13,914	5,764	236	25,345	24,985	685	25,670	-324	-1.3
GCT3-17	5,300	186	14,465	5,535	268	25,754	25,121	307	25,428	326	1.3
GCT3-18	5,300	187	15,062	5,497	630	26,675	26,207	265	26,472	203	0.8
GCT3-19	5,300	186	15,353	5,551	1,196	27,586	27,080	240	27,320	266	1.0
GCT3-20	5,300	107	14,771	5,580	1,219	26,976	26,128	233	26,361	615	2.3
GCT3-21	5,300	106	14,842	5,406	1,184	26,838	26,096	218	26,314	524	2.0
GCT3-22	5,300	106	15,195	5,356	1,167	27,124	26,620	215	26,835	288	1.1
GCT3-23	5,300	185	15,311	5,395	1,220	27,411	26,858	209	27,067	344	1.3
GCT3-24	5,300	185	15,761	5,269	1,208	27,722	27,283	204	27,487	236	0.9
GCT3-25	5,300	184	15,029	5,355	1,146	27,015	26,263	217	26,480	534	2.0

Notes:

1. Nitrogen-feed rate reduced by 1,000 lb per hour to account for losses in feed systems and seals.
2. Steam rate taken from FIC289 since FI204 was not reading accurately.

Table 4.4-2

Nitrogen, Sulfur, Hydrogen, and Oxygen Mass Balances

Operating Period	Nitrogen		Sulfur		Hydrogen		Oxygen		Calcium		Inerts		Feed Ca/S M/M
	(In- Out) In %	In - Out lb/hr	(In- Out) In %	In - Out lb/hr	(In- Out) In %	In - Out lb/hr	(In- Out) In %	In - Out lb/hr	(In- Out) In %	In - Out lb/hr	(In- Out) In %	In - Out lb/hr	
GCT3-1	-3.9	-727	32.4	4.7	-20.0	-47	1.4	74.0	-3.4	-3.0	10.3	20	2.2
GCT3-2	0.9	167	42.4	6.4	-39.3	-95	-8.7	-446	-15.7	-14	3.1	6	2.2
GCT3-3	-1.0	-173	25.7	3.9	-21.3	-73	-4.1	-245	-0.3	0	3.6	7	3.0
GCT3-4	-1.8	-330	32.7	5.0	-18.9	-65	-2.5	-152	1.0	1	2.5	5	3.0
GCT3-5	-1.2	-213	31.9	4.7	-3.0	-10	4.1	245	2.7	3	-0.1	0	3.1
GCT3-6	-1.5	-269	34.0	4.9	-52.3	-136	-10.3	-557	9.4	10	10.3	17	3.2
GCT3-7	-1.0	-164	60.1	9.9	-21.9	-56	-2.2	-111	13.8	14	18.9	32	2.8
GCT3-8	-1.6	-262	52.4	7.8	-16.0	-43	-1.2	-62	15.4	16	21.0	35	3.1
GCT3-9	-2.3	-385	41.0	5.6	-9.3	-28	2.0	108	10.5	11	22.4	36	3.4
GCT3-10	-1.7	-290	54.8	7.3	-13.3	-42	1.4	78	25.0	34	27.5	46	5.4
GCT3-11	-0.8	-146	60.9	7.7	-29.6	-84	-5.3	-301	36.7	50	45.6	84	5.6
GCT3-12	0.8	125	63.5	5.9	-15.6	-32	-0.4	-15	37.6	28	62.7	87	3.5
GCT3-13	-0.1	-9	52.1	4.2	-32.2	-51	-2.8	-95	42.6	55	38.7	46	9.8
GCT3-14	-4.7	-783	-0.5	-0.1	-30.5	-80	-2.4	-122	5.5	5	14.3	25	2.7
GCT3-15	-4.8	-784	-7.8	-0.9	-29.0	-74	-3.3	-168	4.7	4	12.9	23	2.7
GCT3-16	-4.4	-718	-6.9	-0.8	-30.5	-79	-4.3	-221	4.7	4	11.8	21	2.7
GCT3-17	-3.3	-537	34.3	4.2	-31.0	-82	-2.3	-124	40.4	42	49.2	90	3.8
GCT3-18	-3.5	-588	41.7	5.1	-19.5	-59	-0.6	-33	44.4	47	49.0	89	3.8
GCT3-19	-7.5	-1,286	27.8	3.4	-6.9	-25	5.9	378	45.9	48	47.1	83	3.8
GCT3-20	-4.1	-689	36.0	5.1	-12.2	-45	3.6	221	32.5	26	38.2	66	1.9
GCT3-21	-4.0	-665	34.1	4.8	-5.1	-19	3.6	222	43.2	35	45.4	79	1.9
GCT3-22	-4.4	-746	33.4	4.7	-7.8	-29	2.2	137	46.1	37	47.7	82	1.9
GCT3-23	-4.3	-728	42.2	6.0	-8.1	-30	2.3	146	60.0	63	48.9	86	3.2
GCT3-24	-3.7	-639	38.4	5.4	-14.1	-52	1.2	77	61.2	64	49.1	86	3.2
GCT3-25	-3.7	-623	37.0	5.2	-8.5	-31	1.8	110	54.8	57	46.5	81	3.2

Notes:

1. Nitrogen-feed rate reduced by 1,000 lb per hour to account for losses in feed systems and seals.
2. Reactor gaseous sulfur emissions calculated from synthesis gas combustor SO_2 measurement.

Table 4.4-3

Typical Component Mass Balances

	Nitrogen	Sulfur	Hydrogen	Oxygen	Calcium	Inerts
Operating Period	GCT3-18	GCT3-18	GCT3-18	GCT3-18	GCT3-18	GCT3-18
Date	1/30/01	1/30/01	1/30/01	1/30/01	1/30/01	1/30/01
Time Start	20:15	20:15	20:15	20:15	20:15	20:15
Time End	23:45	23:45	23:45	23:45	23:45	23:45
Fuel	PRB	PRB	PRB	PRB	PRB	PRB
Sorbent	OH LS	OH LS	OH LS	OH LS	OH LS	OH LS
Mixing Zone Temperature, ^{O}F	1,766	1,766	1,766	1,766	1,766	1,766
Pressure, psig	225	225	225	225	225	225
In, pounds/hr						
Fuel	39	12.2	213	1,537	47	175
Sorbent				87	58	6
Air	11,341		21	3,597		
Nitrogen	5,497					
Steam			70	560		
Total	16,877	12.2	304	5,780	105	181
Out, pounds/hr						
Fuel Gas	17,465	5.5	363	5,775		
PCD Solids		1.6	1	38	58	92
Total	17,465	7.1	364	5,813	58	92
(In-Out)/In, %	-3.5%	41.7%	-19.5%	-0.6%	44.4%	49.0%
(In-Out), pounds per hour	-588	5.1	-59	-33	47	89

Table 4.4-4

Carbon Balances

Operating Period	Feeds (In)			Products (Out)			In - Out	(In- Out)/In	Carbon Conversion		
	Coal lb/hr	Sorbent lb/hr	Total lb/hr	Syngas lb/hr	PCD Solids lb/hr	Total lb/hr	lb/hr	%	Solids %	Products %	Gas %
GCT3-1	2,978	15	2,994	2,221	287	2,508	486	16.2	90.7	87.5	74.6
GCT3-2	2,973	15	2,988	2,524	293	2,817	171	5.7	90.5	88.8	84.9
GCT3-3	2,975	21	2,997	2,445	267	2,711	285	9.5	91.4	89.5	82.2
GCT3-4	3,005	22	3,027	2,447	246	2,693	334	11.0	92.2	90.4	81.4
GCT3-5	3,037	22	3,058	2,271	231	2,503	556	18.2	92.7	90.2	74.8
GCT3-6	3,095	22	3,117	2,462	212	2,674	443	14.2	93.5	91.8	79.6
GCT3-7	3,111	22	3,133	2,263	199	2,462	670	21.4	93.9	91.7	72.7
GCT3-8	3,125	22	3,147	2,297	195	2,491	656	20.8	94.1	92.0	73.5
GCT3-9	3,004	22	3,026	2,240	175	2,415	611	20.2	94.5	92.7	74.6
GCT3-10	3,007	34	3,041	2,213	148	2,361	680	22.4	95.4	93.8	73.6
GCT3-11	3,111	34	3,145	2,561	163	2,724	421	13.4	95.1	94.0	82.3
GCT3-12	2,266	15	2,282	1,874	78	1,951	330	14.5	96.8	96.1	82.7
GCT3-13	2,019	37	2,056	1,403	134	1,537	519	25.3	94.0	91.4	69.5
GCT3-14	3,082	15	3,097	2,325	300	2,625	473	15.3	90.6	87.5	75.4
GCT3-15	3,082	15	3,097	2,298	338	2,636	461	14.9	89.3	85.7	74.6
GCT3-16	3,081	15	3,097	2,364	355	2,720	377	12.2	88.8	85.4	76.7
GCT3-17	3,081	22	3,103	2,378	95	2,474	629	20.3	97.0	96.2	77.2
GCT3-18	3,085	22	3,106	2,604	65	2,669	437	14.1	98.0	97.6	84.4
GCT3-19	3,085	22	3,106	2,311	47	2,358	749	24.1	98.6	98.1	74.9
GCT3-20	3,085	12	3,097	2,342	34	2,376	721	23.3	99.0	98.6	75.9
GCT3-21	3,085	12	3,097	2,493	44	2,538	559	18.1	98.6	98.3	80.8
GCT3-22	3,088	12	3,101	2,556	49	2,605	496	16.0	98.5	98.2	82.8
GCT3-23	3,090	22	3,111	2,574	44	2,618	494	15.9	98.6	98.3	83.3
GCT3-24	3,090	22	3,111	2,687	40	2,727	384	12.3	98.8	98.6	87.0
GCT3-25	3,090	21	3,111	2,446	35	2,482	630	20.2	98.9	98.6	79.2

Note:
See Table 4.2-1 for synthesis gas composition assumptions.

Table 4.4-5

Energy Balance

	Feeds (In)				Products (Out)					
Operating Period	Coal 10^6 Btu/hr	Air 10^6 Btu/hr	Steam 10^6 Btu/hr	Total 10^6 Btu/hr	Syngas 10^6 Btu/hr	PCD Solids 10^6 Btu/hr	Heat Loss[1] 10^6 Btu/hr	Total 10^6 Btu/hr	In - Out 10^6 Btu/hr	(In- Out)/In %
GCT3-1	47.2	0.8	0.0	48.1	33.5	4.5	1.5	39.5	8.6	17.9
GCT3-2	47.2	0.8	0.2	48.2	38.2	4.6	1.5	44.4	3.8	7.9
GCT3-3	47.0	0.8	1.7	49.5	37.3	4.2	1.5	43.0	6.6	13.3
GCT3-4	47.6	0.8	1.8	50.2	37.2	3.9	1.5	42.6	7.6	15.2
GCT3-5	47.9	0.8	1.8	50.5	34.0	3.7	1.5	39.2	11.4	22.5
GCT3-6	49.0	0.8	1.5	51.4	38.1	3.4	1.5	42.9	8.4	16.4
GCT3-7	49.3	0.8	1.4	51.5	33.9	3.2	1.5	38.5	12.9	25.2
GCT3-8	49.5	0.8	1.4	51.8	34.2	3.1	1.5	38.7	13.0	25.1
GCT3-9	47.6	0.7	1.8	50.2	33.5	2.8	1.5	37.8	12.4	24.6
GCT3-10	47.7	0.8	1.9	50.4	33.1	2.4	1.5	37.0	13.4	26.5
GCT3-11	49.0	0.8	1.0	50.8	38.0	2.6	1.5	42.1	8.7	17.2
GCT3-12	35.6	0.6	1.3	37.5	27.4	1.2	1.5	30.1	7.4	19.7
GCT3-13	32.2	0.5	1.5	34.2	20.7	2.0	1.5	24.2	10.0	29.2
GCT3-14	48.8	0.7	0.3	49.8	35.9	4.6	1.5	42.1	7.7	15.5
GCT3-15	48.5	0.7	0.3	49.5	35.0	5.2	1.5	41.8	7.7	15.6
GCT3-16	48.5	0.7	0.3	49.5	36.0	5.4	1.5	42.9	6.6	13.3
GCT3-17	48.5	0.8	0.3	49.6	36.5	1.6	1.5	39.6	10.0	20.2
GCT3-18	48.5	0.8	0.8	50.1	39.5	1.1	1.5	42.2	8.0	15.9
GCT3-19	48.5	0.8	1.6	50.9	35.6	0.8	1.5	37.9	13.0	25.6
GCT3-20	48.6	0.8	1.6	51.0	37.0	0.6	1.5	39.1	11.9	23.4
GCT3-21	48.6	0.8	1.6	51.0	37.8	0.8	1.5	40.1	10.9	21.4
GCT3-22	48.6	0.8	1.6	51.0	38.6	0.8	1.5	41.0	10.0	19.6
GCT3-23	48.6	0.8	1.6	51.0	38.7	0.8	1.5	41.0	10.0	19.7
GCT3-24	48.6	0.8	1.6	51.0	41.2	0.7	1.5	43.5	7.6	14.9
GCT3-25	48.6	0.8	1.6	50.9	36.5	0.7	1.5	38.7	12.2	24.0

Notes:

1. Reactor heat loss estimated from combustion test run data.
2. Standard state assumed to be 100°F.
3. Fluidization and instrument nitrogen inlet temperature assumed to be at 100°F and to have zero standard-state enthalpy.
4. Limestone sorbent inlet temperature assumed to be at 100°F and to have zero standard-state enthalpy.

Table 4.4-6

Gasification Efficiencies

Operating Period	Raw Cold Gas Efficiency			Raw Hot Gas Efficiency			N_2 Corrected Gas Efficiency	
	Gas %	Solids %	Products %	Gas %	Solids %	Products %	Cold Products %	Hot Products %
GCT3-1	46.1	64.3	56.3	70.9	89.0	86.6	63.2	84.5
GCT3-2	55.9	63.9	60.7	81.0	89.1	88.1	66.9	86.5
GCT3-3	52.9	66.9	61.5	79.3	93.3	92.2	68.3	90.9
GCT3-4	51.5	67.6	61.4	78.1	94.2	93.1	68.3	91.9
GCT3-5	44.8	68.6	58.8	70.9	94.7	93.0	66.6	91.6
GCT3-6	52.7	69.9	63.6	77.7	94.9	93.8	70.4	92.7
GCT3-7	46.1	72.4	62.5	68.7	95.0	93.2	69.6	92.0
GCT3-8	46.5	72.7	63.0	69.0	95.2	93.5	69.8	92.4
GCT3-9	47.2	73.1	63.7	70.4	96.3	95.1	70.9	94.1
GCT3-10	45.3	73.3	62.9	69.3	97.3	96.3	70.4	95.4
GCT3-11	52.8	70.6	64.3	77.5	95.3	94.3	70.2	93.5
GCT3-12	49.7	70.5	62.7	77.0	97.8	97.2	72.8	96.1
GCT3-13	40.1	71.1	58.1	64.4	95.4	93.4	69.5	91.3
GCT3-14	50.9	66.7	60.5	73.7	89.6	87.6	65.8	86.2
GCT3-15	49.7	65.7	59.1	72.2	88.2	86.0	64.2	84.5
GCT3-16	51.6	65.2	59.7	74.2	87.8	85.9	64.6	84.4
GCT3-17	51.1	71.8	64.4	75.2	95.9	94.8	70.4	94.0
GCT3-18	56.1	72.6	67.2	81.5	97.9	97.5	73.1	97.0
GCT3-19	46.7	73.6	63.9	73.4	100.2	100.3	70.6	100.0
GCT3-20	49.9	74.5	66.2	76.1	100.7	101.0	73.0	100.7
GCT3-21	52.1	74.5	67.2	77.8	100.2	100.3	73.5	100.0
GCT3-22	53.4	74.0	67.2	79.6	100.1	100.1	73.4	99.8
GCT3-23	53.4	74.1	67.4	79.6	100.3	100.4	73.5	100.1
GCT3-24	57.7	73.3	68.4	84.8	100.5	100.5	74.2	100.3
GCT3-25	49.3	74.5	65.9	75.1	100.4	100.5	72.4	100.2

Notes:

1. Reactor heat loss (1.5×10^6 Btu/hr) estimated from combustion test run data.
2. Standard state assumed to be 100 ° F.
3. Fluidization and instrument nitrogen inlet temperature assumed to be 100 ° F and to have zero standard-state enthalpy.

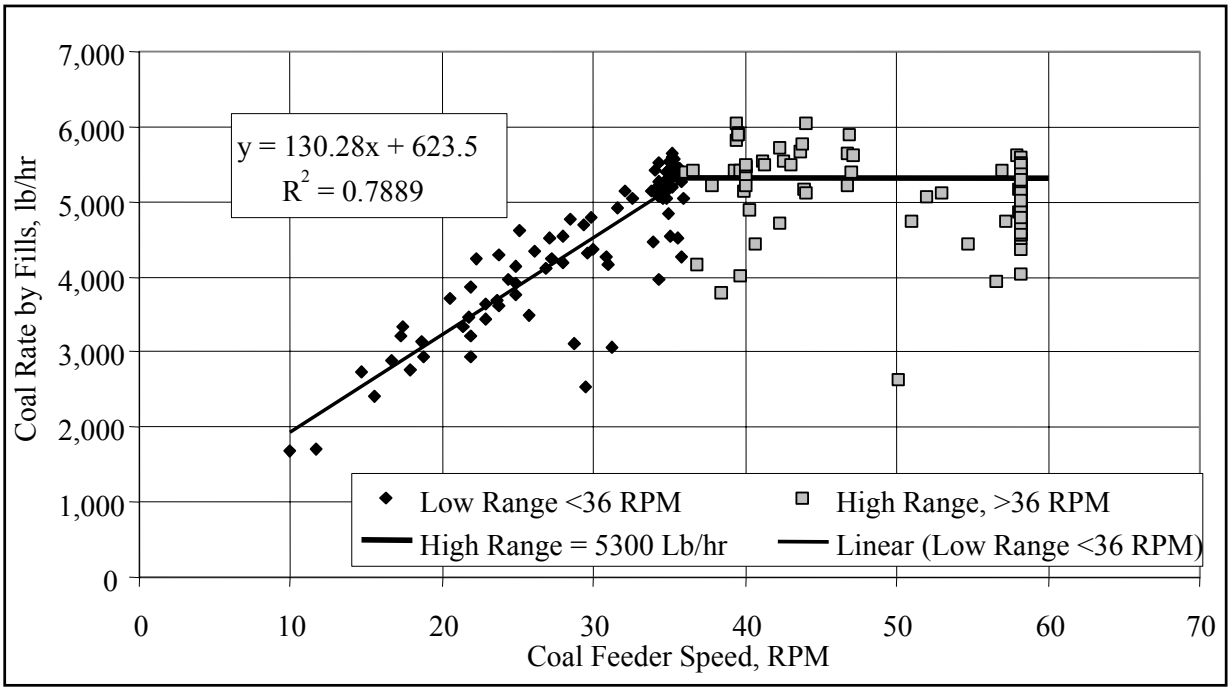

Figure 4.4-1 Coal Feeder Correlation

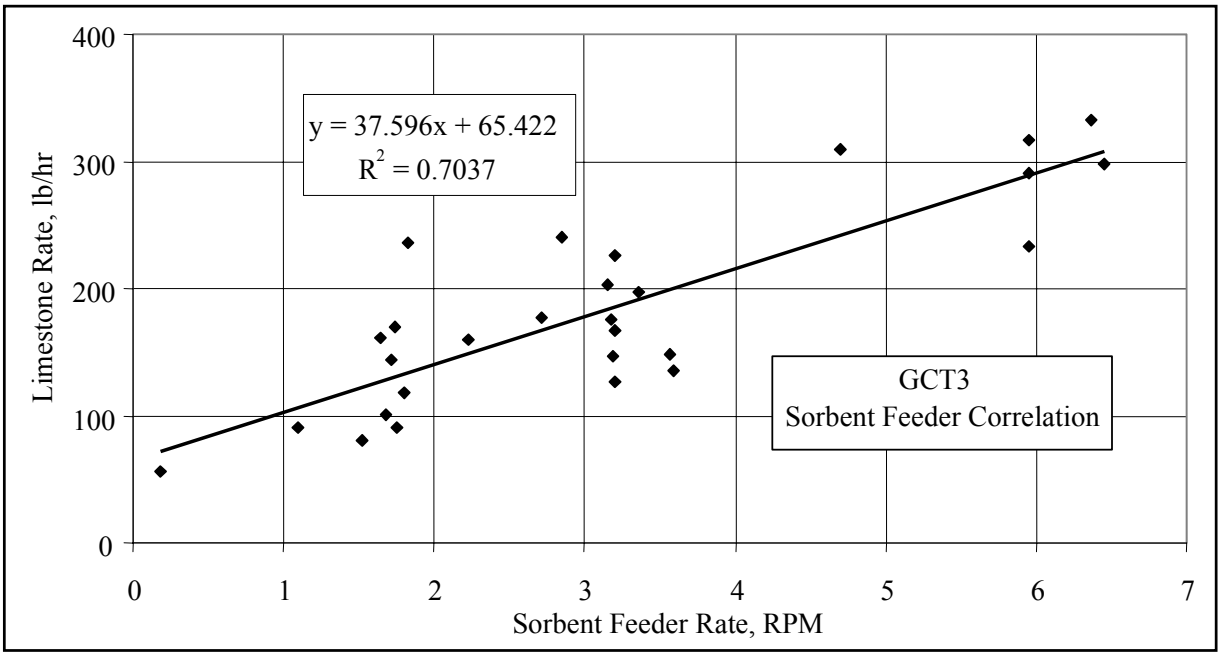

Figure 4.4-2 Sorbent Feeder Correlation

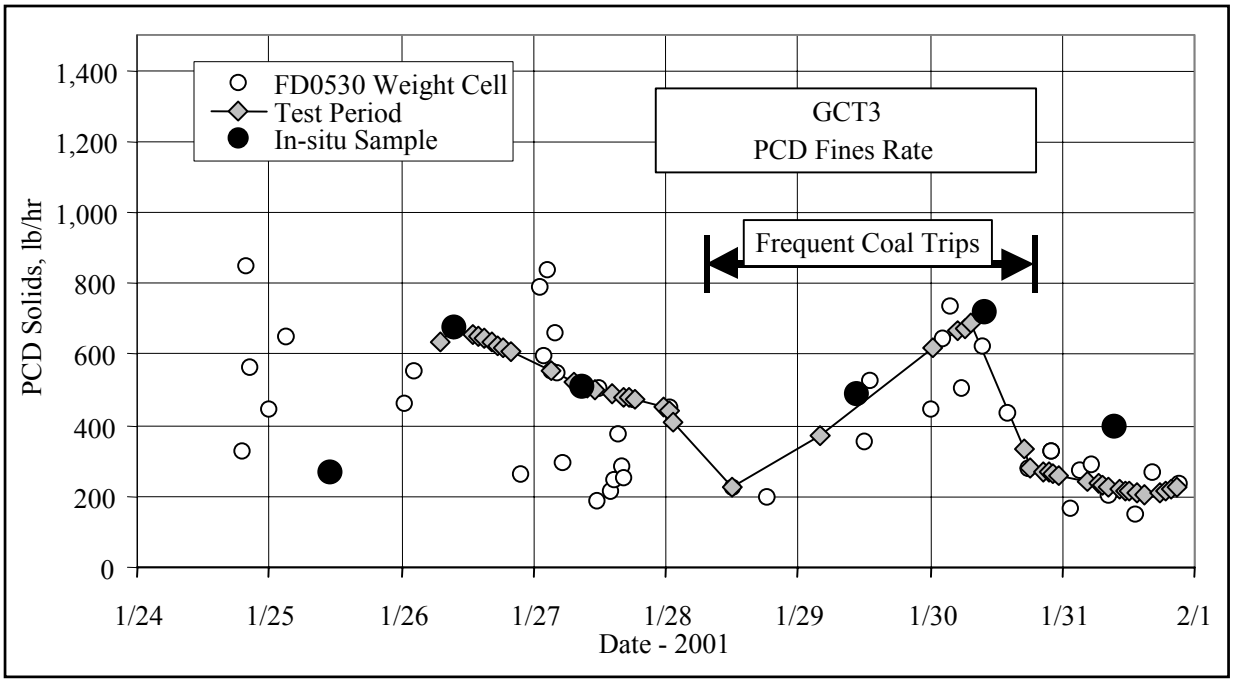

Figure 4.4-3 PCD Fines Rate

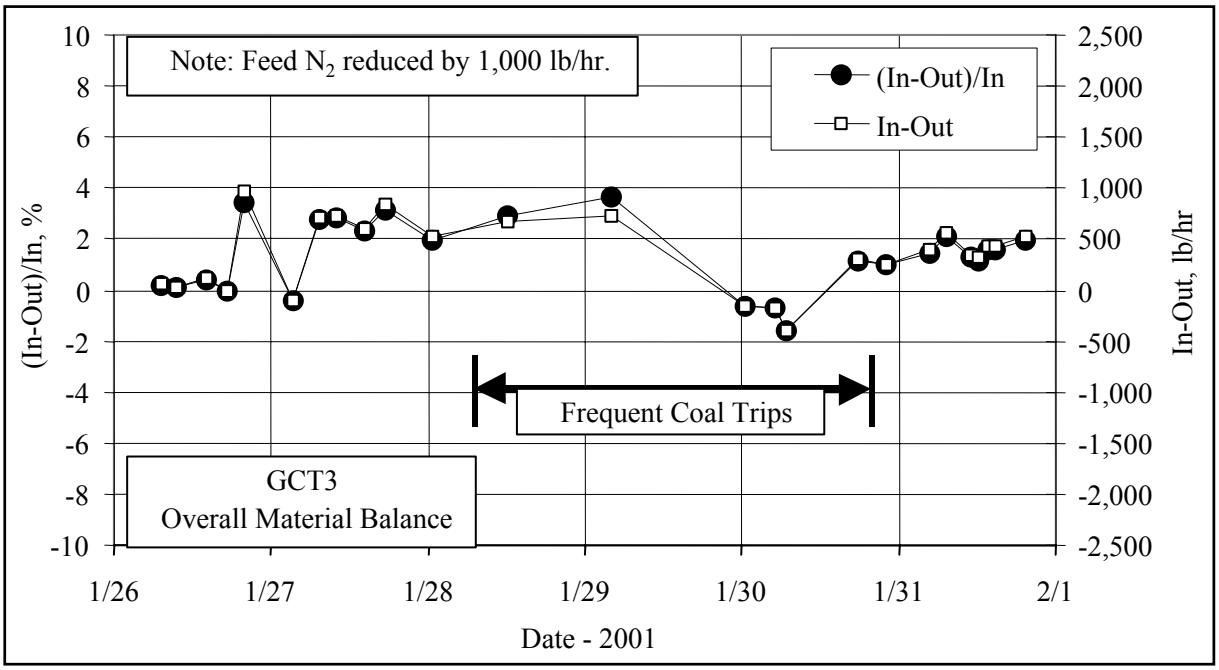

Figure 4.4-4 Overall Material Balance

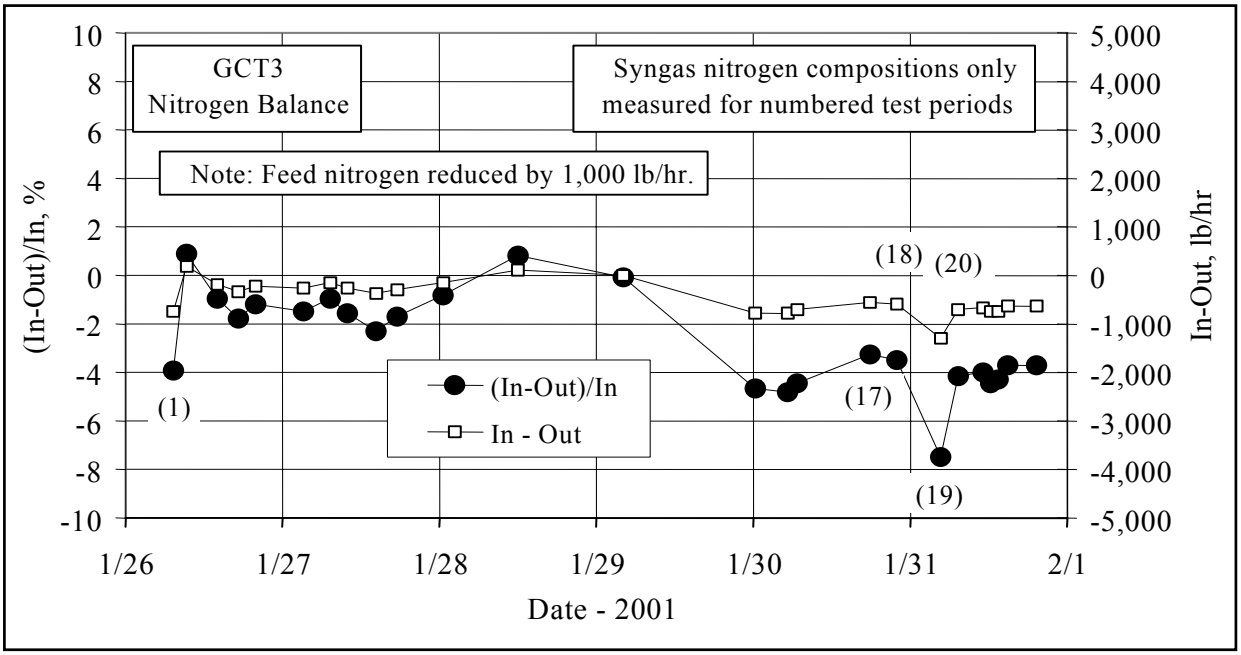

Figure 4.4-5 Nitrogen Balance

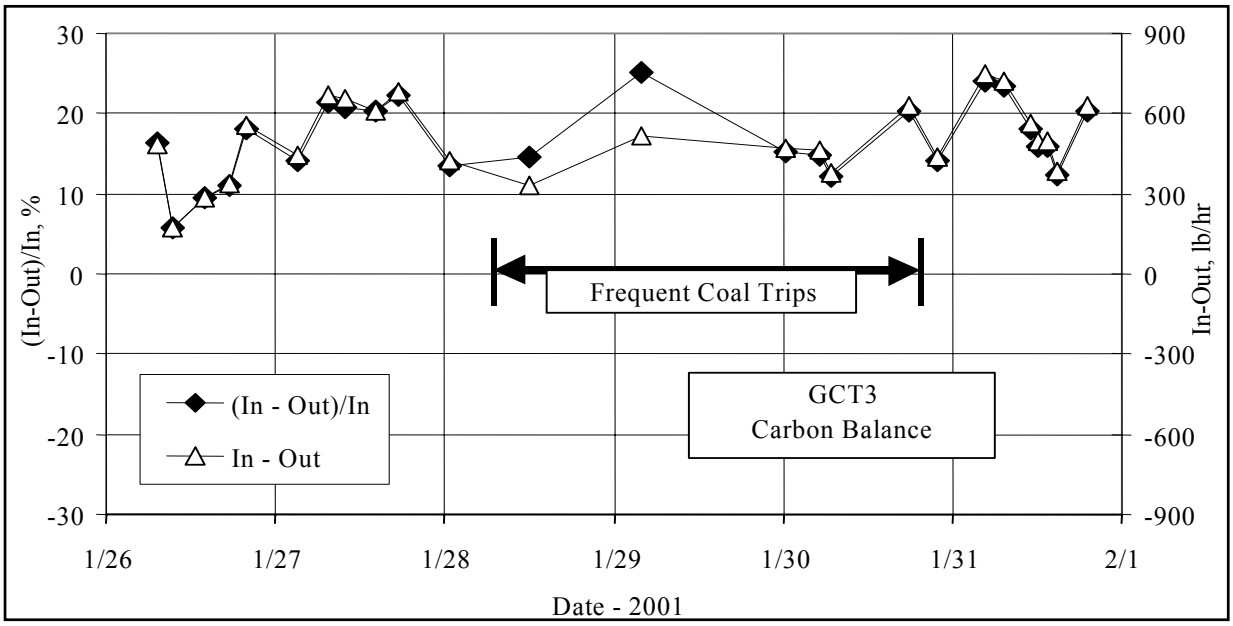

Figure 4.4-6 Carbon Balance

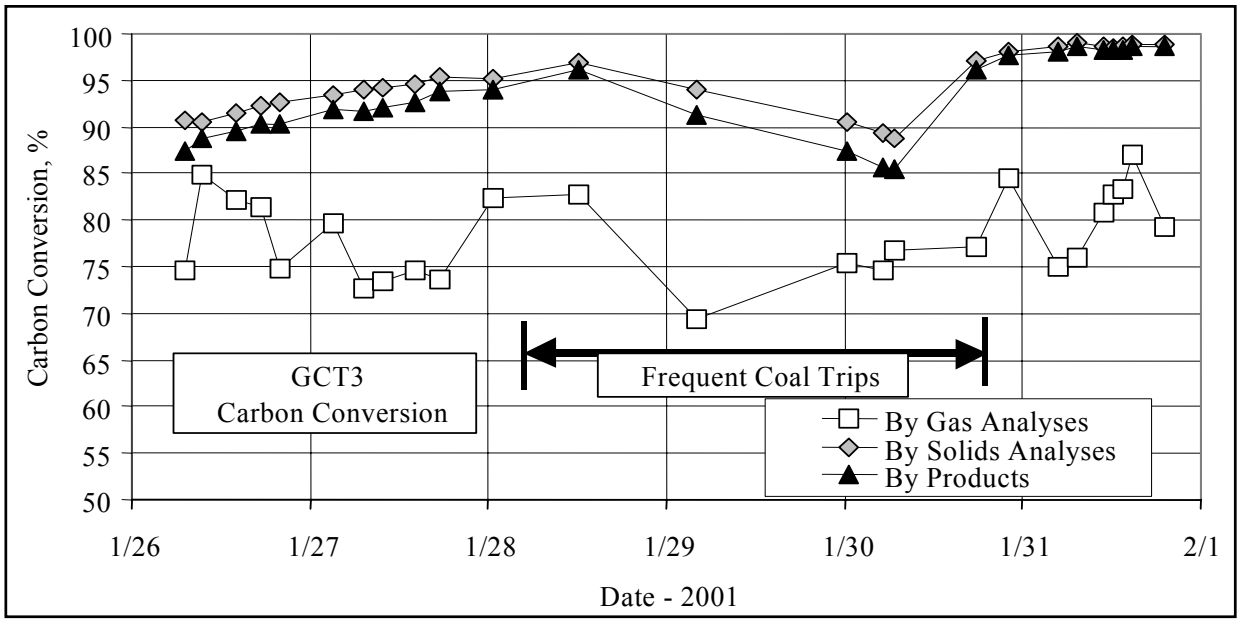

Figure 4.4-7 Carbon Conversion

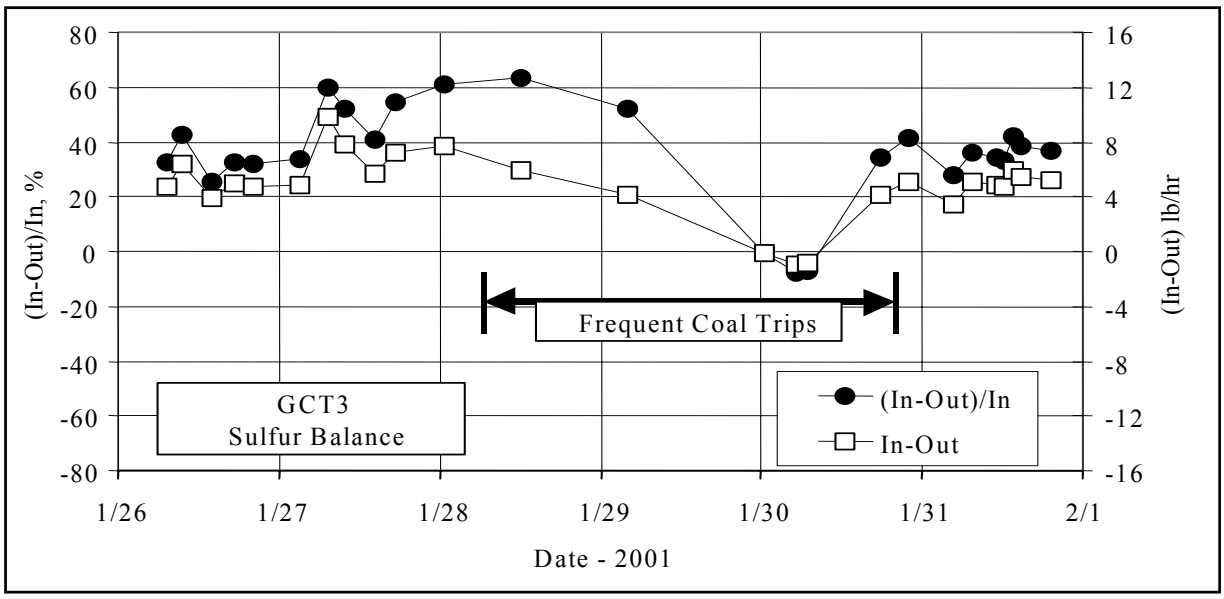

Figure 4.4-8 Sulfur Balance

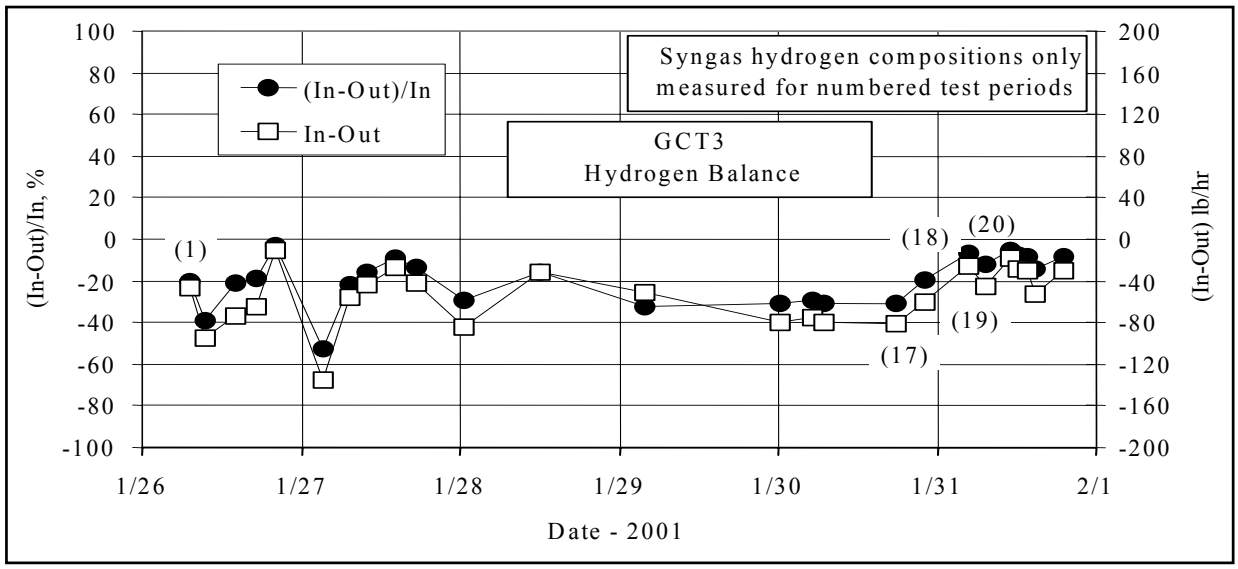

Figure 4.4-9 Hydrogen Balance

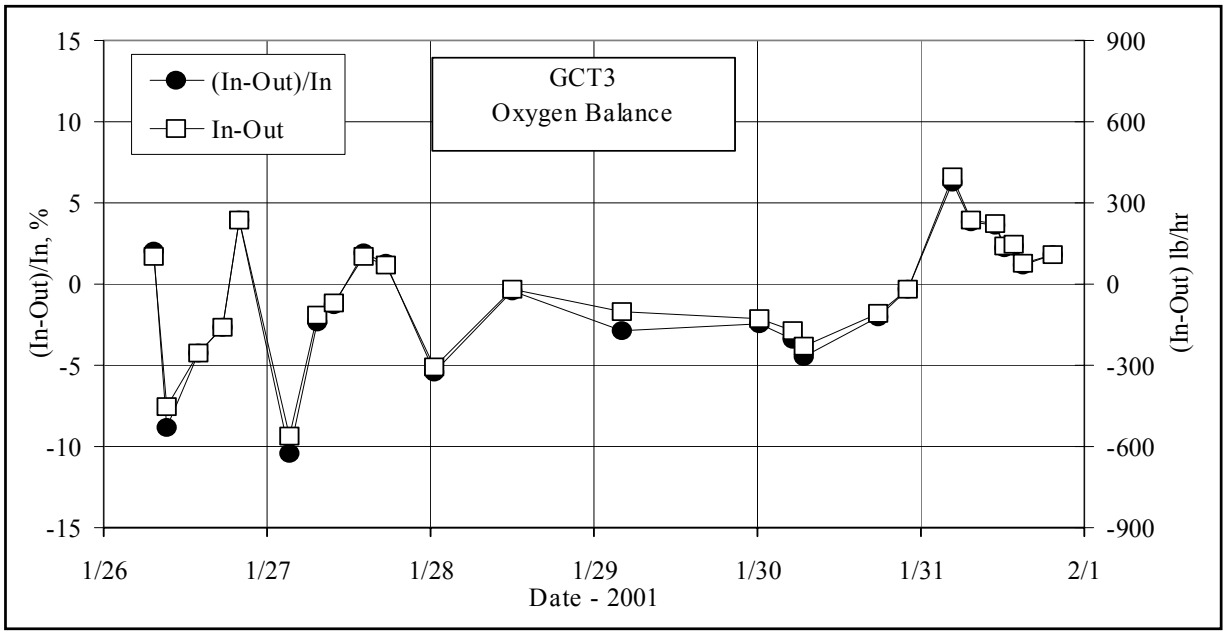

Figure 4.4-10 Oxygen Balance

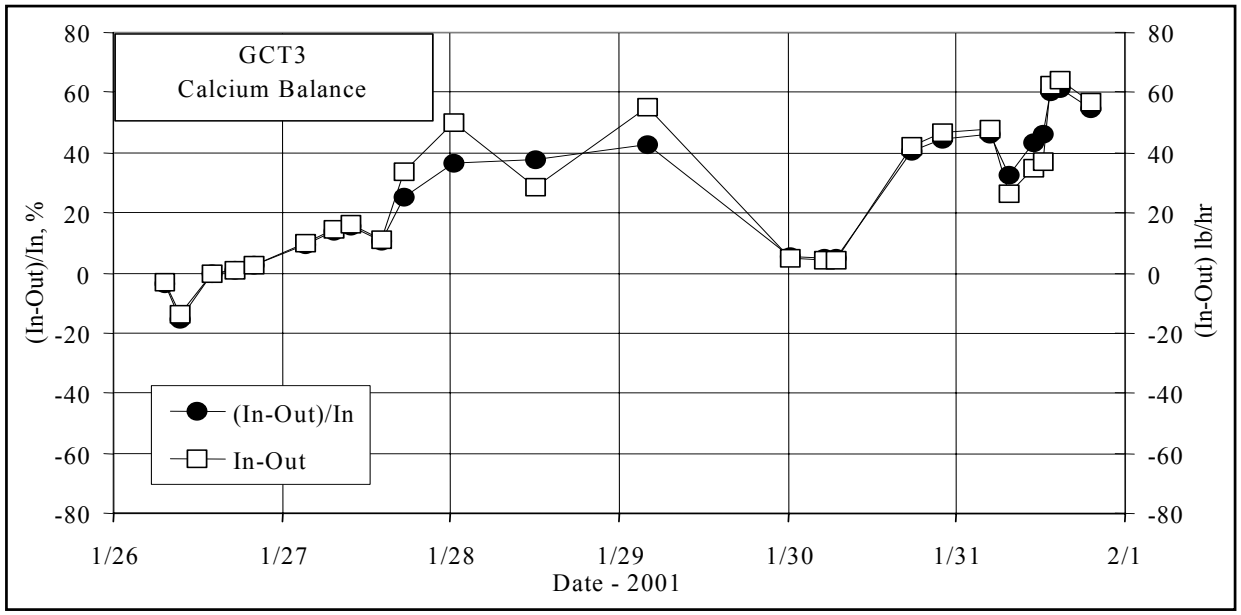

Figure 4.4-11 Calcium Balance

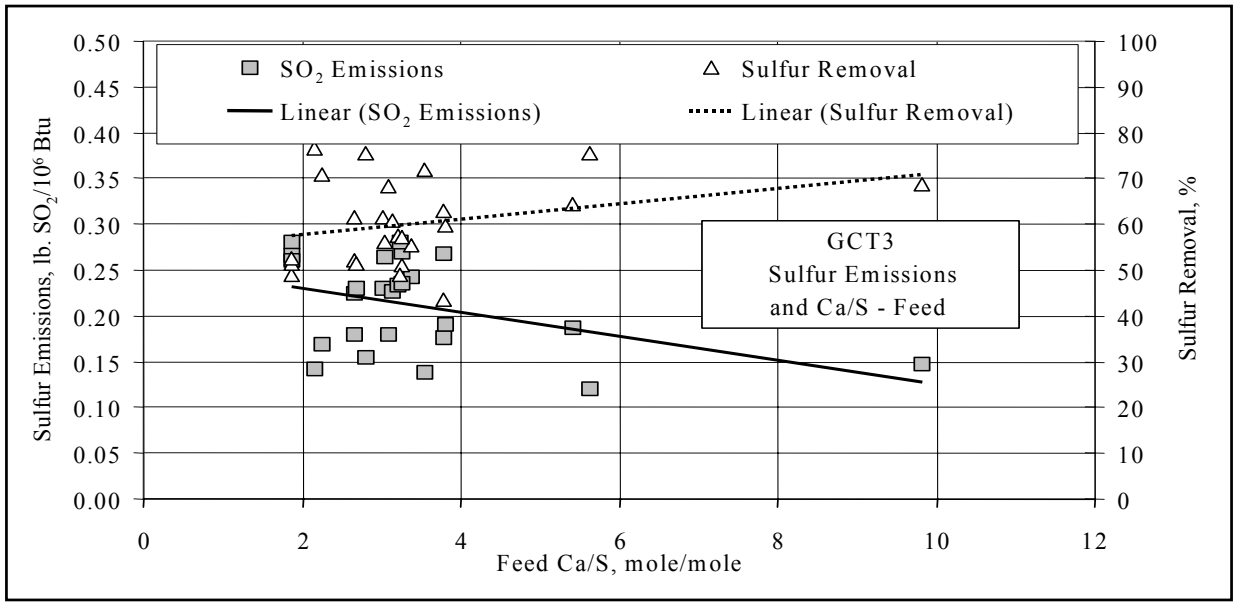

Figure 4.4-12 Sulfur Emissions and Feeds Ca/S Ratio

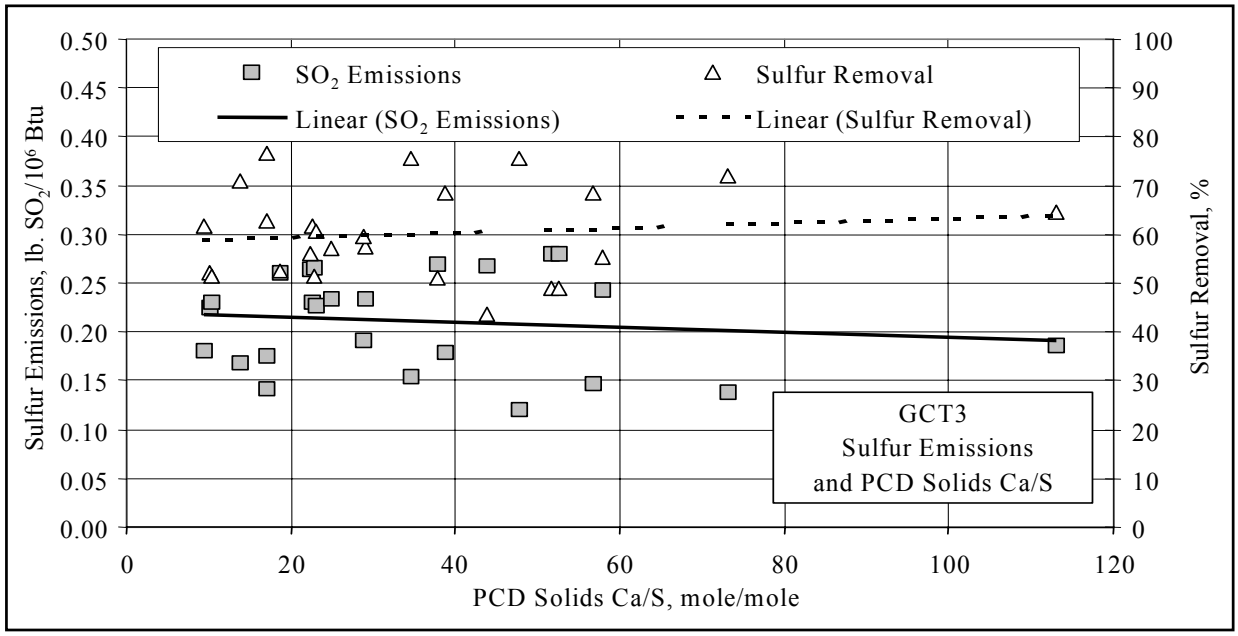

Figure 4.4-13 Sulfur Emissions and PCD Solids CA/S Ratio

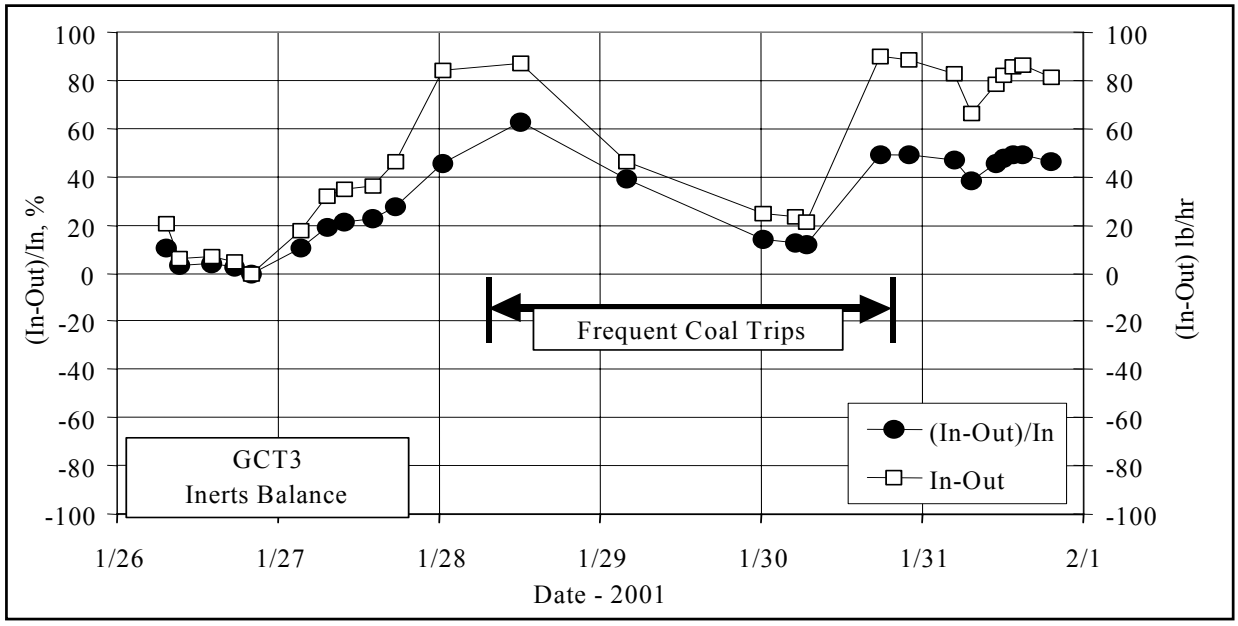

Figure 4.4-14 Inerts Balance

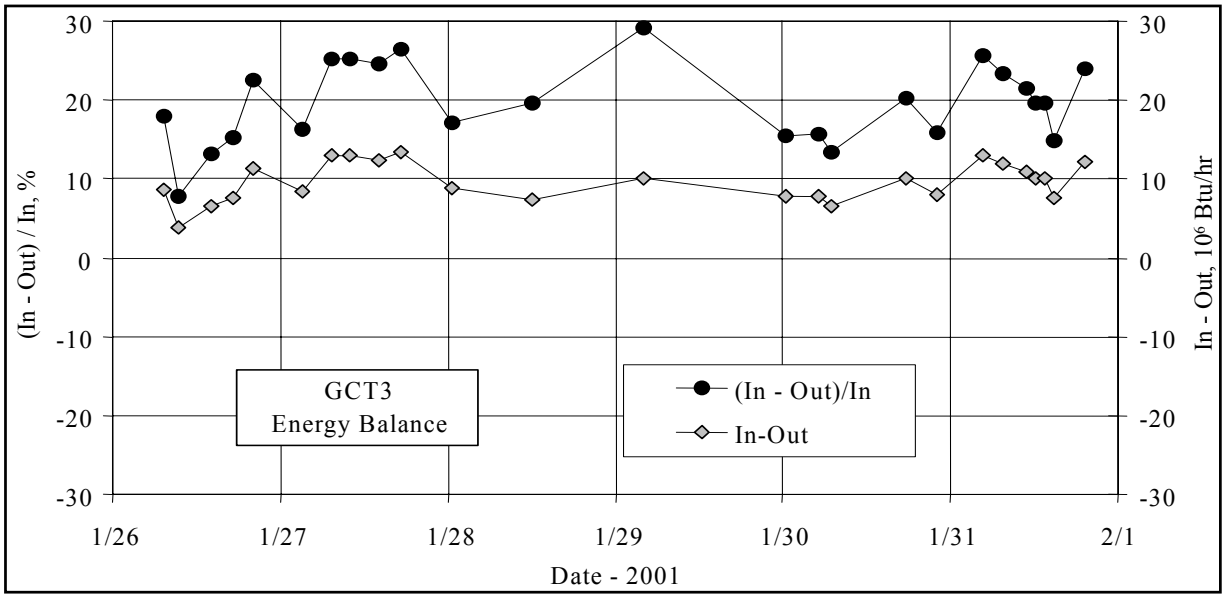

Figure 4.4-15 Energy Balance

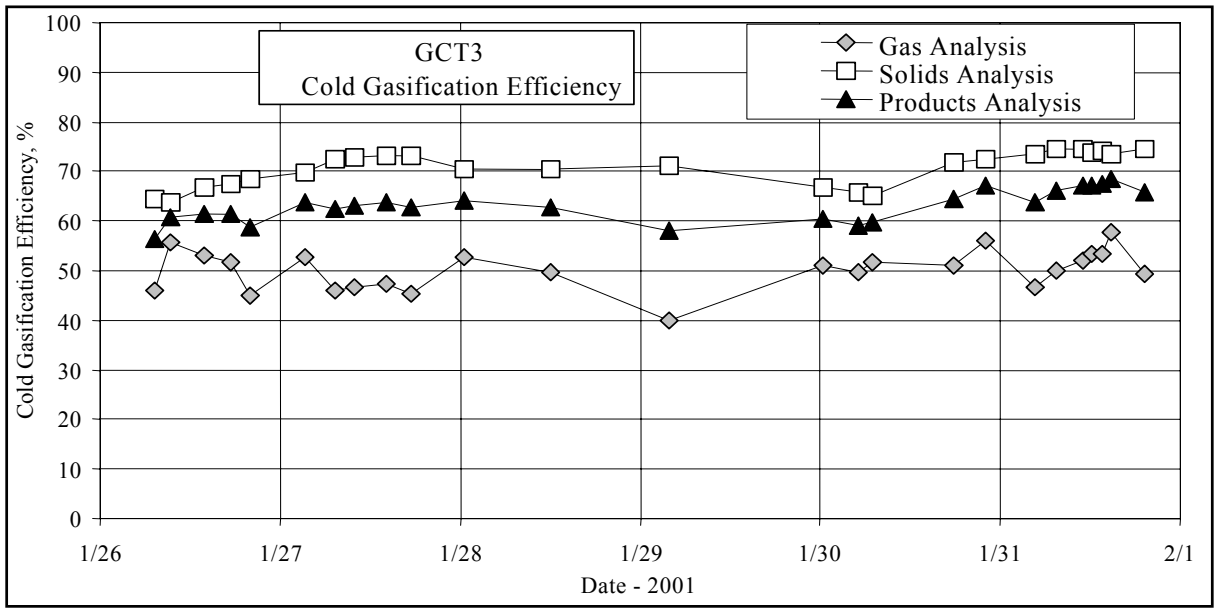

Figure 4.4-16 Gasification Efficiency – Cold

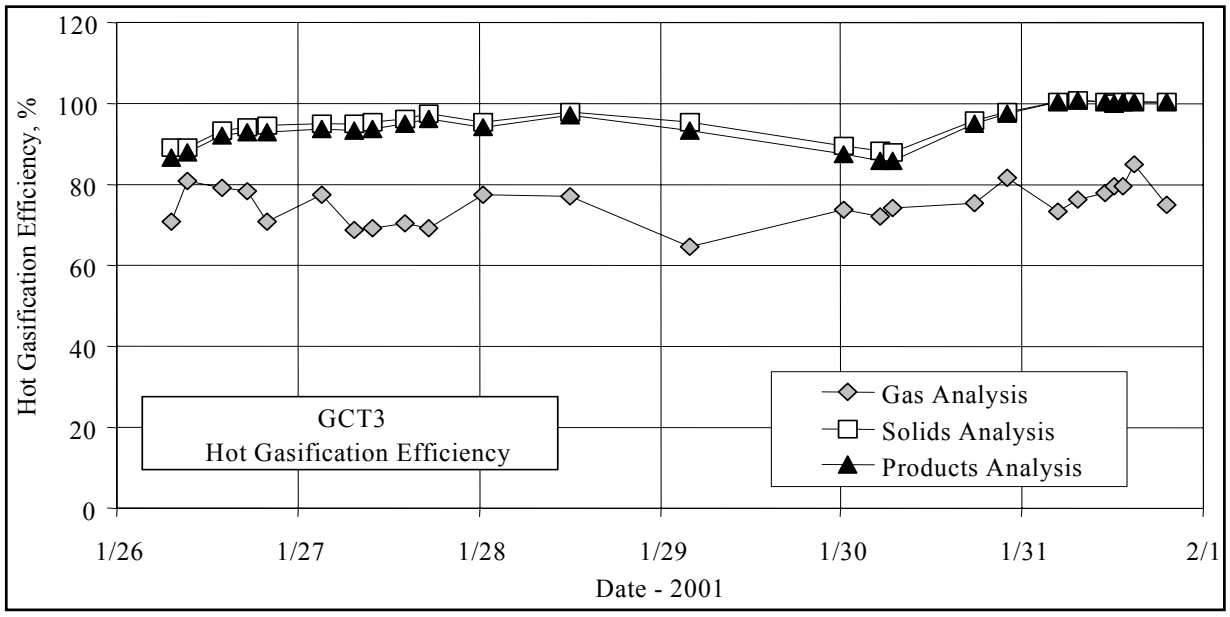

Figure 4.4-17 Gasification Efficiency – Hot

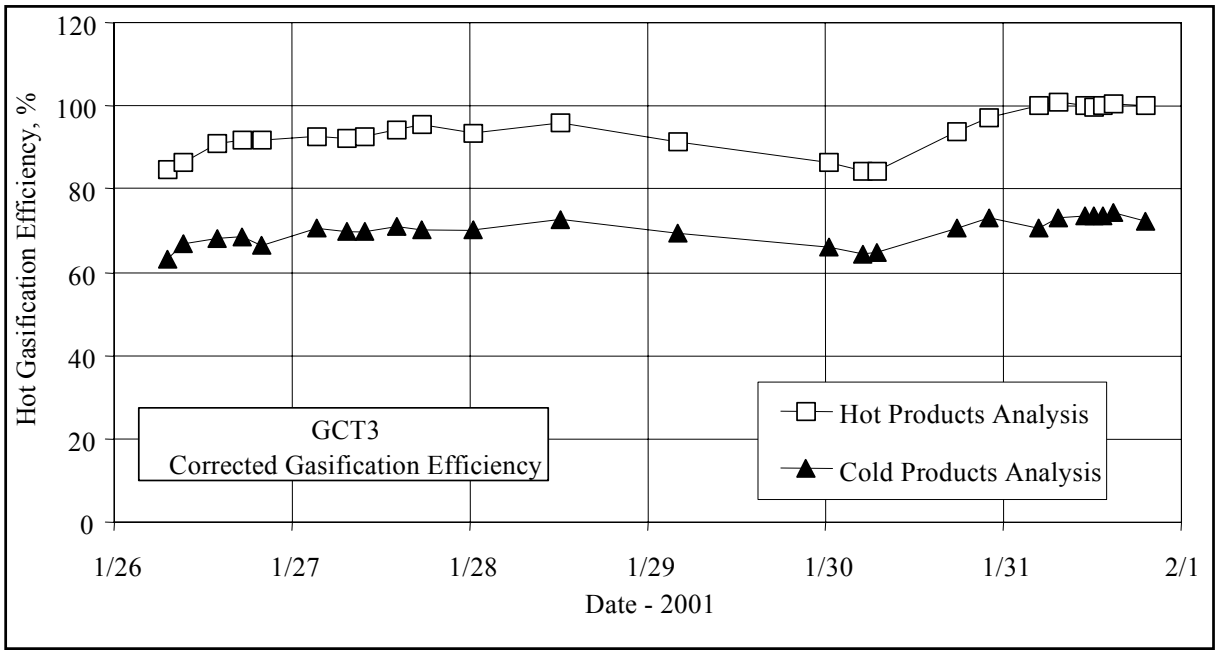

Figure 4.4-18 Corrected Gasification Efficiencies

4.5 PROCESS GAS COOLERS

Heat transfer calculations were performed on the primary gas cooler (HX0202) and secondary gas cooler (HX0402) to determine if their performance had deteriorated during GCT3 due to deposits of tar or other compounds on the tubes.

The HX0202 is between the transport reactor cyclone (CY0201) and the Siemens Westinghouse PCD (FL0301). During GCT3, HX0202 was not bypassed and took the full gas flow from the transport reactor. The HX0202 is a single-flow heat exchanger with hot gas from the transport reactor flowing through the tubes and with the shell side operating with the plant steam system. The pertinent equations are:

$$Q = UA\Delta T_{LM} \tag{1}$$

$$Q = c_p M(T_1 - T_2) \tag{2}$$

$$\Delta T_{LM} = \frac{(T_1 - t_2) - (T_2 - t_1)}{\ln \frac{(T_1 - t_2)}{(T_2 - t_1)}} \tag{3}$$

Q = Heat transferred (Btu/hour)
U = Heat transfer coefficient (Btu/hr/ft^2/°F)
A = Heat exchanger area (ft^2)
ΔT_{LM} = Log mean temperature difference (°F)
c_p = Gas heat capacity (Btu/lb/°F)
M = Mass flow of gas through heat exchanger (lb/hr)
T_1 = Gas inlet temperature (°F)
T_2 = Gas outlet temperature (°F)
$t_1 = t_2$ = Steam temperature (°F)

Using Equations (1) through (3) and the process data, the product of the heat transfer coefficient and the heat exchanger area (UA) can be calculated. The UA for GCT3 is shown in Figure 4.5-1 as hourly averages, along with the design UA of 5,200 Btu/hr/°F and the pressure drop across HX0202. If HX0202 is plugging, the UA should decrease and the pressure drop should increase. The UA deterioration is a better indication of heat exchanger plugging because the pressure drop is calculated by the difference of two numbers of about the same size, usually from 150 to 240 psig, resulting in pressure drops of 1 to 2 psi.

The UA slowly increased from 4,000 to 8,000 Btu/hr/°F during the first 10 hours of testing, higher than the design value of 5,200 Btu/hr/°F. The UA was then constant from early on January 25 to January 28 at between 8,000 and 9,000 Btu/hr/°F. During the periods of numerous coal trips from January 28 to January 30 the hourly average UA was very irregular and

went as low as 3,800 Btu/hr/°F. After the coal feed was stabilized the UA increased from 8,000 to 9,000 Btu/hr/°F for the last 2 days of the run. Heat exchanger HX0202 performance did not decrease during GCT3. The performance of HX0202 in GCT3 was better than in GCT2 with a higher synthesis-gas rate. The GCT2 UA was typically at 4,000 Btu/hr/°F for most of GCT2, which resulted in a higher PCD inlet temperature.

The pressure drop was essentially constant at around 1.5 psi during the entire run except for the 2 days of frequent coal feed trips. During the coal feed trips from January 28 to January 30 the heat exchanger pressure drop decreased due to the lower synthesis gas-flow rate.

The secondary gas cooler is a single-flow heat exchanger, with hot gas from the PCD flowing through the tubes and with the shell side operating with plant steam system. Some heat transfer and pressure drop calculations were done around HX0402 to determine if there was any plugging or heat exchanger performance deterioration during GCT3. HX0402 is not part of the combustion gas turbine commercial flow sheet. In the commercial gas turbine flow sheet the hot synthesis gas from the PCD would be sent directly to a combustion gas turbine. HX0402 would be used commercially if the synthesis gas were to be used in a fuel cell or as a chemical plant feedstock.

Using Equations (1) through (3) and the process data, the product of the heat transfer coefficient and the UA can be calculated. The UA for the GCT3 testing is shown in Figure 4.5-2 as hourly averages, along with the design UA of 13,100 Btu/hr/°F and the pressure drop across HX0402. If HX0402 is plugging, the UA should decrease and the pressure drop should increase.

The UA increased during the first day of testing from 14,000 to 16,000 Btu/hr/°F, above the design UA of 13,100 Btu/hr/°F. The UA then held steady at 16,000 Btu/hr/°F for the next several days, until the period of numerous coal trips. During the coal trips the UA decreased to 13,000 Btu/hr/°F. After the coal feed was stabilized the UA was constant at 15,000 Btu/hr/°F.

The pressure drop was constant at 2.5 to 3.3 psi for the first 3 days of operation. During the periods of frequent coal trips the pressure drop varied between 1.0 and 3.0 psi. After the coal feed was stabilized the pressure drop increased to 3.0 psi. There was no evidence of heat exchanger plugging during the run since the UA and the pressure drop were essentially the same at the end of the run as at the start of the run.

The GCT2 test run had HX0402 UAs in the same range as GCT3 at 14,000 to 16,000 Btu/hr/°F at full synthesis gas flow. The pressure drops for HX0402 occurring during GCT2 were also comparable to GCT3, with pressure drops of 2 to 3 psi.

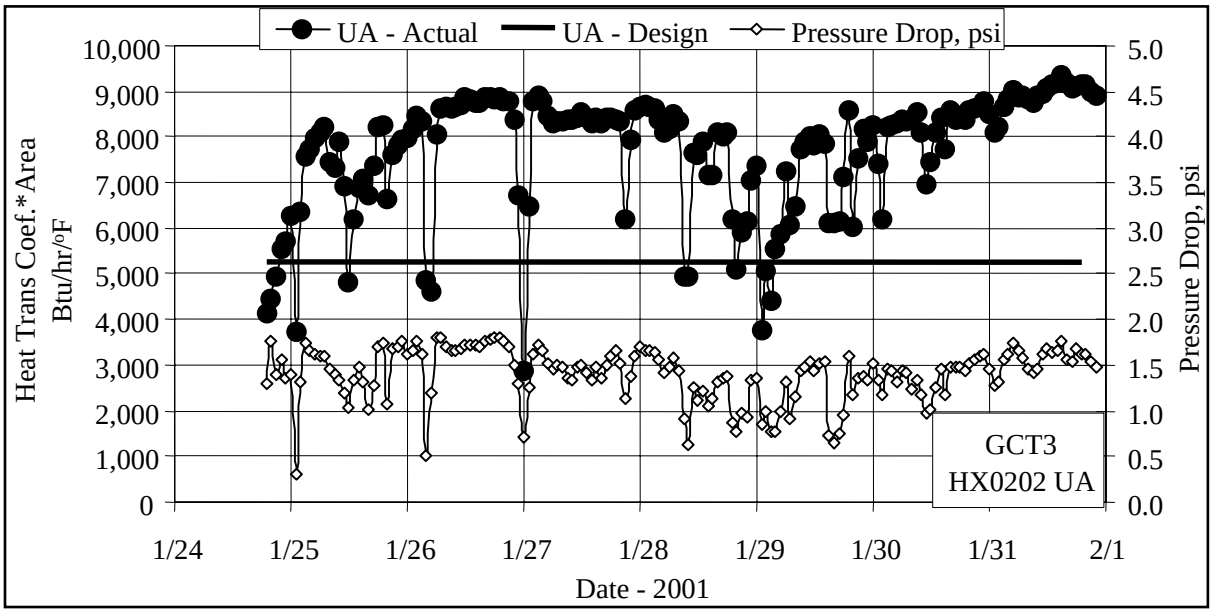

4.5-1 HX0202 Heat Transfer Coefficient and Pressure Drop

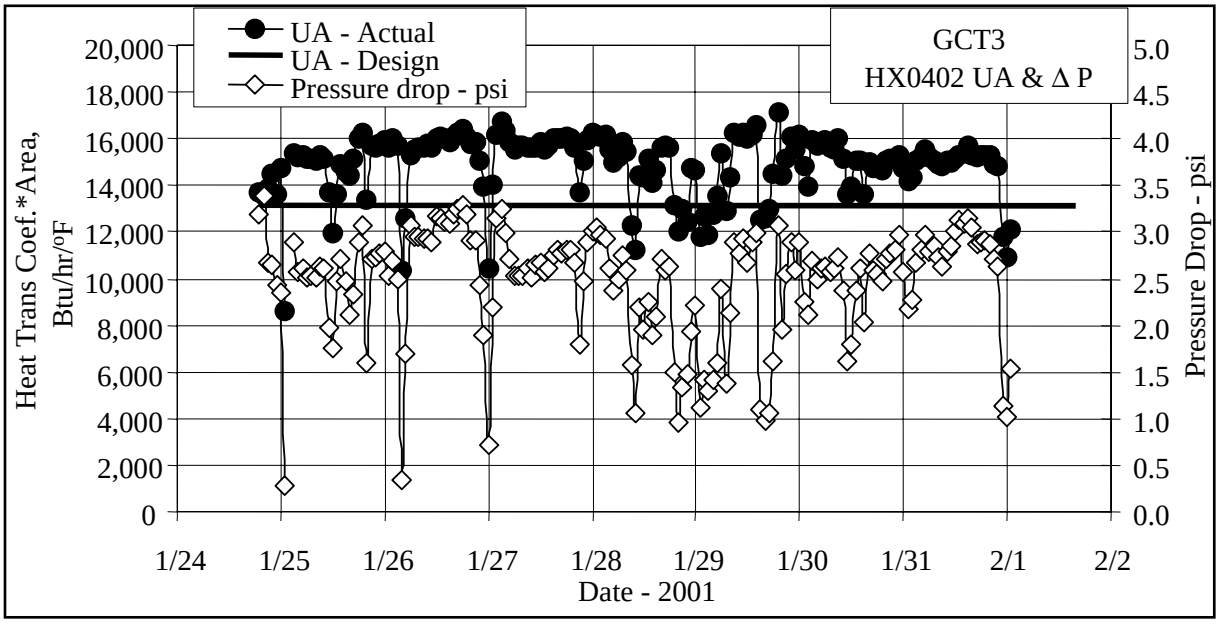

4.5-2 HX0204 Heat Transfer Coefficient and Pressure Drop

TERMS

Listing of Abbreviations

AAS	Automated Analytical Solutions
ADEM	Alabama Department of Environmental Management
APC	Alabama Power Company
APFBC	Advance Pressurized Fluidized-Bed Combustion
ASME	American Society of Mechanical Engineers
AW	Application Workstation
BFI	Browning-Ferris Industries
BFW	Boiler Feed Water
BMS	Burner Management System
BOC	BOC Gases
BOP	Balance-of-Plant
BPIR	Ball Pass Inner Race, Frequencies
BPOR	Ball Pass Outer Race, Frequencies
BSF	Ball Spin Frequency
CAD	Computer-Aided Design
CEM	Continuous Emissions Monitor
CFB	Circulating Fluidized Bed
CFR	Code of Federal Regulations
CHE	Combustor Heat Exchanger
COV	Coefficient of Variation (Standard Deviation/Average)
CPC	Combustion Power Compay
CPR	Cardiopulmonary Resuscitation
CTE	Coefficient of Thermal Expansion
DC	Direct Current
DCS	Distributed Control System
DOE	U.S. Department of Energy
E & I	Electrical and Instrumentation
EERC	Energy and Environmental Research Center
EPRI	Electric Power Research Institute
EDX	Energy-Dispersive X-Ray
ESCA	Electron Spectroscopy for Chemical Analysis
FCC	Fluidized Catalytic Cracker
FCP	Flow-Compacted Porosity
FFG	Flame Front Generator
FI	Flow Indicator
FIC	Flow Indicator Controller
FOAK	First-of-a-Kind
FTF	Fundamental Train Frequency
FW	Foster Wheeler
GBF	Granular Bed Filter
GC	Gas Chromatograph
GEESI	General Electric Environmental Services, Inc.
HP	High Pressure

HRSG	Heat Recovery Steam Generator
HTF	Heat Transfer Fluid
HTHP	High-Temperature, High-Pressure
I/O	Inputs/Outputs
ID	Inside Diameter
IF&P	Industrial Filter & Pump
IGV	Inlet Guide Vanes
IR	Infrared
KBR	Kellogg Brown & Root
LAN	Local Area Network
LIMS	Laboratory Information Management System
LOC	Limiting Oxygen Concentration
LOI	Loss on Ignition
LPG	Liquefied Propane Gas
LSLL	Level Switch, Low Level
MAC	Main Air Compressor
MCC	Motor Control Center
MS	Microsoft Corporation
NDIR	Nondestructive Infrared
NETL	National Energy Technology Laboratory
NFPA	National Fire Protection Association
NOx	Nitrogen Oxides
NPDES	National Pollutant Discharge Elimination System
NPS	Nominal Pipe Size
OD	Outside Diameter
OSHA	Occupational Safety Health Administration
OSI	OSI Software, Inc.
P&IDs	Piping and Instrumentation Diagrams
PC	Pulverized Coal
PCD	Particulate Control Device
PDI	Pressure Differential Indicator
PDT	Pressure Differential Transmitter
PFBC	Pressurized Fluidized-Bed Combustion
PI	Plant Information
PLC	Programmable Logic Controller
PPE	Personal Protection Equipment
PRB	Powder River Basin
PSD	Particle Size Distribution
PSDF	Power Systems Development Facility
ΔP	Pressure Drop
PT	Pressure Transmitter
RFQ	Request for Quotation
RO	Restriction Orifice
RSSE	Reactor Solid Separation Efficiency
RT	Room Temperature
SCS	Southern Company Services, Inc.
SEM	Scanning Electron Microscopy

SMD	Sauter Mean Diameter
SRI	Southern Research Institute
SUB	Start-up Burner
TCLP	Toxicity Characteristic Leaching Procedure
TR	Transport Reactor
TRDU	Transport Reactor Demonstration Unit
TSS	Total Suspended Solids
UBP	Uncompacted Bulk Porosity
UND	University of North Dakota
UPS	Uninterruptible Power Supply
UV	Ultraviolet
VFD	Variable Frequency Drive
VOCs	Volatile Organic Compounds
WPC	William's Patent Crusher
XRD	X-Ray Diffraction
XXS	Extra, Extra Strong

Listing of Units

acfm	actual cubic feet per minute
Btu	British thermal units
°C	degrees celsius or centigrade
°F	degrees fahrenheit
ft	feet
FPS	feet per second
gpm	gallons per minute
g/cm^3	grams per cubic centimeter
g	grams
GPa	gigapascals
hp	horsepower
hr	hour
in.	inches
inWg	inches, water gauge
°K	degrees kelvin
kg	kilograms
kJ	kilojoules
kPa	kilopascals
ksi	thousand pounds per square inch
m	meters
MB	megabytes
mm	millimeters
MPa	megapascals
msi	million pounds per square inch
MW	megawatts
m/s	meters per second
MBtu	Million British thermal units
m^2/g	square meters per gram
μ or μm	microns or micrometers
dp_{50}	particle size distribution at 50 percentile
ppm	parts per million
ppm (v)	parts per million (volume)
ppm (w)	parts per million (weight)
lb	pounds
pph	pounds per hour
psia	pounds per square inch
psig	pounds per square inch gauge
ΔP	pressure drop
rpm	revolutions per minute
s or sec	seconds
scf	standard cubic feet
scfm	standard cubic feet per minute
V	volts
W	watts